CHEMICAL MECHANISMS UNDERLYING SOME BIOLOGICAL REACTIONS MEDIATING THE CYTOTOXICITY AND THERAPEUTIC POTENTIAL OF NITRIC OXIDE

Douglas Mackay Short

A Thesis Submitted for the Degree of PhD
at the
University of St Andrews

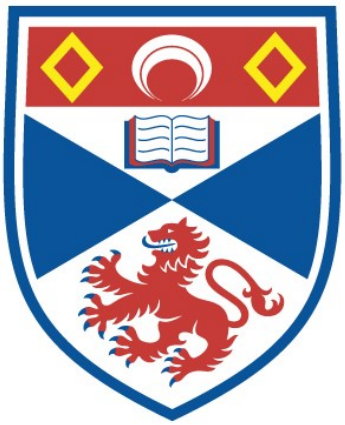

1999

CHEMICAL MECHANISMS UNDERLYING SOME BIOLOGICAL REACTIONS MEDIATING THE CYTOTOXICITY AND THERAPEUTIC POTENTIAL OF NITRIC OXIDE

A thesis presented by

Douglas Mackay Short B.Sc. (Hons) Dunelm. GRSC

to the

UNIVERSITY OF ST. ANDREWS

in application for

THE DEGREE OF DOCTOR OF PHILOSOPHY

St. Andrews September 1998

DECLARATION

I, Douglas Mackay Short, hereby certify that this thesis, which is approximately 38,000 words in length, has been written by me, that it is the record of work carried out by me and that it has not been submitted in any previous application for a higher degree.

25. 2. 99

Date Signature of candidate

I was admitted as a research student in October 1995 and as a candidate for the degree of Doctor of Philosophy in October 1996; the higher study for which this is a record was carried out in the University of St. Andrews between October 1995 and September 1998.

25. 2. 99

Date Signature of candidate

I hereby certify that the candidate has fulfilled the conditions of the Resolution and Regulations appropriate for the degree of Doctor of Philosophy in the University of St. Andrews and that the candidate is qualified to submit this thesis in application for that degree.

25-2-99

Date Signature of supervisor

COPYRIGHT

In submitting this thesis to the University of St. Andrews, I understand that I am giving permission for it to be made available for use in accordance with the regulations of the University Library for the time being in force, subject to any copyright vested in the work not being affected thereby. I also understand that the title and abstract will be published, and that a copy of the work may be made and supplied to any *bona fide* library or research worker.

25·2·99

Date Signature of candidate

"Education is what survives when what has been learned has been forgotten".

B. F. Skinner, *New Scientist*. 21st May 1964.

Dedicated to my mum with enduring love and appreciation

ACKNOWLEDGEMENTS

I owe a debt of gratitude to many more people than can be mentioned here, so this is not meant to be in any way exhaustive. First and foremost, I thank Dr. Tony Butler for his first rate supervision, guidance, charm and wit. Other academic staff who deserve recognition include: Professor John Ridd for help with understanding the CIDNP phenomena, the 'sultan of shim' Dr. Trevor Rutherford for his NMR expertise, Dr. Phil Lightfoot for running the crystal structure and Professor John Walton for assistance with the EPR spectroscopy. For helpful suggestions or discussions: Professors Keith Ingold of the NRC in Ottawa, Ron Lawler of Brown University, RI, Manfred Lehnig of the University of Dortmund and Lyn Williams of Durham University. I am indebted to Dr. Brian Cox of Zeneca in Huddersfield for providing a copy of the 'Scientist' computer program and training in its use.

I have been privileged to share many memorable experiences during my time in St. Andrews. It was the best of times, it was the worst of times and never has so much been owed to so few by one person. The few include the members of lab. 408b for creating a conducive and fun working environment: Doug Robertson, Elaine, Francesca, Garry, Haitham, Hazel, Iain, Judy, Kate, Louise, Nicola Bainbrigge, Phillippa and Zeljka. Arwel, Colin and Nicola Davidson deserve special thanks for being especially supportive housemates, friends and colleagues. I would like to acknowledge several of my secondary school teachers at St. Bees. In particular, my chemistry masters Philip Barratt for warning me not to be over-confident and Dr. Philip Etchells for reporting that I appeared to be someone who only works when he

has to and that this would be my downfall, either at A-level or beyond. He may be right, but thankfully I haven't come unstuck yet. In fact it was 'Doc. Etch.' who first brought the apt B.F. Skinner quote to my attention: usually immediately prior to a tri-weekly test. Dr. Tony Winzor's dedication and faith in me was a great inspiration. I feel that Malcolm Thyne (currently head of Fettes College, Edinburgh) played a pivotal role in 'catalysing' my interest in chemistry from a tender age. I still have fond memories of his equation-balancing wagers with the class, the 'magical' colour-changing liquid as it was poured from flask to flask and his 'one collar and two socks are necessary/acid plus base equals salt plus water' mnemonics. The latter of which proved to me that rote learning can have its merits.

I thank the Biotechnology and Biological Sciences Research Council (BBSRC) for a grant to allow me to pursue this work and The Wellcome Trust for provision of high-field NMR facilities.

ABSTRACT

Some *in vitro* reactions of peroxynitrite are examined using ^{15}N CIDNP NMR spectroscopy to elucidate more information about the radical nature of nitration, nitrosation and isomerisation mechanisms. Preliminary work on the nitration of tyrosine with $H^{15}NO_3$ confirms that 3-nitrotyrosine forms predominantly by the same radical mechanism established for other activated aromatic compounds such as 4-methylphenol. Reaction of alkaline [^{15}N] peroxynitrite with biotarget-type molecules such as tyrosine, a tyrosine-containing tripeptide and thiol-containing amino acids allows nuclear polarisation effects to be discerned which are consistent with free and solvent-caged $NO_2^{\bullet}$ and $HO^{\bullet}$ or $CO_3^{\bullet-}$. The phase of the nitrate signal observed during peroxynitrite isomerisation at pH 7.4 is opposite to that observed during reaction with a biotarget-type molecule, suggesting dimerisation of $NO_2^{\bullet}$ to N_2O_4 and its subsequent hydrolysis in addition to in cage geminate pair collapse. Mechanisms in accord with the observations are suggested and their implications and extent to which they concur with established theories are discussed. Kinetic simulations are used to estimate the relative importance of nitryl chloride and peroxynitrite as *in vivo* reactive nitrogen species. Three furazan 2-oxide (furoxan) derivatives with potent NO-donating activity were synthesised according to literature methods and their decomposition in aqueous solution to yield NO was examined using EPR spectroscopy by spin trapping with Fe^{2+}-*N*-methyl-D-glucamine dithiocarbamate (Fe^{2+}–MGD). Ammonia, arising from thiol-mediated reductive decomposition pathways, was also detected in quantities up to approximately 8% of the nitrogen-containing decomposition products. A commercially-available enzymatic assay based on reductive amination of 2-oxoglutarate using L-glutamate dehydrogenase and NADPH was used. The proportion of furoxan giving rise to these products is estimated and possible mechanisms for their generation are suggested.

List of Acronyms and Abbreviations Used

N.B. Common abbreviations listed in the *Journal of the Chemical Society* instructions for authors are not defined here.

S_{RN}(ANRORC)	Nucleophilic Substitution by Addition of Nucleophile, Ring-Opening, Ring Closure
CIDNP	Chemically Induced Dynamic Nuclear Polarisation
CYS	L-Cysteine
DBNBS	Sodium 3,5-dibromo-4-nitrosobenzene
DMPO	5,5-Dimethylpyrroline-*N*-oxide.
DOPA	3,4-Dihydroxyphenylalanine
ET	Electron transfer
GSNO	*S*-Nitrosoglutathione
MAH	Molecule-assisted homolysis
NAC	*N*-Acetyl-L-cysteine
NAP	*N*-Acetyl-DL-penicillamine
NO	Nitric oxide (IUPAC nitrogen monoxide)
$ONOO^-$/ONOOH	Peroxynitrite anion/peroxynitrous acid (IUPAC oxoperoxonitrate(1–) and hydrogen oxoperoxonitrate
PEN	DL-Penicillamine
RNS	Reactive Nitrogen Species
ROS	Reactive Oxygen Species
SNAP	*S*-Nitroso-*N*-acetyl-DL-penicillamine
SNHP	*S*-Nitroso-*N*-heptanoyl-DL-penicillamine
TYR/Y	L-Tyrosine

CONTENTS

List of Figures and Tables.

1 Introduction

1.1 The *in vitro* and *in vivo* chemistry of NO

1.1.1 *In vitro* chemistry

Nitric oxide (NO) is possibly the most important member of a family of nitrogen oxides including nitrous oxide or 'laughing gas' (N_2O), dinitrogen trioxide (N_2O_3), nitrogen dioxide ($NO_2^{\bullet}$) and its dimeric form dinitrogen tetraoxide (N_2O_4) and dinitrogen pentaoxide (N_2O_5) shown in Fig 1.1. It is often confused with nitrous oxide, even by professional bodies.[1] Together with N_2O and $NO_2^{\bullet}$, NO has been known for over 200 years as together they were the first gaseous compounds isolated by Joseph Priestley and others in the 1770s.

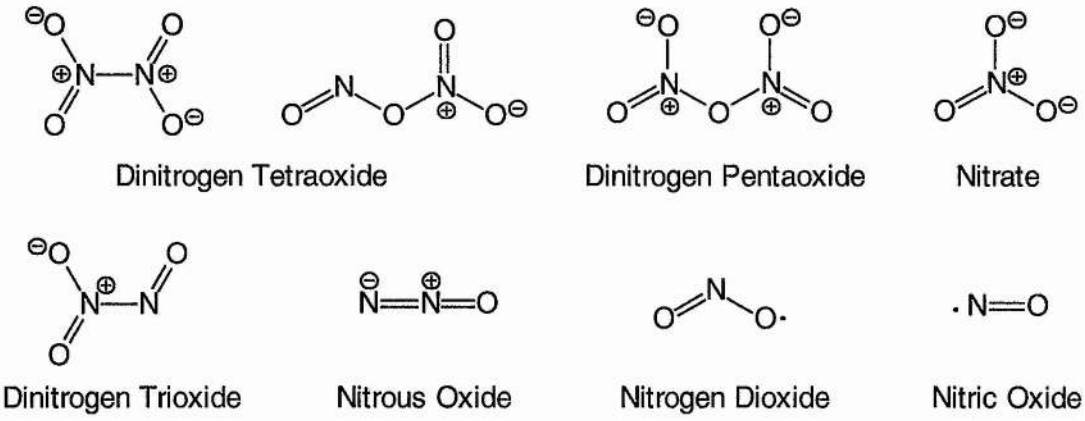

Fig. 1.1 Structures of some nitrogen oxides.

However, it was not until the 1990s that NO's importance in biological systems was fully appreciated. In 1992 it was elected as "Molecule of the Year" by the American popular journal Science[2] and in 1993, Chemical and Engineering News proclaimed it "biochemistry's unexpected new superstar".[3] The 1998 Nobel Prize in Physiology or Medicine was awarded jointly to Robert F. Furchgott, Louis J. Ignarro and Ferid

Murad for their discoveries concerning NO as a signalling molecule in the cardiovascular system. Nitric oxide itself is a colourless, monomeric gas and the extra electron in the antibonding π^* orbital renders it also paramagnetic. Some physical properties of NO are outlined in Table 1.1.

Table 1.1 Some physical properties of NO.[4]

MP/° C	BP/° C	μ/D	Distance (NO)/pm	$\Delta H_f^{\ominus}$/ kJ mol^{-1}	$\Delta G_f^{\ominus}$/ kJ mol^{-1}	E_i/ kJ mol^{-1}	Bond order
– 163.6	– 151.8	0.15	115	90.2	86.6	890.6	~ 2.5

The molecule is therefore a radical species, but a rather unreactive one. This is due to the delocalised nature of the unpaired electron - several resonance structures can be written. It is thermodynamically unstable at 25 °C and 1 atm. The ionisation energy is low compared with nitrogen (1500 kJ mol^{-1}), oxygen (1170 kJ mol^{-1}) and carbon monoxide (1350 kJ mol^{-1}); therefore the molecule will ionise easily to NO^+. NO reacts with oxygen to give nitrogen dioxide according to eqn. (1).

$$2NO\cdot + O_2 \longrightarrow 2NO_2\cdot \qquad (1)$$

1.1.2 *In vivo* chemistry

The oxidation of NO in the gaseous phase and in solution is first order in oxygen and second order in NO. Therefore under physiological conditions where the concentrations can be as low as 10^{-9} M, the reaction is slow enough not to be a significant sink reaction for NO as the physiological half life ranges from 4 to 50 s.[5] The third order rate constant[6,7] for the oxidation process is 6.3 ($\pm$ 0.4) $\times$ 10^6 M^{-2} s^{-1}.

The final oxidation products of NO in the blood are nitrite and nitrate represented by eqns. (1)–(3) and detection of residual nitrite produced by the Griess test[8] provides evidence of NO formation.

$$2NO_2 \cdot \longrightarrow N_2O_4 \qquad (2)$$

$$N_2O_4 + H_2O \longrightarrow NO_2^{\ominus} + NO_3^{\ominus} + 2H^{\oplus} \qquad (3)$$

1.1.2.1 The role of NO in vascular smooth muscle relaxation

Vascular smooth muscle (VSM) cells surround arteries and arterioles and their collective contraction and relaxation contracts and relaxes the arteries thus regulating blood pressure. The contractile state of VSM is determined by the interaction of two proteins, actin and myosin - the process being regulated by the intracellular concentration of calcium $[Ca_i^{2+}]$ which is in turn regulated by another 'messenger molecule' - guanosine 3', 5' cyclic monophosphate (cGMP). This is synthesized from guanosine triphosphate (GTP) in a reaction catalysed by guanylate cyclase (GC). The structures are illustrated in Fig. 1.2.

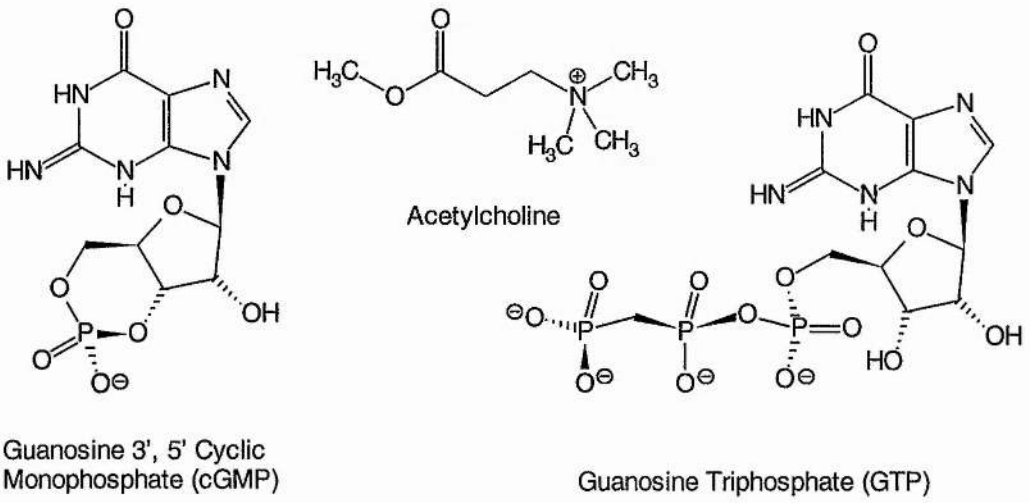

Fig. 1.2 Structures of important species in the process of smooth muscle relaxation: GTP and cGMP and acetylcholine.

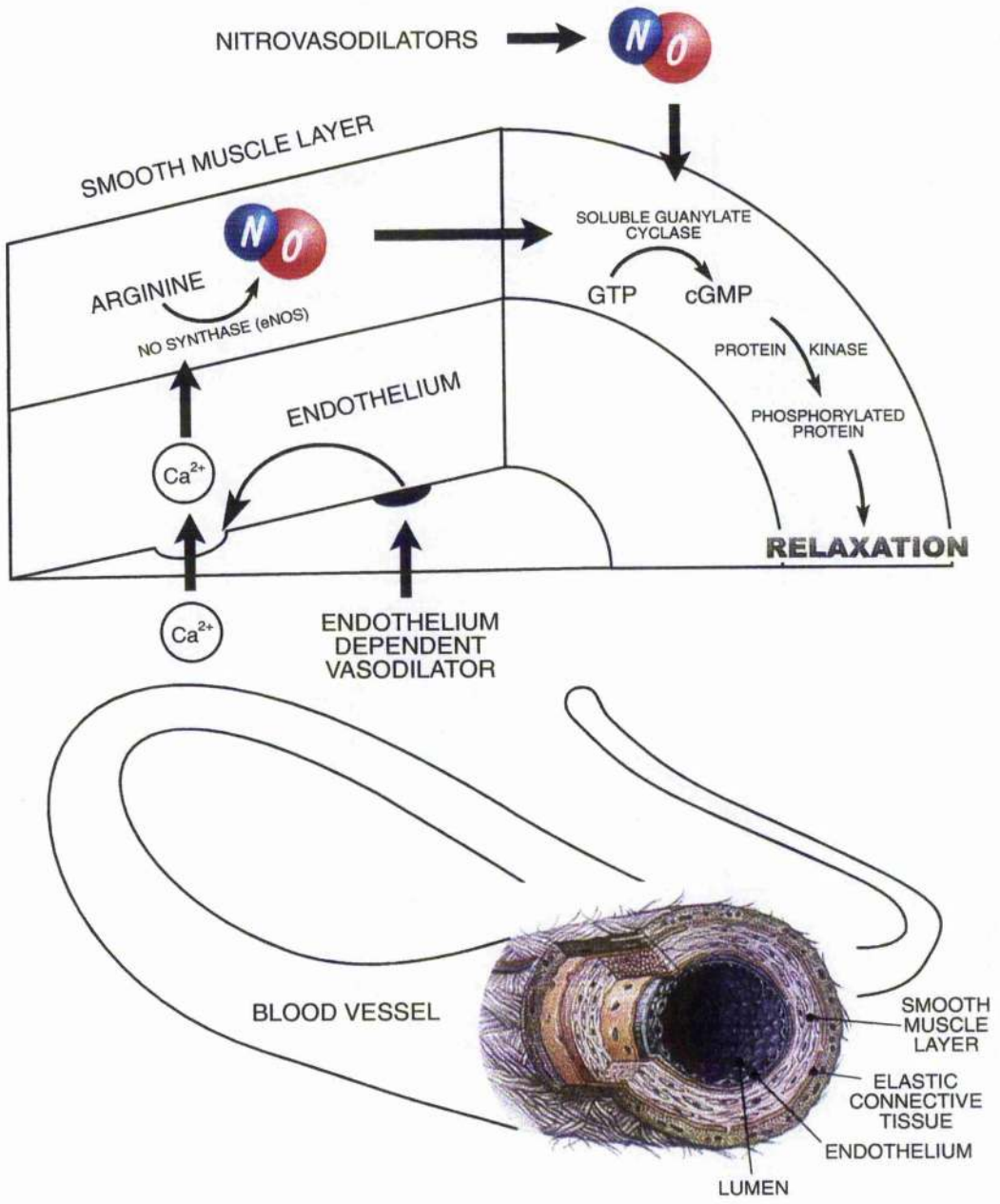

Fig. 1.3 Schematic diagram illustrating the role of NO in smooth muscle relaxation.

Furchgott and Zawadzki showed that injections of acetylcholine (Fig. 1.2) lower blood pressure by relaxing VSM *in vivo*.[9] Thus acetylcholine is a vasodilator. However they also showed, in working with sections of aorta *ex vivo*, that it is necessary to preserve the endothelial layer to observe the vasodilatory effect. Hence acetylcholine acts in the endothelium to produce a vasodilatory substance which diffuses to the outer layers of

the artery causing the VSM to relax. The unknown substance was dubbed the endothelium-derived relaxing factor or EDRF.

Furchgott suggested that NO was the EDRF based on the observation that certain NO-containing compounds like glyceryl trinitrate, sodium nitroprusside and Roussin's Black Salt (RBS) illustrated in Fig. 1.4 activated guanylate cyclase *in vitro*. Moncada *et al.* and Ignarro independently ratified these results.

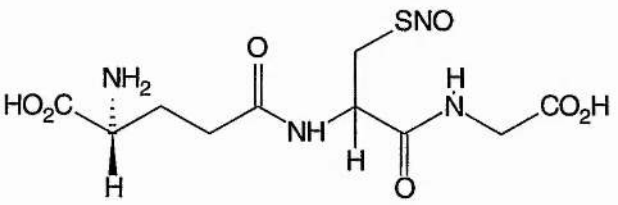

S-nitrosoglutathione (GSNO)

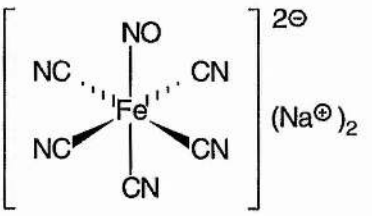

Sodium nitroprusside (SNP)

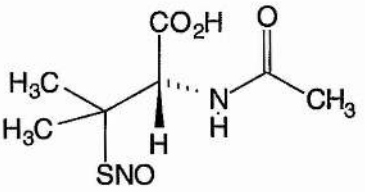

S-nitroso-*N*-acetyl-DL-penicillamine (SNAP)

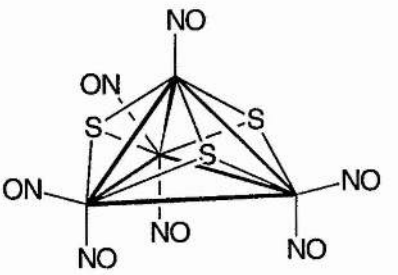

Roussin's Black Salt, $Na[Fe_4(NO_7)S_3]$

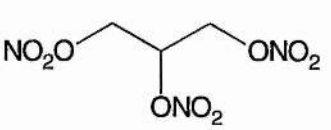

Glyceryl trinitrate (GTN)

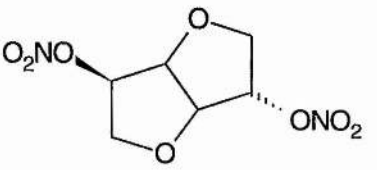

Isosorbide dinitrate

Fig. 1.4 Structures of existing NO donor drugs.

1.1.2.2 Activation of guanylate cyclase by NO

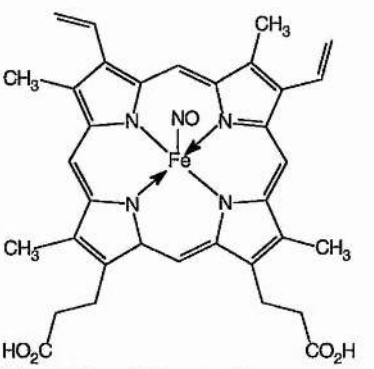

Fig. 1.5 Nitroso-haem unit.

In 1978 Craven and DeRubertis[10] showed that the responsiveness of purified soluble guanylate cyclase (sGC) to NO, nitrite, nitroprusside and *N*-methyl-*N'*-nitro-*N*-nitrosoguanidine (MNNG) could be restored by the addition of low concentrations of free haematin, haemoglobin, methaemoglobin or catalase. However, high concentrations proved to be inhibitory. Furthermore, these responses were markedly increased by the presence of a $1e^-$ reducing agent such as ascorbate, cysteine, dithiothreitol, or glutathione. This had the result of keeping the haem-bound iron in ferrous form and favouring the formation of paramagnetic nitrosyl•haem complexes from the activating species. Addition of preformed nitrosyl haemoglobin increased the activity of the purified enzyme 10–100 fold over the basal depending on the metal cofactor. These results led to the obvious conclusion that the paramagnetic nitrosyl•haem complex (Fig. 1.5) was required for the activation of guanylate cyclase.

1.1.2.3 The role of NO in platelet aggregation

Nitric oxide also plays a role in the process of platelet aggregation. More specifically, NO inhibits this process. The formation of thrombi involves the binding together of blood platelets which fasten to sites where endothelial cells have been removed and the NO used in this process is derived from the endothelial cells (Fig. 1.6). The anti-platelet aggregatory effects of NO are synergistic with that of prostacyclin (or prostaglandin I_2, PGI_2) which is also synthesised in the endothelium. Thrombus formation can result in a myocardial infarct *via* formation in sites where scar tissue replaces normal cardiac muscle. They may also form where arteries have become coated with atherosclerotic plaque. The administration of NO donor drugs, such as

those already mentioned and others based on thionitrites, *e.g.* *S*-nitroso-*N*-acetyl-DL-penicillamine (SNAP) and *S*-nitrosoglutathione (GSNO) illustrated in Fig. 1.4, will prevent platelet aggregation.

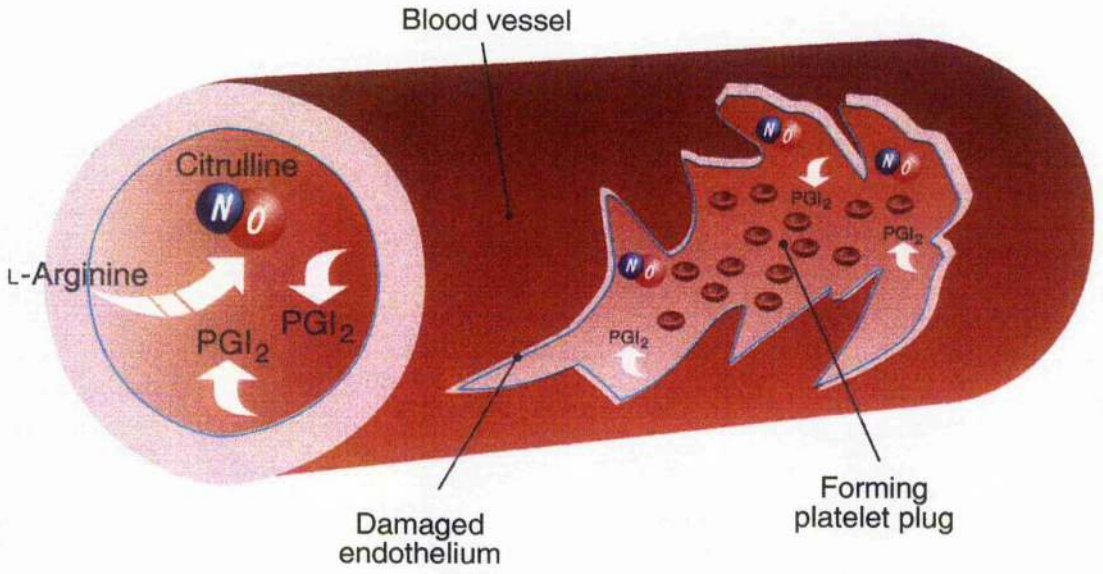

Fig. 1.6 Schematic diagram illustrating the role of NO in platelet aggregation.

1.1.2.4 The role of NO in the immune system

The rate of production of NO will be increased in response to pathological stimuli due to the inducible form of NO synthase, iNOS. The activated immune system also produces reactive oxygen species (ROS), including superoxide, which react with nitric oxide to produce reactive nitrogen species (RNS). The main reactive species produced from the reaction of nitric oxide with superoxide is peroxynitrite which subsequently isomerises to benign nitrate. Hence high levels of nitrate are found in patients with gastroenteritis. The reactive species are collectively responsible for the destruction of pathogens such as *Leishmania*, *Mycobacterium tuberculosis*, malaria parasites, fungi which are toxic to tumours and certain host cells.

1.1.2.5 The role of NO in the nervous system

NO is known to be responsible for the increased cGMP levels after stimulation of nerve cells in the central nervous system (CNS). In the peripheral autonomic nervous system, which controls involuntary body functions, NO induces smooth muscle relaxation in non-adrenergic, non-cholinergic (NANC) nerves. NO, or NO-containing compounds at least, are now believed to be responsible for neurotransmission due to the finding that NANC nerve induced smooth muscle relaxation can be prevented by the use of NO-synthase inhibitors. NO is involved with the development of the male penile erection as the use of NO-synthase inhibitors can prevent relaxation of the smooth muscle in the *corpus cavernosum*. This is a topical issue as Viagra®, Pfizer's recently launched treatment for erectile dysfunction (ED) shown in Fig. 1.7 has already become the fastest selling prescription drug in the USA to date.

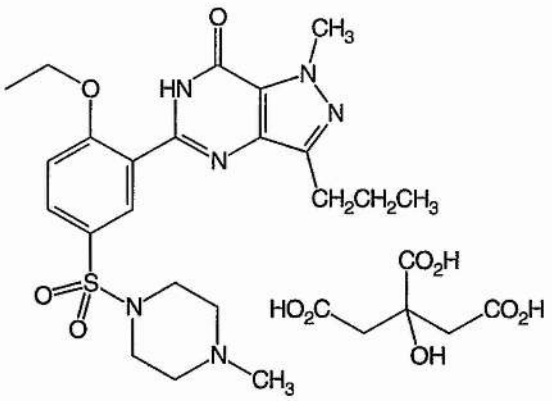

1-[[3-(6,7-dihydro-1-methyl-7-oxo-3-propyl-1H-pyrazolo [4,3-d]pyrimidin-5-yl)-4-ethoxyphenyl]sulfonyl]-4-methylpiperazine citrate

Fig. 1.7 The structural formula and IUPAC name of Viagra® (sildenafil citrate).

Sildenafil has no direct relaxant effect on isolated human *corpus cavernosum*, but enhances the effect of NO by inhibiting phosphodiesterase type 5 (PDE5), which is responsible for degradation of cGMP. When sexual stimulation causes local release of NO, inhibition of PDE5 by sildenafil causes increased levels of cGMP in the *corpus cavernosum*, resulting in smooth muscle relaxation and inflow of blood. NO has been

proposed to be a 'retrograde messenger' by feeding back to the pre-synaptic neuron[11,12] thus prompting it to increase its output of neurotransmitters (Fig. 1.8).

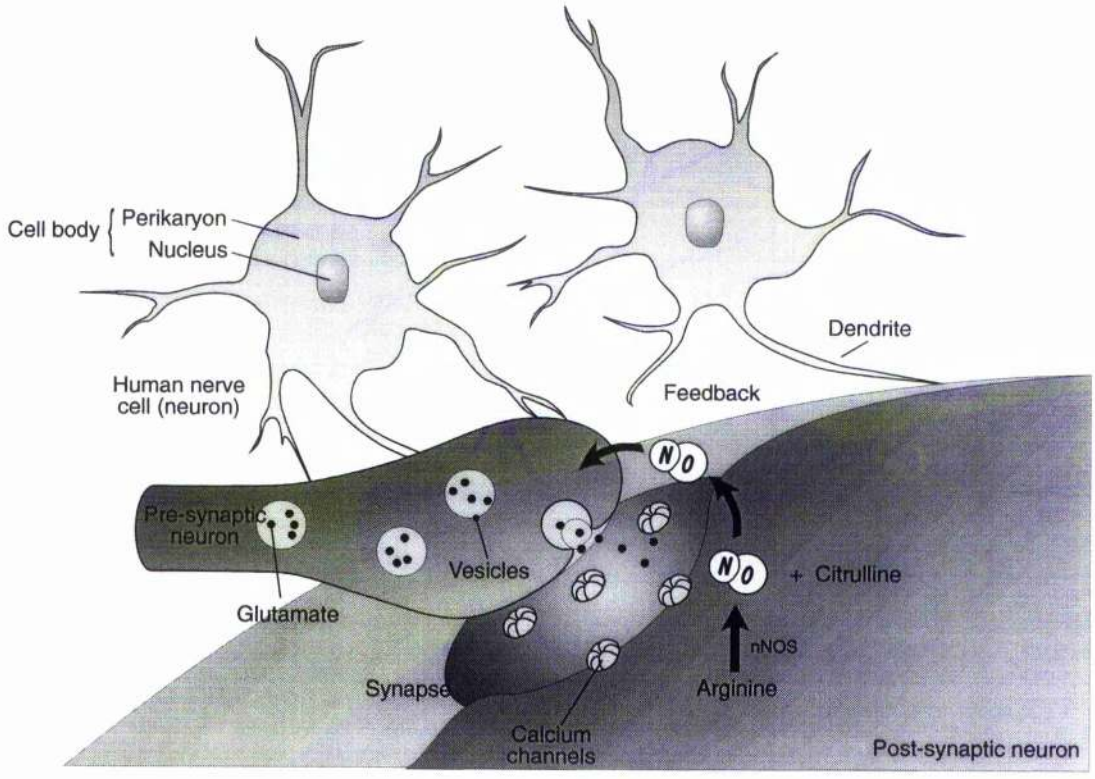

Fig. 1.8 Schematic diagram illustrating the role of NO in neurotransmission.

1.1.2.6 Biosynthesis of NO by the oxidation of L-arginine

Nitric oxide is synthesized as required *in vivo* by the oxidation of the amino acid L-arginine and the reaction is catalysed by NO-synthase (NOS). The product of the reaction is citrulline which is reconverted to L-arginine *via* the urea cycle. Some analogues of L-arginine are effective NOS inhibitors (Fig 1.9). There are at least three NO-synthases which catalyse NO production in a variety of different tissue types: endothelial (eNOS), neuronal (nNOS) and macrophage (inducible, or iNOS). They are invariably large, complex proteins with oxidative and reductive portions possessing features in common with cytochrome P450 reductase. The mechanism of this oxidation process[13] involves a hydroxylation to N^{ω}-hydroxy-L-arginine (Scheme 1.1).

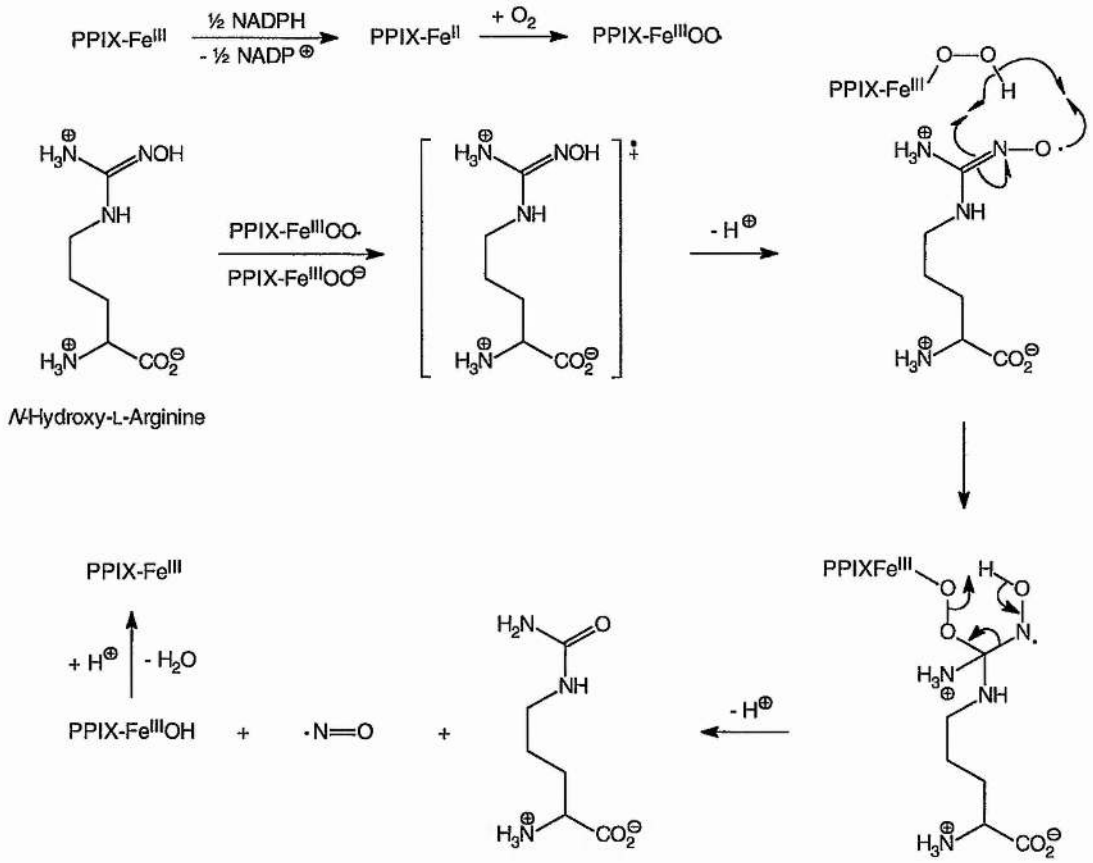

Scheme 1.1

This oxidation process requires biopterin, NADPH and oxygen.[14] The presence of the superoxide dismutase enzyme (SOD) enhances the biological activity of NO (almost doubling its half life *in vivo*) which suggests that superoxide is responsible for the inactivation of NO in tissues. Defects in the L-arginine–NO system are responsible for hypertension (high blood pressure) and diabetes.

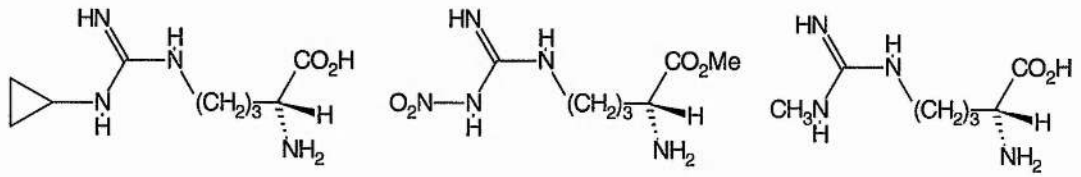

Fig. 1.9 Some inhibitors of NO synthase.

1.2 The *in vitro* and *in vivo* chemistry of peroxynitrite

1.2.1 Notes on the nomenclature used

The systematic names for the species ONOOH and the conjugate base $ONOO^-$ are hydrogen oxoperoxonitrate and oxoperoxonitrate(1–) respectively. The literature convention is to use peroxynitrite as a generic term for the sum of the concentrations of both species as well as the conjugate base itself. Where it is necessary to refer to the protonated form individually, peroxynitrous acid is used. In the body of the discussion, this convention has been adopted. However, I.U.P.A.C nomenclature has been retained in the experimental sections consistent with *J. Chem. Soc.* convention. It should be noted that the terms peroxonitrite and pernitrite have been used in older and particularly inorganic literature in place of peroxynitrite.

1.2.2 *In vitro* chemistry

The chemistry of peroxynitrite has been comprehensively reviewed by Edwards and Plumb[15] in 1994 and Pryor and Squadrito[16] in 1995. Peroxynitrous acid was first prepared by Baeyer and Villiger[17] as an unknown, unstable oxidising species formed during the oxidation of acidified aqueous solutions of nitrites to nitrates using H_2O_2. In these early studies, it was thought[18] to be HNO_4 (presumably peroxynitric acid, $HOONO_2$) described later for the purpose of comparison.

1.2.2.1 Syntheses of peroxynitrite

The yellow peroxynitrite ion is stable for several hours in 0.1 M base (pH 12–13). It can be generated under these conditions by reaction of $O_2^{\bullet-}$ with NO in one of the few examples of a radical–radical coupling of superoxide.[19] Papée and Petriconi[20] were the first to report that peroxynitrite could be formed by irradiation of nitrate solutions with

UV light. However, three alternative preparations offer greater convenience; the choice of synthetic procedure being influenced by the available equipment and the intended application. The method of Leis *et al.*,[21] employed in this study, is the simplest and exploits the strong nucleophilicity of HOO^- against the nitroso group in alkyl nitrites of average reactivity, such as 1-methoxy- or 1-ethoxy-2-nitrosooxy-ethane; *tert*-butyl nitrite does not react as quickly or as cleanly. A reaction spectrum generated under similar conditions is illustrated in Fig 1.10. The characteristic features are an isosbestic point at 263 nm and λ_{max} at 300–302 nm (ε = 1670 ± 50 M^{-1} cm^{-1}). Quantitative (>97%) formation of peroxynitrite takes places in about 5 min from the point of addition of the alkyl nitrite (equimolar with the hydrogen peroxide). The second order rate constant for the reaction between 1-ethoxy-2-nitrosooxy-ethane and HOO^- was measured as 2.2 M^{-1} s^{-1}.

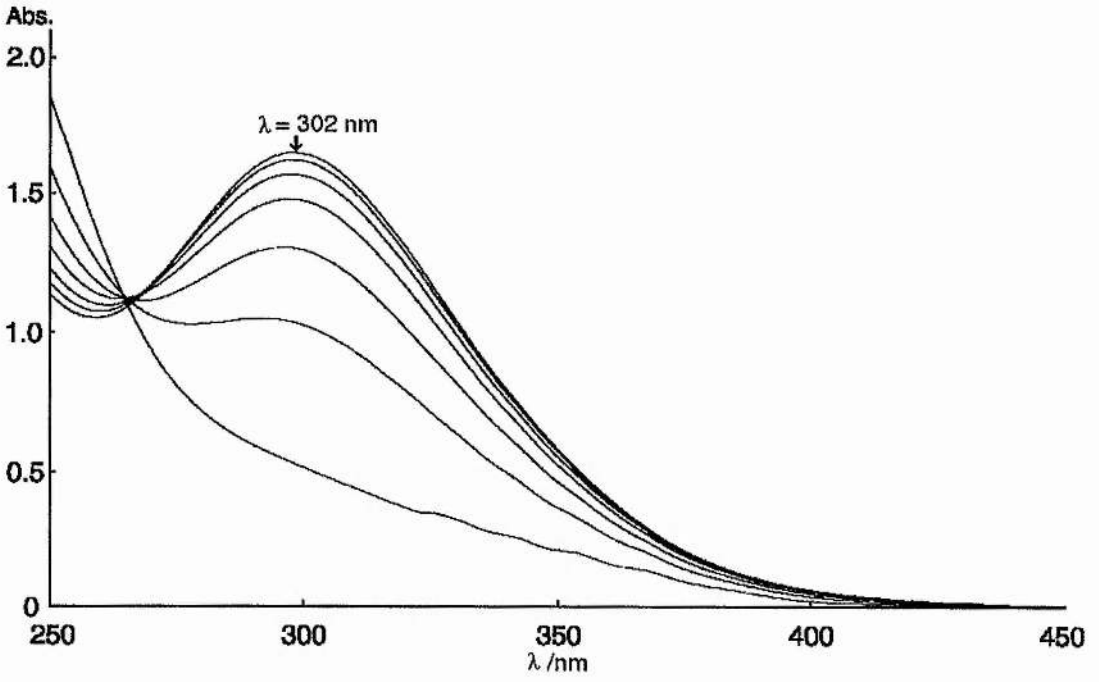

Fig. 1.10 UV-visible spectrum showing the formation of peroxynitrite from equimolar (1.01 mM) alkaline hydrogen peroxide and 1-ethoxy-2-nitrosooxy-ethane.

Perhaps the most widely used procedure employs a quenched flow reactor to mix solutions of acidified hydrogen peroxide and nitrite then rapidly increase the pH. However, peroxynitrite synthesised by this method is invariably contaminated with peroxides or nitrite. Only recently Saha *et al.*[22] studied the optimum conditions for this process and found that (*a*) ClO_4^-, NO_3^-, SO_4^- and phosphate ions have no effect on the formation and decay rates. (*b*) Cl^- enhances the rate of formation of ONOOH at low $[H_2O_2]$, and has no effect at high $[H_2O_2]$. This suggests that at relatively low $[H_2O_2]$, Cl^- competes with H_2O_2 for nitrous acidium ion to yield nitrosyl chloride, which may also nitrosate H_2O_2. (*c*) An excess of more than 10% of H_2O_2 over nitrite, or *vice versa*, is sufficient to yield *ca.* 85–90% of peroxynitrite. Prior to the availability of any accurate data on this reaction, residual peroxides were removed by passing down an MnO_2 column while nitrites and nitrates were removed by passing through anionic exchange columns and elution with formate. Yields were at best 45–50% and the slow rate of flow through the exchange columns meant that isomerisation of the anion to nitrate became a significant source of losses. The formation of peroxynitrite was shown by Anbar and Taube[23] using ^{18}O as an isotopic tracer to involve several steps shown in eqns. (4)–(6).

$$HNO_2 + H^{\oplus} \rightleftharpoons H_2NO_2^{\oplus} \quad (4)$$

$$H_2NO_2^{\oplus} \rightleftharpoons NO^{\oplus} + H_2O \quad (5)$$

$$NO^{\oplus} + H_2O_2 \longrightarrow HOONO + H^{\oplus} \quad (6)$$

The third procedure, first reported by Gleu and Roell[24] involves the reaction of ozone with azide ion and has been subsequently reexamined by Pryor *et al.*[25] A speculative mechanism for this process is illustrated in Scheme 1.2.

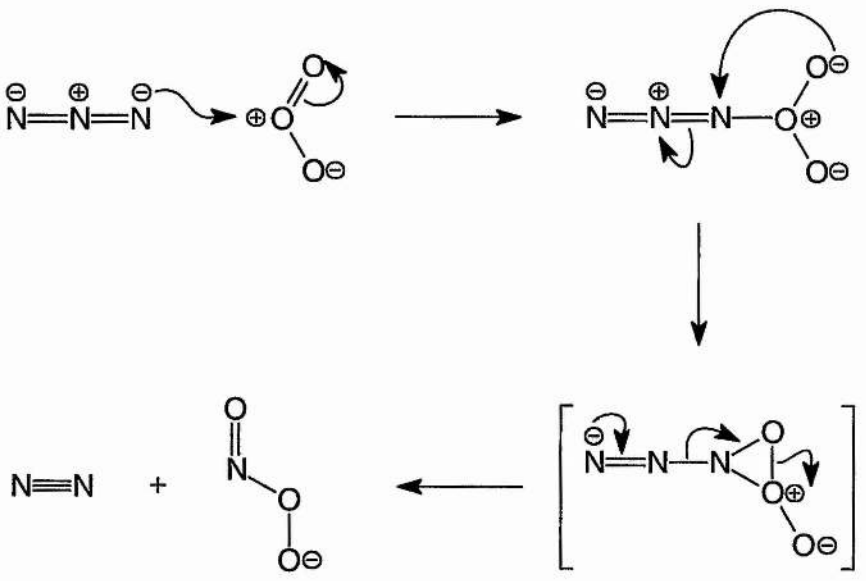

Scheme 1.2

The kinetics of decomposition of peroxynitrite in an excess of alkali were measured by Hughes and Nicklin[26] at 25, 30, 35, 40 and 45 °C (pH 12–13). They claimed that decomposition takes place through the protonated form, ONOOH and not *via* homolysis into hydroxyl radical and nitrogen dioxide radical followed by recombination as suggested by Halfpenny and Robinson.[27] $\Delta H^{\ddagger}$ was found to be 18 ± 1 kcal mol^{-1} (52.3 kJ mol^{-1}) and $\Delta S^{\ddagger}$ to be 3 ± 2 cal mol^{-1} K^{-1} (26 J K^{-1} mol^{-1}). The corresponding kinetics at 1 °C ± 1 °C (pH 4–9) were determined by Keith and Powell.[28] The rate law is shown in Scheme 1.3. The pK_a was measured to be 7.42 ± 0.06 at 37 °C.

$$k = k_{HA}\frac{[H^+]}{[H^+] + K_a}$$

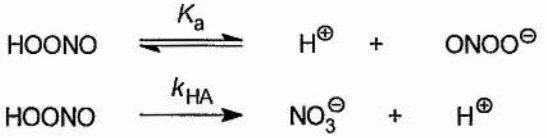

Scheme 1.3

When stored frozen at – 20 °C, peroxynitrite solutions decompose at a rate of about 1.7% per day and should be used within 2–4 weeks. For short-term storage of about 1 week or less, these solutions can be stored at refrigerator temperatures (*ca.* 3–5 °C) where $t_{½}$ is about 7 days.[29]

Reliable spectroscopic evidence exists in support of the theory that peroxynitrite may exist in either *cis* or *trans* forms. Vibrational spectroscopic data for the tetramethylammonium salt were elucidated by Bohle *et al.*[30] and are illustrated in the Table 1.2. It is apparent from a cursory examination that the peroxide bond is the weakest and the central N–O bond has substantial π character. However, an additional band observed only in the Raman spectrum correlates well with calculated values for the *trans* isomer. This is important since only the *cis* isomer can be detected in the NMR spectrum. Presumably electrostatic repulsion between the terminal oxygen atoms, one of which carries a negative charge, accounts for the *cis* isomer having the larger vibrational energy: δ(ONOO) in table 1.2.

trans *cis*

Furthermore, Beckman and co-workers[31] have succeeded in producing both conformers of potassium peroxynitrite (KOONO) in an argon matrix containing potassium nitrate at 13 K by means of *in situ* photolysis with an ArF excimer laser at 193 nm. Photoconversion between the *cis* and *trans* conformers was achieved by irradiation of the matrix with a laser at varied wavelengths. Identification of the absorption maxima (approx. 325 and 375 nm for *cis* and *trans* KOONO, respectively)

were determined with reference to the relative intensities of IR absorption lines observed for each species at each stage of photolysis.

Table 1.2 Observed and calculated vibrational modes for peroxynitrite.

		observed ν_{max}/cm^{-1}		calculated ν_{max}/cm^{-1}	
mode	isomer	IR	Raman	$O^{14}NOO^-$	$O^{15}NOO^-$
ν(N=O)	*trans*	1496 (n/a)	1483 (1448)	1488	1460
ν(N–O)	*trans*	1224 (1199)	(n/a)	1221	1198
η(OO)	*trans*	932 (927)	955 (945)	947	947
δ(ONOO)	*cis*	809 (797)	813 (803)	847	846
δ(ONOO)	*trans*	(n/a)	645 (635)	663	661

1.2.2.2 Comparison with peroxynitric acid ($HOONO_2$)

The chemistry of peroxynitric acid ($HOONO_2$) has been studied by Appelman and Gosztola.[32] It may be prepared in aqueous solution by the reaction of HNO_2 with an excess of H_2O_2 at or below 0 °C. In contrast with peroxynitrite it is stable in acid solution ($t_{½}$ *ca.* 30 min) but undergoes fast decomposition in alkaline solution. Like peroxynitrite it is a potent oxidising agent producing nitrite ion and dioxygen on decomposition. A sharp chemical shift of δ_N – 28.3 ppm referenced to $H^{15}NO_3$ (~ 0.25 M) was reported which corresponds to δ_N 344.6 ppm relative to the chemical shift of $H^{15}NO_3$ (~ 2.3 M) in this work (referenced to liquid ammonia at 25 °C). Appelman and Gosztola proposed a speculative mechanism shown in eqns. (7)–(10) to account for the formation of peroxynitric acid. This mechanism involves the formation of peroxynitrite and its subsequent decomposition into $HO^\bullet$ and $NO_2^\bullet$.

$$HNO_2 + H_2O_2 \longrightarrow HOONO + H_2O \qquad (7)$$

$$HOONO \rightleftharpoons \cdot OH + \cdot NO_2 \quad (8)$$

$$\cdot OH + H_2O_2 \longrightarrow \cdot HO_2 + H_2O \quad (9)$$

$$\cdot NO_2 + \cdot HO_2 \rightleftharpoons HOONO_2 \quad (10)$$

and these reactions would compete with eqns. (11)–(14).

$$HOONO \longrightarrow H^{\oplus} + NO_3^{\ominus} \quad (11)$$

$$\cdot OH + HNO_2 \longrightarrow \cdot NO_2 + H_2O \quad (12)$$

$$2HO_2\cdot \longrightarrow H_2O_2 + O_2 \quad (13)$$

$$2NO_2\cdot + H_2O \longrightarrow HNO_2 + H^{\oplus} + NO_3^{\ominus} \quad (14)$$

1.2.3 *In vivo* chemistry

In a landmark paper published in 1990, Beckman *et al.*[33] proposed that peroxynitrite may be formed by mammalian immune systems through the reaction of endogenously produced nitric oxide and superoxide at the diffusion-controlled limit (Scheme 1.4).

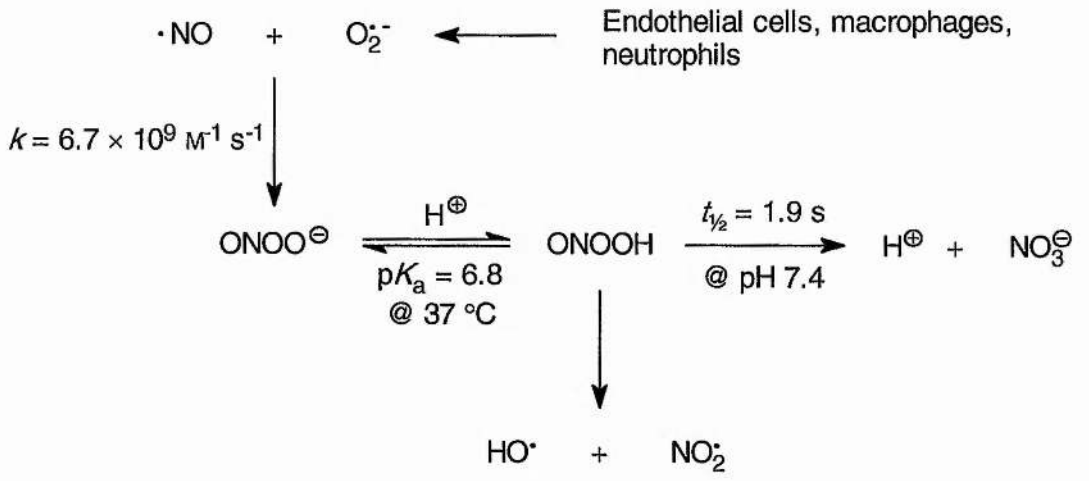

Scheme 1.4

That proposal (which has subsequently received 2,100 citations) spawned a great deal of research interest resulting in an average of over 80 publications per year covering chemistry, biochemistry and physiology. As mentioned earlier, NO is known to be

produced enzymatically in endothelial cells, neutrophils and macrophages by Ca^{2+}-activated NADPH oxidation of L-arginine[34] while superoxide is a reactive oxygen species (ROS) formed during normal cellular metabolism.[35] Peroxynitrite-induced pathogenesis has been implicated in a variety of inflammatory tissue disorders[36–40] such as atherosclerosis,[41,42] sepsis, cerebral reperfusion injury (ischaemic stroke) and neurological diseases characterised by the progressive onset of dementia including Huntington's, Alzheimer's and Parkinson's diseases and AIDS.[43] It also contributes to the microbicidal activity of phagocytes,[44] will oxidise thiols, iron-sulfur centres, DNA and nitrate tyrosine residues in proteins, inactivating them towards phosphorylation.[45,46] Although other radical mechanisms for *in vivo* tyrosine nitration have been proposed,[47] casting doubt on its specificity as a marker for peroxynitrite, it is nevertheless widely accepted. 3-Nitro-L-tyrosine has also been discovered in the brains of multiple sclerosis victims.[48] Peroxynitrite has also been shown to be a vascular smooth muscle relaxing agent and a platelet aggregation inhibitor.

1.2.3.1 Pathological implications of tyrosine nitration

The phosphorylation of protein-bound tyrosine residues is associated with many important physiological processes, despite the fact that phosphorylation of serine and threonine residues may account for 99.95% of such reactions. Examples include evidence that tyrosine-specific protein kinases (TSPK's) are coded for by oncogenes (responsible for triggering the transformation of normal cells to tumour cells) and are involved with epidermal growth factor (EGF) and platelet-derived growth factors (PDGF). These are mitogenic polypeptides which bind to receptors in cell membranes and stimulate cell division (mitosis). This strongly suggests that at least one pathway of cell growth involves tyrosine phosphorylation. The process is catalysed by protein kinases in the forward direction (transfer of $-PO_3^{2-}$, from ATP to the hydroxyl group)

and protein phosphatases in the reverse direction (hydrolysis of the phosphorylated hydroxyl group). The net effect is to change the charge density at the site of phosphorylation which triggers subtle reorientations of the local protein structure. This, in turn, may then trigger a cascade of reorientations throughout other regions or through the entire molecule; its activity being modified, but not entirely lost. The introduction of a nitro group at the 3-position of tyrosine may have two effects; the electron-withdrawing ability sufficiently reduces the nucleophilic character of the tyrosine hydroxyl to prevent attack on the terminal phosphoryl group on ATP (illustrated in Scheme 1.5) or the altered electron-density profile of the nitrated tyrosine residue causes deleterious conformational changes to the protein resulting in a loss of activity.

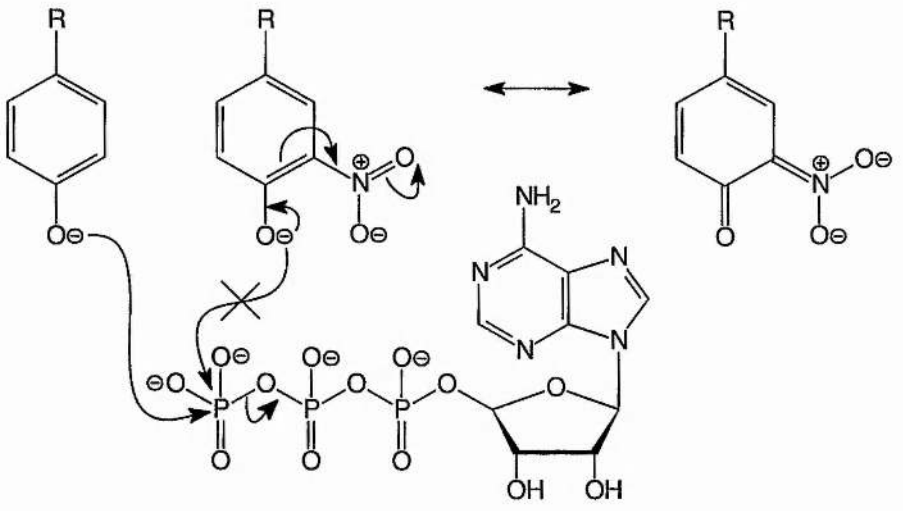

Scheme 1.5

1.2.3.2 Possible role of peroxynitrite in the oxidation of L-tyrosine to L-DOPA in melanogenesis

L-Tyrosine and L-DOPA (3,4-dihydroxy-L-phenylalanine) can be oxidised enzymatically by tyrosinases and copper oxidases to dopaquinone which may then

undergo a series of complex spontaneous reactions involving cyclisation and oxidative polymerisation to form mammalian skin pigments classed as melanins (Scheme 1.6). The process[49] is termed melanogenesis. The involvement of reactive oxygen species (ROS), specifically singlet oxygen ($^1O_2$) and the superoxide radical anion ($O_2^{\bullet -}$) in skin sensitisation and tanning has been demonstrated.[50] It seems reasonable to speculate that peroxynitrite may at least be partially involved in this oxidative process as it is formed where there exists a source of superoxide in addition to NO. It is now well established that peroxynitrite is a source of hydroxyl radicals and in the presence of tyrosine can react *via* a radical pathway to form DOPA[51] in addition to small quantities of radical combination products, of those, the major being *o,o'*-dityrosine[52,53] which is intensely fluorescent.[54,55]

Peroxynitrite has already been implicated in a variety of inflammatory conditions and is likely also to be involved in the pathogenesis of sunburn erythema. In support of this theory, a recent paper[56] demonstrated that on skin exposure to UV-B radiation, endothelial nitric oxide synthase (eNOS) and xanthine oxidase (XO) were activated to release NO and produce peroxynitrite. Other recent developments[57] show that the neurohormone, melatonin, produced in the pineal gland is a scavenger of peroxynitrite. Melatonin (Fig 1.11) regulates the circadian rhythm or 'body clock' and is currently available as a treatment for sleep disorders such as insomnia and 'jet-lag'.

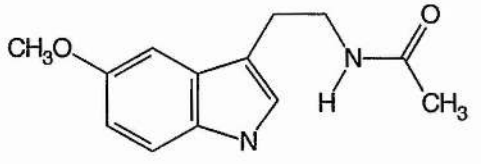

Fig. 1.11 Structure of melatonin

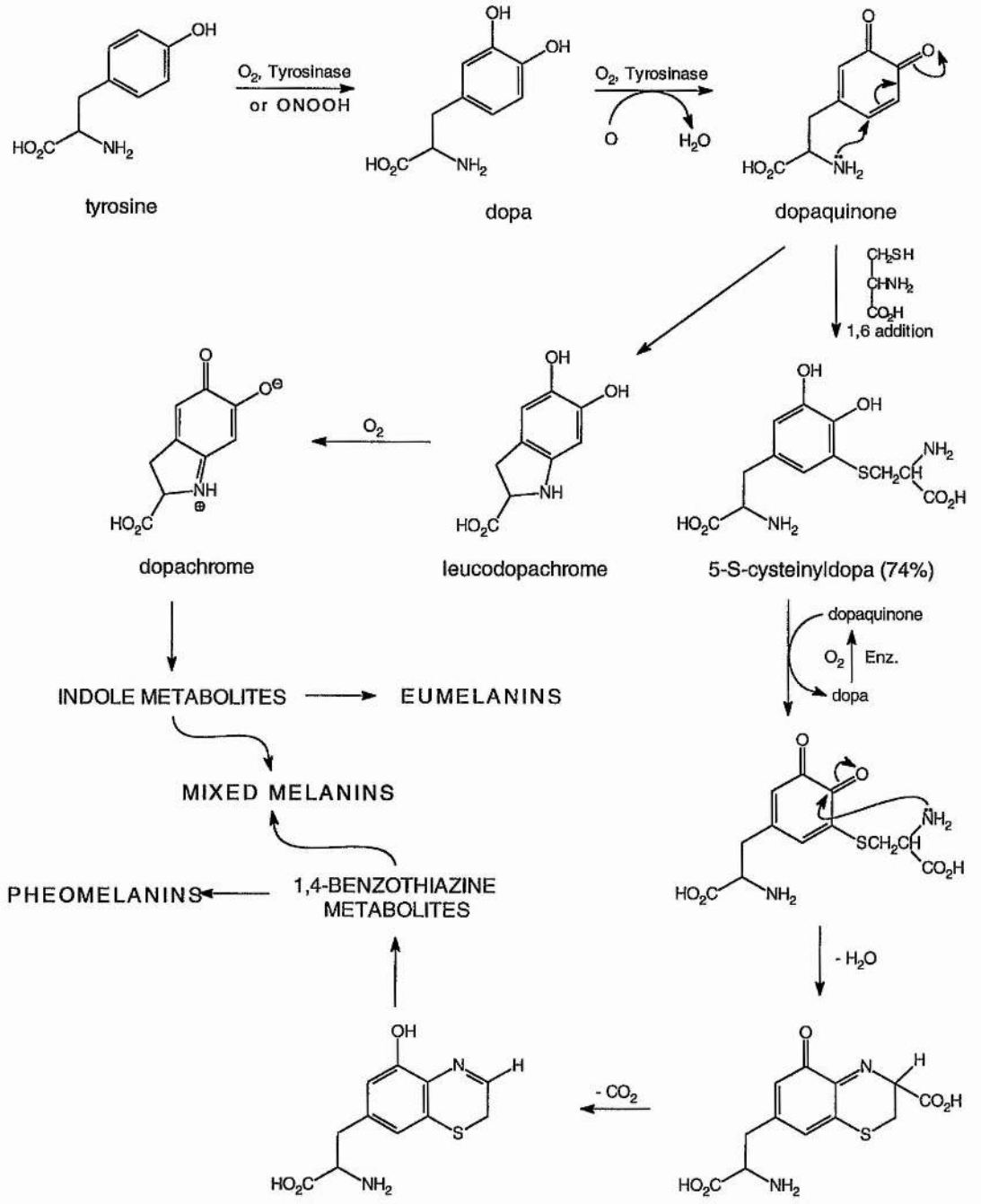

Scheme 1.6

1.3 The reactivity of peroxynitrite

Beckman *et al.*[33] have demonstrated that the oxidation product yield from peroxynitrite when reacted with deoxyribose and DMSO decreased at higher pH. This, they commented, was curious because they allowed sufficient time (8 half lives at pH

9.0) for the peroxynitrite anion to become protonated and decompose as peroxynitrous acid. The rationalisation they proposed was that peroxynitrous acid decays by two pathways; direct rearrangement of *cis* peroxynitrite by attack of the terminal oxygen atom on the nitrogen to form nitrate without forming strong oxidants and the homolytic fission of the *trans* form to form nitrogen dioxide and hydroxyl radicals.

They also proposed that the transition state for internal rearrangement may have a shorter half life, due to a lower activation energy. Therefore it may be less likely to be deactivated due to the loss of a proton. Another theory is that the energy required to break the O–OH bond is dissipated more readily throughout the molecule by loss of a proton.

1.3.1 Radical reactivity - evidence for and against the cage mechanism

One of the most significant hypotheses concerning the oxidative chemistry of peroxynitrite is that it may undergo homolytic fission of the O–O bond to form hydroxyl radical and nitrogen dioxide radical. Initially, a solvent cage surrounds the so-called 'geminate' pair of radicals. The radicals may either diffuse from the confines of the cage and undergo reaction or recombine within the cage. When the product reforms, the process is known as cage return. The unpaired electron density of $NO_2^{\bullet}$ resides partly on the central nitrogen atom and partly on the terminal oxygen atoms. Thus, $NO_2^{\bullet}$ is an ambident radical illustrated in eqn. (15). This important characteristic has the implication that it may recombine with hydroxyl radical in two ways, either to form peroxynitrite or nitrate.

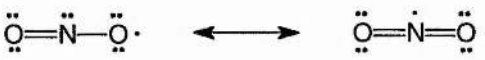

(15)

The cage mechanism explains a large number of the mysterious subtleties encountered in peroxynitrite chemistry. For instance a large amount of cage-return accounts for the decomposition to nitrate having a low entropy of activation. This is the case because a large positive entropy of activation is indicative of a transition-state complex which is less geometrically constrained than one with a lower value of $\Delta S^{\ddagger}$. Therefore, by definition, caged radicals are confined to a greater extent than free radicals and so formation of nitrate by recombination within the cage will have a lower entropy of activation than nitrate formed by combination of free radicals. It is also observed that hydroxyl radical scavengers such as ascorbic acid do not exclusively inhibit oxidation of thiols by peroxynitrite. The cage mechanism provides a ready explanation of this finding since cage return and diffusion are fast processes occurring near the diffusion-controlled limit and scavengers cannot trap 100% of the radicals formed as the rates of these reactions are too slow.

The confining properties of the solvent molecules forming the cage are directly related to the viscosity of the solvent. Therefore the enthalpy of diffusion will be greater at higher solvent viscosity. This theory was tested by Pryor *et al.*[58] who found that increasing the viscosity of buffered solutions of peroxynitrite by introducing polyethylene glycols (PEG's) has no significant effect on the decomposition of peroxynitrite. This paper is confusing if not interpreted carefully as it seems to provide conclusive evidence against the formation of radicals in this system. In fact, it simply provides evidence against *free* radical formation during the decomposition of peroxynitrite at pHs close to its pK_a. Clearly, external agents will not influence the rate of processes occurring within the confines of the solvent cage. This observation is neither in conflict with evidence presented in this work, which indicates that formation of nitrate occurs within the cage, nor does it require the presence of an

'activated intermediate' (discussed briefly in section 1.3.2) to be invoked. Internal rearrangement of peroxynitrous acid[28] (illustrated in Scheme 1.7) provides a simple alternative explanation for this result. However, it can only partially account for the isomerisation to nitrate.

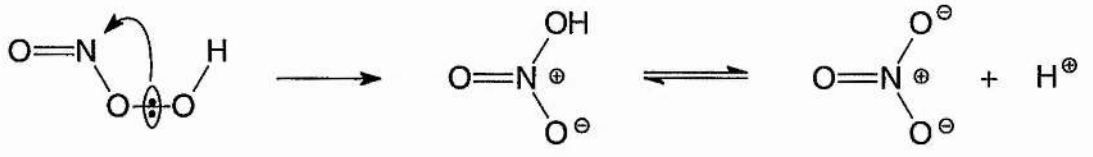

Scheme 1.7

Tsai *et al.* have made *ab initio* studies on peroxynitrite anion, peroxynitrous acid[59] and alkali metal salts of peroxynitrite.[60] They report that there is a large rotational barrier between the *cis* and *trans* isomers of peroxynitrite of approximately 24 kcal mol^{-1} because of the partial π-nature of the central N–O bond. They reported that this predicted vibrational frequencies closer to the empirical values in related alkali-peroxynitrite salt systems than HF, MP2 and all other DFT methods.

1.3.2 The 'activated intermediate': ONOOH*

In order to explain the low yield of radicals from trapping experiments carried out under physiological conditions, it has been suggested that peroxynitrite may exist in an electronically-excited form, dubbed ONOOH* and that this species has 'radical-like' reactivity. Hence an alternative nitration pathway may exist at pHs approaching 7.4. In an extensively quoted work (with over 370 citations) Koppenol *et al.*[61] claim that thermodynamic calculations preclude the formation of hydroxyl radical from ONOOH. This paper describes the activated form as a specific geometrical isomer. However this cannot be the case as all calculations by Koppenol indicate that geometrical isomer interconversion is faster than peroxynitrite decay. The calculations

were formulated around a rate determining homolysis of ONOOH (k_f) with subsequent recombination of hydroxyl and nitrogen dioxide radical to form nitrate (k_b). The Gibbs free energy was calculated from empirical activation parameters. Hence k_b was calculated from eqn. (16) to be in the range 10^{13}–10^{15} M^{-1} s^{-1}.

$$\Delta G^{\ddagger} = \Delta H^{\ddagger} - T\Delta S^{\ddagger} = -RT\ln(k_f/k_b) \tag{16}$$

Since this rate constant would be greater than the diffusion limit, then it was concluded by Koppenol that the decomposition of peroxynitrite to form hydroxyl radicals was highly unlikely. However eqn. (16) does not apply when one of the reactions is already diffusion-controlled as opposed to activation-controlled. Furthermore, although the empirical value for $\Delta H^{\ddagger}$ agreed well with the calculated value, the value for $\Delta S^{\ddagger}$ was smaller than that found for O–O bond homolysis in peroxides (3 versus 12 cal mol^{-1} K^{-1} so this was taken to be further evidence against homolysis. Evidently the lack of freedom in the transition state of peroxynitrite is indicative either of a strong structural interaction with the solvent, or simply extensive cage return of the radical pair. Co-author Pryor has discredited Koppenol's work[62] by admitting that serious mistakes were disseminated in this publication and that the most likely situation is that a rather long-lived 'sticky cage' exists which holds together the radicals. This is in accord both with the low activation enthalpy, is borne out by the observations later in this work, and also effectively invalidates the conclusions drawn from evidence previously used to support the existence of an 'activated intermediate' including the viscosity work.

1.3.3 Peroxynitrite and bicarbonate

Lymar and Hurst[63] have demonstrated that peroxynitrite reacts rapidly with CO_2 (k = 3×10^4 M^{-1} s^{-1}). Under physiological conditions, the reaction of peroxynitrite with

CO_2 is likely to be of dominating importance since bicarbonate is present in both intracellular (12 mM) and interstitial (30 mM) tissue fluids. The rate of reaction of bicarbonate with peroxynitrite in biological systems is greater than decomposition of peroxynitrite. Therefore it is likely that *in vivo* reactions will be mediated by intermediates derived from reaction with carbon dioxide rather than those derived solely from peroxynitrite. A reaction scheme to account for the reactive intermediates has been proposed by Pryor and co-workers[64–67] and is summarised in Scheme 1.8.

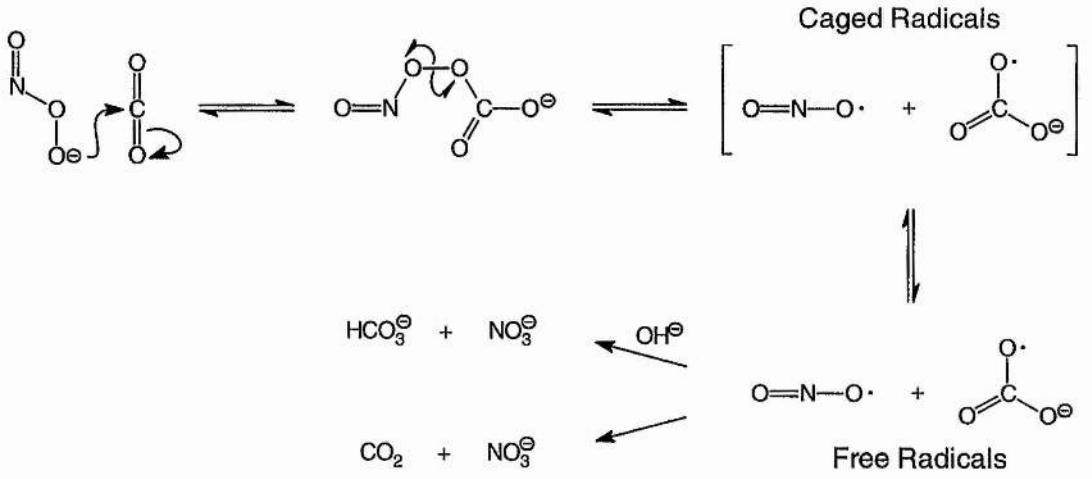

Scheme 1.8

1.4 Chemistry of the furazan 2-oxide (furoxan) ring system

The previous sections of this introduction are intended provide a background to the biochemistry of nitric oxide in the immune system and set the scene for chapters 2 and 3. What follows introduces the material in chapter 4; a study on the mechanism by which a particular class of heterocyclic compound releases NO. The fact that these two topics appear to be chemically disparate and contrasting in terms of the biochemistry provides some justification for treating them separately. However, they share the common underlying themes of both being mechanistic investigations involving the chemistry of nitrogen oxides and radiofrequency spectroscopy.

1.4.1 Notes on the nomenclature used

The 'furoxan' nomenclature is not recognised by either Chemical Abstracts or the International Union of Pure and Applied Chemistry because they are considered to be the *N*-oxides of 1,2,5-oxadiazoles. The latter are given the trivial name furazans for use in fusion nomenclature. However, following RSC journal convention and the recommendation of Gasco and Boulton,[68] main compounds will be referred to as furoxan **1**, **2**, *etc.* in the body of the discussion to save repetition of 'furazan oxide' and the formation of names containing awkward conjunctions of noun elements. I.U.P.A.C nomenclature has been retained in the experimental sections for the purpose of clarity. Accepted trivial names are used to refer to intermediate compounds mentioned in passing.

1.4.2 History

The source material for most of the discussion in this section is a comprehensive review by Gasco and Boulton.[68] The history leading up to discovery of the furoxan ring system and the subsequent elucidation of its reactivity shares similarities with that of peroxynitrite. Namely these particular aspects of the chemistry of each species have been the subject of a great deal of debate and controversy up until relatively recently. Although the earliest literature references to peroxynitrite[17] date back to the early 1900s, the first preparations of furoxans came almost half a century earlier. Kekulé[69] is now credited with the first synthesis from mercury fulminate and bromine. Although, as no means existed to determine the structure unambiguously at the time, his discovery passed unrecognised.

1.4.2.1 Structure determination

Several structures were proposed to account for the formula of the compounds prepared during the early work in the latter half of the 19th century (Fig. 1.12).

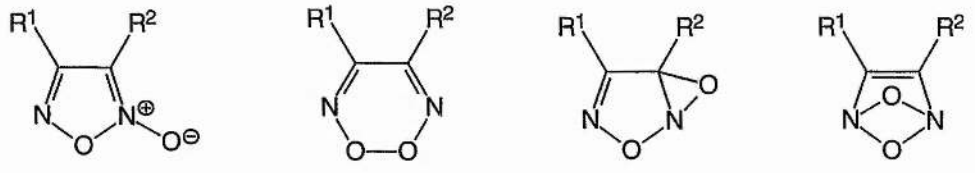

1 2 3 4

Fig. 1.12 Proposed structures for the furoxan ring system.

The correct structure, **1**, was initially proposed by Wieland,[70] though he rejected it in favour of the 2,6-dioxa-1,3-diaza-bicyclo[3.1.0]hex-3-ene structure **3** which was also independently suggested by Werner.[71] The [1,2,3,6] dioxadiazine structure, **2**, was proposed by Koreff[72] to satisfy the requirement for the symmetrical structure produced in furoxan syntheses from 1,2-dioximes (glyoximes) by oxidation and by the action of nitrogen oxides on alkenes.[73,74] However, it was eventually rejected on account of inconsistency with the stability and lack of oxidising ability of furoxans. Furthermore, **2** and the 5,6-dioxa-1,4-diaza-bicyclo[2.1.1]hex-2-ene structure **4** could not account for the existence of geometric isomerism when $R^1 \neq R^2$. The crystal structure of 3-nitro-4-phenylfuroxan,[75] a by-product of the reaction of phenyl-substituted alkenes with nitrogen oxides is illustrated in Fig. 1.13. This simple structure exhibits the general features of the furoxan ring system. Most noteworthy is the particularly long O1–N2 ring bond. The length of this bond renders it susceptible to cleavage under thermal and photochemical conditions whereupon the furoxan will undergo isomerisation.

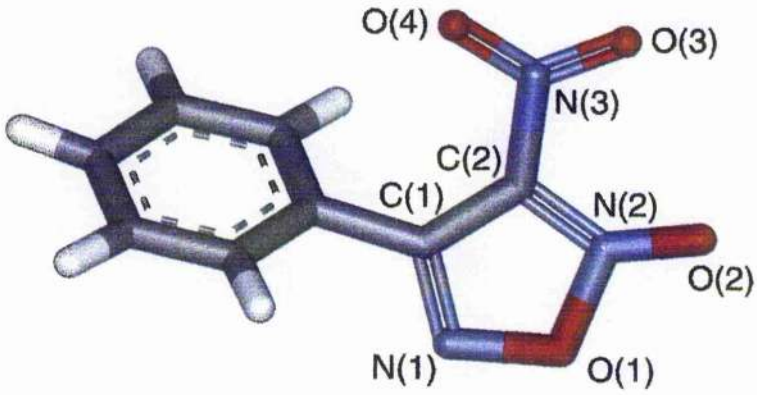

Bond	Length/pm
C(1)–C(2)	1.410
N(1)–O(1)	1.386
O(1)–N(2)	1.440
N(2)–O(2)	1.204
N(2)–C(2)	1.316

Fig. 1.13 Crystal structure of 3-nitro-4-phenylfuroxan projected onto the plane of the oxadiazole ring.

The remainder of this introduction is concerned with selected syntheses and ring reactions relevant to those aspects of furoxan chemistry utilised and investigated later in this work. Mechanisms are suggested where appropriate if they are interesting or relevant to a particular aspect of the work.

1.4.3 Preparations of furoxans

1.4.3.1 From nitrile oxides

The dimerisation of nitrile oxides is the final step in the mechanism of production of many symmetrically-substituted furoxans ($R^1 = R^2$). The reaction proceeds readily due to the thermodynamic instability of certain aliphatic or aromatic nitrile oxides and thus will occur spontaneously in neutral solutions at room temperature or with mild heating. The reaction is reversible and competes with dyotropic rearrangement[76] (simultaneous movement of two σ bonds) to the isocyanate. These processes are illustrated in Scheme 1.9.

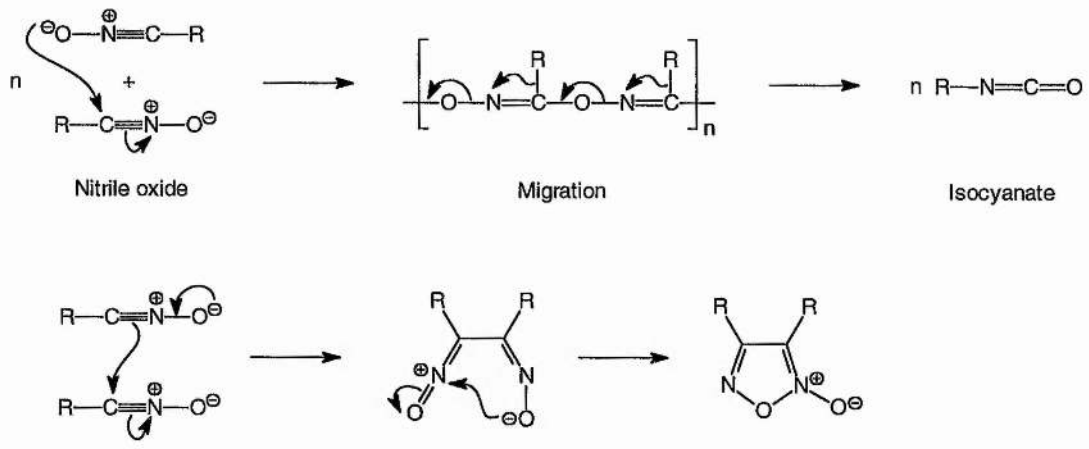

Scheme 1.9

The mechanism has been the subject of some debate with a concerted cycloaddition[77] and a two-step radical cycloaddition[78] being proposed. Second order kinetics,[79] a low solvent dependence and an entropy of activation of approximately – 80 J K^{-1} mol^{-1} are observed and are consistent with the concerted cycloaddition mechanism.[77]

1.4.3.2 From alkenes and nitrogen oxides

The action of nitrous acid on suitable arylpropene derivatives (*e.g.* anethole, cinnamaldehyde, isosafrole, *etc.*) provides a convenient synthetic route to 4-aryl substituted furoxans (Scheme 1.10). Although the mechanism has not been elucidated, the reaction can be conveniently formulated as Markovnikov addition of N_2O_3 across the double bond. Intermediate 'pseudonitrosites' and α-nitroketone oximes have been identified, although it is not known whether the nitro group supplies one or both furoxan oxygen atoms. Osawa *et al.*[80] made the interesting observation that sorbic acid (*trans*, *trans*-hexa-2,4-dienoic acid), which has been widely used as a food preservative of low toxicity, may react with sodium nitrite; also used as a food preservative in meat processing, to form 3-methylfuroxan propenoic acid *via* the nitrolic acid derivative. It appears that the strong bactericidal activity may be due to production of this furoxan derivative. If R is also a carbocation destabilising

substituent, then the reaction will not proceed. This synthetic strategy provides the most convenient route to $[^{15}N]_2$ furoxans, as $Na^{15}NO_2$ is the most cost-effective and readily available $[^{15}N]$ starting material.

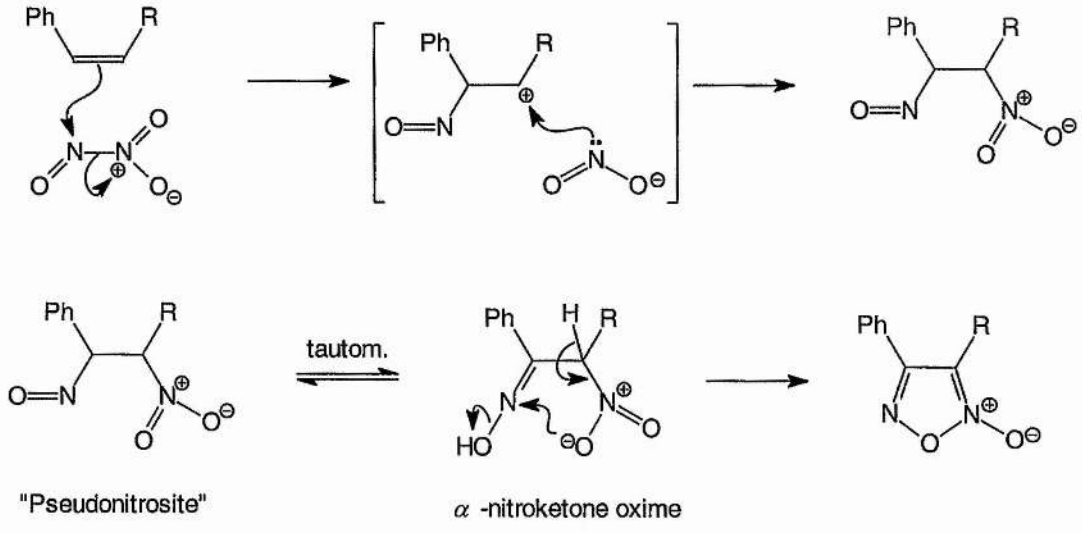

Scheme 1.10

1.4.3.3 From nitroalkanes

Primary nitro compounds also provide a synthetic route to furoxans as they form nitrile oxides on dehydration which subsequently dimerise (in the absence of a dipolarophile) in the manner previously described. Suitable dehydrating systems include acetic anhydride or sulfuric acid. However, when electron-withdrawing groups are present, to increase the acidity of the α-protons, milder systems such as $BF_3{\cdot}OEt_2/Ac_2O$ or $(CF_3CH_2)O_2/Et_3N$ may be employed. Later in this work, HNO_3/AcOH is used to convert phenylnitromethylsulfone into bis(phenylsulfonyl)furoxan.

1.4.3.4 From nitrolic acids

Aryl, alkyl and acyl nitrolic acids (1-nitroketone oximes) may yield furoxans under a variety of conditions by loss of nitrous acid: either spontaneously,[81,82] by the action of heat[83–85] or sodium bicarbonate.[86] A number of furoxan-producing transformations brought about by nitrogen oxides are thought to proceed *via* nitrolic acid intermediates (Fig. 1.14); the general requirement being that the substrate has a methylene group that may enolise or form a stabilised carbocation.

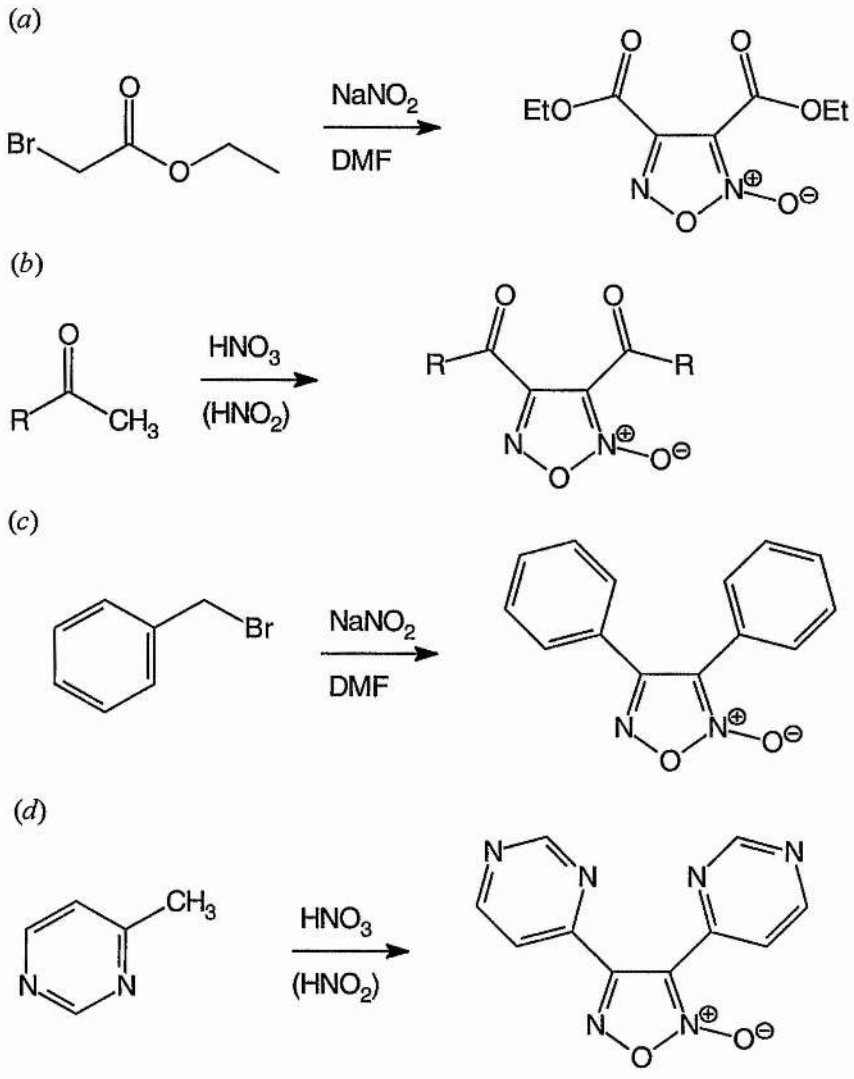

Fig. 1.14 Furoxan syntheses thought to proceed *via* nitrolic acid intermediates.

A formally correct, but speculative mechanism is suggested in Scheme 1.11, where the initial step is attack of the enol form of the substrate on a suitable carrier of NO^+. When the reagent is nitric acid this would be either nitrous acidium ion or dinitrogen trioxide. In the case of N_2O_4, a plausible nitrosating agent is the nitro-nitrito isomer: covalent nitrosyl nitrate. It is likely that the subsequent step may proceed *via* a radical mechanism, since the nitro-nitro isomer of N_2O_4 is in equilibrium with $NO_2^{\bullet}$.

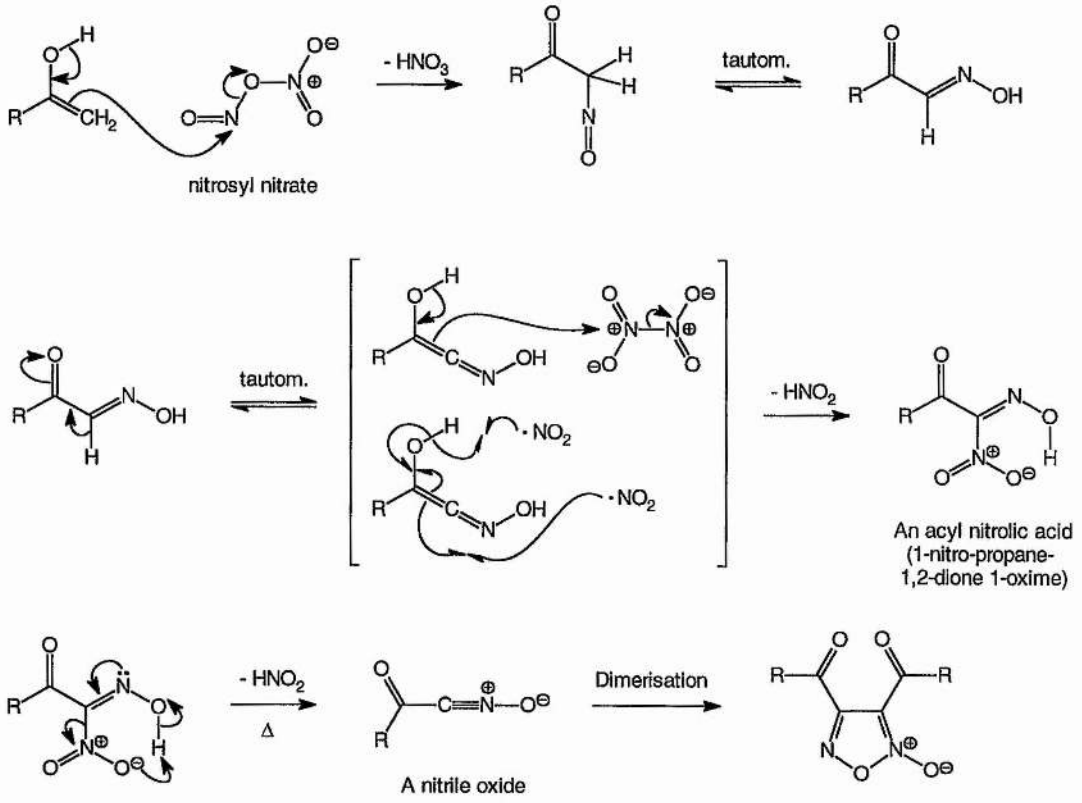

Scheme 1.11

When R = CH_3 (acetone) the nitrolic acid intermediate was identified by its IR spectrum and the nitrile oxide trapped as its 1,3-dipolar cycloadduct with dimethylacetylene dicarboxylate.

1.4.3.5 From diazo compounds and nitrosating agents

Yet another route to furoxans which involves the dimerisation of a nitrile oxide in the final step is the nitrosation of electron-deficient diazo compounds followed by loss of nitrogen. Suitable diazomethanes include the perfluoroalkyl[87] and the α-diazosulfones.[88] A speculative mechanism is illustrated in Scheme 1.12. An electron withdrawing group must be present since simple diazoalkanes do not react in this way to give furoxans.

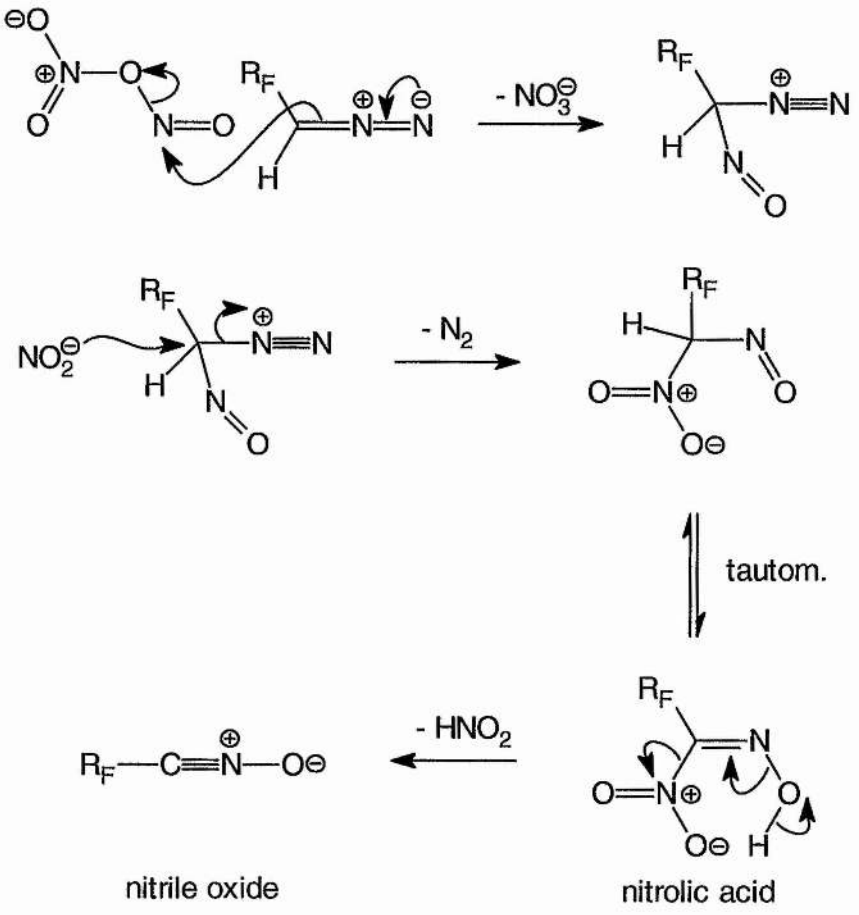

Scheme 1.12

2 ^{15}N CIDNP NMR studies on the interactions of RNS with potential biotargets

2.1 Introduction

2.1.1 Aims of this work

This subject will be discussed in the context of the mechanism and implications of the interaction of endogenously produced peroxynitrite with various forms of superoxide dismutase. Yamakura[89] has demonstrated that the nitration of tyrosine residue no. 34 in human recombinant Mn SOD is known to be responsible for inactivation of the enzyme with IC_{50} = 6 μM at 1.7 μM of Mn SOD and IC_{50} = 170 μM at 45.6 μM of Mn SOD. The work of MacMillan-Crow *et al.*[90] supports this result and shows, additionally, that only three tyrosine residues are nitrated by peroxynitrite. Their observations are consistent with previous work on chronically rejecting human kidney transplants. This is important as nitration and inactivation of Mn SOD would dramatically increase mitochondrial superoxide levels, leading to formation of more peroxynitrite in a positive feedback loop which could cause further damage to other proteins. Tyrosines 45 and 193 are surrounded by areas of positive charge (blue colour in Fig. 2.1) and glutamate residues: a feature which has been observed in other proteins to direct peroxynitrite to specific tyrosine residues.

The nitration of protein-bound tyrosine residues by peroxynitrite has been proposed by Ischiropoulos *et al.*[91] to involve the nitronium ion (NO_2^+) in a metal-ion catalysed mechanism on the bovine Cu, Zn SOD enzyme. The reasons why this mechanism must be considered in detail here are twofold. Apart from the questionable relevancy of working with the bovine enzyme (although human Cu, Zn SOD does contain no

tyrosine residues), the evidence presented in support of this highly speculative mechanism is flawed yet it has been embraced with little question by workers in this field (receiving some 380 citations). Second, a heterolytic mechanism for the cleavage of peroxynitrite seems unlikely even under these conditions given that most of the evidence in the literature points to a radical mechanism. Indeed, positively establishing this latter point forms part of the *raison d'être* for this investigation.

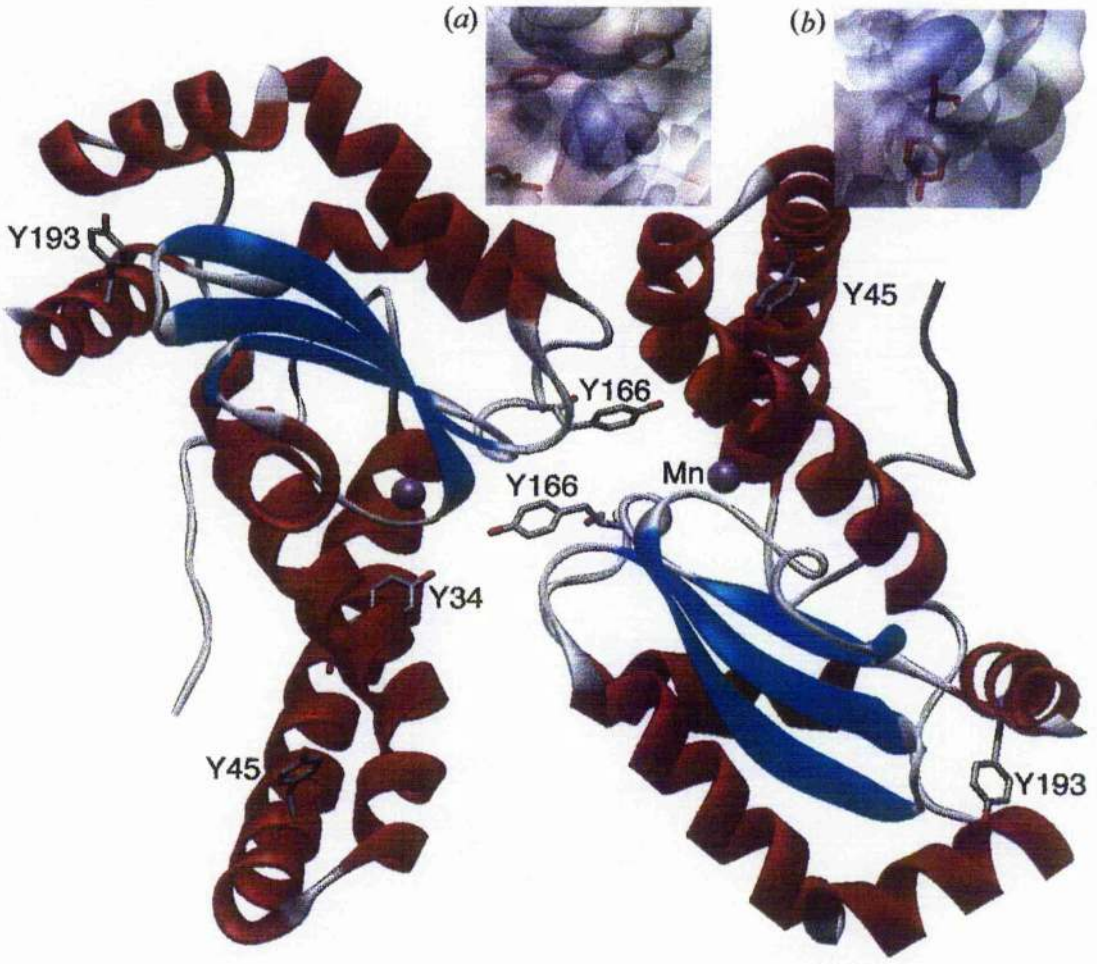

Fig. 2.1 Computer visualised image of the X-ray crystal structure of human Mn SOD homodimer with the peptide backbone represented as a ribbon. All tyrosine residues that are nitrated are labelled together with the putative dityrosine cross-link at Y166. Inset (*a*) shows the charge surface around the Mn/Y34/Y166 area and inset (*b*) around the Y193 area.

Some of the factors influencing the nature of the nitration mechanism are discussed in the next section, but the remainder of this section is confined to a critical discussion of the heterolytic mechanism proposed by Ischiropoulos *et al.*[91] Careful examination of the crystal structure shows that their schematic diagram is both inaccurate and misleading. The position of the positively charged Lys120 which attracts peroxynitrite into the hydrophobic pocket of the active site should be almost directly above the Cu ion and Arg141, Thr56 is shown to be on the wrong side of the channel and the histidine residue between and liganding both the Cu^{2+} and Zn^{2+} ions is residue 61, not 42. However, these errors are relatively trivial and are not sufficient to invalidate the proposed mechanism. Fig. 2.2 illustrates a detailed molecular model of the active site and selected other important structural features together with a modified schematic diagram. It has been constructed from accurate crystallographic data and illustrates the features described in this mechanism more clearly. Before considering the likely situation with peroxynitrite, it is sensible to review the mechanism derived by Tainer *et al.*[92] for the dismutation of superoxide radical anion to dioxygen and hydrogen peroxide (Scheme 2.1).

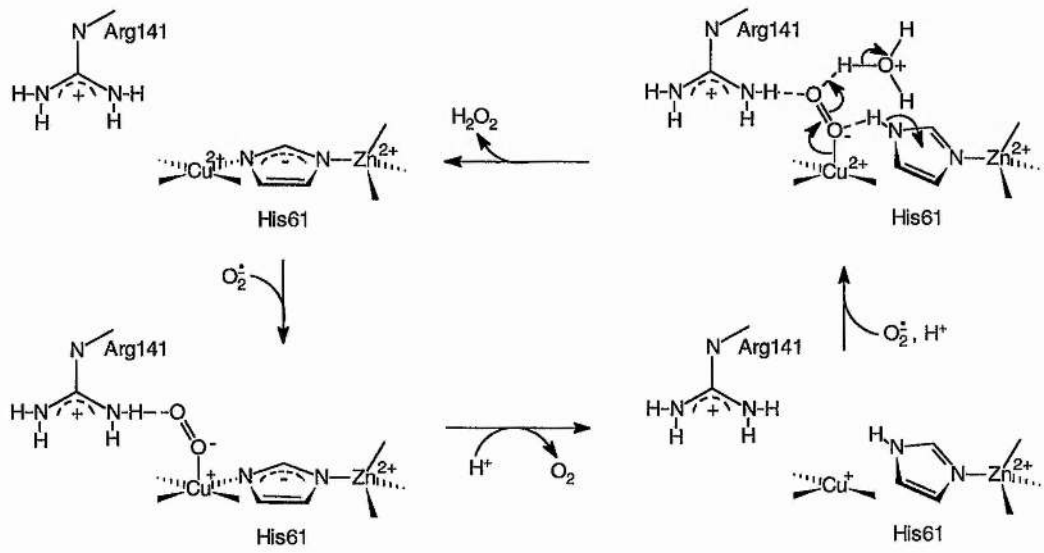

Scheme 2.1

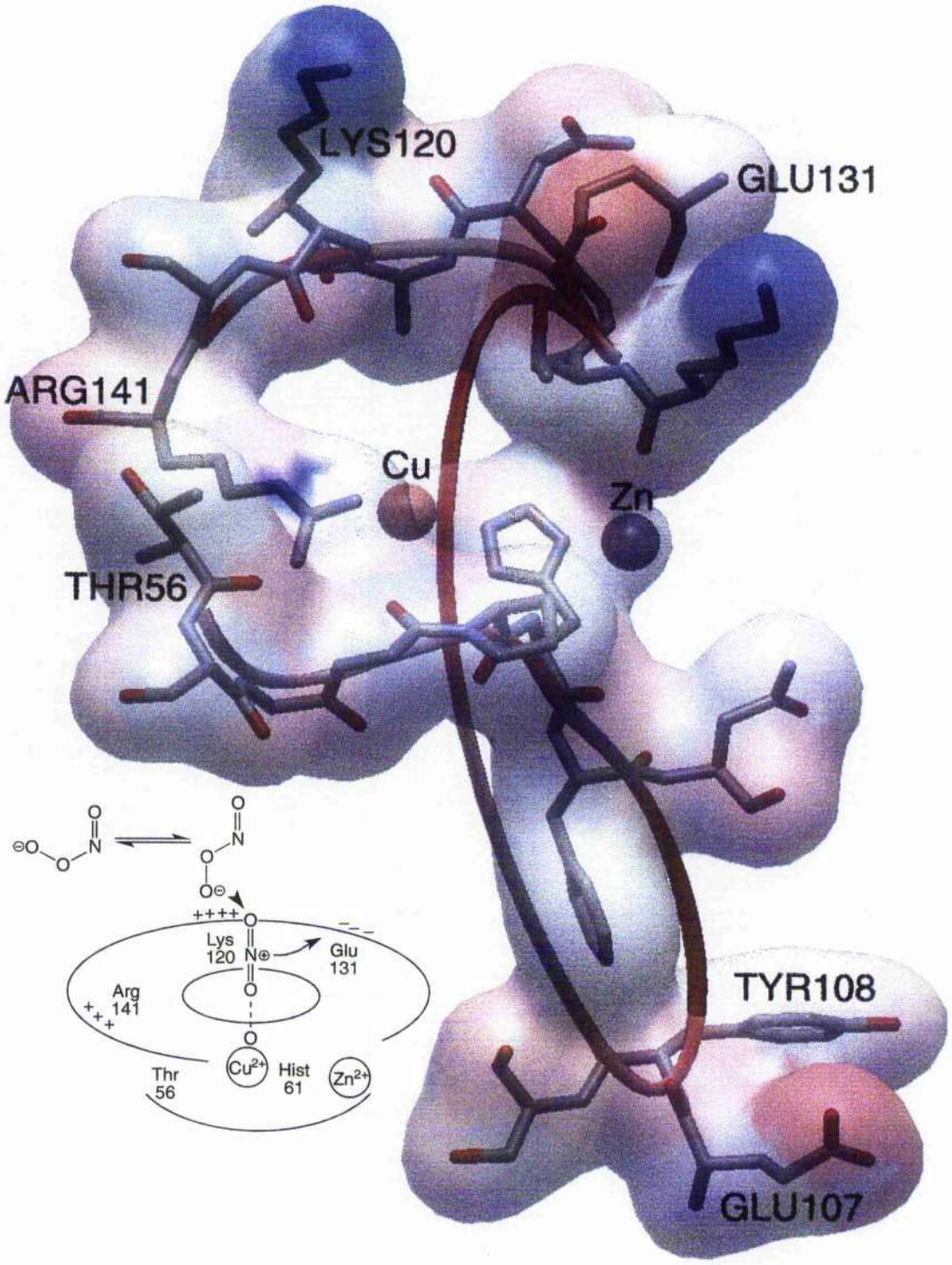

Fig. 2.2 Computer visualised image of the active site of bovine Cu, Zn SOD derived from Tainer *et al.*[92] illustrating the features described in the mechanism proposed by Ischiropoulos *et al.* for the heterolytic cleavage of peroxynitrite. Amino acid residues are represented as sticks and the peptide backbone as a solid ribbon.

Blue colours in the simulated surface indicate areas of positive charge and red colours areas of negative charge.

In step 1 the superoxide radical anion binds to the Cu^{2+} displacing one axial water molecule with the second oxygen atom H-bonding to a guanidinium nitrogen of Arg141. The unpaired electron reduces the d^9 Cu^{2+} centre to a d^{10} Cu^{+} centre with simultaneous breaking of the bond between His61 and copper; dioxygen is released. Step 2 involves electron transfer from Cu^{+} to a second molecule of superoxide regenerating Cu^{2+}. Proton transfer from His61 gives Cu-hydroperoxide. Addition of a second proton from a water molecule in the active site yields the neutral H_2O_2 leaving group. Assuming that the estimate of the oxidation potential of the peroxynitrite anion to the nitrosodioxyl radical[61] is reliable and this value is almost the same as the reduction potential of Cu^{2+} to Cu^{+}, 0.42 V, then peroxynitrite can reduce the active site copper.

The proposals of Ischiropoulos *et al.* appear to be contradictory since they state that "...once in the active site, *one* electron from peroxynitrite may be transferred to the copper to form a cuprous intermediate." as in eqns. (1) and (2).

$$ONOO^- + Cu^{+2}\text{,Zn SOD} \Rightarrow ONOO\text{—}Cu^{+1}\text{,Zn SOD} \quad (1)$$

$$ONOO\text{—}Cu^{+1}\text{,Zn SOD} + H^+ \Rightarrow NO_2^+ + HO\text{—}Cu^{+1}\text{,Zn SOD} \quad (2)$$

Clearly, one electron transfer, as with superoxide, could not lead to heterolytic cleavage of the peroxide bond required for formation of nitronium ion. The mechanism they propose would be correct if the Cu^{2+} centre was not reduced to a Cu^{+} centre as written. Since the principle author[93] does not discuss the mechanism in terms of one electron processes, it has to be assumed that introduction of Cu^{+} was

unintentional. If one electron oxidation of peroxynitrite and reduction of Cu^{2+} were to occur, then this would allow a radical decomposition leading to release of nitrogen dioxide as shown in Scheme 2.2 (*a*) or NO and dioxygen as in pathway (*b*).

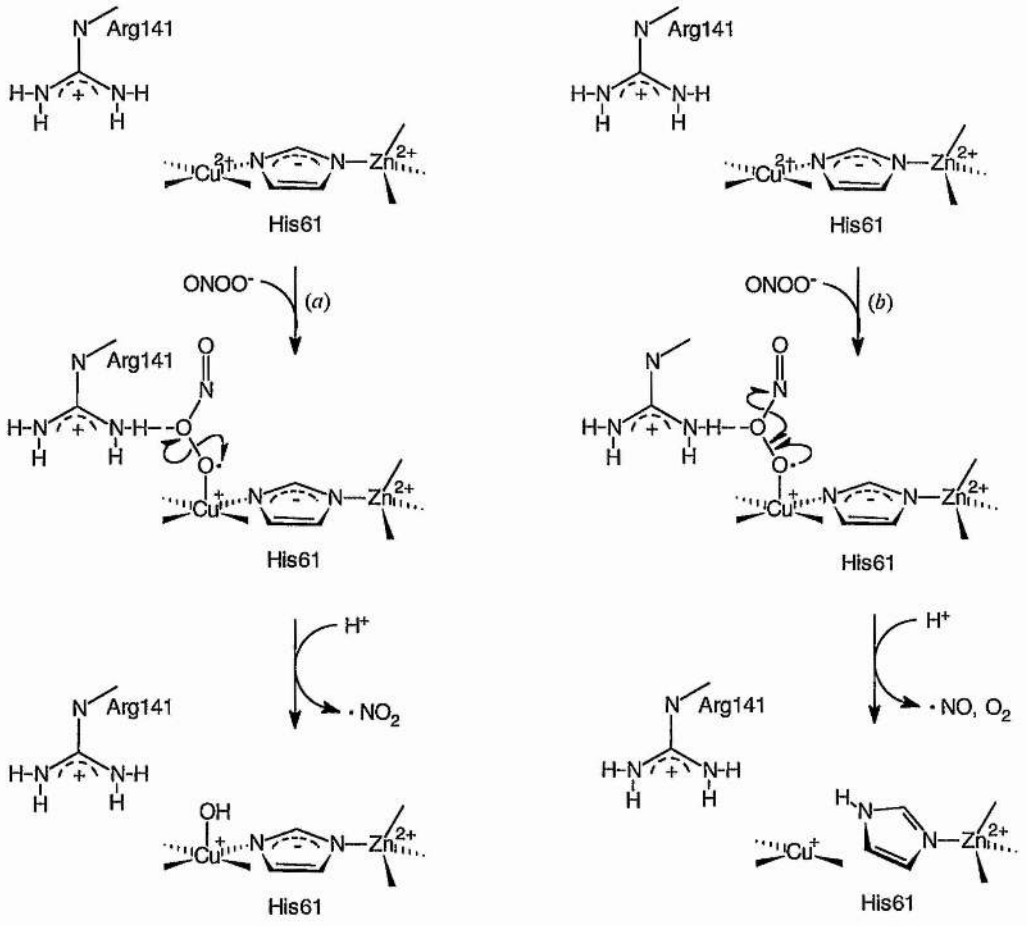

Scheme 2.2

Since Ischiropoulos *et al.* do not observe the accumulation of reduced (Cu^{+})-SOD in the system, if the nitration does occur *via* the routes shown in Scheme 2.2, then some form of recycling would have to be in operation. Speculative pathways for this process are outlined in Scheme 2.3.

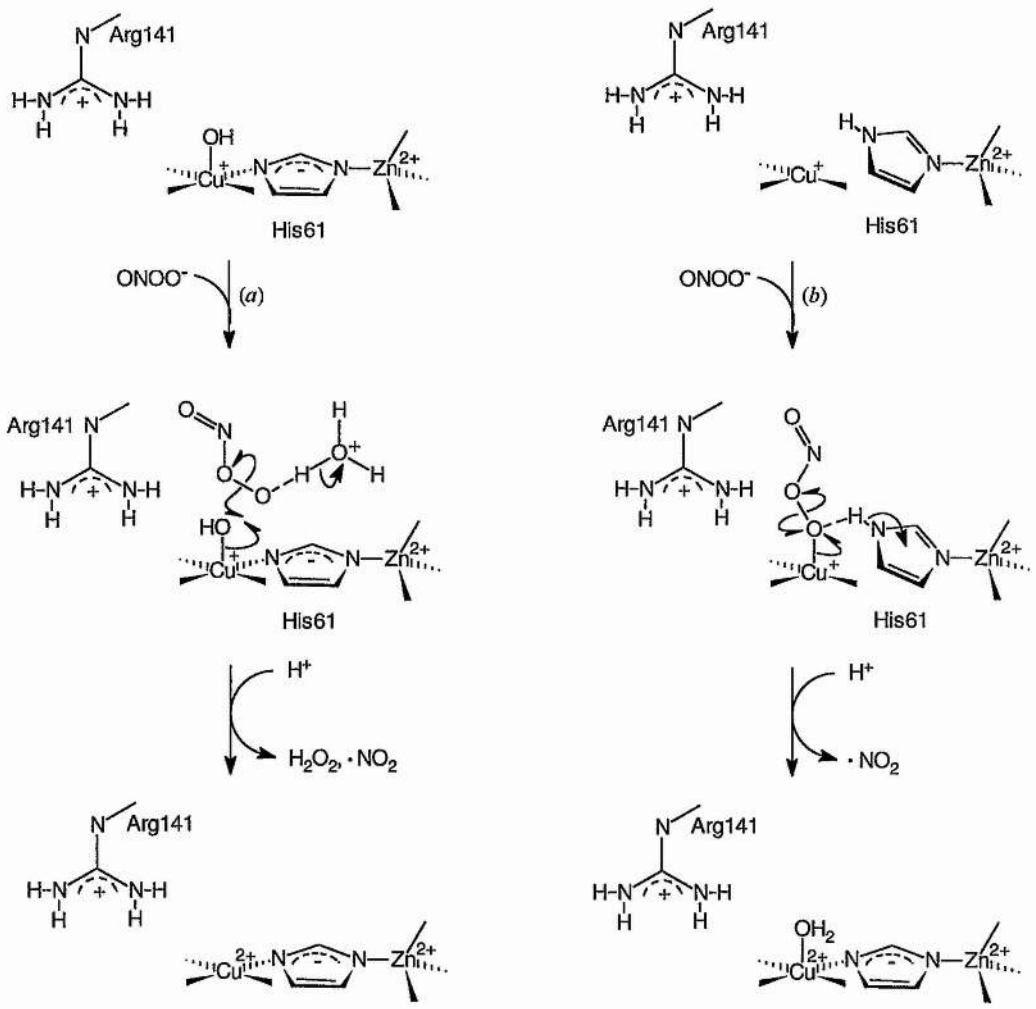

Scheme 2.3

Furthermore, it is not surprising that the series of experiments described by Ischiropoulos *et al.*[91] in which $NO^{\bullet}$, $NO_2^{\bullet}$, NO_2^- and NO_3^- are reacted with solutions of Cu, Zn SOD buffered at pH 7.4 result in no 'significant' formation of nitrotyrosine residues. $NO^{\bullet}$ is not reactive enough to nitrate even activated aromatic compounds such as tyrosine and solutions of nitrite or nitrate will not effect nitration reactions near neutral pH. The fact that nitrogen dioxide did not give any significant nitrotyrosine may simply be due to dimerisation to N_2O_4 and subsequent hydrolysis. Since the electrostatic interaction between the negative charge on peroxynitrite anion

and the positively charged areas of the enzyme surface is crucial to the observed activity, it cannot be expected that addition of uncharged $NO_2^{\bullet}$ to native SOD will result in an effect analogous to that in which it is generated at the active site by homolytic cleavage of ligand-bound, oxidised peroxynitrite.

2.1.2 Possible mechanisms of aromatic nitration

An enzymatic mechanism of aromatic nitration involving nitronium ion seems unlikely as the usual conditions required to produce this species are the high acidities encountered in mixtures of concentrated H_2SO_4 and HNO_3. The mechanism is outlined in Scheme 2.3.

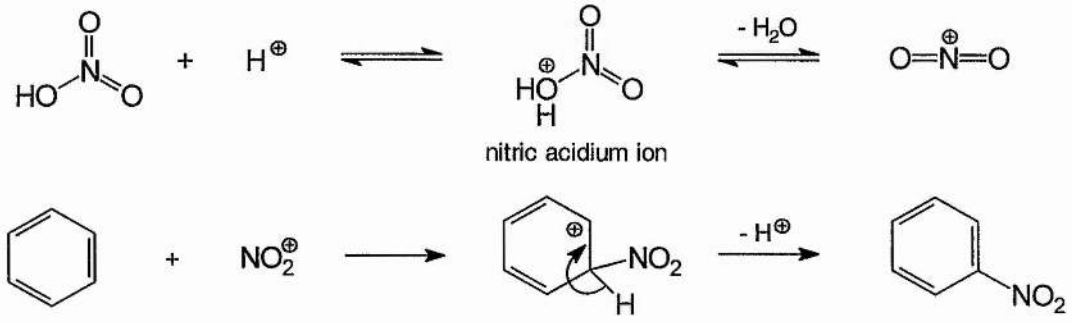

Scheme 2.4

In dilute solutions of nitric acid, two distinct mechanisms predominate: a classical nitrosation-oxidation mechanism (Scheme 2.4) and one involving radicals described in a series of papers by Ridd and co-workers[94] (Scheme 2.5). The range of radical processes encountered during nitration by nitric acid has been reviewed by Ridd.[95] The salient points are that nitrous acid catalysed nitrations normally occur through the radical cation pathway outlined in Scheme 2.5 although the classical reaction path (Scheme 2.4) contributes to the rate when the acidity is relatively low and [HNO_2] is relatively high. It is important to note that there must be at least some separation of the

$\overline{ArH^{\bullet+}\ NO_2^{\bullet}}$ radical pair in the radical cation pathway, otherwise no CIDNP effect would be observed.

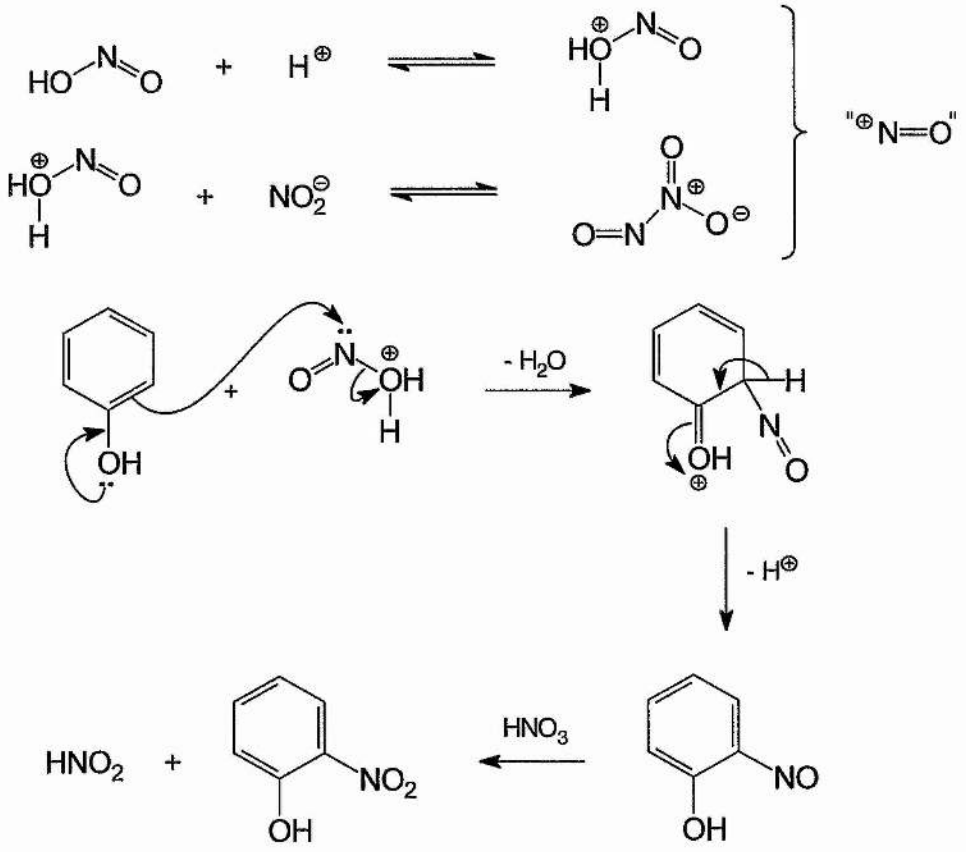

Scheme 2.5

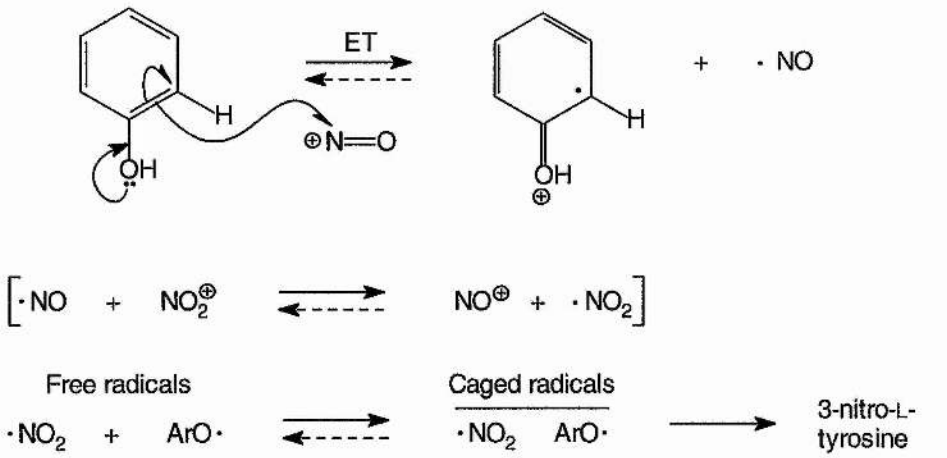

Scheme 2.6

2.1.3 Chemically Induced Dynamic Nuclear Polarisation (CIDNP)

The technique of Chemically Induced Dynamic Nuclear Polarisation[96,97] (hereafter referred to as CIDNP) is a means of probing the mechanism of reactions which are believed to involve free radicals. The product(s) of the reaction are observed during or shortly after their formation which contrasts with electron paramagnetic resonance (EPR) spectroscopy in which the radical intermediates are observed directly. The advantages of CIDNP over EPR are that CIDNP does not require the introduction of an additional species into the system to trap the radicals, so the technique is non-invasive in that sense. Furthermore, with CIDNP, the spectral changes over time of several species can be monitored simultaneously without the deconvolution necessary with EPR. The technique can provide several different classes of mechanistic information ranging from simply evidence for radical precursors to the reaction products through to the identity and characteristics of the precursors. In addition, further information can be gleaned in the form of the pair formation, polarisation identity and radical lifetimes/separations. However a drawback is that whilst EPR is a quantitative technique, the fact that dynamic signals are displayed in CIDNP NMR precludes estimation of the proportion of the products formed *via* a radical process without some knowledge of the kinetics of the reactions being studied. The products can only arise from two radicals paired in a singlet multiplicity and the formation of this multiplicity is dependent on the nuclear spin state. When two radical precursors come together with a triplet multiplicity, then one radical must undergo spin inversion before reaction can occur. Those precursors with nuclear spin states which do not favour spin inversion will exhibit a sufficiently long lifetime in order to escape the cage.[98] The sign of the polarisation in the CIDNP effect observed will be opposite for products derived from singlet precursors than from those derived from triplet precursors.

2.1.3.1 Qualitative sign rules

Kaptein[99] formulated two simple qualitative sign rules by which the direction of the net effect shown in eqn. (3) or multiplet effect [eqn. (4)] can be predicted. Conversely, empirical observations may be used to derive one of the parameters if the others are known.

$$\Gamma_{ne} = \mu \times \varepsilon \times a_i \times \Delta g \tag{3}$$

$$\Gamma_{me} = \mu \times \varepsilon \times a_i \times a_j \times J_{i,j} \times \sigma_{i,j} \tag{4}$$

The following sign convention is employed:

μ + if the radical pair is formed from a triplet precursor or by an encounter of free radicals.

– if the radical pair is formed from a singlet precursor.

ε + for products formed by coupling or disproportionation ('in cage').

– for products formed by cage-escape reactions.

$a_{i,j}$ + if the nucleus under consideration has a positive hyperfine coupling constant.

– if the nucleus under consideration has a negative hyperfine coupling constant.

Δg + if the observed radical has the higher g factor.

– if the observed radical has the lower g factor.

$J_{i,j}$ + if nuclei i and j have a positive spin-spin coupling constant.

– if nuclei i and j have a negative spin-spin coupling constant.

$\sigma_{i,j}$ + when nuclei i and j belong to the same radical.

– when nuclei i and j belong to different radicals.

Γ_{ne} + enhanced absorption, A.

– emission, E.

Γ_{me} + the low-field signal(s) of a multiplet shows E, whereas the high-field signal(s) shows A. (E/A).

– the low-field signal(s) of a multiplet shows A, whereas the high-field signal(s) shows E. (A/E).

Table 2.1 Magnetic properties of nitrogen nuclei.[100] The Varian Unity*plus* spectrometer used in this work operates at 11.74 T bringing protons into resonance at 500 MHz.

	^{14}N	^{15}N
Natural abundance/%	99.64	0.36
Spin quantum number	1	½
NMR frequency (11.74 T/MHz)	36.12	50.66
Sensitivity relative to ^{1}H	0.00101	0.00194
Sensitivity relative to ^{13}C at natural isotopic abundance	17.22	0.0214

Before undertaking a CIDNP study using [^{15}N] peroxynitrite, it was considered appropriate to undertake preliminary work with $H^{15}NO_3$ in order to gain experience in the technique and assess how easy it would be to detect CIDNP enhancement effects with L-tyrosine as the aromatic substrate.

2.1.3.2 General problems

The extraction of meaningful results from these systems is hampered by several general problems, some specific to the chemical systems and some due to the NMR operation. The fact that chemically unstable intermediates are involved in the chemical system causes problems with timing of the experiments. Many of the reactions about which information is required are non-stoichiometric. This factor in conjunction with the relative insensitivity of ^{15}N NMR compared with ^{1}H NMR or EPR, say, makes observation of low-yield products and any nuclear polarisation

induced in them difficult. Irreproducibility between runs on the same chemical system is deleterious and commonplace. On several occasions, particularly where long acquisition times were required, extraneous noise was also observed.

2.2 Results and discussion

2.2.1 Reaction of $H^{15}NO_3$ with *N*-acetyl-L-tyrosine

It is desirable to match $t_{½}$ for the reaction with the relaxation time of the ^{15}N nucleus (*ca.* 3 min in the nitro group) in order to achieve optimal enhancement in the ^{15}N NMR spectrum. To this end, the kinetics of nitration of *N*-acetyl-L-tyrosine were followed by uv-visible spectrophotometry at various concentrations of sodium nitrite added to catalyse the reaction. Typical individual runs are shown in Fig. 2.3; the sigmoid form results from the autocatalytic nature of the nitrous acid catalysed mechanism illustrated in Scheme 2.6.

During the nitration of L-tyrosine with $H^{15}NO_3$ it was observed that quantities of gas collected inside the NMR tube. This was sufficient to prevent a satisfactory lock signal being achieved on the NMR spectrometer. It is likely that the gas was $^{14}N{\equiv}^{15}N$, formed as a result of *N*-nitrosation of the amino group by species able to transfer NO^+ present in the $H^{15}NO_3$ followed by subsequent diazotisation[101] and nucleophilic substitution[102] to form, presumably, either 2-hydroxy-3-(4-hydroxy-phenyl)-propionic acid or 2-hydroxy-3-(3-nitro-4-hydroxy-phenyl)-propionic acid (Scheme 2.7). To circumvent this problem, *N*-acetyl-L-tyrosine was used with the rationale that introduction of an acetyl group at the amino nitrogen would discourage the *N*-nitrosation pathway long enough to observe the expected CIDNP effects for electrophilic aromatic nitration.

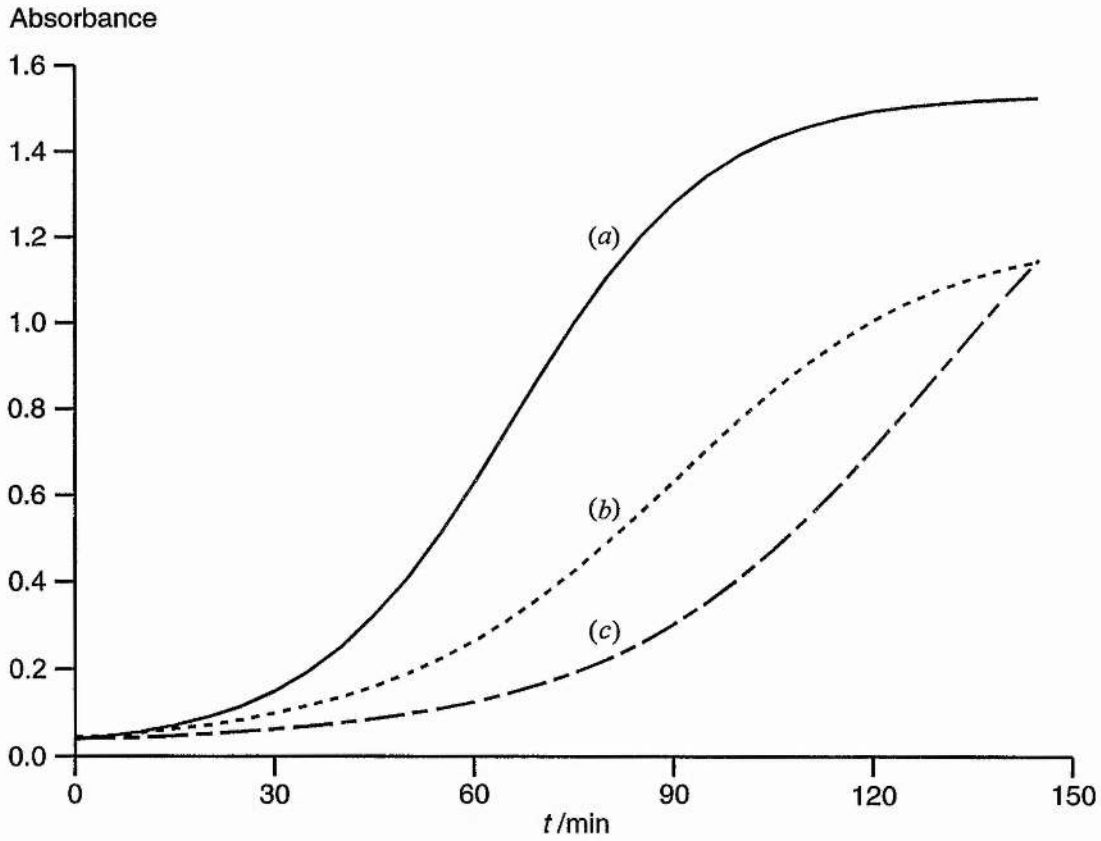

Fig. 2.3 Typical sigmoid shaped curves generated by an autocatalytic process. (*a*) 1:1, (*b*) 3:2 and (*c*) 2:3 mixtures of HNO_3 (40%, 9.01 M) containing residual nitrous species and L-tyrosine (1 mM). Individual data points have been omitted for clarity.

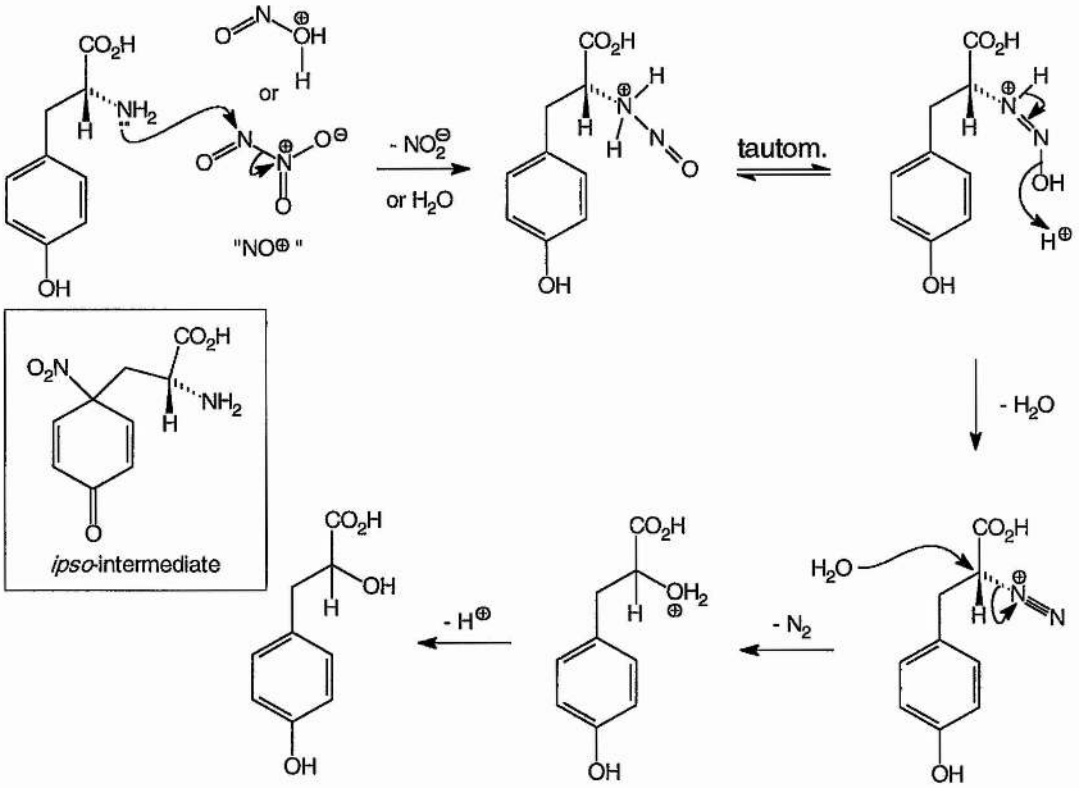

Scheme 2.7

Fig. 2.4 shows the signals in the ^{15}N NMR spectrum during the reaction of $H^{15}NO_3$ and *N*-acetyl-L-tyrosine. A red-orange precipitate formed during the experiment which analysed as $[^{15}N]_1$ 3-nitro-*N*-acetyl-L-tyrosine. The spectrum displays a strong emission signal at δ_N 370.3 ppm analogous to that observed in the nitrous acid catalysed nitration of mesitylene[94a] and *p*-nitrophenol[94b] in trifluoroacetic acid; the mechanism (represented in Scheme 2.6) can therefore be explained in the same way. The smaller peak at δ_N 368.6 ppm is due to the $[^{15}N]$ nitrobenzene reference.

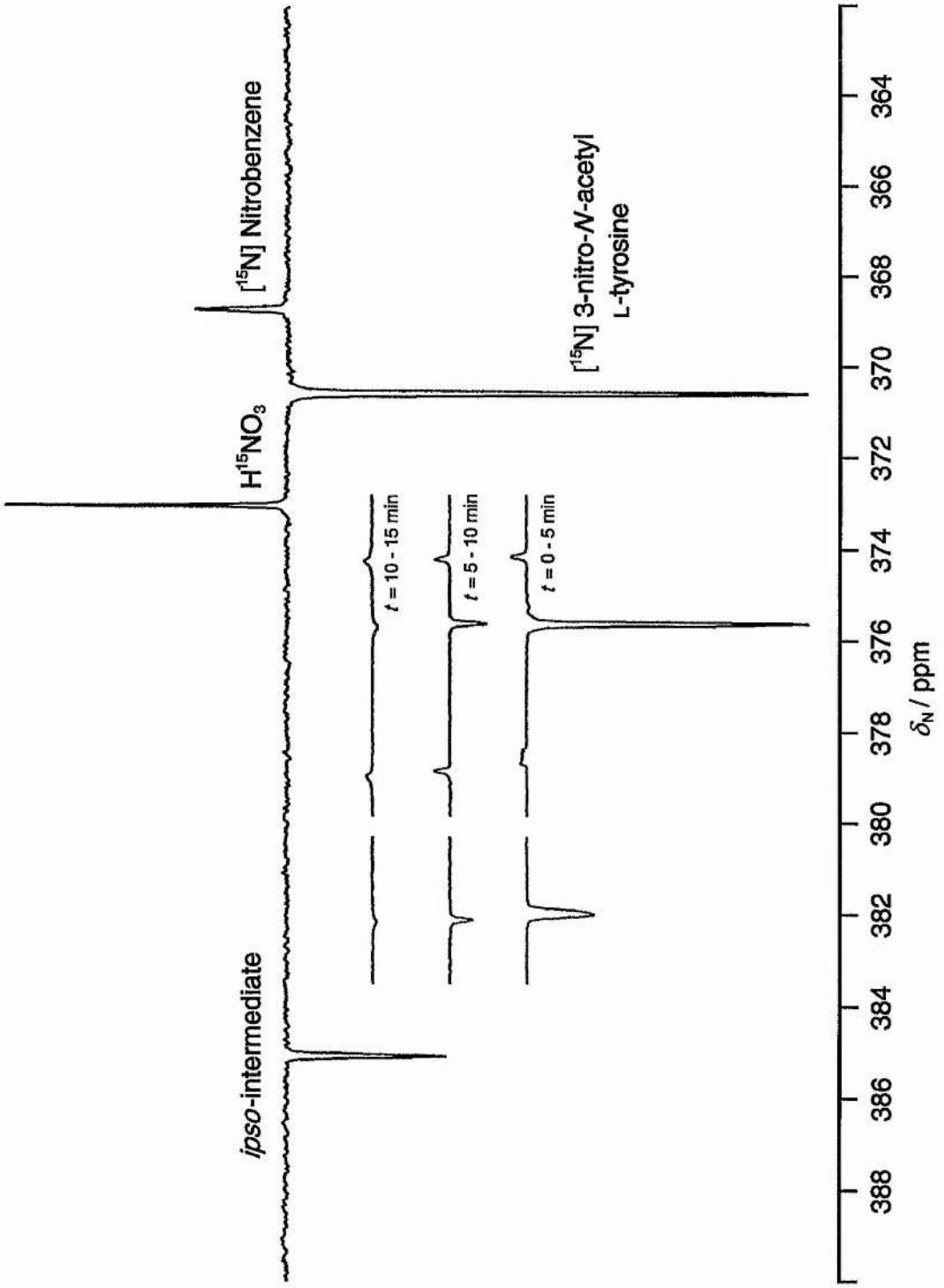

Fig. 2.4 ^{15}N NMR spectrum obtained some 2–4 min after addition of $H^{15}NO_3$ (2.25 M) to *N*-acetyl-L-tyrosine (0.100 M) at 37 °C. [$NaNO_2$] = 0.001 M. Inset: time course of signals.

It has been suggested that the smaller of the two emission signals at δ_N 385.0 ppm may be due to the reaction of $NO_2^{\bullet}$ at the amine group to form an *N*-nitro derivative. This is unlikely for two reasons. First, there is no precedent for the observation of an emission signal corresponding to an *N*-nitro product during a nitration reaction, although it has been shown to occur[103] when labelled and unlabelled nitramines are rearranged together. Second, typical chemical shifts for aliphatic nitramines[104] range from δ_N 313–370 ppm. A more convincing explanation is that the signal corresponds to the *ipso*-intermediate (Scheme 2.7) resulting from attack by $NO_2^{\bullet}$ at the 1 position of the aromatic ring observed for the structurally similar compound 4-methylphenol by Coombes *et al.*[105] in sulfuric acid. Not only is the chemical shift close to that reported for the analogous species during nitration of 4-methylphenol by Ridd *et al.*[106] in acetic anhydride at 2 °C, but also when nuclear polarisation had ceased after approximately 11–13 min, no regular signal could be detected for this species.

The signal at δ_N 372.9 ppm is due to $H^{15}NO_3$, being a weighted average of the species $H^{15}NO_3$, $^{15}NO_2^-$ and $^{15}NO_3^-$. Hence the 3.0 ppm difference in chemical shift between $H^{15}NO_3$ in acid and nitrate ion in alkaline medium. Broadening and shift *ca.* 0.5 ppm downfield of the peak for $H^{15}NO_3$ shown inset in Fig 2.3 derives from exchange with nitrous species produced during the autocatalytic process and perhaps also between N^{III} and N^V states. Nitric acid is the most extensively dissociated of all the mineral acids, with the equilibria shown in eqns. (5) and (6) existing in solution.

$$2HNO_3 \rightleftharpoons H_2NO_3^{\oplus} + NO_3^{\ominus} \rightleftharpoons H_2O + NO_2^{\oplus} + NO_3^{\ominus} \quad (5)$$

$$HNO_3 + H_2O \rightleftharpoons H_3O^{\oplus} + NO_3^{\ominus} \quad (6)$$

In original studies with *p*-nitrophenol, the reaction was represented as occurring through the phenoxide ion, but this may not be correct for the substrate used here; the O–H proton is however probably lost at the time of formation of the radical pair shown. The second reaction shown in Scheme 2.6 is shown in brackets to indicate that this representation indicates merely the stoichiometry of the process; the mechanism must be more complex as the rate of these nitrous acid catalysed nitrations can greatly exceed the rate of formation of nitronium ions in solution.

2.2.1.1 Other considerations and caveats

In the absence of nuclear polarisation, it would be possible to argue that the initial electron transfer to the nitrosonium ion is followed by the partitioning of the radical pair $\overline{\text{ArO}^{\bullet}\ \text{NO}^{\bullet}}$ between combination and dissociation and that the nitroso compound so formed is rapidly oxidised to a nitro compound. However, from the *g*-values reported[107] for nitric oxide (1.909–1.983) and the fact that this radical pair has a singlet precursor (since the initial reactants have no unpaired electrons) it follows that any nuclear polarisation should lead to enhanced absorption and not the emission signal observed. Furthermore, nuclear polarisation could be generated, in principle, through reaction of the nitric acid with the nitrous species in the solution then carried over into the nitrated product by an electrophilic aromatic substitution reaction. Lippmaa *et al.*[108] have observed this phenomenon in the products of diazo-coupling as the nuclear polarisation observed results from a direct electrophilic aromatic substitution reaction. However, were this mechanism to be in operation here, then emission would be seen in the nitric acid signal.

It is important to note that the presence of ^{15}N nuclear polarisation for the nitrated tyrosine derivative does not imply that this product is exclusively formed by a radical

pathway, but the unusual kinetic forms shown in the nitration of *p*-nitrophenol in aqueous nitric acid[109] imply that the radical reactions of Scheme 2.3 are then the only or predominant reaction path. The strength of the emission signals observed in the nitration of *N*-acetyl-L-tyrosine here are consistent with the same conclusion.

More generally in ^{15}N NMR spectroscopy, emission (E) signals may be observed if there is a nuclear Overhauser (NOE) coupling with nearby protons. Emission arises because of the negative magnetogyric ratio[110] of the ^{15}N nucleus. Complete ^{15}N–^{1}H dipolar relaxation in small-medium sized organic molecules such as the phenolic substrate tyrosine used here gives rise to an NOE of – 4.93. When added to the original signal intensity, the result is an NOE enhancement factor of *ca.* – 4. However all ^{15}N NMR spectra in this work were carried out without proton-decoupling and the magnitude of the enhancement factor is clearly much greater than 4.

2.2.1.2 Analysis by Kaptein's rule

When eqn. (1) is applied to the polarisation of ^{15}N nuclei, an additional negative sign has to be added[111] because of the negative magnetogyric ratio of the ^{15}N nucleus. The following discussions are concerned only with the polarisation of the ^{15}N nucleus in products derived from nitrogen dioxide and, in this radical, the negative magnetogyric ratio of the ^{15}N nucleus also causes the relevant hyperfine coupling constant (a_N) to be negative. Kaptein's rule then takes the following form: $\Gamma_{ne} = \mu \times \varepsilon \times \left(g_{NO_2\cdot} - g_b\right)$. This analysis can be simplified further since the value[112] of $g_{NO_2^\cdot}$ (2.0000; ref. 15(*a*) has a discussion of this value) is less than that for the tyrosyl radical[113] (2.0046), organic cation radicals[114] and hydroxyl radicals[115] (2.0119†). Hence Δg is negative as the observed nucleus has the lower g factor. The conclusions of Kaptein's rule can then be

† Generated from Ti^{3+} and H_2O_2 in water at 300 K. Values from γ-irradiation in water at 77 K range from 2.005 to 2.025. All values were obtained by EPR techniques.

related simply to how the radicals are formed and how they react to form the products (Table 2.2).

Table 2.2 The phase of ^{15}N nuclear polarisation in the products formed from radical pairs involving nitrogen dioxide and organic or hydroxyl radicals.

Formation of radical pair	Reaction of radicals	
	Within radical pair	After separation from pair
From singlet precursor	A	E
From triplet precursor	E	A

The mechanism can be explained by the partitioning of the $\overline{ArO^{\bullet}\ NO_2^{\bullet}}$ radical pair between combination and dissociation. Since the radical pair is formed by the diffusion of the radicals together, this is equivalent, according to Kaptein's rule, to derivation from a triplet precursor and, since the product is formed by combination within this radical pair, it follows that the polarisation should lead to an emission signal, as observed.

In conclusion it is important to note that even when polar mechanisms are possible, the nitration of activated aromatic compounds such as tyrosine proceed *via* a radical pathway. This basic and well established fact which Ischiropoulos *et al.* appear not to have considered very carefully is central to understanding both the rationale for this investigation and the conclusions drawn from it.

2.2.2 ^{15}N NMR spectrum of 1-ethoxy-2-nitrosooxy-ethane

The ^{15}N NMR spectrum of neat 1-ethoxy-2-nitrosooxy-ethane, shown in Fig. 2.5, was taken to ascertain the chemical shift and thus facilitate identification of any unreacted

material remaining after synthesis of peroxynitrite. It exhibits several signals in addition to those expected for the reference δ_N 0 (370.3 ppm relative to liquid ammonia at 25 °C) and 1-ethoxy-2-nitrosooxy-ethane at δ_N 207.2 (577.5) ppm. Since only a small quantity of the labelled material was synthesised in any one batch, it was neither distilled nor dried. This latter fact accounts for the presence of the additional signals since it is likely that a small amount of strong acid remained in the essentially neat organic liquid. The broad signal centred at δ_N 202.5 (572.8) ppm is assigned to HNO_2 on the basis of the findings of Bonner and co-workers[116] that the chemical shift for nitrite (which varies with strict linearity to the fraction of NO_2^- protonated, based on $pK_a = 3.09$) appears at δ_N 200.3 (570.6) ppm in 42.4% D_2SO_4. The broadening is due to exchange equilibrium between HNO_2 and the nitrous acidium ion illustrated in Scheme 2.7 (*a*); tautomerisation being a common cause of line broadening even in ^{15}N NMR spectra. The signal at δ_N – 23.8 (346.5) ppm requires more careful attention. Bonner and co-workers report a sharp resonance assignable to the nitrosonium ion (NO^+) appearing at δ_N – 10.1 (360.2) ppm in 42.4% D_2SO_4. However, given the close match in chemical shifts for HNO_2 between their conditions and the conditions here, this signal seems to be too far upfield to correspond to nitrosonium ion. They also report that under conditions of high acidity (0.1 M HNO_3 in 70% $HClO_4$), a signal for nitrate can be detected at δ_N – 23.6 (346.7) ppm. This is a more likely candidate for the signal since nitrate may arise from the synthesis of the alkyl nitrite either by disproportionation of nitrous acid, represented in Scheme 2.8 (*b*), or simply by oxidation of nitrite. The feature at approximately δ_N 240 (610) ppm is likely to be a spectrometer artefact which is discussed later.

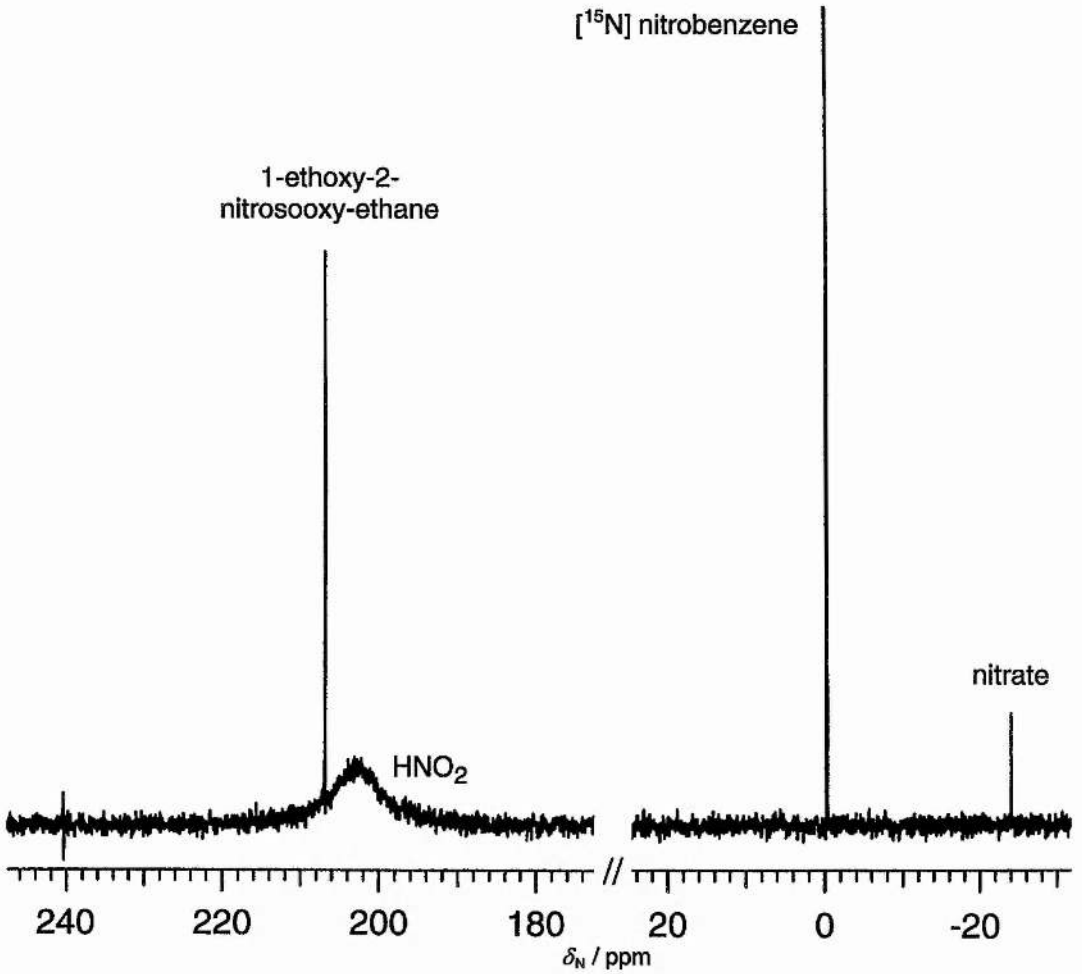

Fig. 2.5 ^{15}N NMR spectrum of 'neat' 1-ethoxy-2-nitrosooxy-ethane (containing some residual strong acid) taken at 0 °C with 28 scans.

(*a*)

$$HNO_2(aq) + H_3O^{\oplus}(aq) \rightleftharpoons H_2NO_2^{\oplus}(aq) + H_2O$$

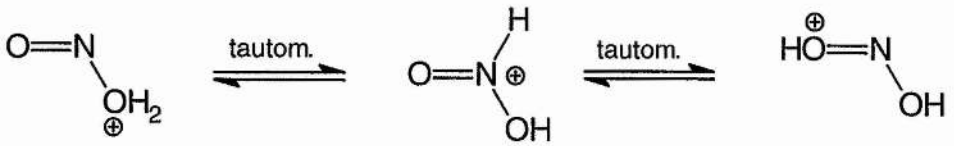

(*b*)

$$3HNO_2(aq) \rightleftharpoons 2NO(g) + H^{\oplus}(aq) + NO_3^{\ominus}(aq) + H_2O$$

Scheme 2.8

2.2.3 Reaction of [^{15}N] peroxynitrite with L-tyrosine (final pH 12.5)

Fig. 2.6 shows the time course of the CIDNP enhancement effects in the ^{15}N NMR spectrum of the reaction of alkaline peroxynitrite with L-tyrosine. Three signals were detected in the initial spectrum: at δ_N 609.1 ppm due to nitrite ions, δ_N 554.6 ppm due to peroxynitrite ions and δ_N 375.9 ppm due to nitrate ions. That due to nitrite initially showed emission (E) before reverting to the expected signal. The peroxynitrite signal decreased linearly over time displaying no obvious enhancement whilst that for nitrate showed enhanced absorption (A) before reverting to the normal signal. This accords with the reaction path shown in Scheme 2.9. Spectra were acquired every 5 min until no further change was observed. Enhancement effects persisted for approximately 25 min.

On occasions during early investigations, the peroxynitrite decomposed with evolution of a gas before it could be effectively used. Since it is known that transition metal ions, particularly Cu^{2+} catalyse the decomposition to, exclusively, nitrite and dioxygen[117] several precautionary measures were adopted to prevent this. A small amount of EDTA (approx. 10^{-5} M) was added to the premixed alkaline hydrogen peroxide and all glassware was carefully washed with 3–5 M HCl, deionised water, and finally acetone. Still under the same conditions, when L-tyrosine was replaced with *O*-methyl-L-tyrosine, slow conversion of peroxynitrite to nitrate was observed with no CIDNP enhancement effects visible in the ^{15}N NMR spectrum. However, when alkaline peroxynitrite (0.05 M) was added in a 1:1 ratio to a solution of *O*-methyl-L-tyrosine (0.025 M) contained in pH 7.0 phosphate buffer, the solution immediately turned bright yellow, indicating the formation of 3-nitro-*O*-methyl-L-tyrosine.

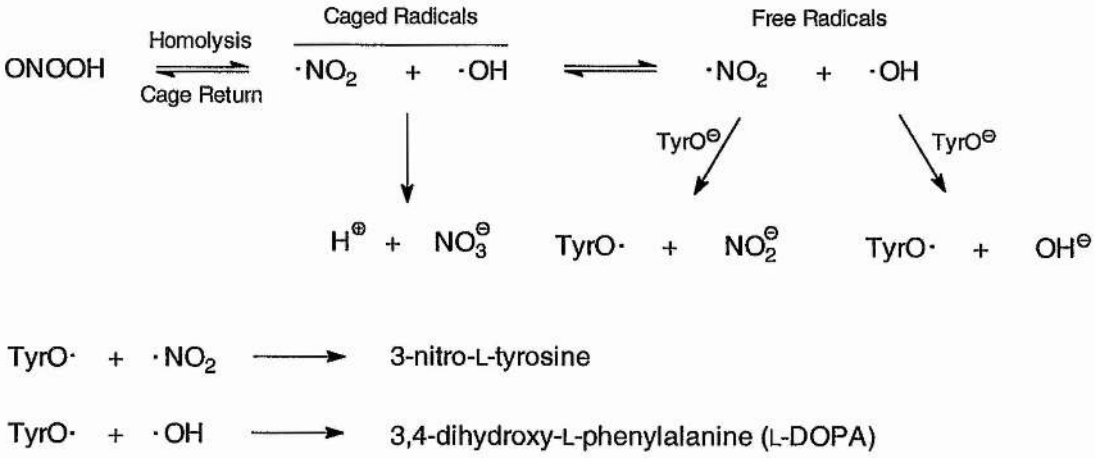

Scheme 2.9

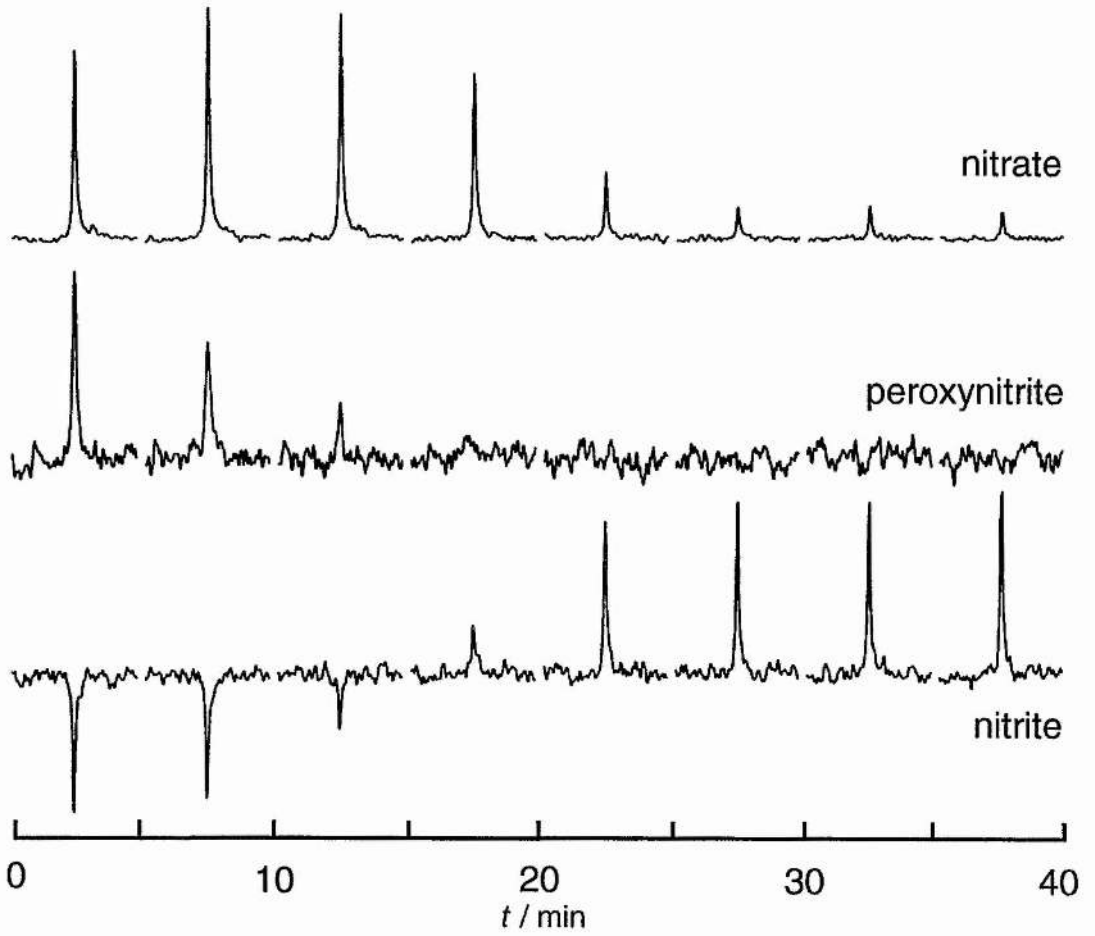

Fig. 2.6 Time course of the ^{15}N NMR signals in the reaction of alkaline peroxynitrite (approx. 0.10 M) with L-tyrosine (0.0045 g, 0.025 M). [NaOH] = 0.15 M.

Maximum enhancement factors of the CIDNP signals are quantified, where possible, using the formula $V_{max} = (I_{max} - I_0)/I_0$. Since V_{max} values are dependent on the reaction time and the relaxation times (T_1) of the nucleus being observed, this treatment is only useful for a qualitative description of CIDNP effects.

Table 2.3 Summary of the characteristics of the ^{15}N NMR spectra shown in Fig. 2.6.

Signal	δ_N/ppm	Summary of CIDNP effects
NO_2^-	238.8 (609.1)	$V_{max} \simeq -1.8$
$ONOO^-$	184.2 (554.5)	Small initial A
NO_3^-	5.7 (376.0)	$V_{max} \simeq 8$

Signals were unambiguously identified by spiking the reaction mixtures with authentic samples of nitrate. The chemical shift of the expected product 3-nitro-L-tyrosine (also determined by spiking) was found to appear very close to nitrate ions at δ_N 5.1 (375.3) ppm. The effects on the signal intensities of adding authentic material to the reaction mixtures are shown in Fig. 2.7. In order to check that the solution of alkaline nitrate and nitrite was not itself responsible for the nitration, a similar solution was made up according to the approximate proportions indicated by the final ratio of signals in the ^{15}N NMR spectrum. This was 0.0875 M in nitrite, 0.0225 M in nitrate and 0.15 M in NaOH; the total concentration of nitrogen containing species was equal to the initial concentration of peroxynitrite from which they were derived (approximately 0.1 M). L-Tyrosine was added so as to produce a final concentration of 0.025 M as in the NMR experiments. The reaction spectrum of the mixture (250 nm to 450 nm) was taken every five minutes on a uv-visible spectrophotometer for the same duration as the NMR experiment (approximately 1 h). After this time, it could clearly be seen that there was no peak at 360 nm corresponding to 3-nitro-L-tyrosine. The

reaction was repeated in pH 7.4 buffer and still no 3-nitro-L-tyrosine could be detected.

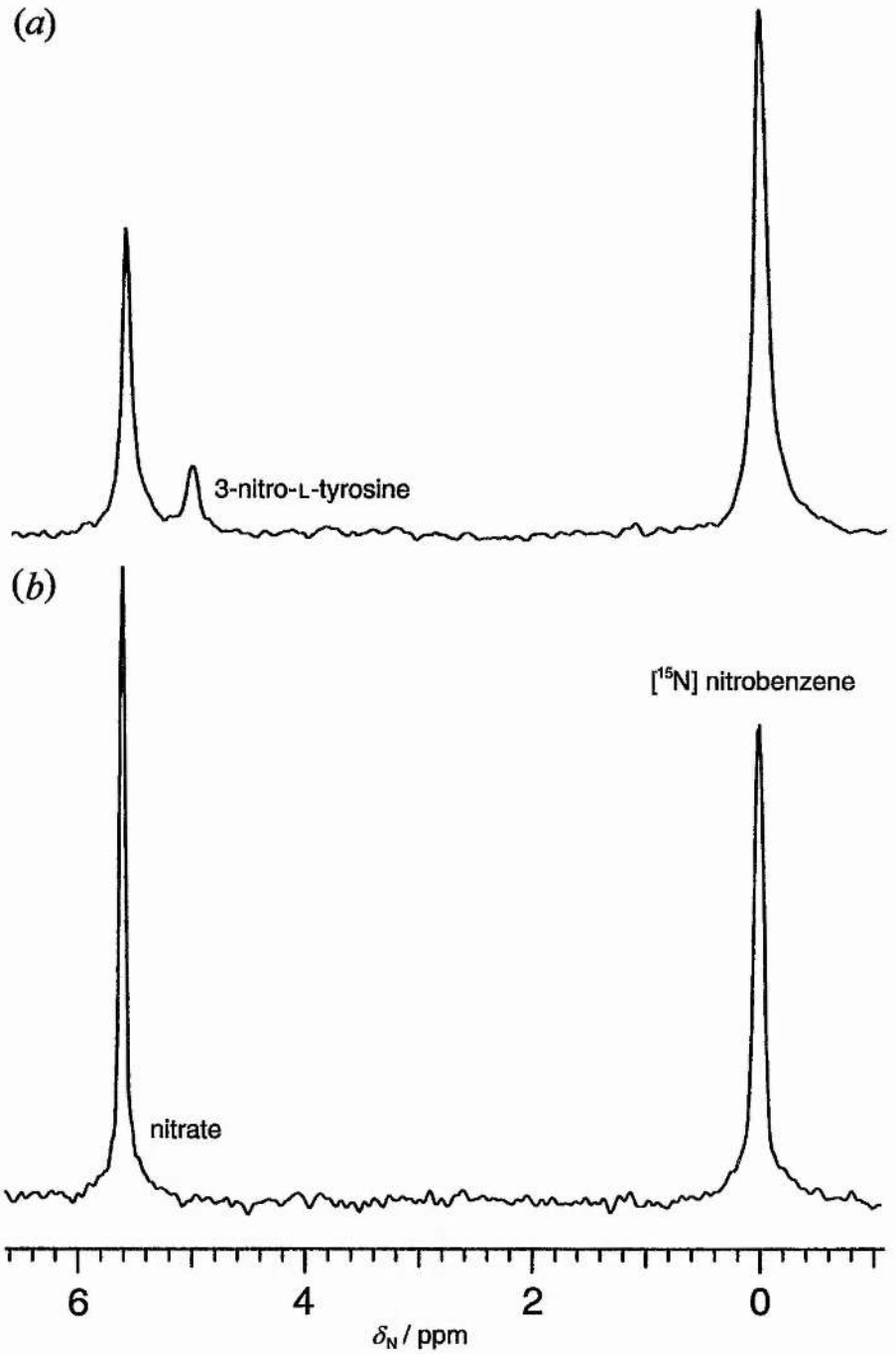

Fig. 2.7 The effects on the signal intensities of adding authentic material to the reaction mixtures: (*a*) addition of 3-nitro-L-tyrosine, (*b*) addition of nitrate.

2.2.4 Reaction of [^{15}N] peroxynitrite with AYV (final pH 12.5)

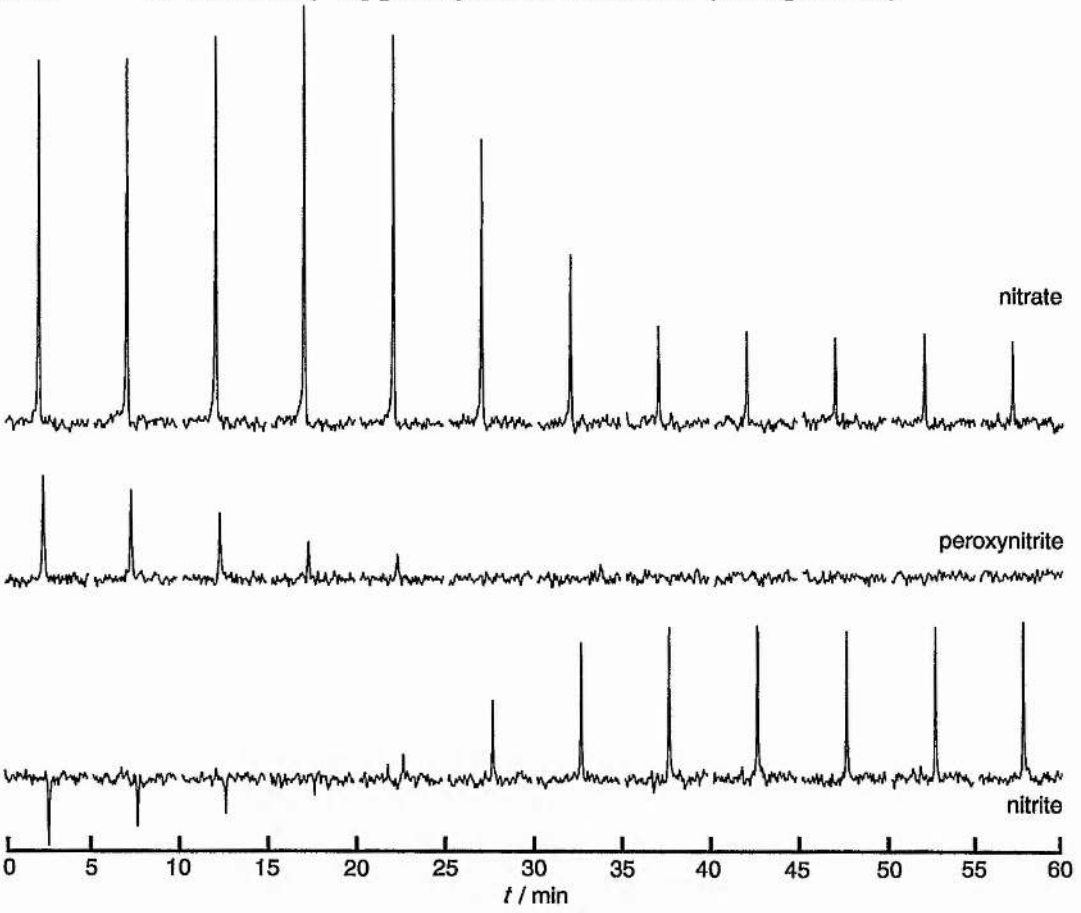

Fig. 2.8 Time course of the ^{15}N NMR signals in the reaction of alkaline peroxynitrite (approx. 0.10 M) with AYV (0.0351 g, 0.05 M). [NaOH] = 0.15 M.

Table 2.4 Summary of the characteristics of the ^{15}N NMR spectra shown in Fig. 2.8.

Signal	δ_N/ppm	Summary of CIDNP effects
NO_2^-	238.8 (609.1)	$V_{max} \simeq -1.5$
$ONOO^-$	184.2 (554.5)	Small initial A
NO_3^-	5.7 (376.0)	$V_{max} \simeq 5.3$

No obvious signal for 3-nitrotyrosine was present in the ^{15}N NMR spectra from these experiments, even allowing for CIDNP enhancement which would be expected if the product formed from tyrosyl radicals and nitrogen dioxide. However, a small signal which may be due to 3-nitrotyrosine, close to that for nitrate ions can be observed in

Fig. 2.6. This appears to change to a shoulder in the nitrate peak as the experiment progresses. It was evident from the yellow colour of the solutions after the runs were complete that some 3-nitrotyrosine clearly did form. In order to estimate the amount of 3-nitrotyrosine present after nitration by alkaline peroxynitrite, uv-visible spectra of the solutions were taken. Since it is more soluble than tyrosine, the AYV tripeptide was added to a solution of peroxynitrite so that the nominal concentrations corresponded to those in the NMR experiments. When the reaction was complete, the uv-visible spectrum was taken. The absorbance at one λ_{max} of 3-nitrotyrosine in AYV (356 nm) was 0.303. Since nitrate and nitrite ions also have a small absorbance at this wavelength, it was necessary to determine this (0.05) and subtract the two values to obtain the absorbance due to the 3-nitrotyrosine residue in AYV alone (0.253). If the molar extinction coefficient of 3-nitro-AYV at 356 nm is assumed to be the same as 3-nitrotyrosine (2339 M^{-1} cm^{-1})[†] then it can be seen that approximately 1.08×10^{-4} M of 3-nitrotyrosine forms. This corresponds to 0.11% of the peroxynitrite and 0.43% of the added AYV. Since a concentration of about 0.05 M is required to give a signal to noise ratio in the ^{15}N NMR spectrum of about 12:1, then clearly with CIDNP enhancement factors less than 10, as observed here, no signal will be seen at concentrations lower than about 1–5 mM.

2.2.4.1 Mechanistic interpretation of spectral changes

The spectral changes observed for the reaction of both L-tyrosine and the AYV tripeptide with alkaline peroxynitrite are very similar and can be explained in terms of the same mechanism (represented in Scheme 2.9). The radical pair shown in the Scheme is formed by the homolysis of a singlet precursor (the O–OH bond in peroxynitrous acid) and so, from Table 2.2 the product formed by reaction within the

[†] A molar extinction coefficient of 2910 M^{-1} cm^{-1} (in 0.01 M HCl) has been reported by R. W. Giese and J. F. Riordan, *Anal. Biochem.*, 1975, **64**, 588.

radical pair (nitric acid) should show enhanced absorption signals and that formed from the nitrogen dioxide radicals that escape from the cage (nitrite ions) should show emission signals. Nitrophenols are known to be formed by the reaction of phenoxy radicals with nitrogen dioxide[118] and aromatic hydroxylation by peroxynitrite ions has been described previously.[51] In a preliminary communication[119] on the subject, it was noted that the peroxynitrite signal intensity appeared to decrease in an exponential manner with time consistent with a first order process. Hence the conclusion was drawn that the homolysis of peroxynitrous acid was essentially irreversible in the presence of a reactive substrate. If this were not so, the reformation of peroxynitrite from the polarised radicals in the $\overline{NO_2^{\bullet}\ HO^{\bullet}}$ radical pair should initially confer some enhancement on the ^{15}N NMR signals for peroxynitrite and hence cause some distortion of the exponential plot. However, the intensity variation of the ^{15}N NMR signal for peroxynitrite taken during the related reaction of this species in the presence of the AYV tripeptide has a sigmoid form and is consistent with some back reaction of the radical pair to reform peroxynitrite. This back reaction is therefore included in Scheme 2.9. It is possible to observe this feature in Fig. 2.6, as the signal intensity in fact decreases *linearly*, not exponentially, due to distortion caused by residual enhanced absorption. However, the small number of signals and the fact that the latter stages of the reaction with L-tyrosine were being observed caused this subtlety to be overlooked initially. The representation of these reactions in Scheme 2.9 must be an oversimplification for several reasons. Firstly, it fails to explain adequately how the organic substrates increase the reaction rate. The subsequent reduction to hydroxide and nitrite ions of the initially formed radicals would lead to some apparent rate increase since these species might otherwise recombine to reform peroxynitrous acid. Since nitrogen dioxide is an ambident radical, recombination events could occur through either of the oxygen atoms so favouring the formation of peroxynitrous acid.

But it seems unlikely that reduction to hydroxide and nitrite ions is sufficient to explain the large difference between the observed rate and that expected at the pH used. Considering the low value for the activation entropy of nitrate formation ($\Delta S^{\ddagger}$ = 3 cal K^{-1} mol^{-1}) it might be expected that cage return to form peroxynitrous acid would be disfavoured. The increase in rate is clearly connected with the ionisation of the phenolic OH group as the decomposition of alkaline peroxynitrite in the presence of *O*-methyl-L-tyrosine is very slow. ET from phenoxide ion to peroxynitrous acid cannot account for this result since homolysis of the species ONOOH· would not give rise to a radical pair and hence would not generate nuclear polarisation. However an interaction between the phenoxide ion and peroxynitrous acid which takes place through a charge-transfer complex as represented by the highly speculative reactions in Scheme 2.10 provide a more likely explanation.

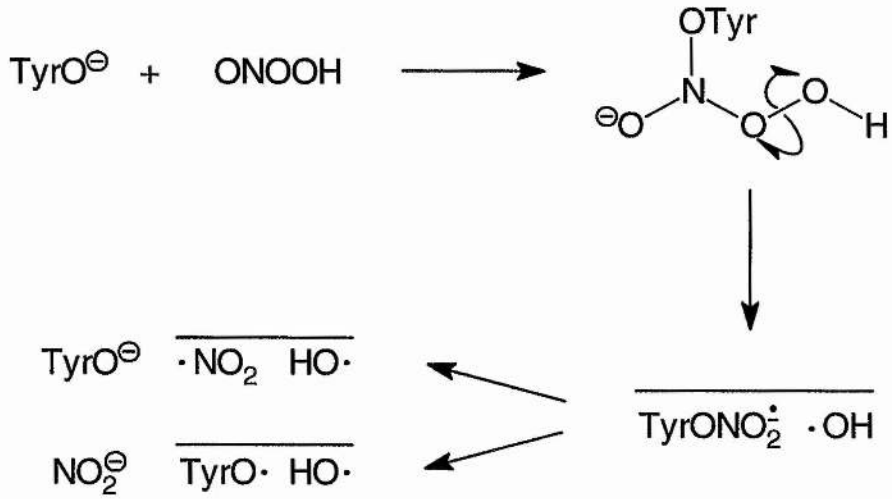

Scheme 2.10

Another difficulty with Scheme 2.9 arises from the fact that very little 3-nitro-L-tyrosine can be detected at the end of the reaction. The reactions of Scheme 2.10 show how some of the peroxynitrite could be converted to nitrite ions without passing through nitrogen dioxide as an intermediate and hence without the possibility of forming 3-nitro-L-tyrosine. It is also possible to argue that the tyrosyl radicals react

preferentially with the hydroxyl radicals. Presumably any difference in reactivity may be accounted for by the fact that the unpaired electron density can exist on three atoms in $NO_2^{\bullet}$ compared with one in the case of $HO^{\bullet}$. In an analogous argument, the ambident nucleophilicity of nitrite accounts for the fact that it is a less powerful nucleophile compared with hydroxide ion. If an excess of nitrogen dioxide developed in the solution, this would be converted by the conventional hydrolysis reaction into nitrite and nitrate ions as represented in eqn. (7) but, from the ^{15}N NMR spectrum, this is unlikely to be the predominant mechanism for the formation of nitrate ions.

$$2 \cdot NO_2 \longrightarrow N_2O_4 \xrightarrow{H_2O} NO_2^{\ominus} + NO_3^{\ominus} + 2H^{\oplus} \qquad (7)$$

Since the dinitrogen tetraoxide in eqn. (7) is formed from nitrogen dioxide radicals that have escaped from the radical pair, the nitrogen nuclei in this molecule and in the nitrite and nitrate ions formed from it must carry with them the nuclear polarisation present in the original nitrogen dioxide radicals. Nitrate ions formed *via* this pathway should therefore give an emission signal. However, it is quite likely that while some nitrate ions are formed in this way, the majority result from recombination of the geminate radical pair. The net observed signal would be the sum of the smaller emission contribution and the larger enhanced absorption contribution. The irregular initial rise in intensity of the nitrate signal, most obvious in Fig. 2.8, is probably best explained in terms of the subtle balance between these two contributions.

2.2.5 Other observed phenomena

On occasions during early experiments, a signal approximately 1.5 ppm downfield from nitrite appeared which exhibited oscillation between emission and absorption with a period of approximately 30 min (Fig. 2.9).

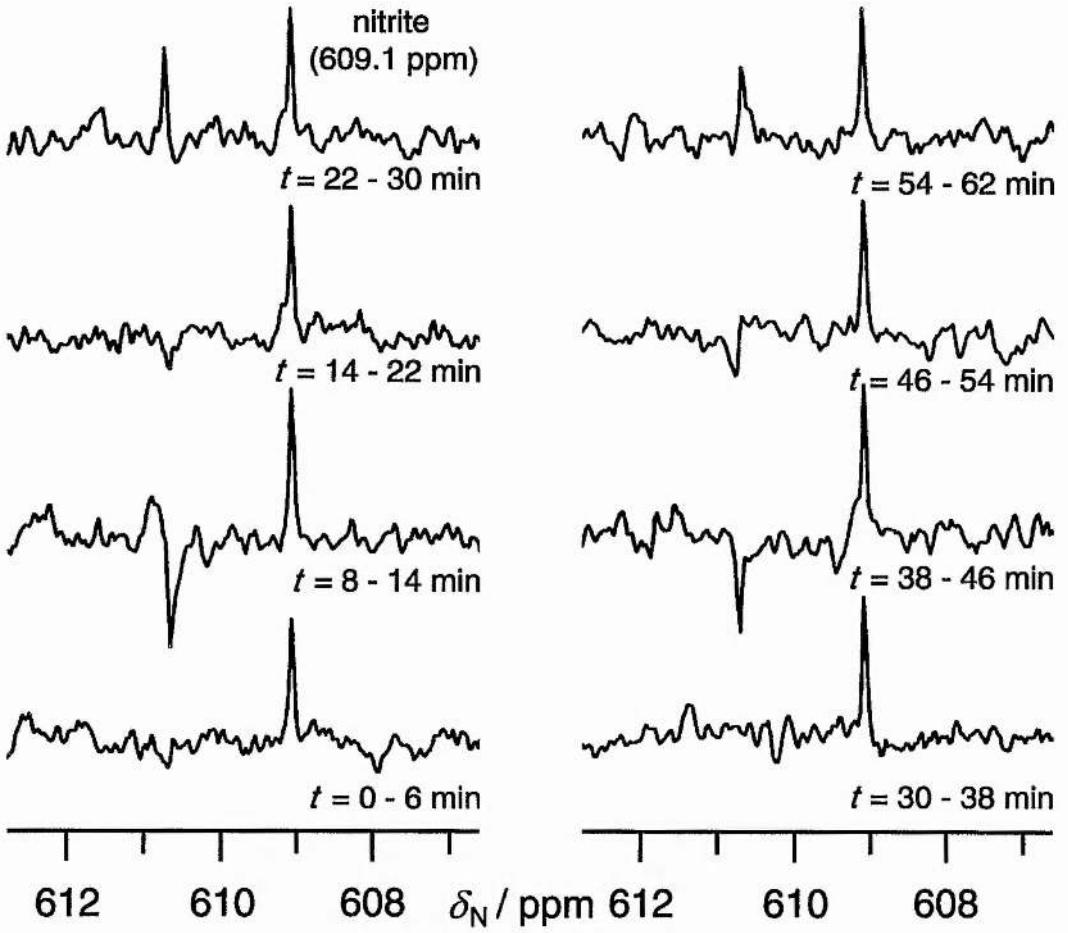

Fig. 2.9 Time course of an oscillating signal observed in the ^{15}N NMR spectrum recorded on addition of peroxynitrite (approx. 0.1 M) to L-tyrosine.

All the peroxynitrite appeared to have reacted within 2–3 min of initiating the run and very little nitrate was formed. It is difficult to find a reasonable explanation for the nature of this phenomenon which may be generated either by the chemistry of the system or through the characteristics of the NMR parameters. The proximity of the chemical shift to nitrite would tend to indicate a species with a similar chemical and thus magnetic shielding environment around the nitrogen atom. In this respect the most reasonable candidates for the signal are N_2O_4, formed by dimerisation of free nitrogen dioxide radicals or nitrosyl peroxynitrite (ONOONO). Normally it is not

possible to observe radicals (such as nitrogen dioxide which differs from nitrite by only one electron) in NMR spectra unless their lifetime is greater than about 10^{-4} s.

It might be intuitively expected that hydrolysis of N_2O_4 in aqueous alkaline solution would be very fast and thus formation of dinitrogen tetraoxide would be kinetically disfavoured in this medium. However in a study of the *N*-nitrosation and nitration of aqueous piperidine by N_2O_3 and N_2O_4, Challis and Kyrtopoulos[120] report that hydrolysis of N_2O_4 in aqueous solution was slower than expected, and in particular, not catalysed by hydroxide ion. Furthermore, in water at 20 °C, the rate of recombination[121] of $NO_2^{\bullet}$ is 4.5×10^8 M^{-1} s^{-1} and $K_{N_2O_4} = 1.53 \times 10^{-5} mol^{-1}$. Challis and Kyrtopoulos conclude that under aqueous alkaline conditions, significant nitration by $NO_2^{\bullet}$ can be ruled out because hydrolysis produces an excess of NO_2^- over NO_3^- whenever $NO_2^{\bullet}$ is present *and* reacting with water. In addition, N_2O_4 is thought to exist in two geometrically isomeric forms and that the nitro-nitro isomer is formed as a result of the recombination of $NO_2^{\bullet}$ in aqueous solution. However this signal can not arise from recombination of $NO_2^{\bullet}$ as this would not produce the phase characteristics observed. Nitrosyl peroxynitrite has been considered before as a potential intermediate in reactions of nitrogen dioxide with alkenes[122] but there is no physical evidence for this species and quantum mechanical calculations by Ridd and co-workers[123] and McKee[124] conclude that it is too unstable to be an effective intermediate. The only other likely explanation is a spectrometer artefact. It is generally possible to infer from the linewidth of a signal whether it is due to a genuine chemical moiety or a spurious signal or 'spike'. In many of the spectra reported here, a signal appears at δ_N 131.0 (501.3) ppm due to the transmitter offset. Apart from extraneous noise, which did not appear to a significant extent in this acquisition, no other signals are unaccounted for. In addition, the linewidth of the oscillating signal was the same as that measured for nitrite. Hence the only sensible conclusion to be

drawn from this evidence is that the oscillating signal is an artefact of the particular spectrometer conditions used in this experiment.

2.2.6 NMR experiments with substrate contained in frozen buffer solution

This technique has been used by Ridd and co-workers[125] to observe ^{15}N nuclear polarisation in reactions where the speed would otherwise make this difficult such as where peroxynitrite reacts at pHs below 9. The spectral changes in reactions where the mixture is initially frozen are more complicated than those in the experiments described previously and thus need to be treated with extra caution. There are several straightforward reasons for this. The presence of D_2O is required to obtain a frequency lock signal on the spectrometer. Although Ridd and co-workers initially kept both components of the reaction frozen, in this work, the aqueous ^{15}N peroxynitrite containing approximately 10% D_2O was initially in the liquid phase in order to achieve a satisfactory frequency lock signal at the beginning of the run. As the frozen solution melts, the temperature of the reaction mixture changes to a large enough extent to cause the lock signal to drop from between typically 25–30% at the beginning of the experiment to around 5–10% at the end. This effect causes the intensity of all the detected signals to alter during the course of the temperature change. Most importantly the intensity of the external reference signal will concomitantly change, when all other things being equal, it ought not to. However, these phenomena can be accommodated by reporting the intensities as a ratio of the reference if this is necessary to aid interpretation of the results. Although the change in lock level will affect the intensity of the external reference signal to a different extent than the species in the reaction mixture, the difference is slight enough to allow the correction to be valid for the purpose of comparing intensity changes in a non-quantitative sense. No changes are observed in chemical shift with temperature for

any of the species present. Detection of signals is made very difficult due to the low-sensitivity characteristics of this particular system. The intrinsic sensitivity of ^{15}N NMR is low compared to ^{1}H NMR (Table 2.1). In addition to this, acquisition time for individual spectra is only 4½ min. Given that signal to noise ratio increases proportional to the square root of the number of transients, then poor signal to noise ratios can be expected with such small acquisition times.

2.2.6.1 Decomposition of [^{15}N] peroxynitrite in frozen phosphate buffer (final pH 7.6)

This experiment was carried out as a control so effects due to nuclear polarisation observed in the presence of substrates can be compared with any effects that occur when no substrate is present. Fig. 2.10 shows the signals from the first five individual acquisition periods phased consistent with previous figures and stacked horizontally.

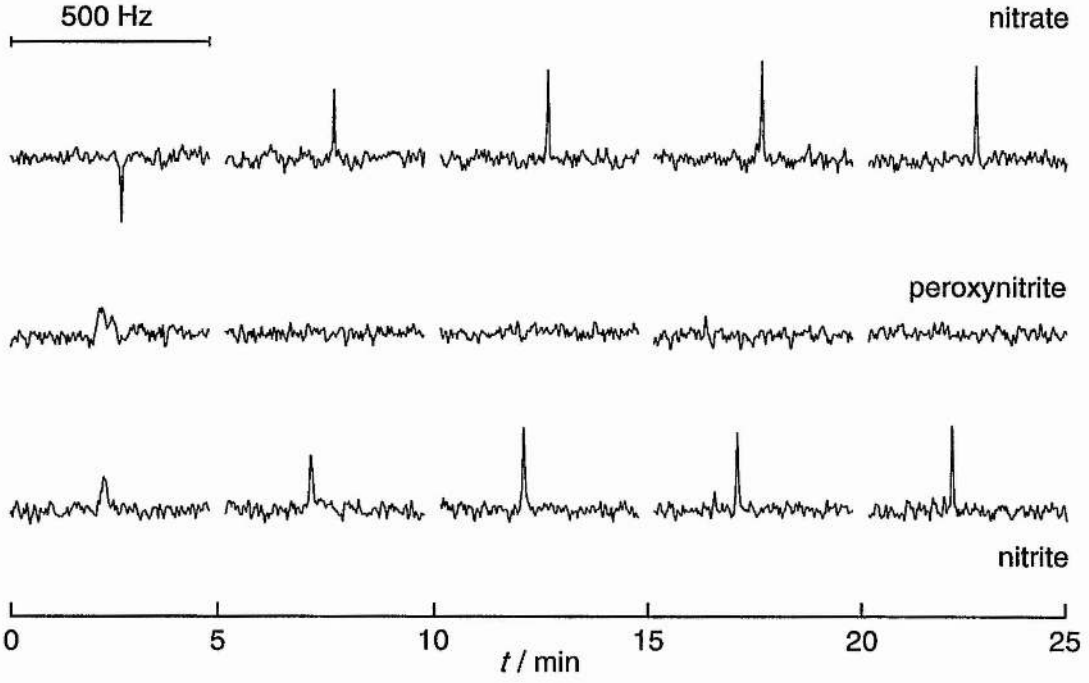

Fig. 2.10 Time course of the ^{15}N NMR signals in the reaction of alkaline peroxynitrite (approx. 0.10 M) with frozen phosphate buffer.

Table 2.5 Summary of the characteristics of the ^{15}N NMR spectrum in Fig. 2.10.

Signal	δ_N/ppm	Summary of CIDNP effects
NO_2^-	238.8 (609.1)	Possible initial E
$ONOO^-$	184.2 (554.5)	No obvious enhancement
NO_3^-	5.7 (376.0)	$V_{max} \simeq -1.6$

2.2.6.1.1 Mechanistic interpretation of spectral changes

It is not obvious how nitrite ions could be formed since the expected stoichiometry of the decomposition should lead only to nitrate ions. Another remarkable feature of the reaction was that the initial signal for the nitrate ions appeared in emission but there was no sign of nuclear polarisation in the signals for nitrate, nitrite and peroxynitrite ions. A possible explanation of the stoichiometry of the reaction is shown in Scheme 2.10. This argument is based on the fact that, at approximately pH 7, there will be a significant concentration of peroxynitrous acid in solution. The assumption is then made that when hydroxyl radicals are generated in the presence of peroxynitrous acid, one of the major reaction paths is hydrogen abstraction by the hydroxyl radicals. The resulting nitrosodioxyl radicals then dimerise and the dimer breaks down by loss of dioxygen. the overall stoichiometry of this reaction depends on partitioning of the $HO^{\bullet}$ and $NO_2^{\bullet}$ radicals produced in the first step between recombination within the radical pair to form nitric acid and escape into the solution. However, significant concentrations of nitrite ions could be formed. This explanation also requires that the signal for the nitrite ions displays polarisation in the same sense, but the relaxation time of this species may be much less due to its greater basicity.

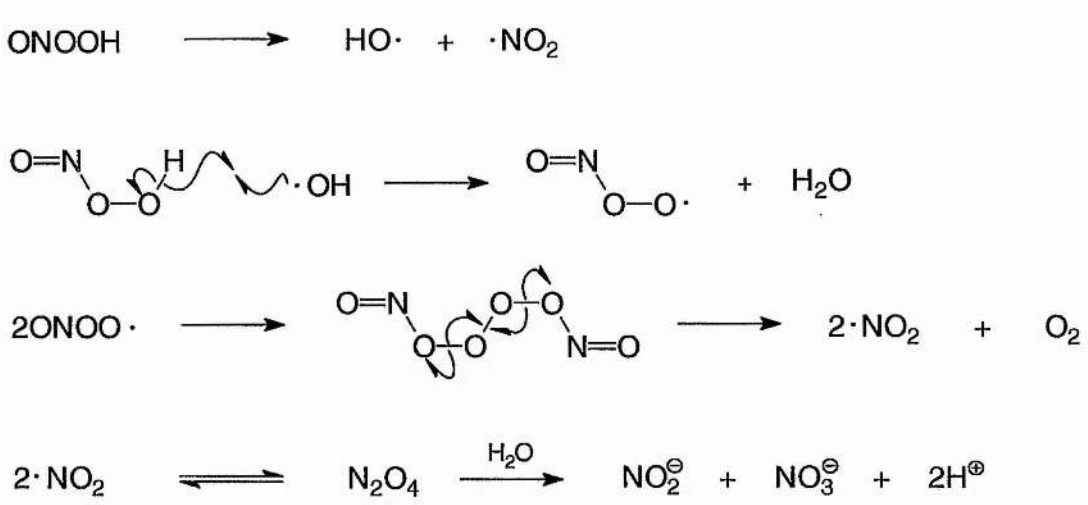

Scheme 2.11

It is more difficult to explain the emission signal on the nitrate ions that occurs in the first acquisition period, but it may be significant that some of the nitrate ions produced by the reactions in Scheme 2.11 must derive from nitrogen dioxide radicals that have escaped from the initial radical pair and are therefore polarised in the direction required to give an emission signal.

Since the nitrosodioxyl (peroxynitrite) radical has cropped up once more, it may be worthwhile to discuss two matters which may be related by it. Beckman and co-workers have estimated the standard reduction potential of the nitrosodioxyl radical to peroxynitrite anion[61] to be + 0.43 V. Hence the reverse process, *i.e.* oxidation of peroxynitrite anion to the radical will have a redox potential of – 0.43 V. It has been reported by Hughes *et al.*[117] that Cu^{2+} ions can bring about the catalytic decomposition of peroxynitrite to nitrite and oxygen, with ONOO· suggested as a potential intermediate. Since around 75% of the peroxynitrite was converted to nitrite, then it does not seem unreasonable to suggest that the dimerisation pathway outlined in Scheme 2.11 may also be in operation, yielding some nitrate. At pH 7.0 and 25 °C, the reduction potential of Cu^{2+} to Cu^{+} ($E^{\ominus}$ = + 0.15 V) is not positive enough to render the

oxidation of peroxynitrite spontaneous. If only *standard* reduction potentials are considered then other transition metal ion couples which may also effect the catalytic oxidation of $ONOO^-$ to $ONOO\cdot$ are Ag^{2+}/Ag^+ ($E^\ominus = +1.98$ V), Co^{3+}/Co^{2+} ($E^\ominus = +1.82$ V), Fe^{3+}/Fe^{2+} ($E^\ominus = +0.77$ V), Mn^{3+}/Mn^{2+} ($E^\ominus = +1.51$ V) and Pb^{4+}/Pb^{2+} ($E^\ominus = +1.69$ V). The Sn^{4+}/Sn^{2+} redox potential ($E^\ominus = +0.15$ V) is similar to the Cu^{2+}/Cu^+ value.

It is intriguing to note that Ingold and co-workers[126] theorize that the formation of methanol from the reaction of peroxynitrite and DMSO may involve the trapping of methyl radical by dioxygen illustrated in eqns. (8) and (9).

$$CH_3^{\cdot} + O_2 \longrightarrow CH_3OO\cdot \quad (8)$$

$$2CH_3OO\cdot \longrightarrow CH_3OH + CH_2O + O_2 \quad (9)$$

Pfeiffer *et al.*[127] have proposed an alternative mechanism for the formation of dioxygen during the decomposition of peroxynitrite (represented in Scheme 2.12).

$$ONOOH \longrightarrow HO\cdot + \cdot NO_2$$

$$HO\cdot + ONOOH \longrightarrow H_2O + \cdot NO + O_2$$

$$\cdot NO_2 + \cdot NO \longrightarrow N_2O_3$$

$$N_2O_3 + H_2O \longrightarrow 2NO_2^{\ominus} + 2H^{\oplus}$$

Scheme 2.12

However, this mechanism cannot be applicable under the conditions employed by Ingold and co-workers. In their experiments, the concentration of DMSO was very much greater than the concentration of peroxynitrite so the reaction of hydroxyl

radical with peroxynitrous acid would not occur. The mechanism must also be rejected in this case since it does not account for the observed stoichiometry.

2.2.6.2 Reaction of [^{15}N] peroxynitrite with L-tyrosine in frozen phosphate buffer (final pH 9.30)

Enhancements in the same sense as with L-tyrosine at pH 12.5 can be observed in Fig. 2.11. However, the lock signal decreases as the temperature increases.

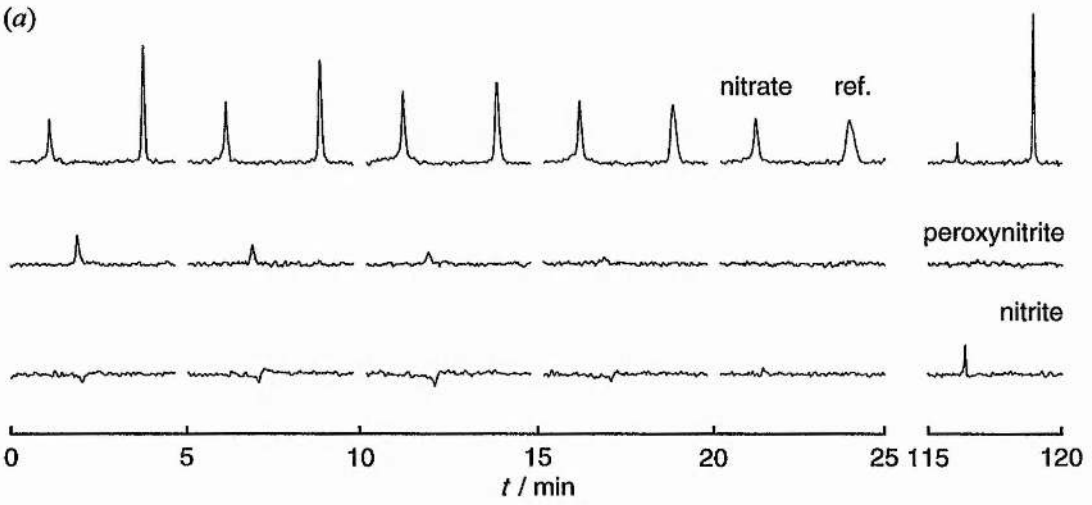

Fig. 2.11 Time course of the ^{15}N NMR signals in the reaction of alkaline peroxynitrite (approx. 0.10 M) with L-tyrosine (0.0181 g, 0.05 M) in frozen phosphate buffer. (*a*) Spectra phased consistent with previous figures with individual signals displayed stacked horizontally. (*b*) Raw spectral arrays.

Table 2.6 Summary of the characteristics of the ^{15}N NMR spectra shown in Fig. 2.11.

Signal	δ_N/ppm	Summary of CIDNP effects
NO_2^-	238.8 (609.1)	$V_{max} \simeq -1.7$
$ONOO^-$	184.2 (554.5)	No obvious enhancement
NO_3^-	5.7 (376.0)	$V_{max} \simeq 4.3$

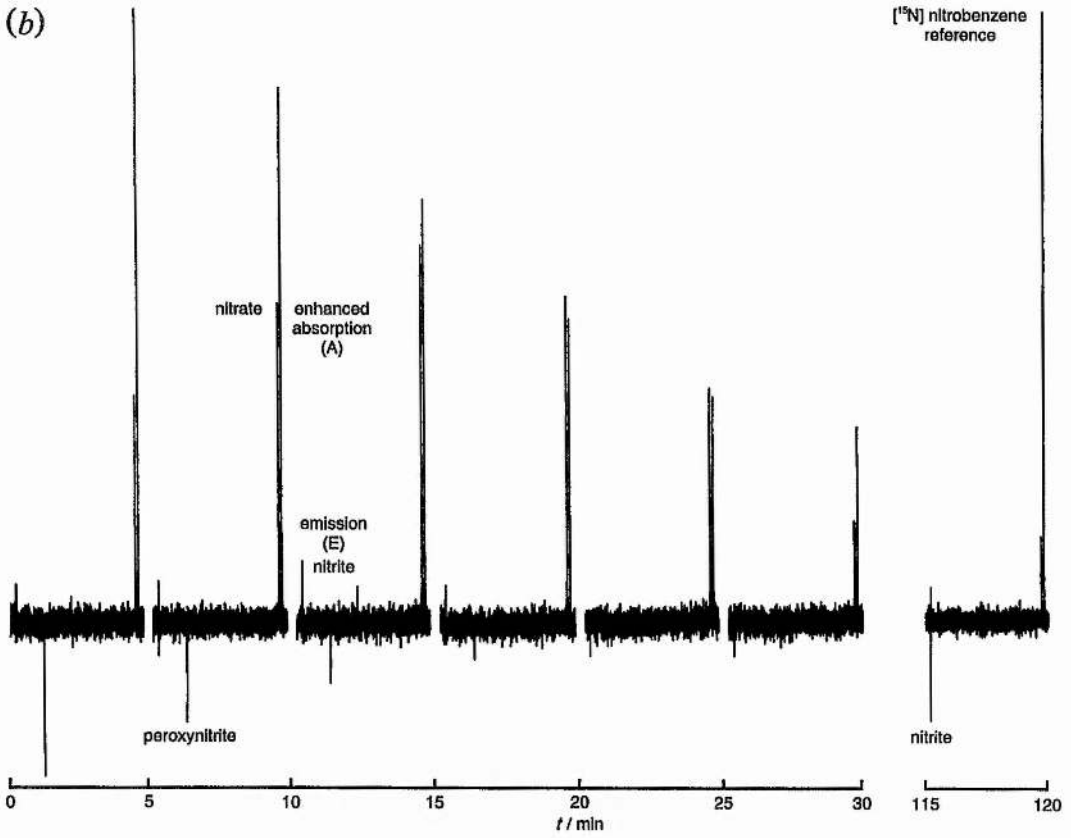

2.2.6.3 Reaction of [^{15}N] peroxynitrite with *O*-methyl-L-tyrosine in frozen phosphate buffer (final pH 9.18)

No CIDNP effects could be observed on any of the signals when peroxynitrite was reacted with *O*-methyl-L-tyrosine at this pH or at pH 7.6. However the formation of 3-nitro-*O*-methyl-L-tyrosine was observed as the characteristic yellow/orange colour.

2.2.6.4 Reaction of [^{15}N] peroxynitrite with L-alanyl-L-tyrosyl-L-valine in frozen phosphate buffer (final pH 7.6)

No enhancement of the ^{15}N NMR signals due to nuclear polarisation could be observed at this pH.

2.2.7 Reaction of [^{15}N] peroxynitrite with frozen bicarbonate buffer (final pH 11.86)

The spectral arrays illustrated in Fig. 2.12 show the changes observed on adding alkaline peroxynitrite to sodium bicarbonate buffer. No signal is present for the reference, [^{15}N] nitrobenzene. This was due to the glass capillary becoming lodged up the NMR tube and thus out of the probe by surface tension of the liquid. It is important to have the reference present when the lock signal alters during a run to provide a comparison of signal intensities. A repeat run with the reference in place produced similar signals.

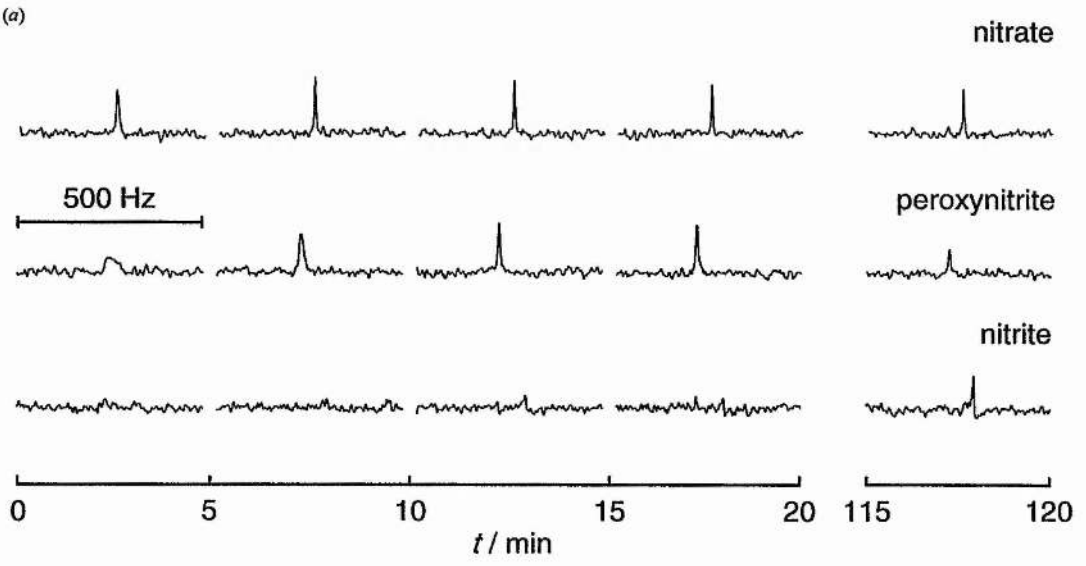

Fig. 2.12 Time course of the ^{15}N NMR signals in the reaction of alkaline peroxynitrite (approx. 0.10 M) with frozen sodium bicarbonate buffer. (*a*) Spectra phased consistent with previous results with signals displayed stacked horizontally. (*b*) Raw spectral arrays.

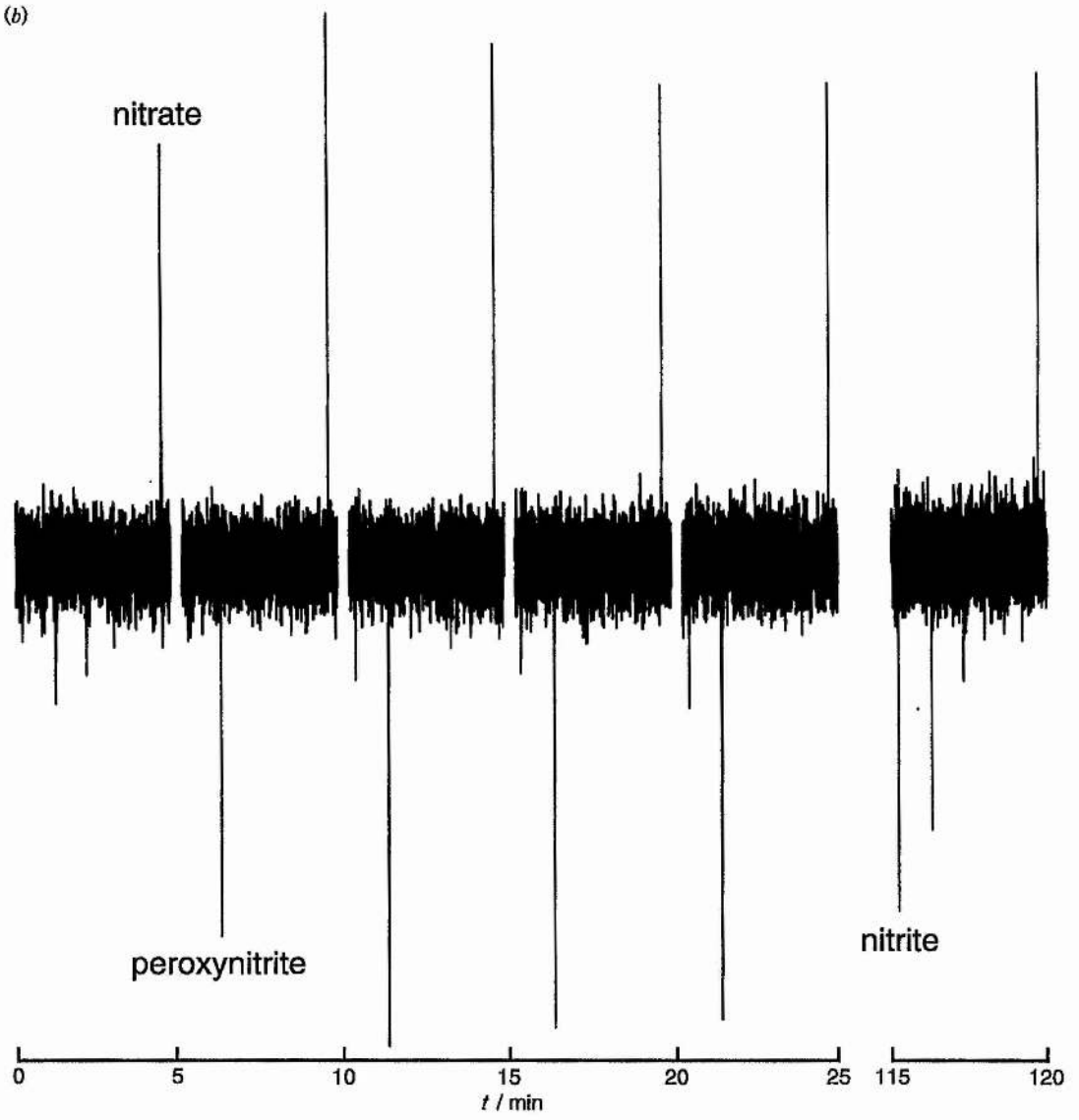

Table 2.7 Summary of the characteristics of the ^{15}N NMR spectra illustrated in Fig. 2.12.

Signal	δ_N/ppm	Enhancement	Phase Change
NO_2^-	238.9 (609.2)	No	No
$ONOO^-$	184.4 (554.7)	Unlikely	No
NO_3^-	5.8 (376.1)	No	No

2.2.7.1 Mechanistic interpretation of spectral changes

It is difficult to draw useful conclusions for this reaction from a mechanistic aspect, but from the presence of a significant peroxynitrite signal after 115 min, the reaction is probably too slow to show significant nuclear polarisation. Therefore the increase in intensity for this signal from the start of the reaction, followed by its steady decay over the course of the second hour is probably due to sharpening of an initially broad signal followed by the slow conversion to nitrate and nitrite.

2.2.8 Reaction of $Na^{15}NO_2$ and NaOCl with L-tyrosine (final pH 7.0)

Eiserich *et al.*[128] have fuelled the recent debate of whether peroxynitrite should be considered as the main RNS responsible for tyrosine nitration by proposing that this reaction may be important in mammalian immune systems. Activated macrophages produce both nitrite and hypochlorous acid (by the action of myeloperoxidase on hydrogen peroxide). Although it is well established that the 6–step reaction occurs by transfer of Cl^+ (*via* intermediate formation of NO_2Cl,[‡]) and not an oxygen atom it is convenient at this stage to represent the overall process by eqn. (10).

$$OCl^{\ominus} + NO_2^{\ominus} \longrightarrow Cl^{\ominus} + NO_3^{\ominus} \qquad (10)$$

Unfortunately, no CIDNP effects could be observed in ^{15}N NMR experiments on the reaction of 0.1 M solutions of NaOCl and $Na^{15}NO_2$ with L-tyrosine in pH 7.4 phosphate buffer. The results of these experiments were erratic, depending unpredictably on the way in which the solutions of NaOCl and sodium nitrite/L-tyrosine in pH 7.4 buffer were mixed. On occasions, the yellow colour of 3-nitro-L-tyrosine formed steadily over 10–15 min, on others the colour formed almost

[‡] This will be further discussed in chapter 3, where references to the original work on the mechanism may be found.

immediately on mixing the solutions. No product could be detected in the ^{15}N NMR spectrum, evidently due to the low yield as with the peroxynitrite reactions. It was also noted that a large proportion of the nitrite did not react, even when the temperature of the reaction was maintained at 50 °C for up to an hour after mixing. Premixed solutions of sodium nitrite in pH 7.4 phosphate buffer and NaOCl had poor nitrating capability presumably since the hypochlorite oxidised the nitrite within 5–10 min. It is interesting to note that when a thiol such as NAP is substituted for L-tyrosine, the dichroic red-green colour of the corresponding *S*-nitrosothiol is observed. Due to the erratic behaviour of this system, no attempts at product identification or quantification were made.

2.2.9 Mechanisms of tyrosine nitration not involving peroxynitrite

Gunther *et al.*[39] have provided evidence which lends credence to an alternative *in vivo* mechanism for formation of 3-nitro-L-tyrosine from nitric oxide which does not require peroxynitrite as an intermediate (Scheme 2.13). There is *in vivo* precedent for this pathway as the same workers have detected tyrosine iminoxyl radicals in the photosystem II/NO system and in prostaglandin H synthase-2 (PHS-2).

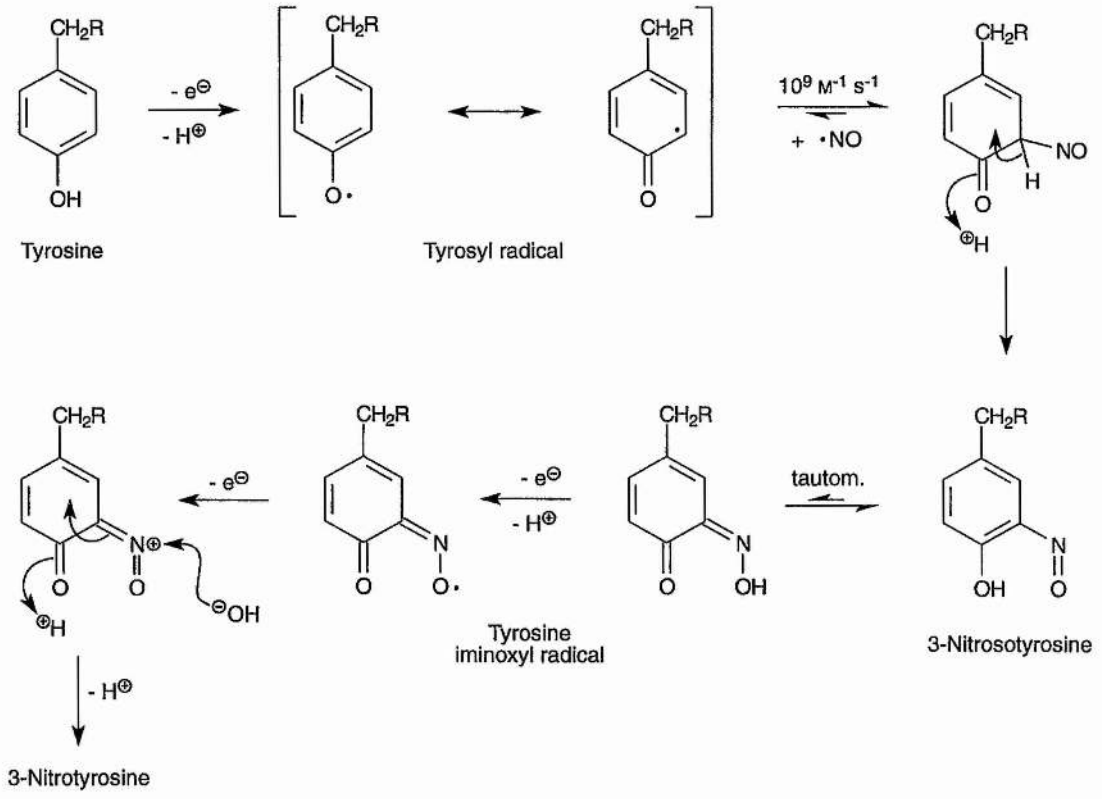

Scheme 2.13

The EPR spectrum of the tyrosine iminoxyl radical was obtained as evidence for the proposed reaction scheme; the Wheland intermediate being EPR-silent. However, although the source of the oxidising equivalents for the oxidations of 3-nitroso-L-tyrosine and the iminoxyl radical were not identified, it is conceivable that hydroxyl radical may be implicated here. Although this work does cast some doubt on the specificity of 3-nitro-L-tyrosine as an assay for peroxynitrite production, the bulk of evidence still points to the peroxynitrite pathway as the major contribution.

2.2.10 Reaction of peroxynitrite with thiols and *S*-nitrosothiol decomposition

The reaction of peroxynitrite with biotarget thiols such as glutathione, penicillamine and the cysteine residues in human serum albumin may be important in two respects. It may represent a significant deactivation pathway for peroxynitrite produced in response to stimulation of the immune system in addition to being a potentially

important means of nitric oxide transport. A certain amount of inconsistency exists in the literature as to whether peroxynitrite can bring about thiol nitrosation. However, in this work, *S*-nitrosothiols produced by the reaction of peroxynitrite with thiols have been unambiguously identified by their characteristic UV-visible spectra (shown in Fig 2.13 with λ_{max} = 340–360 nm and $\varepsilon \simeq 1000$ M^{-1} cm^{-1}) and the concomitant dichroic red–green colour they impart to solutions.

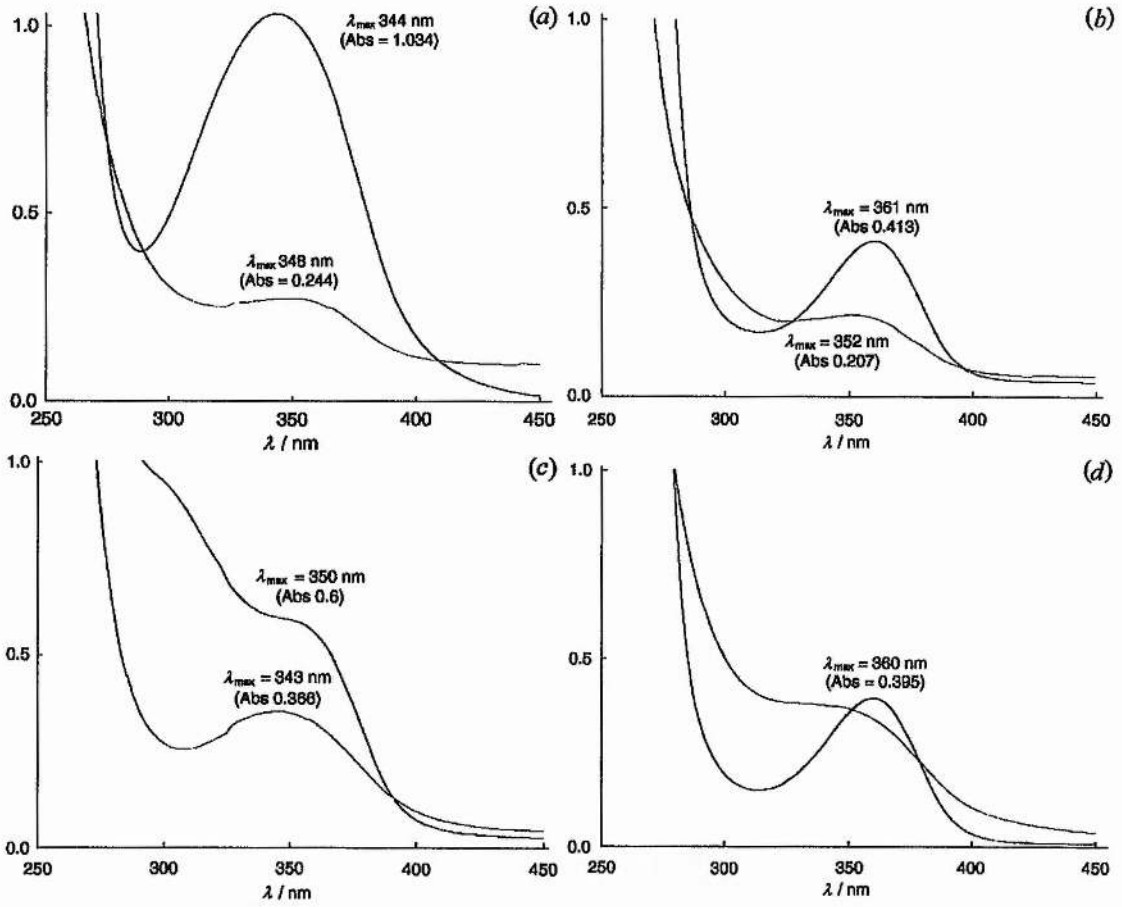

Fig. 2.13 UV-visible spectra resulting from the reaction of alkaline peroxynitrite (6.2 mM) with (*a*) *N*-acetyl-DL-cysteine, (*b*) DL-penicillamine, (*c*) *N*-acetyl-DL-penicillamine and (*d*) L-cysteine. [Thiol] = 62 mM. The smaller absorbances resulted from reaction in pH 7.4 phosphate buffer.

Table 2.8 Amount of *S*-nitrosothiol produced on reaction of alkaline peroxynitrite with various thiols at pH 12.5 and pH 7.4 (data from Fig. 2.13).

	pH 12.5		pH 7.4	
Thiol	[RSNO]/mM	% of $ONOO^-$	[RSNO]/mM	% of $ONOO^-$
N-Acetyl-L-cysteine	1.03	16.7	0.24	3.9
D-Penicillamine	0.41	6.7	0.21	3.3
N-Acetylpenicillamine	0.60	9.7	0.36	5.8
Glutathione	0.578	9.3	—	—
L-Cysteine	0.37	6.0	0.39	6.4

It is apparent from the data in table 2.8 that at alkaline pH, about 10% of the peroxynitrite ends up as *S*-nitrosothiol. (The concentration of *S*-nitrosothiol has been calculated using 1000 M^{-1} cm^{-1} as an average value for the molar extinction coefficient of the -SNO group). This figure drops to about 5% as the pH approaches 7.4 when more peroxynitrite will be protonated and decomposition to form nitrate and nitrite will be more competitive. It is convenient to consider the maximum *S*-nitrosothiol yield as being approximately equivalent to the amount of N_2O_4 (as nitrosyl nitrate) derived from free $NO_2^{\bullet}$ available to bring about nitrosation.

2.2.10.1 Reaction of [^{15}N] peroxynitrite with *N*-acetyl-DL-penicillamine in frozen phosphate buffer (final pH 7.1)

The fast rates of reaction of common thiols with peroxynitrite at room temperature and above (Table 2.8) preclude any observation of nuclear polarisation in the ^{15}N NMR spectrum.

Table 2.9 Second order rate constants for the reaction of alkaline peroxynitrite (final concentration 3.11 mM) with a range of thiols (final concentration 31.1 mM). Followed at 340 nm (pH 10.5 temp. 25 ± 0.1 °C).

Thiol	k_2/ M^{-1} s^{-1}	–SH pK_{a_2}	$t_{½}$/s
DL-Penicillamine	1,740 ± 1.7[a]	7.95[c]	4.5
N-Acetyl-DL-penicillamine	152 ± 0.3[a]	8.0	47
Glutathione	13,060 ± 34[a]	8.72[d]	0.10
N-Acetyl-L-cysteine	7.4 ± 0.05[a]	9.76[e]	20
L-Cysteine	5,900 ± 160[b]	8.21[d,f]	0.03

[a] ref. 129, [b] ref. 40 (measured at 37 °C), [c] ref. 130, [d] ref. 131, [e] ref. 132, [f] ref. 133.

The pH dependence of the second order rate constant as determined by Radi *et al.*[40] for L-cysteine suggests that the undissociated form of the thiol reacts with peroxynitrite anion. The reaction can be described by eqn. (11).

$$k_{obsd} = k_2 \frac{K_{a_1}}{\left(K_{a_1} + [H^+]\right)} \frac{[H^+]}{\left(K_{a_2} + [H^+]\right)} \qquad (11)$$

where k_{obsd} is the observed rate constant at a given pH, k_2 is the second-order rate constant for the reaction of thiols with peroxynitrite anion, K_{a_1} is the dissociation constant of peroxynitrite (6.8 at 37 °C) and K_{a_2} is the dissociation constant of the thiol.

In order to try to detect nuclear polarisation that may arise from the [^{15}N]peroxynitrite/thiol reaction due to contributions from a radical pathway, the technique of freezing the solutions was employed as in the previous experiments with

aromatic substrates. Fig. 2.14 shows the spectral changes during the reaction of [^{15}N] peroxynitrite with *N*-acetyl-DL-penicillamine.

The signal for the nitrate ions shows some signs of enhanced absorption, but there is no emission signal for the nitrite ions; however, the rapid growth of the signal for nitrite ions suggests that only the latter stages of the reaction are being observed, *i.e.* just after the point when the signal for the nitrite ions has passed from an emission signal to a conventional absorption signal. The reaction path is therefore probably the same as that previously described when L-tyrosine is the substrate.

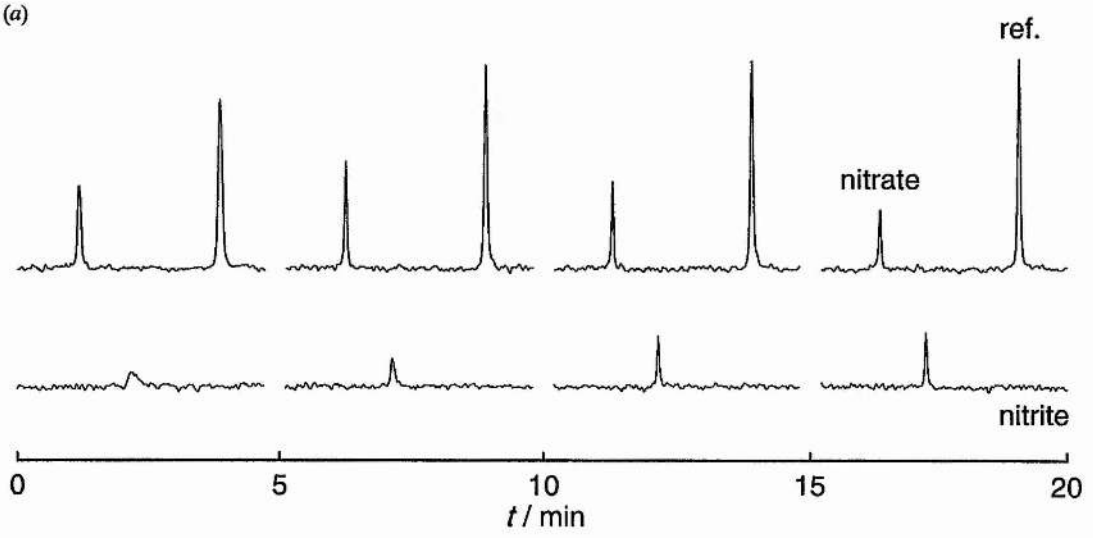

Fig. 2.14 Time course of the ^{15}N NMR signals in the reaction of alkaline peroxynitrite (approx. 0.10 M) with *N*-acetyl-DL-penicillamine (0.0191 g, 0.05 M). in frozen phosphate buffer. [NaOH] = 0.15 M. (*a*) Spectra phased consistent with previous figures with individual signals displayed stacked horizontally. (*b*) Raw spectral arrays.

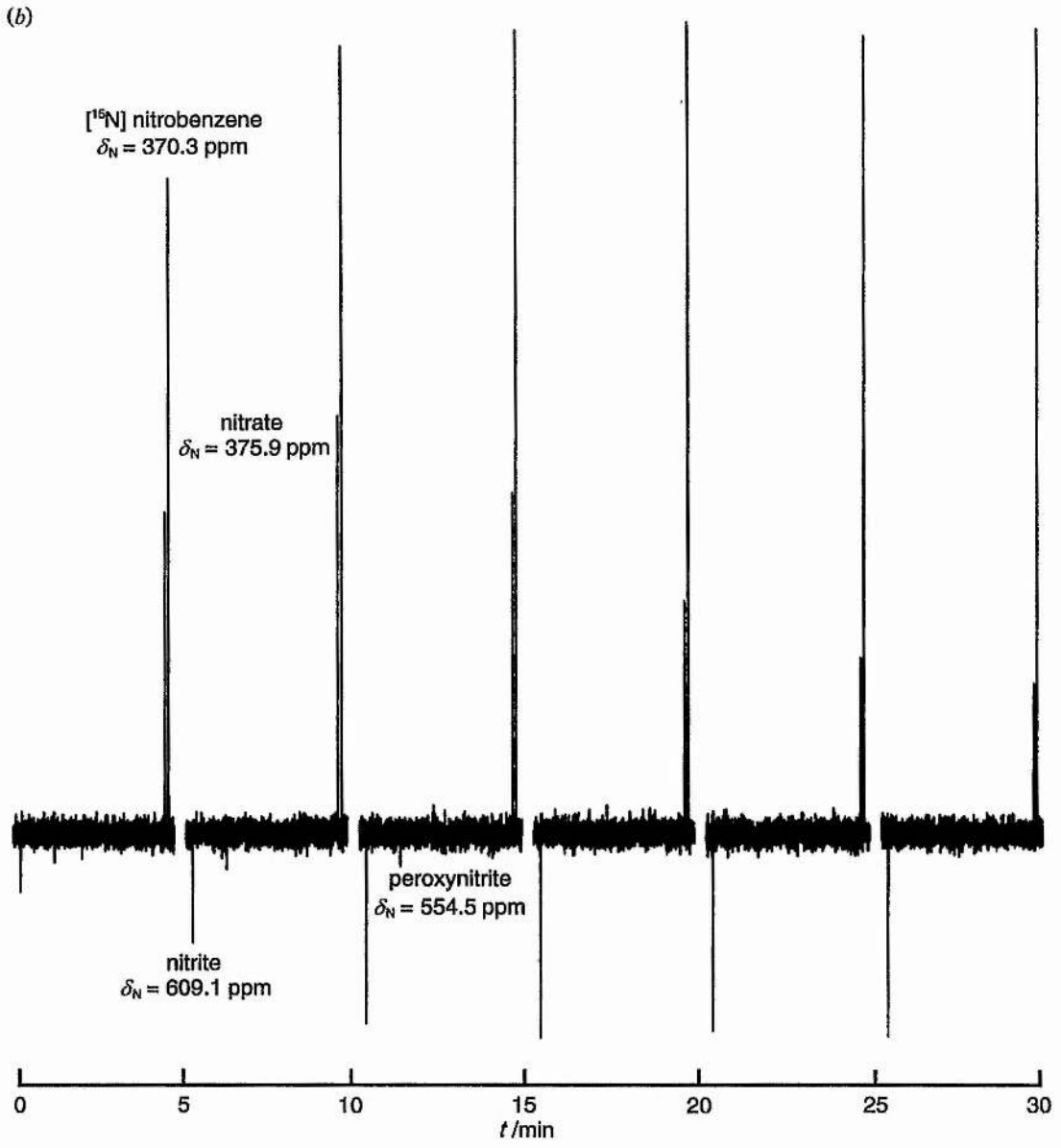

Table 2.10 Summary of the characteristics of the ^{15}N NMR spectra illustrated in Fig. 2.14.

Signal	δ_N/ppm	Enhancement	Phase Change
NO_2^-	238.9 (609.2)	Not observed	Not observed
$ONOO^-$	184.2 (554.5)	No	No
NO_3^-	5.7 (376.0)	$V_{max} \simeq 2.9$	No

Therefore the most appropriate question to address is by what mechanism(s) may peroxynitrite effect nitrosation of thiols? Williams[134] has written a short review on this topic. In principle, peroxynitrite could react with thiols *via* transfer of NO^+ in an S_N2 reaction displacing the peroxide ion (Scheme 2.14).

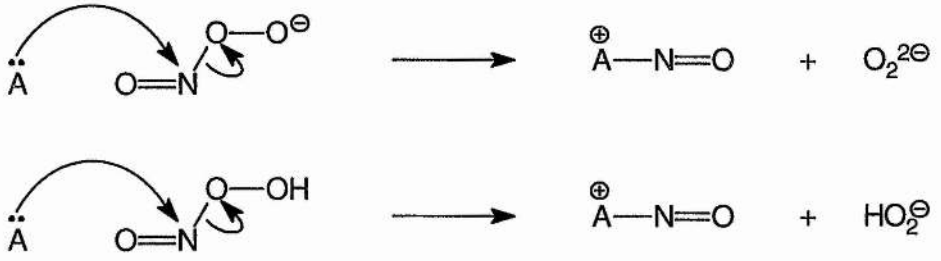

Scheme 2.14

However this pathway is highly unlikely as both species are very poor leaving groups therefore the reaction would be highly disfavoured on both thermodynamic and kinetic grounds. Williams draws an analogy between peroxynitrite and nitrous acid in that the latter species is not itself a nitrosating agent unless protonated to give the nitrous acidium ion such that the leaving group may be water.

The analogy ends there as protonated peroxynitrous acid, $ONO^+(H)OH$, would not exist due to the rapid isomerisation of peroxynitrous acid to nitrate at physiological pH. More likely mechanisms are illustrated in Scheme 2.15.

Pathway (*a*) in Scheme 2.15 is essentially analogous to that proposed earlier with ArO^- as the substrate. Sulfenyl radicals may be generated by an electron transfer either between $HO^\bullet$ or $NO_2^\bullet$ and thiolate ion. Williams concludes[134] that it is reasonable to assume some $NO_2^\bullet$ could become free from the peroxynitrite system and effect nitrosation *via* nitrosyl nitrate as shown in pathway (*b*).

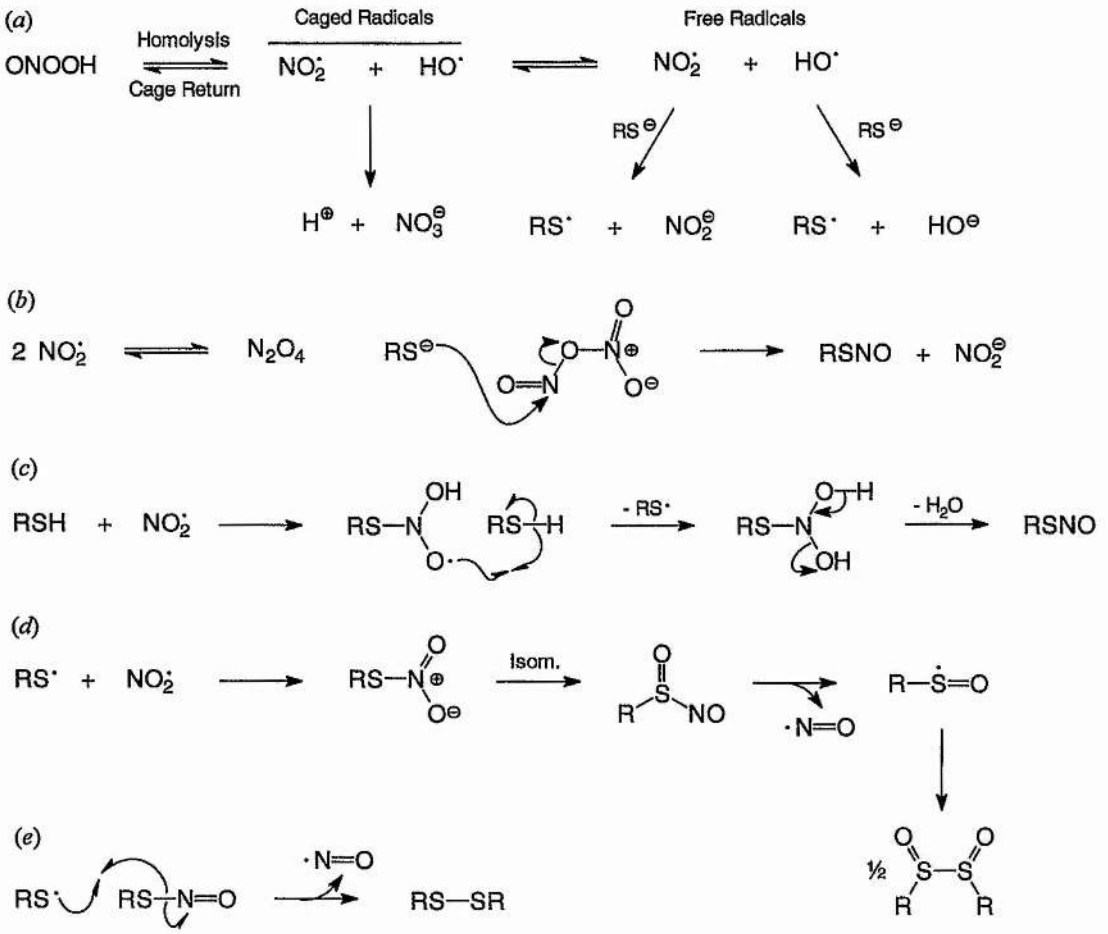

Scheme 2.15

A less likely, but nevertheless possible alternative mechanism is that proposed by Pryor *et al.*[135] Initial attack by $NO_2^{\bullet}$ (derived from homolysis of peroxynitrite) on RSH forms an (alkylthio)(hydroxy)aminoxyl radical. This reacts with a further molecule of thiol to generate an *N,N*-dihydroxyalkanesulfenamide and a sulfenyl radical. Loss of water yields *S*-nitrosothiol. Presumably formation of the kinetically stable disulfide shown in pathway (*e*) provides the driving force for release of NO. An alternative route to release of NO is illustrated in pathway (*d*). This involves isomerisation of the alkyl(nitro)sulfane to an alkyl(nitrosooxy)sulfane and then to an alkyl(nitroso)oxo-$\lambda 4$-sulfane. This may then undergo homolysis to an alkyl(oxo)-$\lambda 4$-sulfanyl radical. Dimerisation would form an *S,S'*-dialkyl-*S,S'*-dioxodi-$\lambda 4$-sulfane.

2.2.10.2 Decomposition of *S*-nitrosothiols

The decomposition of *S*-nitrosothiols has been shown to give different nitrogen-containing products according to the concentration of thiol present. At low or zero [RSH], nitric oxide is produced together with the disulfide, RSSH. However at high [RSH], the R-SNO is also reduced to RSSH, but the principal nitrogen-containing product becomes ammonia together with some N_2O. Clearly this has important ramifications for the toxicity of *S*-nitrosothiols such as glutathione and SNAP, currently undergoing clinical trials as NO-donor drugs, as the intracellular concentration of free and protein-bound RSH in blood plasma can reach millimolar levels. Although the intermediates in the high [RSH] mechanism have not been resolved, it is possible that NO^- (nitroxyl) is produced and may exist as trioxodinitrate (also known as oxyhyponitrite, nitrohydroxylamate, hyponitrate and Angeli's salt). This can account for the formation of both ammonia and N_2O (scheme 4.11). The ^{15}N chemical shift of trioxodinitrate has been determined by Garber *et al.*[136] to be δ_N – 274 ppm relative to nitrite (δ_N – 34.1 ppm relative to ^{15}N nitrobenzene or δ_N 335.1 ppm relative to liquid ammonia at 25 °C). Samples of ^{15}N *S*-nitroso-*N*-heptanoyl-DL-penicillamine (SNHP) and ^{15}N SNAP were prepared in order to ascertain if any intermediates in their decomposition could be identified by their ^{15}N NMR signals. The signal due to the -SNO group appeared at δ_N 466 ppm but suffered approximately fourfold linewidth broadening in both DMSO-d_6 (SNHP) and a 1:1 mixture of methanol and pH 7.4 phosphate buffer (SNAP). A typical value for the linewidth was 20 Hz as compared with 5 Hz for the reference. Since an increase in the width of the signal is accompanied by a decrease in the height by the same factor it is unsurprising that no CIDNP effects could ever be detected for the *S*-nitrosothiol signal. Contributions to broadening in aqueous solution will be made by the equilibria illustrated in Scheme 2.16. In DMSO, clearly hydrolysis will not be significant.

$$RSNO + H_2O \rightleftharpoons RSH + HNO_2$$

$$RSNO + NO_2^{\ominus} \rightleftharpoons RS^{\ominus} + N_2O_3$$

$$RSNO + R'SH \rightleftharpoons RSH + R'SNO$$

Scheme 2.16

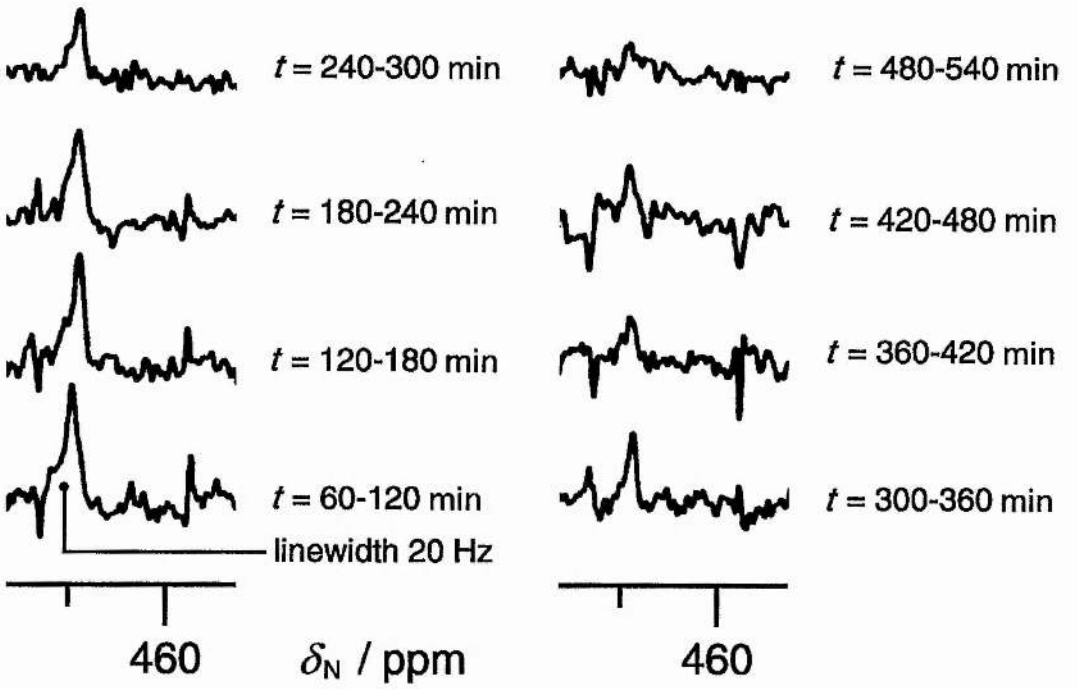

Fig. 2.15 Decomposition of [^{15}N] *S*-nitroso-*N*-acetyl-DL-penicillamine (0.1 g, 0.09 M) in the presence of *N*-acetyl-DL-penicillamine (0.15 g, 0.157 M). Solvent CH_3OH/phosphate buffer, pH 7.0.

Fig. 2.15 shows the time course of the ^{15}N signal for the -SNO group in the decomposition of ^{15}N SNAP in the presence of an excess of the parent thiol. No signals other than that for the nitrosothiol could be detected, a problem which was undoubtedly exacerbated by the occurrence of extraneous noise during the acquisition periods. Furthermore, a significant build up of pressure inside the NMR tube caused

the top to be ejected from the machine providing somewhat anecdotal evidence for the formation of gas in this reaction.

2.2.11 Synthetic procedures

A brief digression into the advantages of TMSI in peptide synthesis and its elegant chemistry seems appropriate in the context of a mechanistic discussion since this reagent is extremely versatile and attractive for this application. It will cleave many commonly encountered protecting groups cleanly and with a high yield of the desired product.

The synthetic strategy involved coupling N^{α}-*tert*-butoxycarbonyl-L-alanine to L-tyrosine benzyl ester, performing a hydrogenation to remove the benzyl ester and then coupling the product thus obtained to L-valine methyl ester. The protected tripeptide was then subjected to cleavage with trimethylsilyl iodide (TMSI) to remove the BOC group and the methyl ester. Mass spectra of the product obtained after 2.5 h reaction time with TMSI at 50 °C showed a mixture of fully protected starting material and methyl ester. Hence the reaction time was increased to 9 h with heating to 60–70 °C followed by stirring at room temperature for a further 12 h. In an early attempt at the synthesis of L-alanyl-L-tyrosyl-L-valine, a benzyl group was used to block the hydroxyl group of tyrosine to discourage formation of the phenyl ester in the first peptide coupling step with activated *tert*-butoxycarbonyl-L-alanine. The strategy was to cleave the *O*-benzyl group from tyrosine, the *tert*-butoxycarbonyl group from the alanine residue and the methyl ester from the valine residue simultaneously using three equivalents of trimethylsilyl iodide, rather than having to perform an acid-catalysed deprotecting step and risk rearrangement by acid catalysed benzylation of the aromatic ring by the benzyl carbocations thus formed.[137–139] It is well

documented[140] that TMSI cleaves benzyl ethers without any problems of rearrangement, but in fact it is unnecessary to block the tyrosine hydroxyl in this case as it is not reactive enough, under the conditions employed, to form significant amounts of undesired phenyl ester. However, the TMSI reagent was still useful in concurrent removal of both the *tert*-butoxycarbonyl group on the alanine and the methyl ester on the valine residue in a modified, simpler synthetic procedure. The reagent is vulnerable to hydrolysis by residual water that may be present in the solvent or in the atmosphere on transferral from the storage bottle, therefore a slight excess is used to ensure a stoichiometric quantity remains.

2.2.11.1 Mechanism of cleavage of *tert*-butoxycarbonyl esters (a monosubstituted *tert*-butyl carbamate)

As illustrated in Scheme 2.17, a transesterification reaction occurs in the first step to form, in this instance, *tert*-butyl iodide, and the corresponding trimethylsilyl carbamate. Quenching with methanol followed by spontaneous loss of CO_2 from the carbamic acid yields the free amine. Olah and Narang report in a review[141] that the lone pair of electrons on the nitrogen atom polarise the carbonyl group so as to favour interaction of the oxygen atom with the electrophilic silicon centre on the trimethylsilyl iodide. Thus, carbamates react faster with the reagent than the corresponding esters. Benzyl and *tert*-butyl carbamates as in this example are cleaved almost instantaneously at 25 °C. Due to the ability of iodide as a good leaving group, all the reactions take place *via* S_N2 pathways, thus intermediate carbocations are not formed and no rearrangement occurs. This is a useful characteristic because the most common benzyl and *tert*-butyl groups form particularly stable carbocations.

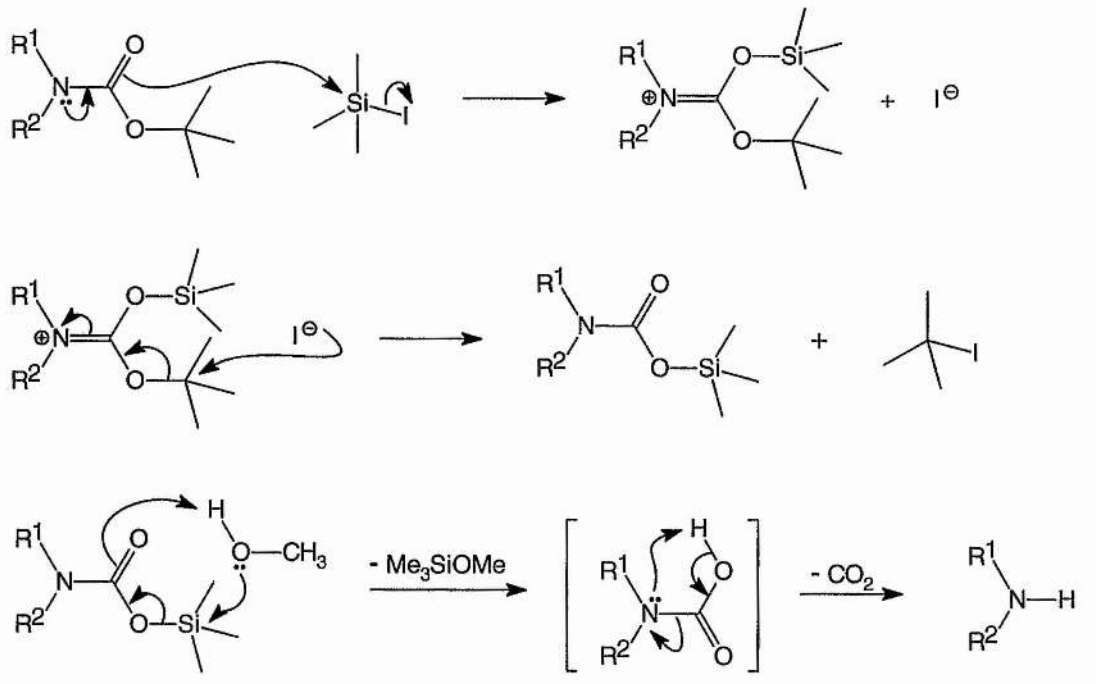

Scheme 2.17

2.2.11.2 Mechanism of cleavage of ethers (benzyl tyrosyl ether)

The mechanism here is trivial and exploits once again the affinity of silicon for oxygen (Scheme 2.18).

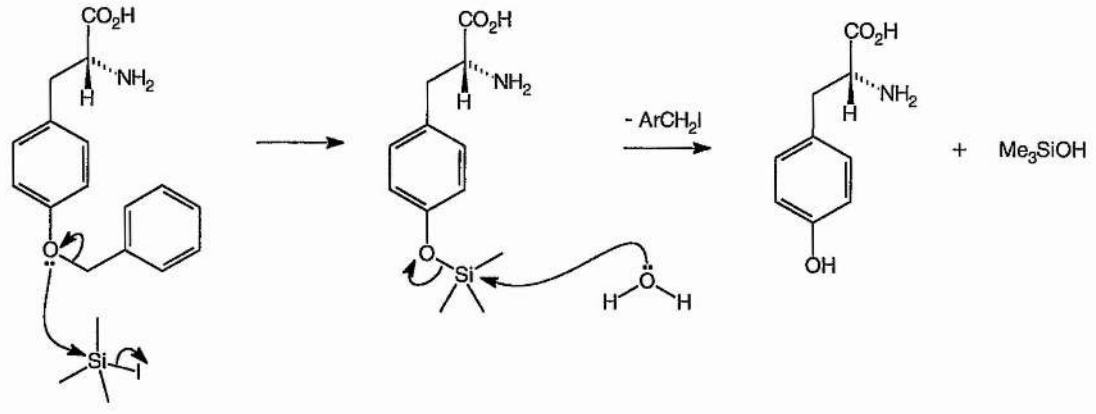

Scheme 2.18

Benzyl ethers, in addition to trityl (trimethylsilyl) and *tert*-butyl ethers react at a much faster rate than other alkyl ethers, hence they can be selectively cleaved. Stammer and

co-workers report that methyl esters require an excess of TMSI and elevated temperatures for reaction times in the region of one hour, and that in the case of Boc-Val-Tyr(Bzl)·OMe, 3.6 equivalents of TMSI at a temperature of 50 °C were required to cleave the methyl ester which did not begin to react until one hour had elapsed.

2.3 Conclusions

As has already been discussed, much doubt and speculation exists in the literature since the seminal discovery of Beckman *et al.*[33] in 1990 that peroxynitrite may be formed *in vivo* and undergo homolysis to hydroxyl and nitrogen dioxide radicals. It is surprising that detection of radicals in the peroxynitrite pathway was possible considering that the yield of radical products peaks close to pH 7.4 and falls off dramatically at higher pH. Since nitration of *O*-methyl-L-tyrosine by peroxynitrite is observed at pH 7.4 and the mechanisms postulated thus far cannot account for this behaviour, an alternative explanation is required. The possibility exists that peroxynitrite may act as a one-electron oxidant in a molecule assisted homolysis (MAH) reaction, directly transferring an electron to the substrate. The products would be a substrate radical (if the substrate carried a negative charge, *e.g.* RS^- or ArO^-) or a radical cation (if the substrate was neutral) and a radical-ion pair ($HO^{\bullet}/NO_2^-$ or $HO^-/NO_2^{\bullet}$). These possibilities are illustrated in Scheme 2.19. For reasons discussed earlier, the latter radical ion pair is more likely. An MAH mechanism, previously characterised in many systems,[142] has been proposed by Pryor to occur in the reaction of thiols with peroxynitrite.[16] This is consistent with the observed second order kinetics and the pH profile which suggests the mechanism involves RS^- as the electron donor and ONOOH as the electron acceptor rather than $ONOO^-$ and RSH.

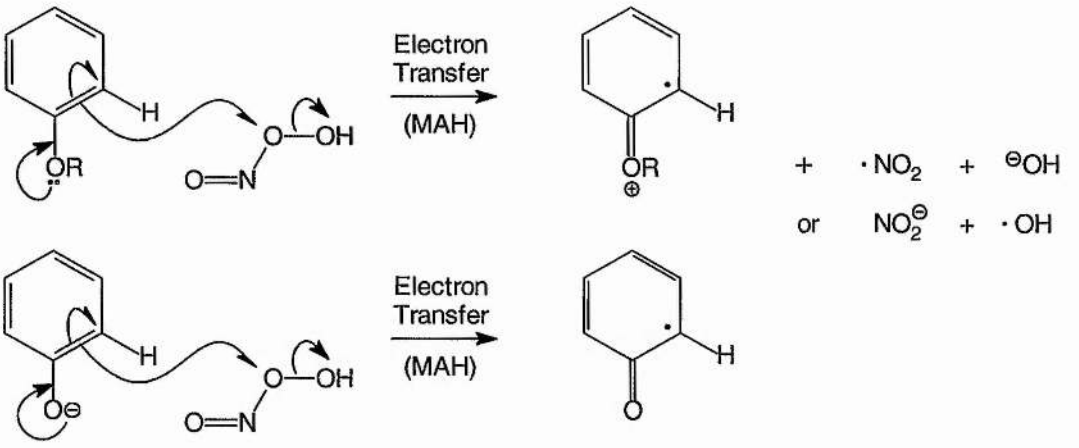

Scheme 2.19

The mechanisms proposed are not in conflict with findings that have otherwise proved contentious in the literature. The cage mechanism can account for the fact that scavengers cannot trap a stoichiometric quantity of radicals since cage recombination occurs at a faster rate than bimolecular reactions. MAH reactions can produce hydroxyl-like adducts without there ever being any freely diffusing hydroxyl radical. Despite these arguments Ingold and co-workers[126] have accumulated convincing evidence that approximately 10% of the peroxynitrite yields freely diffusing hydroxyl radicals at room temperature and pH ~6.8 in deoxygenated and bicarbonate free water. The remaining 90% isomerises to nitric acid by an inefficient in-cage reaction of the geminate radical pair. The findings presented here are supported by this conclusion. Ingold and co-workers have commented[§] that the experiments reported here up to section 2.2.10 do not represent definitive evidence for the formation of radicals from peroxynitrite under CO_2-free conditions. This is obviously true since the experiments were performed before the reaction with CO_2 was considered. However, despite the obvious academic interest and physiological importance, the debate over whether the oxidative chemistry of peroxynitrite is mediated by hydroxyl radical is largely

[§] Ref. 126 and discussion with Prof. K. U. Ingold.

irrelevant to the issues under scrutiny here. Taken at face value, this statement may seem paradoxical, but it has proved possible to establish that radical mechanisms were involved in the reactions of peroxynitrite by considering only the role of nitrogen species. Furthermore, the ongoing preoccupation of many workers with implicating hydroxyl radical in peroxynitrite chemistry has produced enough indirect evidence for its formation that an additional contribution was considered largely superfluous. The motivation for this study, and undoubtedly many others on the chemistry of peroxynitrite, is the underlying theme of its potential role in biological reactions. Therefore since it has been reported widely that, under physiological conditions, the radical reactions of peroxynitrite are mediated by CO_2, its rigorous exclusion reduces the relevance to this situation. It is difficult to retrospectively justify this important oversight and Ingold's comment is certainly valid since the amount of bicarbonate present in the aqueous systems may have been significant due to absorption of CO_2 from the atmosphere by the sodium hydroxide used to keep the peroxynitrite solutions alkaline. It is not surprising that the *in vivo* reactions attributed initially to peroxynitrite are now considered to be mediated by the CO_2 adduct, nitrosoperoxycarbonate, since the electron spin relaxation time of $HO^{\bullet}$ is so short, it will effectively short-circuit the slower nuclear spin dependent singlet-triplet mixing required for CIDNP.[143] The carbonate radical anion formed by homolysis of this adduct will be much less reactive and therefore a more 'CIDNP-competent' radical than $HO^{\bullet}$ due to resonance stabilisation of the unpaired electron density over three oxygen atoms. However, the consensus of opinion is that *freely diffusing* hydroxyl radical is definitely formed; the only remaining source of debate is over the quantity. The most sensible conclusion to draw from the body of evidence is that more stable radicals will be formed if possible (such as the carbonate radical anion derived from homolysis of nitrosoperoxycarbonate), but when such options are not available,

hydroxyl radical will be formed in the manner previously described. The reactions may be attributed to secondary radicals derived from $HO^{\bullet}$ that could form pairs with the ^{15}N-containing radical.[143] In the case of lower pH solutions without tyrosine, it seems likely that the *ca.* 0.1 M 2-ethoxyethanol, present as a by-product of peroxynitrite synthesis, would provide a readily abstractable pool of hydrogen atoms attached to C bound to O. Such C–H bonds react very rapidly with $HO^{\bullet}$ to form radicals which have strong reducing properties. In radiation chemistry, for example, alcohol is often added to convert the oxidising $HO^{\bullet}$ radical to a reducing radical.[143] Either the tyrosyl radical or the α-OR type radical could then react with the $NO_2^{\bullet}$ half of the radical pair to give nitrate or nitrite as required and the products would show CIDNP *via* either recombination or scavenging reactions.[143] Several factors contribute to the different reactivity profile of this caged system than those that have been studied in organic solvents. The unusual 'stickiness' of this cage may be attributed to the strong hydrogen bonding in water together with its high polarity and the large electron exchange energy of this polar radical pair. No evidence is found for the existence of either an electronically-excited or a geometrical conformer of peroxynitrite due to the presence of a single peak in all of the NMR spectra in this work. This indicates that if *cis* or *trans* conformers exist either they interconvert rapidly on the NMR timescale or one is particularly stabilised by interaction with the solvent. It seems that the debate over whether peroxynitrite is the main RNS in mammalian immune systems will continue until such time as developments in NMR or MRI technology allow the monitoring of ^{15}N signals in live mammals which have been fed on a ^{15}N arginine enriched diet and genetically engineered to overproduce reactive species.

3 Kinetic simulations on RNS produced by the immune system

3.1 Introduction and aims

The immune system produces a wide range of reactive oxygen and nitrogen species (ROS and RNS) which have deleterious effects on biotarget molecules such as tyrosine or thiols; *e.g.* nitration of tyrosine residues will deactivate proteins towards tyrosine phosphorylation. With a wide range of potential reactive species available it is difficult to predict the individual contribution to the overall effect (*i.e.* thiol oxidation and nitrosation or tyrosine nitration) each will have. One particular problem which has been raised, but not effectively addressed in the biochemical literature, is whether detection of protein-bound 3-nitro-L-tyrosine by Western blot analysis is sufficiently specific to be considered as an assay for the production of peroxynitrite *in vivo*. One of the aims of this study is to address this problem. However the underlying goal is to clarify whether it is reasonable to consider peroxynitrite as the most significant RNS in the immune system. At least, it is hoped to contextualise the role of peroxynitrite with respect to other potentially important reactive nitrogen species.

The techniques employed in the chemical studies reported earlier in this work require rather special conditions. The corollary is that the biological analogy is tentative at best. It is hoped that by implementing computer-based modelling techniques which utilise information already well established in the literature, the results of the chemical studies will be reinforced. Until more direct and informative ways to probe physiological systems are discovered then the most efficacious means of elucidating the nature of such inherently complicated systems is to combine chemical studies with some form of computer modelling. The software simplifies the handling of relatively complicated systems combining parallel reactions, preequilibria, *etc.*

Some of the species considered in this study are nitric oxide (NO), nitrogen dioxide ($NO_2^{\bullet}$), nitrite (NO_2^-), hypochlorite (HOCl), superoxide radical anion ($O_2^{\bullet-}$), nitryl chloride (NO_2Cl), peroxynitrite ($ONOO^-$), hydroxyl radical ($HO^{\bullet}$) and chlorine radical ($Cl^{\bullet}$).

3.2 Results and discussion

3.2.1 Classification of RNS and ROS

Nitric oxide, superoxide and hydrogen peroxide are produced directly by phagocytic cells (*i.e.* macrophages and neutrophils)[144] in response to foreign stimuli. These are therefore termed 'primary' species. Dioxygen is also considered to be a primary species as it does not necessarily need to have been generated by an *in vivo* synthesis reaction. Secondary species are those formed by reaction of primary species such as peroxynitrite (from NO and superoxide), hypochlorite (produced in a myeloperoxidase catalysed reaction by neutrophils from hydrogen peroxide and chloride) and nitrogen dioxide (from oxidation of NO by oxygen). Dinitrogen trioxide and nitrite must be considered as ternary species as they are formed by reaction of a primary and a secondary species (NO or dioxygen with nitrogen dioxide). It might be intuitively expected that unless synthesis reactions occur at the diffusion limit, then contributions from higher-order species will be greater than from lower-order species. Peroxynitrite occupies a uniquely elevated position in the league of such reactive species for several reasons. It is formed at the diffusion-controlled limit from primary reactants, isomerises to a benign species but also can mediate tissue stress in a variety of fast reactivity modes ($1e^-$ oxidations, nitration and, indirectly, nitrosation).

3.2.2 Peroxynitrite system

The 'immune system' (IS) is modelled here as a source of nitric oxide and superoxide which does not get depleted over the course of the simulation. In widely referenced modelling studies (with around 120 citations) Lancaster[145] has used a value of 1.03×10^{-5} M s^{-1} for the rate of production of NO and superoxide in the stimulated immune system, although Fontecave and Pierre[146] suggest that under pathological conditions a steady-state concentration of 0.1 μM is reasonable. Although Lancaster's value is more extensively referred to, it is probably at least an order of magnitude too high and so both will be accommodated in this work. A recent paper by Laurent *et al.*[147] covers the kinetic modelling of the nitric oxide gradient generated *in vivo*. According to their calculations, the rate of production of nitric oxide is of the order of 10^{-9} M s^{-1}. However this value may more realistically represent the rate of production in the vasculature rather than the immune system.

The formation reaction is set to be zeroth order so that ['immune system'] does not change over the course of the simulation. If the reaction is zeroth order, then the value of the rate constant can take the same magnitude and units as the rate of production. This somewhat artificial situation simplifies the model and is brought about by the fact that IS is not a discrete chemical species but in actual fact a collection of biomolecules (enzymes, proteins, *etc.*). Alternatively the rate of formation of nitric oxide and superoxide would have to have a first order rate constant with a magnitude such that the product k_0[IS] = 1.03×10^{-5} M s^{-1}. The second order rate constant for reaction of superoxide and nitric oxide (k_1) as reported by Huie and Padmaja[148] is set at 6.7×10^{9} M^{-1} s^{-1}. The first order rate constant for rearrangement of peroxynitrite to nitrate (k_2) is set to be 0.36 s^{-1} at pH 7.4 and 37 °C according to Beckman *et al.*[33] The reaction scheme used in the modelling is illustrated in Scheme 3.1.

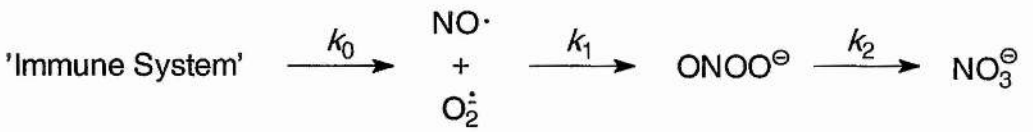

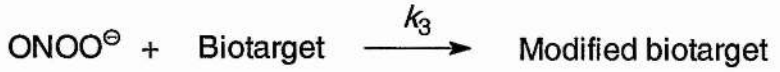

$$\frac{d[\mathrm{IS}]}{dt} = 0 \quad \frac{d[\mathrm{NO}]}{dt} = k_0 - k_1[\mathrm{NO}][\mathrm{O_2^-}\cdot] \quad \frac{d[\mathrm{O_2^-}\cdot]}{dt} = k_0 - k_1[\mathrm{NO}][\mathrm{O_2^-}\cdot]$$

$$\frac{d[\mathrm{ONOO^-}]}{dt} = k_1[\mathrm{NO}][\mathrm{O_2^-}] - k_2[\mathrm{ONOO^-}] - k_3[\mathrm{ONOO^-}][\mathrm{Biotarget}]$$

$$\frac{d[\mathrm{NO_3^-}]}{dt} = k_2[\mathrm{ONOO^-}]$$

Scheme 3.1

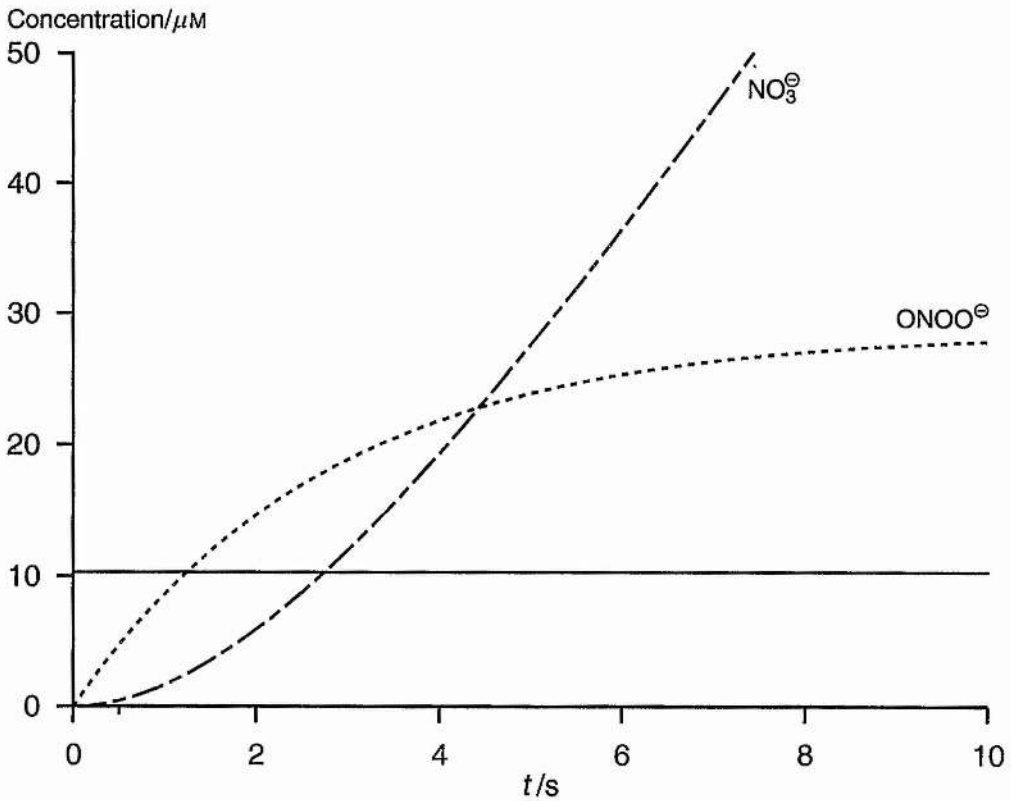

Fig. 3.1 'Scientist' rate profile for the peroxynitrite model. $k_0 = 1.03 \times 10^{-5}$ s^{-1}, $k_1 = 6.7 \times 10^9$ M^{-1} s^{-1}, $k_2 = 0.36$ s^{-1}. $[\mathrm{IS}]_0 = 1.03 \times 10^{-5}$ M, $[\mathrm{NO}]_0$, $[\mathrm{O_2^{\bullet-}}]_0$ and $[\mathrm{ONOO^-}]_0 = 0$ M.

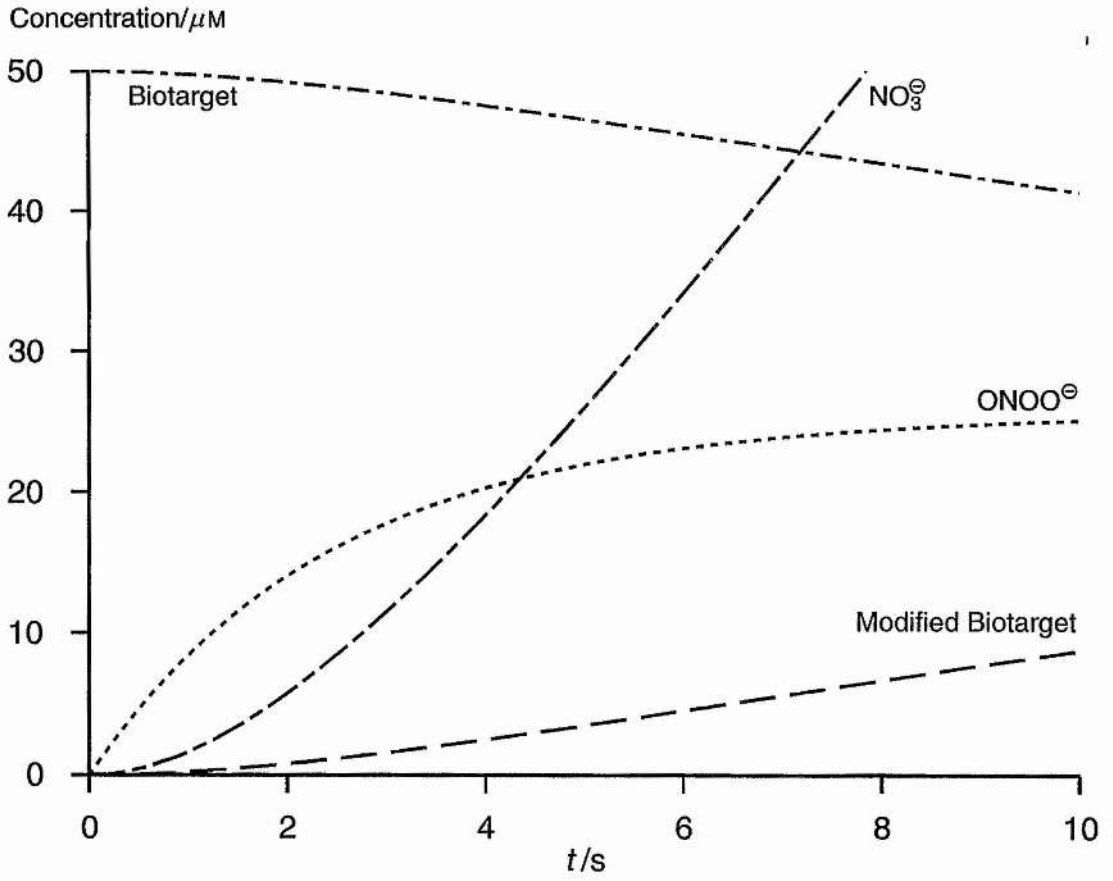

Fig. 3.2 'Scientist' rate profile for the peroxynitrite model modified to include a biotarget competing with isomerisation to nitrate. $k_0 = 1.03 \times 10^{-5}$ s^{-1}, $k_1 = 6.7 \times 10^9$ M^{-1} s^{-1}, $k_2 = 0.36$ s^{-1} and $k_3 = 1000$ M^{-1} s^{-1}. $[IS]_0 = 1.03 \times 10^{-5}$ M, $[NO]_0$, $[O_2^{\bullet-}]_0$, $[ONOO^-]_0 = 0$ M. $[Biotarget]_0 = 50$ μM.

The most useful question to address is how large does the second order rate constant (k_3) for the reaction between a biotarget and peroxynitrite have to be for the modified biotarget to form in significant amounts over the timescale of the simulation? An array of possible values for this rate constant can be found by varying both the initial concentration of the biotarget from 1×10^{-2} M to 1×10^{-6} M and the rate of formation of nitric oxide and superoxide from 10^{-6} M s^{-1} to 10^{-9} M s^{-1}. Results are depicted in Table 3.1 (*a*) and (*b*).

Table 3.1 Results of kinetic simulations on the peroxynitrite/biotarget model. Values reported are the magnitude of the second order rate constant ($k_3/M^{-1}\ s^{-1}$) for reaction of peroxynitrite with a biotarget required to generate [modified biotarget] = (*a*) 0.100 μM and (*b*) 1.00 nM after 10 s. $[Biotarget]_0$ is represented down the left column and k_0 across the top row.

(*a*)	1×10^{-5} M	1×10^{-6} M	1×10^{-7} M	1×10^{-8} M	1×10^{-9} M
1×10^{-2} M	0.0495	0.502	5.5	> diffusn. cntrl	> diffusn. cntrl
1×10^{-3} M	0.495	5.02	55	> diffusn. cntrl	> diffusn. cntrl
1×10^{-4} M	4.95	50.2	550	> diffusn. cntrl	> diffusn. cntrl
1×10^{-5} M	50	502	5500	> diffusn. cntrl	> diffusn. cntrl
1×10^{-6} M	521	5300	57750	> diffusn. cntrl	> diffusn. cntrl

(*b*)	1×10^{-5} M	1×10^{-6} M	1×10^{-7} M	1×10^{-8} M	1×10^{-9} M
1×10^{-2} M	0.000495	0.00502	0.0502	0.510	5.75
1×10^{-3} M	0.00495	0.0495	0.500	5.10	57.5
1×10^{-4} M	0.0495	0.495	5.00	51.0	575
1×10^{-5} M	0.495	4.95	50.0	510	5750
1×10^{-6} M	4.95	49.5	500	5100	57550

The values in the tables above show that the magnitude of the second order rate constant for the reaction between peroxynitrite and a biotarget needs to be between 10^3 and $10^4\ M^{-1}\ s^{-1}$ in order to generate [modified biotarget] of similar order to $[biotarget]_0$ when k_0 is around the value proposed by Fontecave and Pierre. It is unlikely to be coincidental that the values measured for two potential biotarget molecules containing a thiol group, L-cysteine and glutathione reported in table 2.8 are of this order.

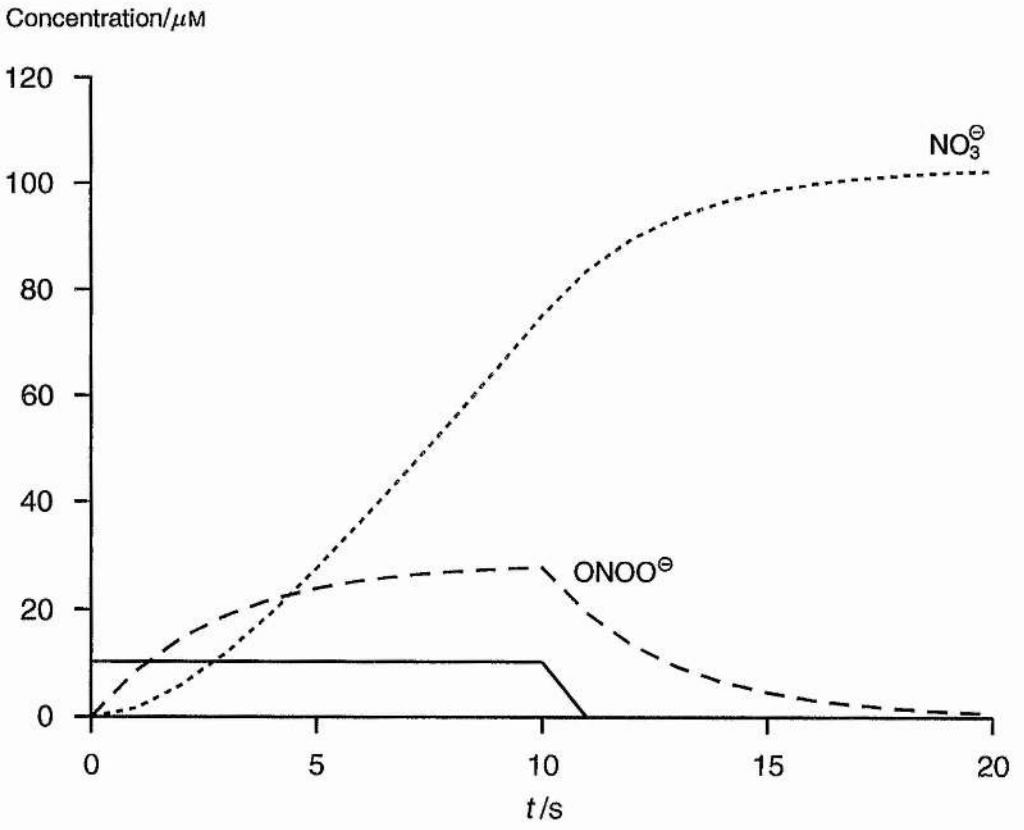

Fig. 3.3 'Scientist' rate profile for the peroxynitrite model modified to allow the 'immune system' to be deactivated after 10 s. Conditions over first 10 s as for Fig. 3.1. Conditions from 10–20 s: $k_0 = 0\ s^{-1}$, $k_1 = 6.7 \times 10^9\ M^{-1}\ s^{-1}$, $k_2 = 0.36\ s^{-1}$. $[IS]_{t=10} = 0$ M, $[NO]_{t=10} = [O_2^{\bullet-}]_{t=10} = 3.92 \times 10^{-8}$ M. $[ONOO^-]_{t=10} = 2.78 \times 10^{-5}$ M. $[Biotarget]_{t=10} = 7.51 \times 10^{-5}$ M.

The timescale of the concentration profiles are in agreement with that predicted by Lancaster (10–20 s to achieve a steady state concentration of peroxynitrite). This provides a useful check of the efficacy of the model. However it is worth noting that the assumptions which Lancaster makes to produce his NO profiles are too elementary and the results may be unsound. He assumes NO is generated by a point source when a cylindrical source is clearly a far more accurate model of the situation in the vasculature. Lancaster's model seems more appropriate for the situation in the brain where it may be more realistic to consider nitric oxide to be produced by point sources

(neurons). Butler *et al.*[149] have addressed these problems and shown that concerns regarding efficacious haem scavenging of endothelial-produced NO are unfounded due to a well-established principle of fluid mechanics; flow rates at the edges of a Newtonian liquid are turbulent and therefore much slower than at the centre.

3.2.3 Nitryl chloride system

An elegant mechanistic study by Johnson and Margerum[150] supplementing earlier work by Cachaza *et al.*[151] on the reaction of hypochlorous acid with nitrite has established that formation of nitryl chloride (NO_2Cl) occurs by transfer of Cl^+. As mentioned previously in section 2.2.8, Eiserich *et al.*[128a,b] have put forward the hypothesis that this species may be responsible for some of the *in vivo* reactions ascribed to peroxynitrite, potentially further undermining the axioms on which much research (including this work) have been justified. The aim of this part of the work is to assess whether nitryl chloride is likely to be a valid RNS in this context.

Nitration by salts of nitronium ion is usually an electrophilic process,[152] but nitration of activated aromatic compounds such as tyrosine can occur by a radical pathway involving ET. Indeed, the work of Eiserich *et al.* has shown that in addition to the expected formation of 3-nitro-*N*-acetyl-L-tyrosine from the reaction of nitryl chloride with *N*-acetyl-L-tyrosine, some of the dityrosine derivative was formed which suggests the presence of radicals on the reaction pathway.

Eqns. (1)–(8) illustrate possible source and sink reactions for nitryl chloride under physiological conditions with eqns. (3)–(7) according to Johnson and Margerum. It can be seen that two paths exist for the decomposition of nitryl chloride; attack by NO_2^- to form N_2O_4 and dissociation to give NO_2^+ and Cl^-. The N_2O_4 path is

preferred over the NO_2^+ path when the nitrite concentration exceeds 4.6×10^{-3} M, however under physiological conditions in the immune system, the concentration of nitrite is not expected to approach this level therefore the contribution from eqns. (4) and (5) would be insignificant.

$$\text{'Immune System'} \xrightarrow{k_0} NO + HOCl \quad (1)$$

$$2NO + O_2 \xrightarrow{k_1} 2NO_2^{\ominus} \quad (2)$$

$$NO_2^{\ominus} + HOCl \underset{k_{-2}}{\overset{k_2}{\rightleftharpoons}} NO_2Cl + OH^{\ominus} \quad (3)$$

$$NO_2Cl + NO_2^{\ominus} \underset{k_{-3}}{\overset{k_3}{\rightleftharpoons}} N_2O_4 + Cl^{\ominus} \quad (4)$$

$$N_2O_4 + OH^{\ominus} \xrightarrow{k_4} NO_3^{\ominus} + NO_2^{\ominus} + H^{\oplus} \quad (5)$$

$$NO_2Cl \underset{k_{-5}}{\overset{k_5}{\rightleftharpoons}} NO_2^{\oplus} + Cl^{\ominus} \quad (6)$$

$$NO_2^{\oplus} + OH^{\ominus} \xrightarrow{k_6} NO_3^{\ominus} + H^{\oplus} \quad (7)$$

$$NO_2^{\oplus} + H_2O \underset{k_{-7}}{\overset{k_7}{\rightleftharpoons}} HNO_3 + H^{\oplus} \quad (8)$$

The fact that eqn. (3) is an equilibrium indicates that the reaction of NO_2Cl with HO^- is not encounter controlled. The rate-determining step in the Scheme is ionisation of NO_2Cl (k_5) to give nitronium ion. Before considering the process of aromatic nitration, it is necessary to ascertain whether hydrolysis of nitronium ion is more likely to occur by reaction with H_2O or HO^-.

Johnson and Margerum conclude from their detailed analysis of the kinetics of this system that, with respect to nitration by NO_2^+, HO^- is a factor of 10^{10} more reactive that H_2O. This value seems to be very high and their kinetic evidence may be questionable on the grounds that the only conditions which might produce such evidence are runs in the presence of high [HO^-] and here the only two [HO^-] used

are 2.06×10^{-6} and 2.13×10^{-6} M. It is possible to compare it with other kinetic data. Ritchie *et al.*[153] have determined the relative nucleophilicities of a number of species with respect to reaction at a carbocation and eqn. (9) represents their general scale for nucleophilicity where k_0 is a characteristic of the electrophile and N_+ is a parameter dependent on the identity of the nucleophile and the solvent.

$$\log k = \log k_0 + N_+ \tag{9}$$

For reaction of triphenylmethyl cation with HO^- and H_2O the N_+ values[154] are 4.75 and 0.73 respectively, so the relative nucleophilicity of HO^- and H_2O in this system is $10^{4.75}/10^{0.73} = 10^{4.75-0.73} = 10^{4.02}$. This is some six orders of magnitude smaller than the value suggested by Johnson and Margerum. Although there is a difference in electronegativity between the two electrophilic centres, there is no suggestion in the work of Ritchie *et al.* that k_0 will change much between a carbon-centered and a nitrogen-centered cation. Furthermore, provided that the nucleophilicity is treated as a relative factor, the difference in steric bulk between NO_2^+ and $(Ph)_3C^+$ need not be taken into account as both HO^- and H_2O are small molecules of similar size. If the N_+ values of Ritchie *et al.* represent a valid description of the relative nucleophilicities of HO^- and H_2O, then the relative concentrations of these species must also be considered in order to gain a correct idea of their bulk reactivity. At pH 7.4 the concentration of hydroxide ions is given by eqn. (10).

$$[OH^-] = \frac{K_W}{[H^+]} = \frac{1.008 \times 10^{-14}}{10^{-7.4}} = 2.53 \times 10^{-7}\ \text{M} \tag{10}$$

Since $[HO^-]$ is very low at this pH and $[H_2O]$ is 55.5 M, reaction of nitronium ion with water will be more likely than with hydroxide ion. Therefore, to establish

whether tyrosine could be nitrated by NO_2^+ at pH 7.4 in an aqueous system it is necessary to determine the relative rates of reaction of H_2O and tyrosine with NO_2^+. The reaction of NO_2^+ with water illustrated in eqn. (8) is accompanied by oxygen exchange and the rate has been measured by Bunton and Halevi.[155] For the nitration of very reactive aromatic substrates according to eqn. (11) where $k_8[NO_2^+][ArH] \gg k_7[NO_2^+][H_2O]$, the autoprotolysis of nitric acid (governed by k_{-7}) will be the rate-determining step and the overall reaction will be zeroth order in substrate.

$$NO_2^{\oplus} + ArH \xrightarrow{k_8} ArNO_2 + H^{\oplus} \qquad (11)$$

Therefore the bulk reactivity of the aromatic substrate must exceed that of water in order for nitration to occur as the rate of nitration depends on the concentration of ArH. Below a certain concentration there will not be a clean zeroth order dependence on the substrate and the value of the threshold concentration is a measure of the reactivity of ArH towards NO_2^+: the lower the threshold concentration, the more reactive ArH is. According to the data of Schofield[156] on the nitration of phenol in 40% H_2SO_4, the half life of nitronium ion is about 10^{-10} s (*i.e.* the reaction is diffusion controlled). Schofield also reports that the zeroth order rate constant (k_7) for reaction of NO_2^+ with *water* (under conditions of similar acidity) can be estimated to be $\simeq 10^6$–10^8 s^{-1}.[157] Therefore, NO_2^+ should be $\simeq 10^2$–10^4 times more reactive towards phenol than water. However, the product ratio resulting from addition of these species will also depend on their relative amounts. For instance, in a 10^{-6} M solution of phenol, the ratio will be reduced by a factor of $(10^{-6}/55.5) \approx 1.8 \times 10^{-8}$ to $\simeq 10^{-4}$–10^{-6}. This indicates that, under physiological conditions where it is reasonable to assume that the concentration of tyrosine can reach μM levels, essentially all the NO_2^+ present reacts with water to form nitric acid. If the assumption that phenol reacts with

electrophiles at a similar rate to tyrosine is reasonable, then it would appear that tyrosine would not be nitrated by $NO_2^{\bullet}$ and that any NO_2Cl formed within the immune system will end up, if it reacts only by an electrophilic mechanism, as nitric acid.

In a different approach, the available kinetic data may be utilised to estimate a rate constant for hydrolysis of NO_2Cl. As no values for k_2, k_{-2}, k_5, k_{-5} or k_6 can be extracted from the data of Johnson and Margerum, it is necessary to make certain assumptions in order to fulfil this objective. It seems reasonable to assume that reaction of NO_2^+ with HO^- (k_6) is encounter controlled at pH 7.4 and 37 °C, leading to $k_6 \gg k_{-5}$ and effectively rendering the back reaction to reform nitryl chloride insignificant. Since $k_6 \gg k_5$ also, then formation of nitronium ion is rate determining and the rate of hydrolysis is simply given by eqn. (12).

$$\frac{d[NO_2Cl]}{dt} = -k_5[NO_2Cl] \tag{12}$$

But since $\frac{k_2}{k_{-2}} = \frac{[NO_2Cl][OH^-]}{[HOCl][NO_2^-]}$ from eqn. (3), substituting in eqn. (12) gives the expression for the rate of hydrolysis in terms of known parameters shown in eqn. (13).

$$\frac{d[NO_2Cl]}{dt} = -\frac{k_2k_5}{k_{-2}}\frac{[NO_2^-][HOCl]}{[OH^-]} \tag{13}$$

The parameter $\frac{k_2k_5}{k_{-2}}$ is defined by Johnson and Margerum to be equal to 2.3×10^{-2} s^{-1} and $[HO^-]$ under physiological conditions is taken from eqn. (10) to be equal to 2.53×10^{-7} M. Therefore in order to achieve steady state conditions on nitryl chloride under the constraints imposed where rate of formation is equal to rate of reaction, it

follows that the second order rate constant governing the reaction of nitrite and hypochlorous acid needs to be equal to 90, 909 $M^{-1} s^{-1}$.

3.3 Conclusions

3.3.1 Peroxynitrite system

The results of the modelling simulations are not startling and this is reassuring from the point of view both of the reliability of the established facts and the confidence that can be held in the conclusions drawn from them. The simple model used here represents good value in terms of convenience but does not account for any significant formation of nitrite. High levels of nitrite are detected both in the reactions studied earlier in this work and in the urine of patients with inflammatory disorders. Clearly the ^{15}N NMR studies intimate that the reactions of peroxynitrite are not trivial. Therefore such mathematical simulations can only offer a minor contribution towards solving the mechanistic problem. However, it is reassuring to note that even a simplified approach yields results that compare sensibly with empirical data. For instance concerning the rate constant for reaction of tyrosine with peroxynitrite, from Table 3.1 (*a*), it can be seen that choosing a reasonable set of values for $[biotarget]_0$ (1×10^{-7} M) and k_0 (1×10^{-5} M) it is estimated to be approximately $5.5 \times 10^3 M^{-1} s^{-1}$. Koppenol and co-workers[158] find that the second order rate constant for this reaction in the presence of Fe^{3+}-EDTA at pH 7.2 is in fact the same ($5.5 \times 10^3 M^{-1} s^{-1}$). However, this is entirely coincidental since one can choose several sets of 'reasonable' values from Table 3.1 (*a*) and (*b*), all of which are open to liberal interpretation as are the physiological relevance of the conditions chosen by Koppenol and co-workers. But the fact that the modelling and empirical data agree even to the same order of magnitude is surely significant.

3.3.2 Nitryl chloride system

The most obvious conclusion from the calculations and simulations here is that nitryl chloride acting as an electrophile is unlikely to be responsible for the tyrosine nitration and oxidative damage in the immune system that has been ascribed to peroxynitrite. This conclusion is supported by Jiang and Hurst[159] who studied the relative chlorinating, nitrating and oxidising capabilities of neutrophils. They also conclude that kinetic arguments suggest the HOCl–NO_2^- reaction will be relatively unimportant in physiological environments. This is unsurprising as they observe the second order rate constant for reaction of NO_2^- and HOCl to form NO_2Cl is $\geq 6 \times 10^2$ M^{-1} s^{-1} (*i.e.* at most three orders of magnitude *less* than the rate constant of hydrolysis estimated here). In addition they observe that this reaction competes with direct chlorination of the phenolic ring by HOCl.

The fact that NO_2Cl (or generally speaking, mixtures of hypochlorite and nitrite) brings about tyrosine nitration is not in dispute, but the work of Eiserich *et al.*[128] does not establish much about the mechanism of this process. Presumably it may occur in an ionic manner or *via* radical species produced by ET between hypochlorous acid and tyrosine according to eqns. (14) and (15) or by the interaction of hypochlorous acid and nitrite [eqns. (16) and (17)].

$$HO{-}Cl + TyrOH \longrightarrow \cdot OH + HCl + TyrO\cdot \quad (14)$$

$$HO{-}Cl + TyrOH \longrightarrow H_2O + Cl\cdot + TyrO\cdot \quad (15)$$

$$HO{-}Cl + NO_2^{\ominus} \longrightarrow \cdot NO_2 + OH^{\ominus} + Cl\cdot \quad (16)$$

$$HO{-}Cl + NO_2^{\ominus} \longrightarrow \cdot NO_2 + \cdot OH + Cl^{\ominus} \quad (17)$$

$$TyrO\cdot + \cdot NO_2 \longrightarrow \text{3-nitrotyrosine} \quad (18)$$

$$TyrO\cdot + Cl\cdot \longrightarrow \text{3-chlorotyrosine} \quad (19)$$

The observation that these mixtures, which have been regarded predominantly in terms of nitrating species may also bring about nitrosation of certain thiols, tempts parallels to be drawn with peroxynitrite. While the purely qualitative experiments described briefly in section 2.2.8 are mostly inconclusive in mechanistic terms, if Scheme 2.15 offers an authentic explanation of this effect, then the radical pathways suggested in eqns. 16–18 are reasonable. Of course, the $RSNO_2$ intermediate which leads to RSNO may also be produced by the reaction of RS^- with $NO_2^{\bullet}$.

A consideration of these matters inevitably leads back to classical discussions on polar aromatic substitution mechanisms and the ET concept.[160] Eberson and co-workers have been involved with work relating to aromatic substitution by the nitronium ion. In a recent paper,[161] they note that two approaches have been pursued, namely (i) to regard the aromatic substitution transition state as a resonance hybrid between the initial state and one[162] in which an electron has been shifted between the substrate ArH and the electrophile E^+ as illustrated in eqn. (20) and (ii) to find evidence for an initial ET step leading to a radical cation $ArH^{\bullet+}$ which combines with E· to give a Wheland intermediate as illustrated in eqn. (21).

$$ArH + E^{\oplus} \longrightarrow \left[ArH\,E^{\oplus} \longleftrightarrow ArH^{\ddagger}\,E\cdot \right]^{\ddagger} \longrightarrow Ar^{\oplus}(H)E \qquad (20)$$

$$ArH + E^{\oplus} \longrightarrow ArH^{\ddagger} + E\cdot \longrightarrow Ar^{\oplus}(H)E \qquad (21)$$

4 Mechanistic investigations on the spontaneous and thiol-mediated decomposition of furoxan derivatives

4.1 Introduction

4.1.1 Background

Feelisch *et al.*[163] have shown that derivatives of the furoxan ring system can release nitric oxide in the presence of thiol co-factors. The activity of the soluble guanylate cyclase enzyme was discovered to be potently increased by administration of furoxans following reaction with sulfhydryl-containing molecules and the levels of cGMP were increased *via* formation of NO. Hence these compounds may be used as vasodilators. Furthermore, certain furoxans can be suitably derivatised so that they possess α_1-antagonist activity[164] by blocking these adrenergic receptors in the plasma membrane which are triggered by epinephrine (adrenaline) and related catecholamines.

Furoxan **1** (Fig. 4.1) proved to be insoluble in aqueous solutions therefore derivatives containing groups conferring water solubility were prepared and investigated for NO release by Gasco *et al.*[165] **3b** Oxalate showed near quantitative (95.3 ± 2.3%) spontaneous release of NO (detected indirectly as nitrite) when incubated under physiological conditions for 1 h. **2b** Oxalate showed near quantitative (91 ± 0.9%) release of NO when incubated with a 50-fold excess of cysteine for 1 h. From a comparison of the EC_{50} values under these conditions, **3b** oxalate was approximately 2½ times less potent, and **2b** oxalate 45 times less potent than GTN and SNP in producing vasodilation on endothelium-denuded strips of rat aorta precontracted with noradrenaline. In the presence of oxyhaemoglobin, a well-known NO scavenger, the

EC_{50} values were respectively increased (and thus the activity decreased) by 6 and 3½ times.

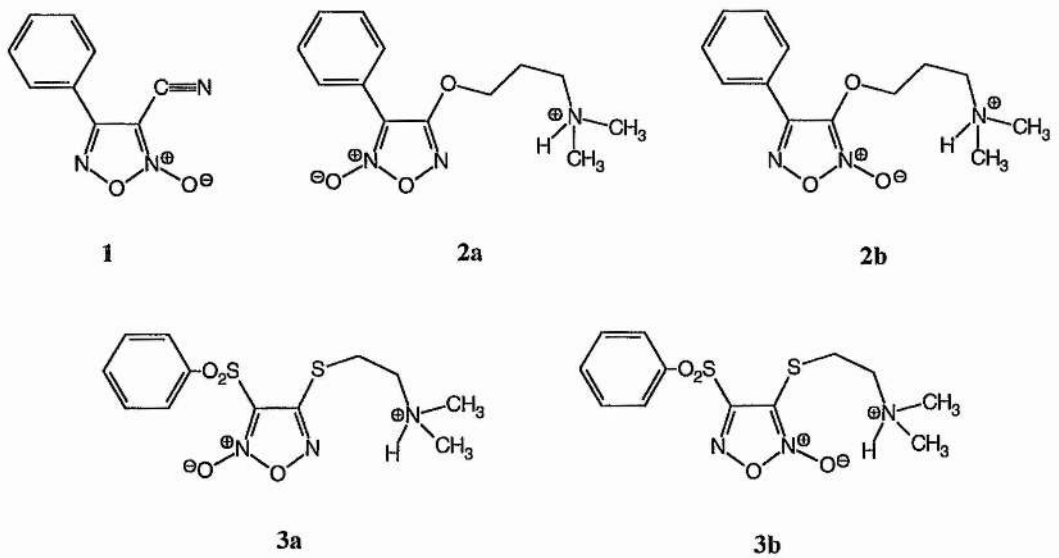

1 **2a** **2b**

3a **3b**

1 2-Oxy-4-phenyl-furazan-3-carbonitrile.

2a Dimethyl-[3-(2-oxy-3-phenyl-furazan-4-yloxy)-propyl]-ammonium oxalate.

2b Dimethyl-[3-(2-oxy-4-phenyl-furazan-3-yloxy)-propyl]-ammonium oxalate.

3a Dimethyl-[2-(2-oxy-3-benzenesulfonyl-furazan-4-ylsulfanyl)-ethyl]-ammonium oxalate.

3b Dimethyl-[2-(2-oxy-4-benzenesulfonyl-furazan-3-ylsulfanyl)-ethyl]-ammonium oxalate.

Fig. 4.1 Main furoxan derivatives referred to in this chapter. (**1**, **2b** and **3b** oxalates studied for mechanism of NO release).

4.1.2 Aims of this work

Although the synthesis and vasodilating activities of furoxan derivatives have been investigated extensively by Gasco and co-workers, the mechanism by which they react is not as well understood. There are several possible mechanisms by which nitrogen-containing products may be produced by their decomposition in aqueous solution. The aims of this study were to investigate, by EPR spectroscopy, the extent to which

furoxan derivatives **1**, **2b** and **3b** oxalates decompose *via* radical pathways to release NO, to identify whether ammonia could account for the remaining 10% of unspecified nitrogen-containing product and to rationalise these results with a general mechanism or mechanisms. Other objectives include gaining evidence for the intermediacy of *S*-nitrosothiols by reaction of a suitable biotarget thiol such as *N*-acetyl-DL-penicillamine or *N*-acetyl-L-cysteine with **1** and **2b** oxalate. Although Feelisch and co-workers reported this in their paper, Gasco and co-workers have no evidence for the intermediacy of *S*-nitrosothiols.

4.1.3 Possible modes of decomposition

The mechanism of release of nitric oxide from furoxan derivatives is unclear. A tentative mechanism for NO release from **1** proposed by Feelisch and co-workers[163] has been further elaborated upon by Gasco and co-workers.[165,166] These proposals are illustrated by the general mechanism shown in Scheme 4.1. Release of nitroxyl (NO^-) was proposed by Gasco and a general mechanism for this is illustrated in pathway (*c*) of Scheme 4.3. When X = S (**3b**), an alternative ionic mechanism involving cleavage of the N2–C3 bond would be reasonable as sulfur stabilises α-carbanions. This process, represented by pathway (*b*) of Scheme 4.3, could lead to nitrite formation by attack of hydroxide ion and transfer of nitrosonium ion shown in pathway (*d*).

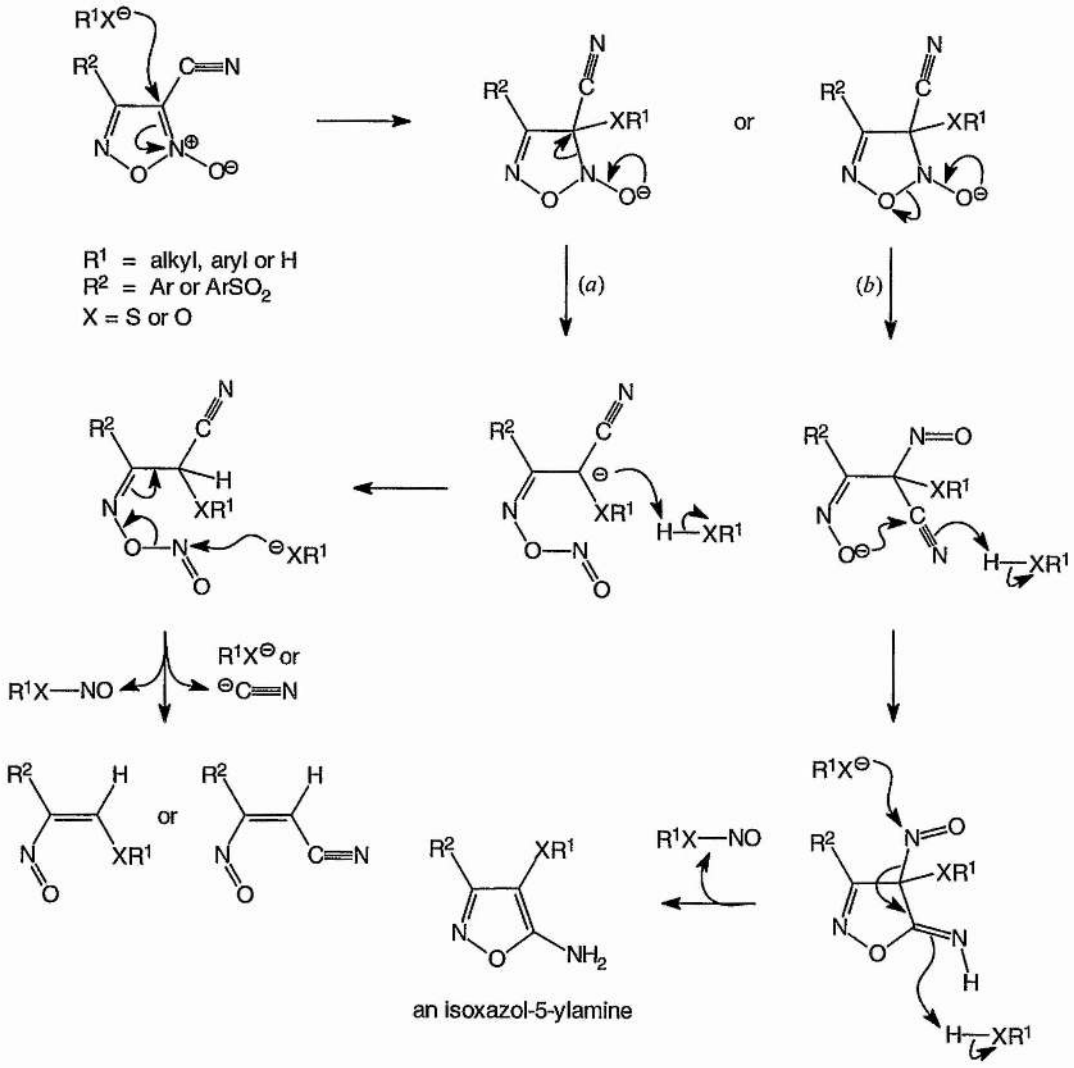

Scheme 4.1

Alternative formally correct mechanisms involving radical intermediates can be written (Scheme 4.2).

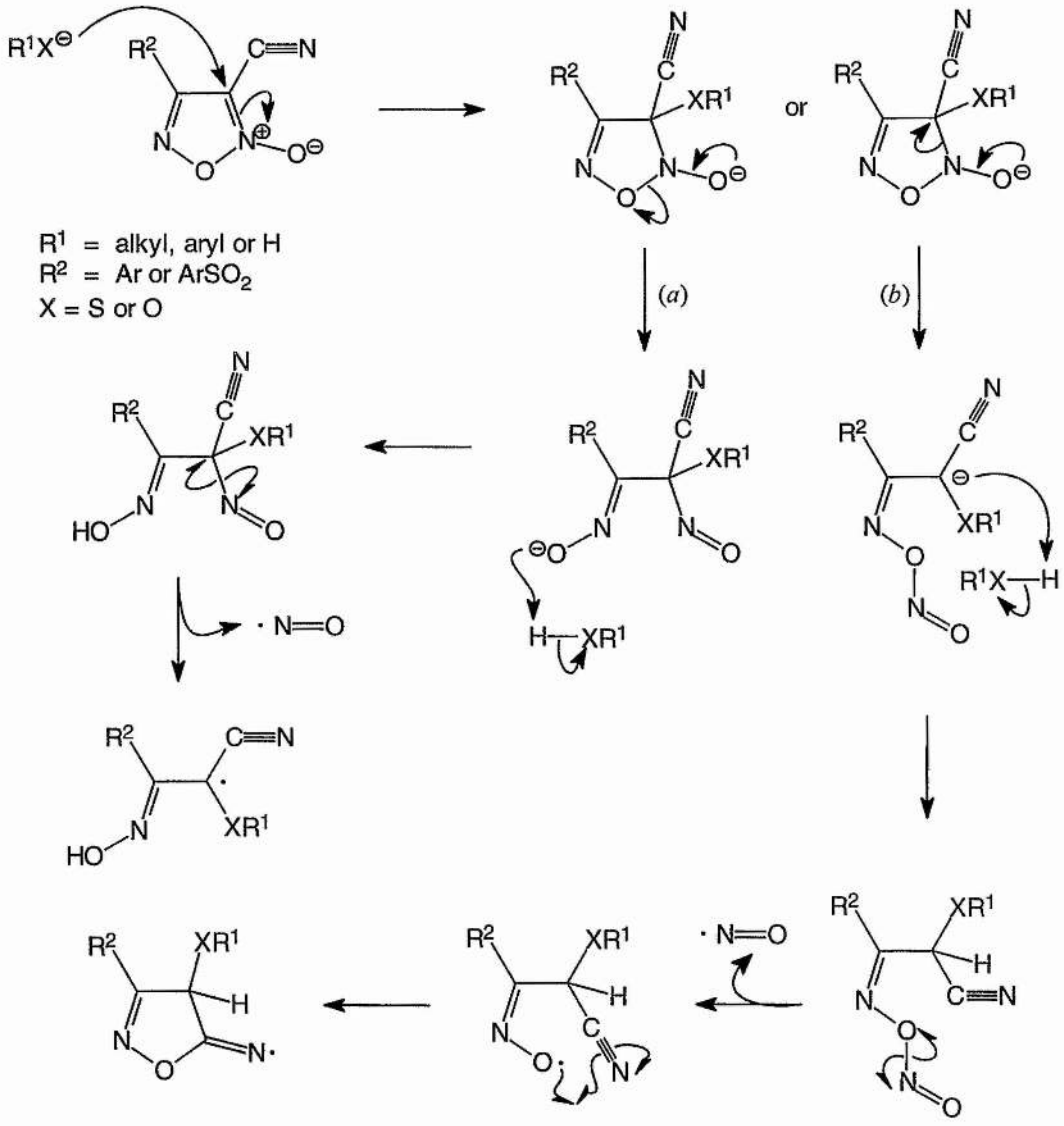

Scheme 4.2

However a distinction must be drawn between those mechanisms which are formally correct and those which are reasonable. The nitrile group and also, if X is sulfur, the R^1X group is carbanion stabilising. Thus cleavage of the N2–C3 or the O1–N2 bond would be reasonable. Clearly since the nitrile group on **1** may participate in a radical or ionic mechanism or indeed act as a leaving group, this is a special case. Pathway (*b*) in Schemes 4.1 and 4.2 forming isoxazol-5-ylamines may be classified as an S_N(ANRORC) mechanism.[167]

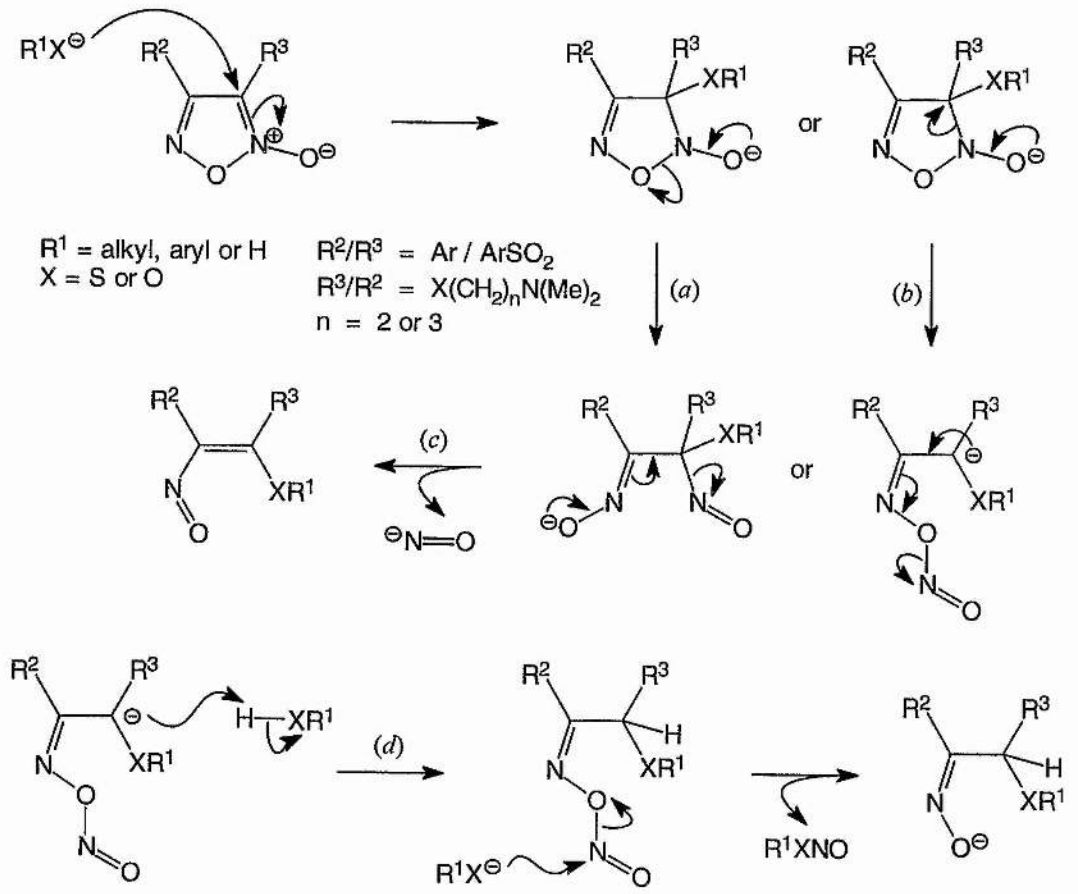
R1X⊖
R2
R3
XR1
or
R1 = alkyl, aryl or H
X = S or O
R2/R3 = Ar / ArSO2
R3/R2 = X(CH2)nN(Me)2
n = 2 or 3
(a)
(b)
(c)
⊖N=O
(d)
R1X⊖
R1XNO

Scheme 4.3

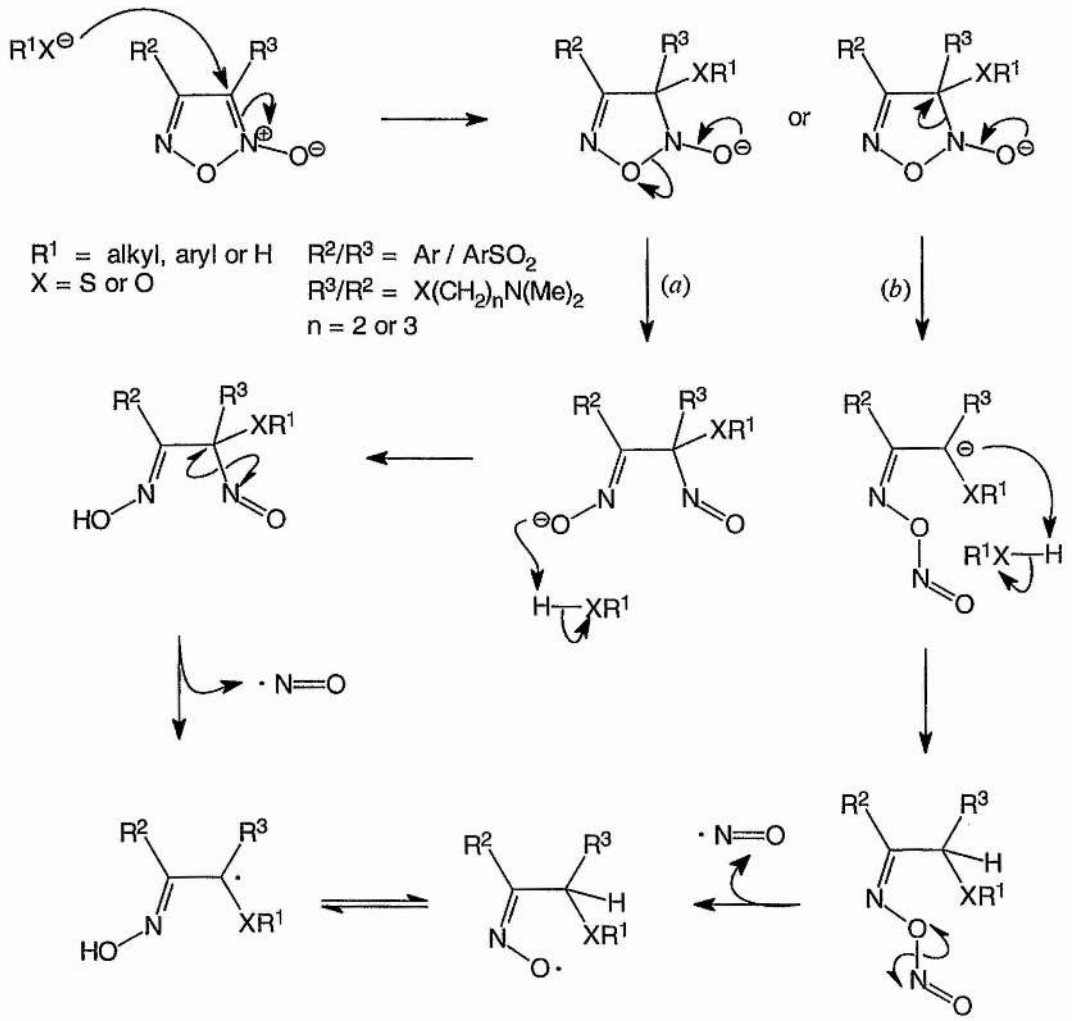

Scheme 4.4

4.2 Results and discussion

4.2.1 Synthetic procedures

The synthetic methods employed closely followed those utilised by Gasco and co-workers and only occasional modification of these procedures were necessary. These are illustrated in Schemes 4.5–4.11. The first step of the four-stage synthesis of **1** (Scheme 4.5) presented some difficulties particularly with the precise reaction conditions and subsequent purification of the target compound due to ambiguities in the literature preparation. Although the reaction proceeds with favourable

regioselectivity (the addition of N_2O_3 is such that the desired isomer is formed in a 96:4 ratio) the product is a viscous red oil that is difficult to purify. It is likely that the main impurity is 3-phenyl-4-nitro furoxan reported by Wieland[168] to be formed during the action of nitrogen oxides on 3-phenyl-propenal (cinnamaldehyde). Nitro groups often impart deep red colours to organic molecules.

A personal communication from Roberta Fruttero,[169] a co-worker of Gasco helped resolve the early experimental difficulties. As discussed earlier, if both substituents on the starting alkene are carbocation destabilising, then no reaction occurs. Unfortunately this factor precludes a single step preparation of **1** from readily available 3-phenyl-acrylonitrile (cinnamonitrile).

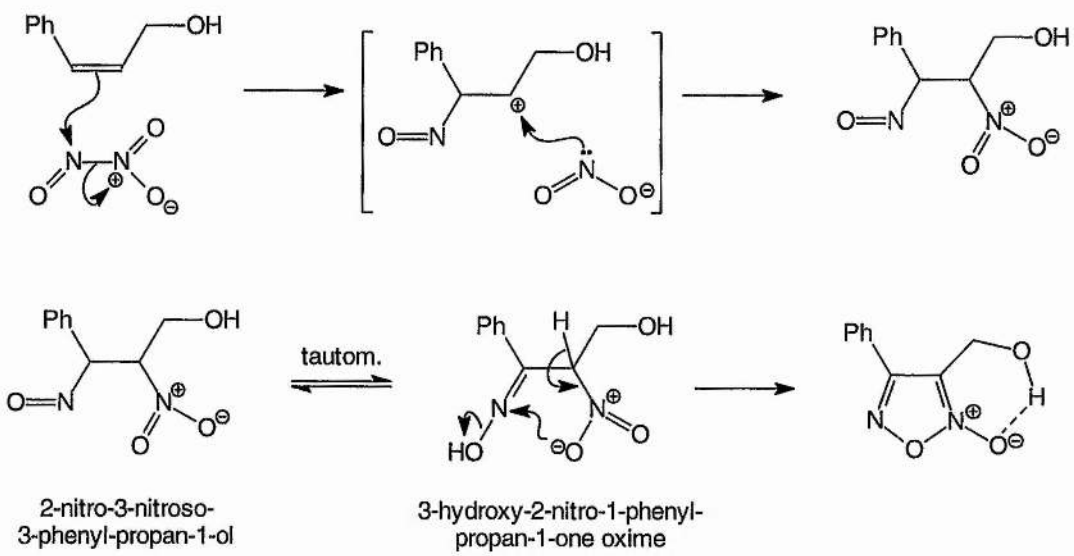

Scheme 4.5

Two methods were employed to convert the 4-phenyl-furoxan carbaldehyde derivative to **1**. The two-step process reported by Gasco *et al.*[165] requiring preparation and isolation of the oxime derivative proved successful. However, the procedure of Capdevielle *et al.*[170] was also attempted since it apparently allowed one-pot

conversion of the carbaldehyde to carbonitrile **1** in high yield without preparation and isolation of the oxime. This would not only remove one step from the synthesis, but also facilitate the introduction of a ^{15}N-labelled atom in the nitrile group. Two ^{15}N-labelled atoms were incorporated into the furoxan ring by simply using $Na^{15}NO_2$ in the synthesis of 4-phenyl-3-furoxan-methanol. In this way, the anticipated preparation of carbonitrile **1** with three ^{15}N-labelled atoms would allow a study of the decomposition by ^{15}N NMR. The procedure reported by Capdevielle *et al.* involves *in situ* oxidation of an intermediate aldimine using NH_4Cl, metallic copper powder and pyridine under an oxygen atmosphere shown in eqn. 1. Fig 4.2 shows the crystal structure and Fig 4.3 the ^{15}N NMR spectrum of the product of this reaction.

$$Cu(0) + 2NH_4Cl + \tfrac{1}{2}O_2 \longrightarrow CuCl_2 + 2NH_3 + H_2O \qquad (1)$$

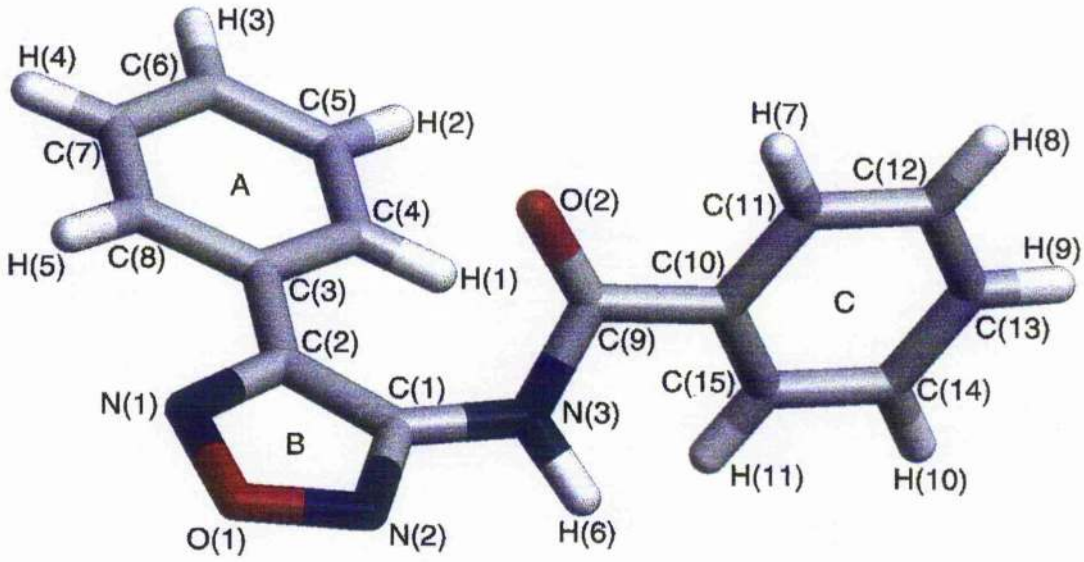

Fig. 4.2 X-ray crystal structure of the product obtained from the attempted synthesis of $[^{15}N]_3$ carbonitrile **1**. Bond lengths, angles, refined coordinates, thermal parameters and their estimated standard deviations are listed in appendix 3.

The crystal structure has few features particularly worthy of note, and here serves only to unambiguously identify the product. Phenyl ring A and furazan ring B are approximately coplanar; the torsion angle being 10.5 °. In contrast, the phenyl ring C is approximately perpendicular to the furazan ring; the torsion angle in this case is close to 83 °. In general, furoxans give good quality crystals and a number of X-ray crystal structures have been published *e.g.* by Gasco *et al.*[75]

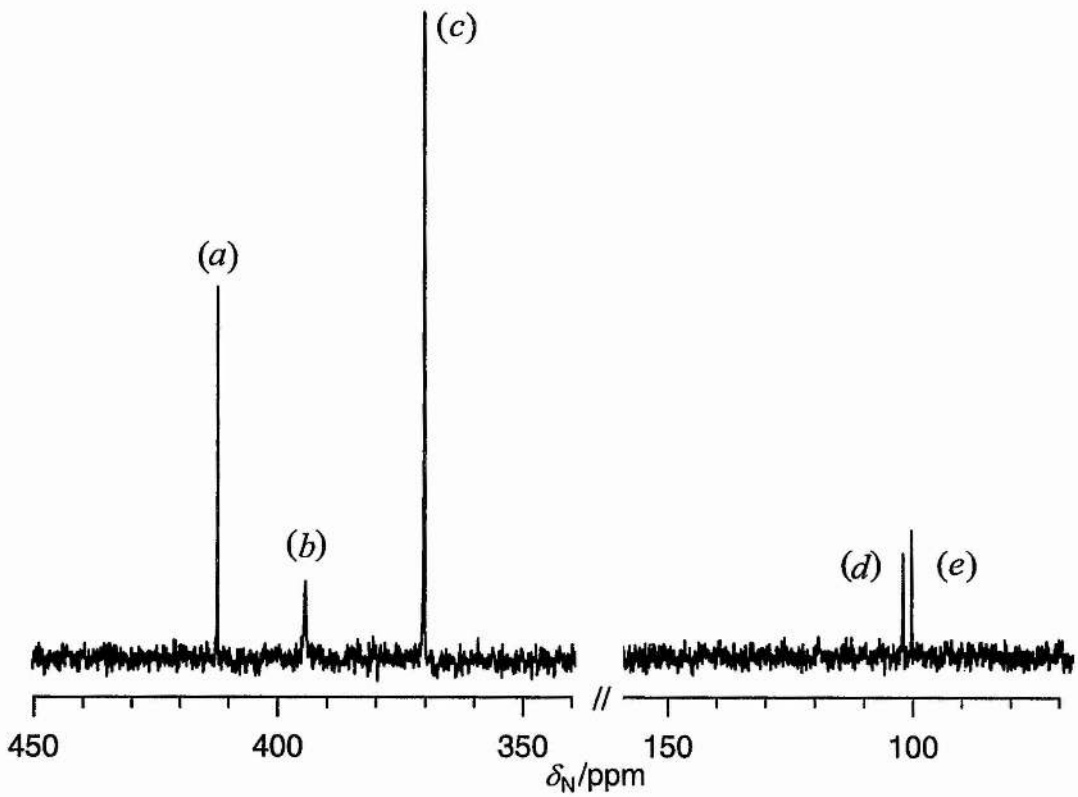

Fig. 4.3 ^{15}N NMR spectrum of furazan **8**. Signals (*a*) δ_N 412.4 ppm: furazan N1, linewidth 3 Hz, (*b*) δ_N 394.5 ppm: furazan N2, linewidth 19 Hz, (*c*) δ_N 374.2 ppm nitrobenzene reference, (*d*) δ_N 102.1 ppm and (*e*) δ_N 100.3 ppm: N3 of tautomers **8b** and **8c**.

The ^{15}N NMR spectrum of this product displays several interesting characteristics. It is perhaps surprising that the difference in the nature of the substituents on the furazan ring has such a profound effect on the ring ^{15}N chemical shifts. The signal at δ_N

394.5 ppm is assigned to N2 as it shows significant broadening due to proton exchange. The signals at δ_N 102.1 ppm and δ_N 100.3 ppm are respectively assigned to the furazanyl benzimidic acid **8b** and [1,2,5]oxadiazol-3-ylidene-benzamide tautomer **8c**.

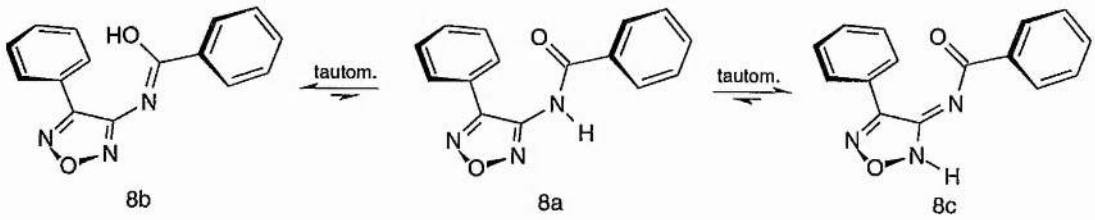

8b 8a 8c

A similar proton-exchange argument must account for the broadening of these signals. It is to be expected that these tautomers are favoured since, in these configurations, the conjugation of double bonds is maximised throughout the molecule.

There is no obvious rationalisation as to how, under these conditions, a phenyl group can have reacted and an amide formed with the observed configuration since Capdevielle *et al.* note only two possible limitations of their synthesis. These are (*a*) enolisable aliphatic aldehydes do not react due to their high instability towards oxidation and aldol condensation and (*b*) some aromatic nitriles cannot be prepared if they are readily oxidisable or contain halogen atoms which can exchange with copper halogen ligands. However, in this case, the explanation for this unpredictable behaviour may be found in a known reaction of acyl furoxans with ammonia, amines and hydrazines and is not an inherent limitation of the Capdevielle reaction with this substrate. An analogous reaction with dibenzoylfuroxan investigated by Bertelson *et al.*[171] is discussed in the review by Gasco and Boulton.[68] It is easier to consider the formation of *N*-(4-phenyl-furazan-3-yl)-formamide **7**, illustrated in Scheme 4.7, and its subsequent reaction with a phenyl residue separately.

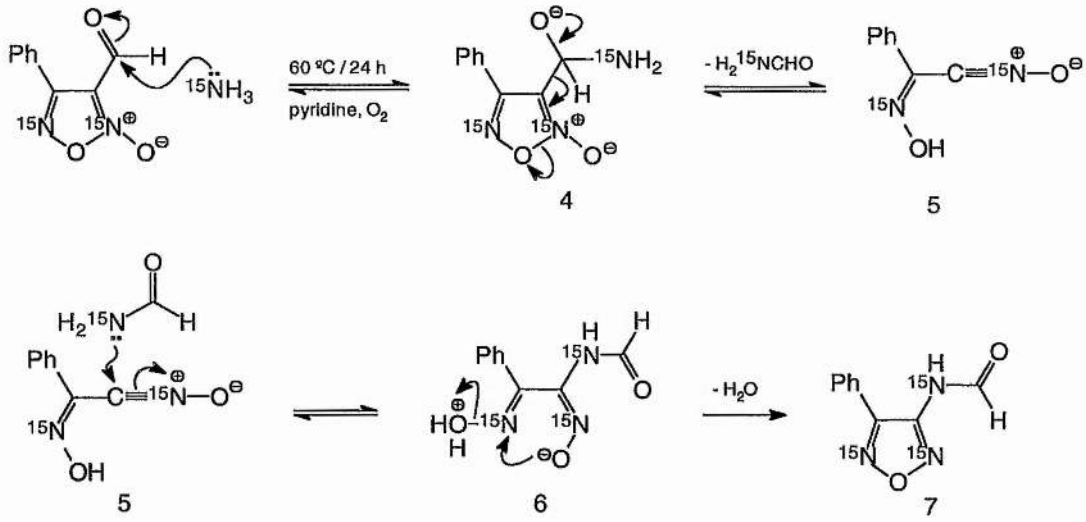

Scheme 4.7

If the carbaldehyde undergoes nucleophilic attack by NH_3 generated by the process outlined in eqn. 1, then formamide may be released from the amino-methanolate ion **4** to yield the intermediate hydroxyimino-phenyl-acetonitrile *N*-oxide **5**. Formamide can then re-attack the nitrile oxide to form *N*-(1,2-bis-hydroxyimino-2-phenyl-ethyl)-formamide **6**. In the case of dibenzoylfuroxan, one of the oxime nitrogen atoms attacks the benzoyl carbonyl to give a nitrosoisoxazole[172] which is unstable and undergoes a rearrangement, either spontaneously, or on heating, to the colourless furazan.[171,173] Boulton and co-workers experienced difficulty in repeating the reaction with dibenzoylfuroxan[174] and found that the proposed open-chain amidoxime structure was actually a 5-hydroxy-3-amino-isoxazol-4-one oxime. However, since a further carbonyl group is unavailable on **6**, the only option is for one of the oxime oxygen atoms to attack the other oxime nitrogen atom with loss of water to generate the furazan directly without going *via* the intermediate isoxazole.

To rationalise how **7** may have reacted with a six-membered ring, the possibility that a Minisci-type reaction had occurred with pyridine was initially considered, since

Minisci *et al.*[175] have reported radical carbamoylation of nitrogen heterocycles by $R_2NC^{\bullet}=O$ generated from formamide or DMF with H_2O_2, H_2SO_4 and $FeSO_4$. However, this theory was quickly discounted on the grounds that the crystal structure data clearly indicated ring C was phenyl, not pyridyl, and one of the fragment ions was due to $PhC=O^+$. Futhermore, protonation of the nitrogen atom in the Minisci reaction brings about an approximately 100-fold increase in reaction rate. Since very little pyridine would be protonated under these reaction conditions, it is highly unlikely that such a carbamoylation would occur. The most likely explanation is that the pyridine was derived from coal tar and contained benzene present as an impurity. With the amount of pyridine used, a benzene level of only 0.1–0.2% would be sufficient to account for the observed reaction yield of around 70%. Given that the Cu^{2+}/Cu^{+} couple has a propensity to participate in one electron catalytic cycles and Cu^{2+} complexes of amino furazans are known,[176] then it appears reasonable to speculate that the substrate acts as a bidentate ligand chelating $CuCl_2$ and the carbamoyl radical cation forms and reacts according to Scheme 4.8.

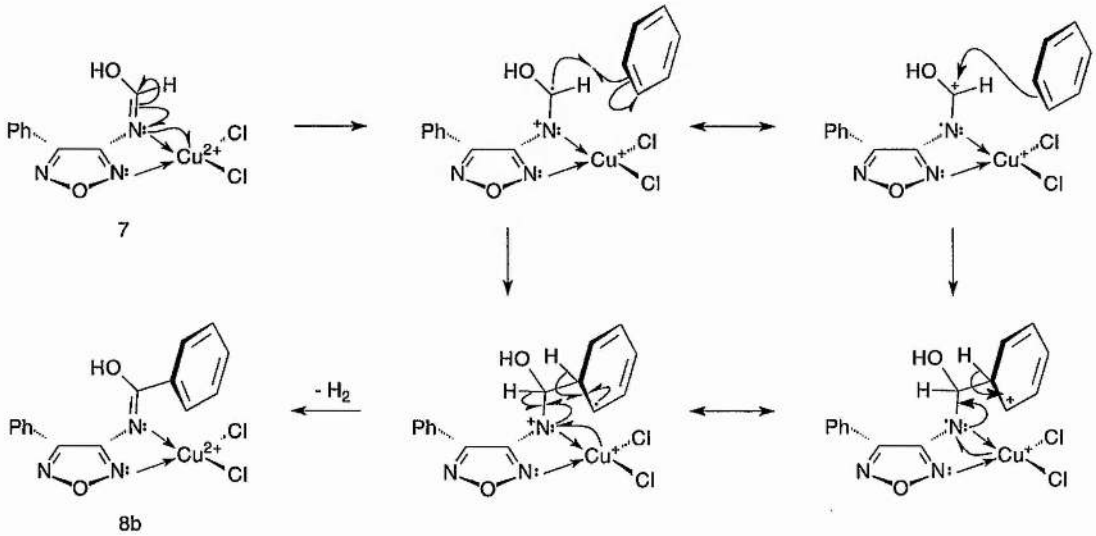

Scheme 4.8

Returning to the synthetic procedures for furoxans **2b** and **3b**, the synthesis of bis(phenylsulfonyl)furoxan illustrated in Scheme 4.9 has several points worthy of comment.

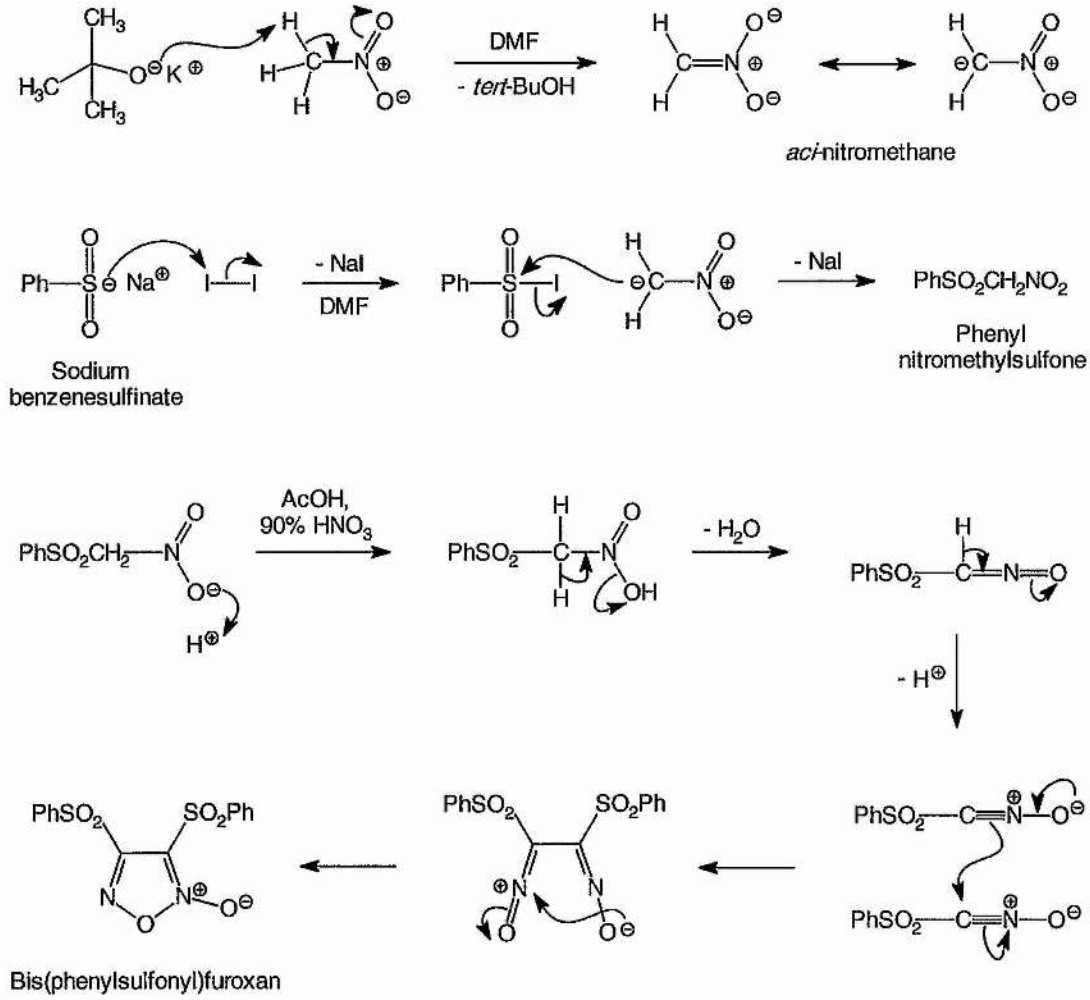

Scheme 4.9

In the formation of phenyl nitromethyl sulfone, poor yields were obtained using sodium methoxide and sodium ethoxide as the base, despite the literature claim that these reagents could be used in preference to the stronger potassium *tert*-butoxide. It was found that yields approaching that reported by Kelley *et al.*[177] could be obtained only by use of the latter base. This is surprising in light of the relatively low pK_a of

nitromethane compared with other carbon acids. The most likely explanation is that the potassium *tert*-butoxide used was a fresh commercial reagent and the sodium methoxide and ethoxide had to be prepared by reacting sodium metal with the appropriate solvent; it is difficult to obtain dry material with this method. Iodide is used here as a good leaving group to convert the sulfur of phenylsulfinate from a strong nucleophilic centre to one which is electrophilic enough to undergo attack by the conjugate base of nitromethane. The result is, in effect, a change from electrophilic to nucleophilic character (*umpolung*) at that sulfur atom. In the next stage, it has been suggested that the furoxan forms *via* dimerisation of a nitrile oxide intermediate. Alternative formally correct mechanisms can be written, but as represented, it can be seen that the reaction is acid catalysed and perhaps the driving force for loss of the proton to form the nitrile oxide is formation of the stable furoxan after dimerisation. It is interesting to note in the context of the biological activity of the other compounds discussed here that certain aromatic nitromethyl sulfone derivatives also display potent biological activity. Zeneca pharmaceuticals have investigated the enzymatic activity of compound ICI215918 and ZD5522 (Fig. 4.4) as potential aldose reductase inhibitors to reduce the complications inherent in diabetes. ZD5522 is undergoing clinical trials (D signifying the drug is in the development phase). It exhibits *in vivo* activity with an ED_{95} of 2.8 mg/kg which corresponds to a daily dosage in the region of 150–200 mg.

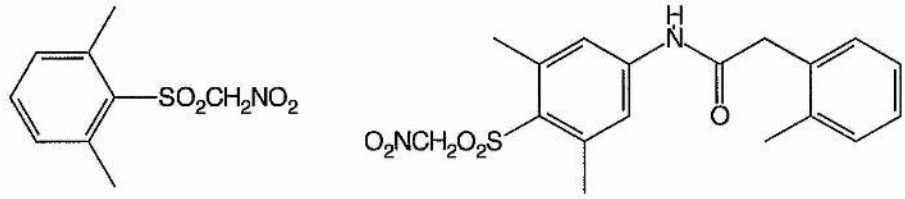

ICI215918 ZD5522

Fig. 4.4 Aryl nitromethylsufone derivatives investigated by Zeneca as aldose reductase inhibitors.

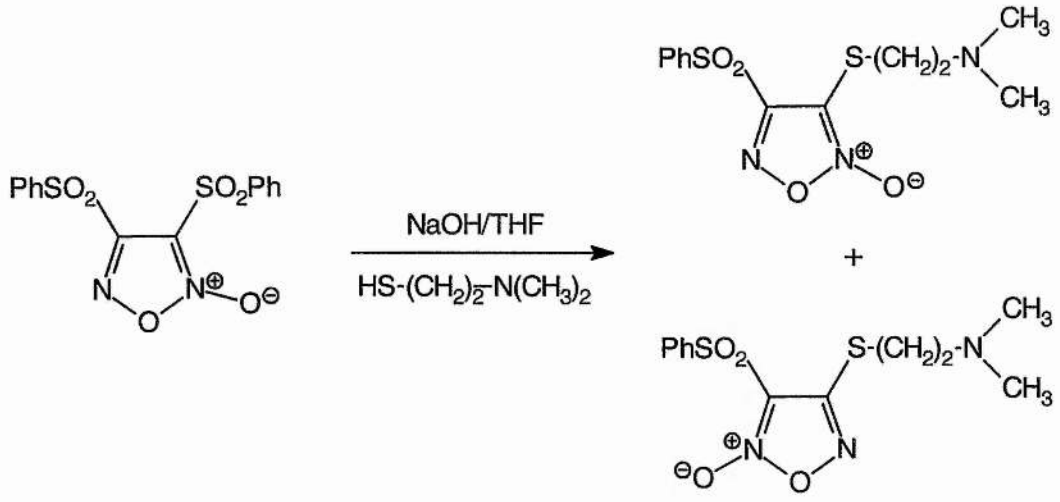

Scheme 4.10

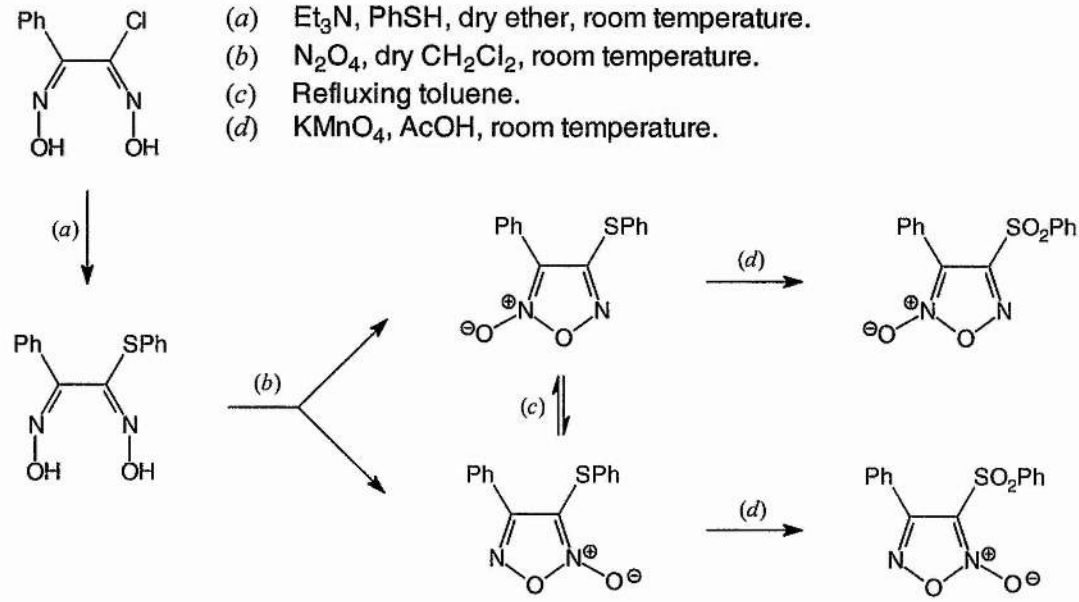

Scheme 4.11

4.2.2 Possible nitrogen-containing products produced by the thiol-mediated decomposition of furoxans 1 and 2b and problems in their identification

Several possibilities exist for the identity of the nitrogen-containing decomposition product(s) of furoxans **1** and **2b** when excess thiol is present depending on whether

the pathway is oxidative or reductive. An oxidative mechanism would, in all likelihood, lead to nitrite (as in the spontaneous decomposition of **3b**) or nitrate. However since thiols are effective reducing agents, the latter pathway ought to apply. In this instance nitroxylic acid (HNO) is a likely candidate for an intermediate species. This would only result from a two-electron reduction according to eqn. (3) as it is likely that nitric oxide is not reactive enough to abstract $H^{\bullet}$ shown in eqn. (2). Nitroxylic acid may then be further reduced to ammonia as represented by eqn. (4) or dimerise to form N_2O (a possible mechanism for this is illustrated in Scheme 4.12).

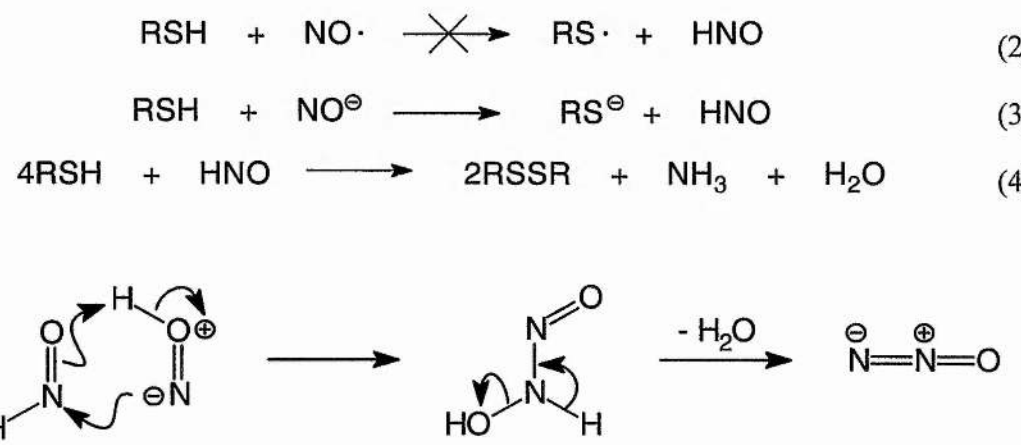

Scheme 4.12

Reduction to ammonia may involve sequential attack of thiolate ion, protonation, then displacement of disulfide by further attack of thiolate ion until eventually hydroxylamine is produced. Presumably this then undergoes thiolate reduction and/or disproportionates to nitrogen and ammonia. This sequence, similar to that proposed by Singh *et al.*,[178] is represented by eqns. (5)–(9).

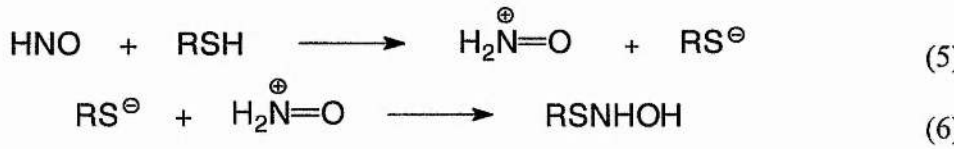

$$RSNHOH + RS^{\ominus} \longrightarrow RSSR + {}^{\ominus}NHOH \quad (7)$$

$$^{\ominus}NHOH + H_2O \longrightarrow NH_2OH + {}^{\ominus}OH \quad (8)$$

$$3NH_2OH \longrightarrow N_2 + NH_3 + H_2O \quad (9)$$

Since nitrous oxide is chemically unreactive, detection would have to involve blowing out any gas formed into a mass spectrometer on a stream of carrier gas. Unfortunately the mass of 44 coincides with carbon dioxide which poses a problem as it appears that unambiguous distinction by accurate mass determination is not practically possible. Bhattacharyya and Dailey[179] have determined NMR parameters for $^{15}N^{15}NO$ gas. In CCl_4 solution at 30 °C the central ^{15}N nucleus gives rise to a low-field doublet at δ_N 139 (508) ppm and the end ^{15}N nucleus to a doublet at δ_N 224 (593) ppm. The values were reported relative to $H^{15}NO_3$ and are approximately corrected relative to ^{15}N nitrobenzene. The values in parentheses are relative to liquid ammonia at 25 °C. It seems unlikely, however, that detection with ^{15}N NMR of N_2O evolved from a reaction will be possible.

It ought to be possible to test the hypothesis that release of nitroxyl from furoxans **1** and **2b** in the presence of excess of thiol yields ammonia as the main nitrogen-containing product. Species thought to release nitroxyl such as *N*-hydroxy-benzenesulfonamide (Piloty's Acid, PA), Angeli's salt or alkali metal nitrosyls such as sodium nitroxyl, NaNO) could be allowed to decompose under physiological conditions in the presence of a suitable thiol and an enzymatic ammonia assay used to quantify the yield. However, the release of nitroxyl from PA has not been unambiguously demonstrated and Zamora *et al.*[180] have shown that nitric oxide can itself be a product of the decomposition of PA (Scheme 4.13).

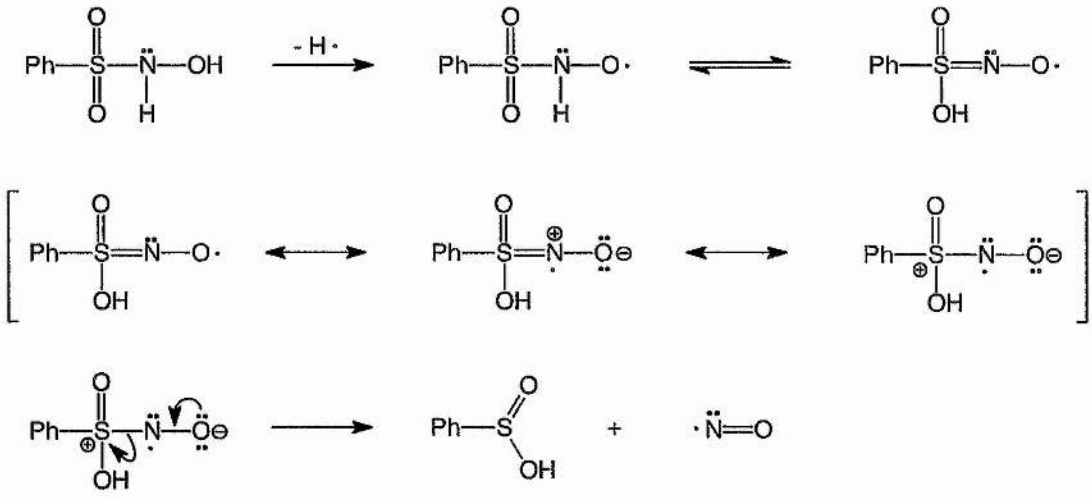

Scheme 4.13

In the case of NaNO, infra red data suggest that alkali metal nitrosyls do not exist as $M^{+}[NO]^{-}$ and might contain the *cis*-hyponitrite ion[181] ($Na_2[O–N=N–O]^{2-}$). It is reported in the literature that in order for decomposition to occur, a 50-fold excess of thiol is required. It is more likely, due to the first order dependency on both reactants giving a second order rate equation, that so long as the concentration of both thiol and furoxan substrate are high enough, one does not need to be present in a large excess. This also applies to the decomposition of *S*-nitrosothiols in the presence of thiols to yield ammonia as the main nitrogen-containing product.

4.2.3 Ammonia assay on decomposition of furoxans 1 and 2b in the presence of *N*-acetyl-DL-cysteine at pH 7.4 and 37 °C

4.2.3.1 Background information

Using the Sigma Diagnostics ammonia kit (procedure no. 171–UV) ammonia can be quantitatively detected in plasma by enzymatic reductive amination of 2-oxoglutarate using L-glutamate dehydrogenase and reduced nicotinamide adenine dinucleotide phosphate (Scheme 4.14).

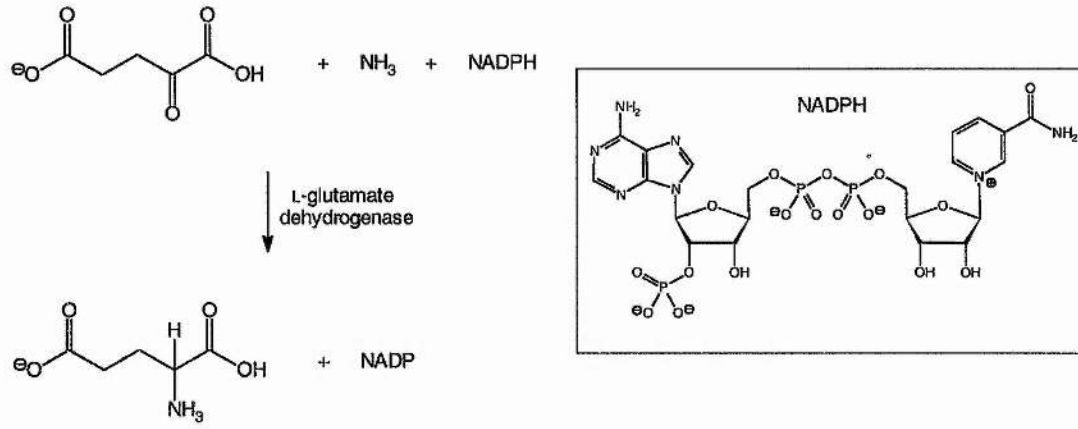

Scheme 4.14

The decrease in absorbance at 340 nm, due to the oxidation of NADPH is proportional to the 'plasma' ammonia concentration.[182,183] The assay is effective for testing with aqueous solutions provided. Methylated amines interfere with diffusion procedures[184] but do not react in the described method using the ammonia specific enzyme.

4.2.3.2 Results

Results are depicted in Tables 4.1–4.3.

Table 4.1 Absorbance changes in decomposition of **1** and **2b** oxalate in the presence of *N*-acetyl-L-cysteine (2.5 mM) at pH 7.4 and 37 °C.

Solution	$A_{initial}$	A_{final}	ΔA
Blank	1.185	1.134	0.051
Control	1.268	1.048	0.220
1, 50 μM	1.217	1.162	0.055
2b, 50 μM	1.216	1.169	0.047

Table 4.2 Absorbance changes in the decomposition of **1** and **2b** oxalate in the presence of *N*-acetyl-L-cysteine (10 mM) at pH 7.4 and 37 °C.

Solution	$A_{initial}$	A_{final}	ΔA
Blank	1.282	1.149	0.133
Control	1.257	0.980	0.277
1, 10 mM	8.448	7.844	0.604
2b, 10 mM	1.294	0.801	0.493

The formation of a bright yellow colour with furoxan **1** caused the absorbance reading to be abnormally high. To compensate for this, the solution was diluted by a factor of 4 before absorbance readings were taken and the result multiplied by 4 before calculation of the difference.

4.2.3.3 Calculations

1. $\Delta A = A_{initial} - A_{final}$
2. Ammonia level in test solution $(\mu g/cm^3) = (\Delta A_{test} - \Delta A_{blank}) \times 30.3$

   Ammonia level in control solution $(\mu g/cm^3) = (\Delta A_{control} - \Delta A_{blank}) \times 30.3$

   Where factor $30.3 = \dfrac{2.22 \times 17}{6.22 \times 0.2}$

   2.22 = Volume of liquid in cuvette.

   17 = Mass/μg of 1 μmol of ammonia.

   6.22 = Millimolar absorptivity of NADPH at 340 nm.

   0.2 = Volume/cm^3 of specimen.

Table 4.3 Amount of ammonia detected on decomposition of **1** and **2b** oxalate in the presence of *N*-acetyl-L-cysteine at pH 7.4 and 37 °C.

Furoxan	ΔA_{test}	ΔA_{blank}	$[NH_3]$/mM	% NH_3
1, 50 μM	0.055	0.051	0.0071	14.2
2b, 50 μM	0.047	0.051	—	—
1, 10 mM	0.604	0.133	0.841	8.4
2b, 10 mM	0.493	0.133	0.641	6.4

4.2.4 EPR investigation of the spontaneous decomposition of furoxan derivatives

If furoxan derivatives decompose, in part, by a radical pathway yielding nitric oxide, then it ought to be possible to trap both the nitric oxide produced in addition to the carbon-centred radical on the substrate and hence quantify the proportion decomposing *via* this route. In order that the work retains a physiological relevancy, it is desirable that the spin traps be soluble and active in aqueous phosphate buffer at pH 7.0–7.4.

4.2.4.1 Attempted detection of NO using *aci*-nitromethane as a spin trap

Reszka *et al.*[185] have utilised the conjugate base form of nitromethane, *aci*-nitromethane, in deaerated aqueous solution as a spin trap for NO. In the presence of strong alkali (0.5 M NaOH) an EPR signal similar to that simulated in Fig 4.5 should be observed from the radical dianion in eqn. (12) obtained after dissociation of a single β H at pH > 12 according to eqn. (11) from the primary spin adduct produced in eqn. (10).

(10)

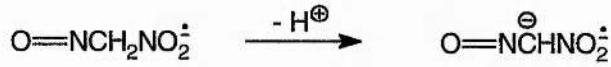

(11)

(12)

Unfortunately no EPR signals could be detected under these conditions. It is likely that if nitric oxide itself is released from furoxan derivatives then this carbon-centred spin trap is not efficient enough to trap nitric oxide released in non-stoichiometric quantities from chemical decomposition. In addition, Park[186] has observed that this technique gave erratic results.

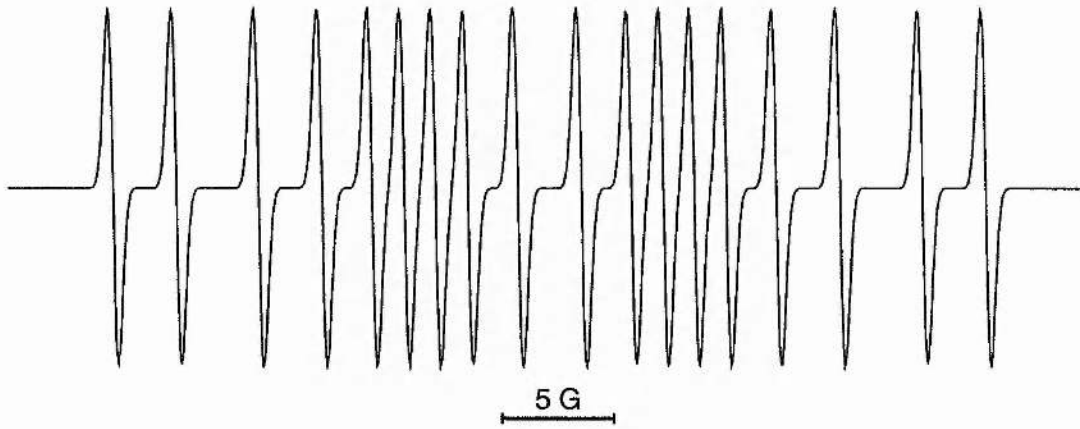

Fig. 4.5 Simulated EPR spectrum for the *aci*-nitromethane-NO spin adduct based on the hyperfine splitting constants $a_N^{NO_2} = 11.56$, $a_N^{NO} = 6.5$ and $a_H^{\beta} = 2.83$.

The *aci*-nitromethane system can also be used to trap $NO_2\cdot$ giving a similar radical dianion according to eqns. (13)–(15). It is interesting to note that Reszka *et al.* report that no signal was observed for the analogous radical dianion even during gassing with O_2 which strongly suggests that free $NO_2^{\bullet}$ is not an intermediate during autoxidation of nitric oxide in aqueous solution.

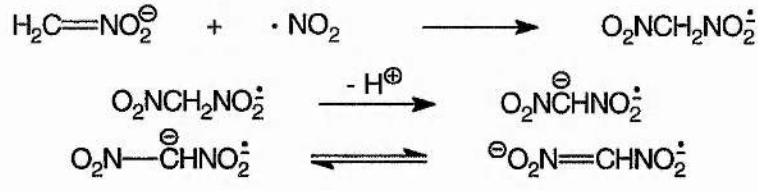

(13)

(14)

(15)

4.2.4.2 Detection of NO using Fe-MGD as a spin trap

In the presence of the NO trap Fe^{2+}-*N*-methyl-D-glucamine dithiocarbamate (Fe–MGD), NO gives rise to characteristic triplet EPR signals[187] with $g = 2.04$ and $a_N = 12.7$ G. Nitroxyl is diamagnetic and thus undetectable under these conditions. Samples of [^{14}N] and [^{15}N] SNAP were used to test the system by acting as an authentic NO donor. The $^{15}NO\cdot$ spin trapped adduct gives rise to a doublet signal due to the spin of the ^{15}N nucleus being ½. A triplet signal occurs with $^{14}NO\cdot$ as the spin of the natural isotope is 1. Quantitative formation of the NO–Fe^{2+}–MGD complexes formed from SNAP can be achieved photolytically in about 5 min by irradiation with a strong light source. In this way, the amount of NO released from furoxan decomposition can be quantified by comparing the double integral with that obtained from a known concentration of NO–Fe^{2+}–MGD adduct. It transpired that strong signals could be observed with 1mM samples of ^{14}N and ^{15}N SNAP in deaerated 50 mM pH 7.4 phosphate buffer in the presence of 10 mM *N*-methyl-D-glucamine dithiocarbamate and ferrous ammonium sulfate (1:5 w/w) without the need for photolysis (Fig. 4.6). Indeed when the sample was exposed to short (approx. 1–5 s) bursts of ultraviolet light the signal displayed transient intensity loss, presumably due to photolysis of the spin adduct followed by its rapid reformation.

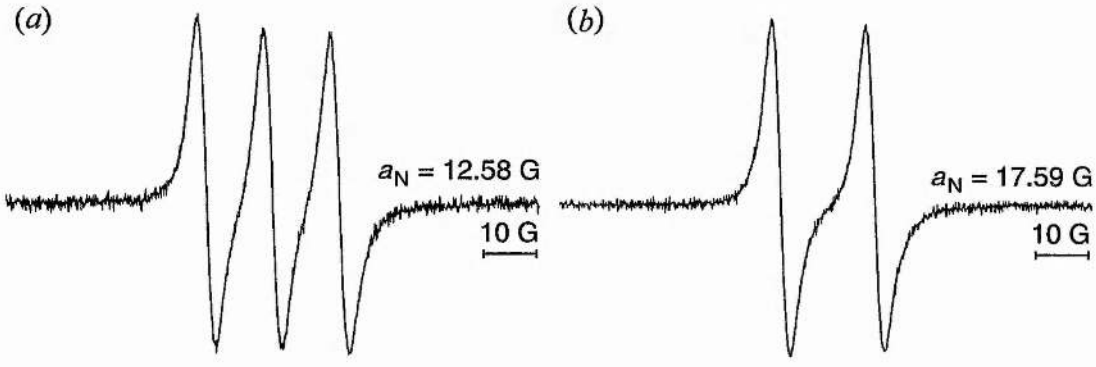

Fig. 4.6 EPR spectra obtained on addition of (*a*) ^{14}N SNAP and (*b*) ^{15}N SNAP to deaerated 50 mM pH 7.4 phosphate buffer in the presence of 10 mM *N*-methyl-D-

glucamine dithiocarbamate and ferrous ammonium sulfate (1:5 w/w) at 21 °C. Microwave frequency = 9.482 GHz and power = 6.346 mW.

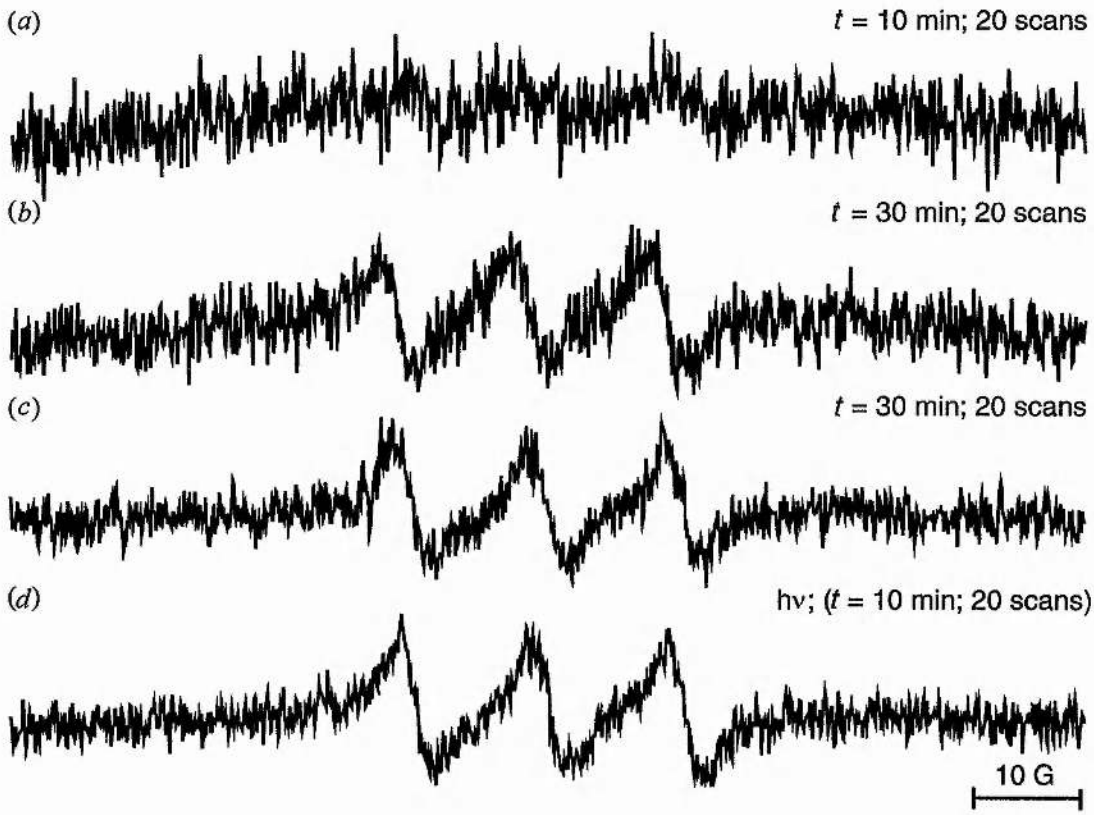

Fig. 4.7 EPR spectra obtained during the decomposition of furoxan derivatives in deaerated pH 7.4 phosphate buffer (50 mM) in the presence of *N*-methyl-D-glucamine dithiocarbamate (10 mM) and ferrous ammonium sulfate (1:5 w/w). (*a*) **1** incubated at 37 °C for 10 min in the presence of *N*-acetyl-DL-penicillamine (10 mM). (*b*) **2b** oxalate incubated at 37 °C for ½ h in the presence of *N*-acetyl-DL-penicillamine (10 mM). (*c*) **3b** oxalate incubated at 37 °C for ½ h. (*d*) **3b** oxalate subjected to photolysis at 21 °C. Microwave frequency = 9.492 GHz and power = 6.362 mW.

1 showed no obvious evidence of any EPR signals for the nitric oxide spin adduct either 10 min after initiating the reaction, incubation at 37 °C for ½ h or upon photolysis for 10 s. However, careful examination of Fig. 4.7 (*a*) reveals a regular

disturbance in the noise which may be a very weak triplet signal. **2b** and **3b** oxalates displayed weak signals for the nitric oxide spin adduct after incubation at 37 °C for ½ h (*b*) and (*c*) and upon photolysis for 10 s without prior incubation (*d*). However photolysis did not significantly alter the signal intensity of incubated samples.

4.2.4.3 Attempted detection of carbon-centred radicals using DBNBS as a spin-trap

The preparation and use of the water-soluble spin trap sodium 3,5-dibromo-4-nitrosobenzenesulfonate (DBNBS) is described by Kaur *et al.*[188] Nitrone traps with hydrophilic character are more commonly used in biological chemistry,[189,190] although the EPR spectra of nitrone spin-adducts are generally less informative[191] than spectra obtained using nitroso spin traps. In the former, the scavenged radical centre is 2-atoms removed from the unpaired electron whereas with nitroso compounds, the EPR spectrum is more likely to reveal splitting from magnetic nuclei in the trapped radical as this centre lies one atom removed from the unpaired electron (Scheme 4.15).

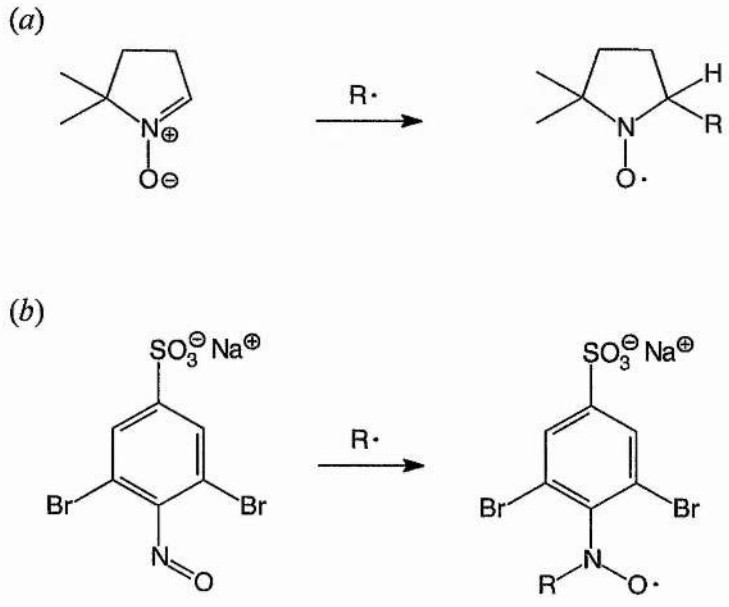

Scheme 4.15

The sulfonate group is necessary in order to confer the desired water solubility on the spin trap, whereas the 2 *ortho* positions are substituted to remove complications due to interaction with aromatic protons. One slight drawback with this system is that at high pH (≥10) signals from methyl radical may be observed[192] due to traces of acetic acid in the trap.

EPR spectra taken under similar conditions to those using the NO spin trap, but with DBNBS are shown in Fig. 4.8. They do not exhibit the characteristic triplet due to interaction of a carbon-centred radical with the nitroso group to form a nitroxide spin adduct. The spike present at 3385 G is an artifact presumably due to paramagnetic impurities present in the soda glass Pasteur pipettes used to contain the sample.

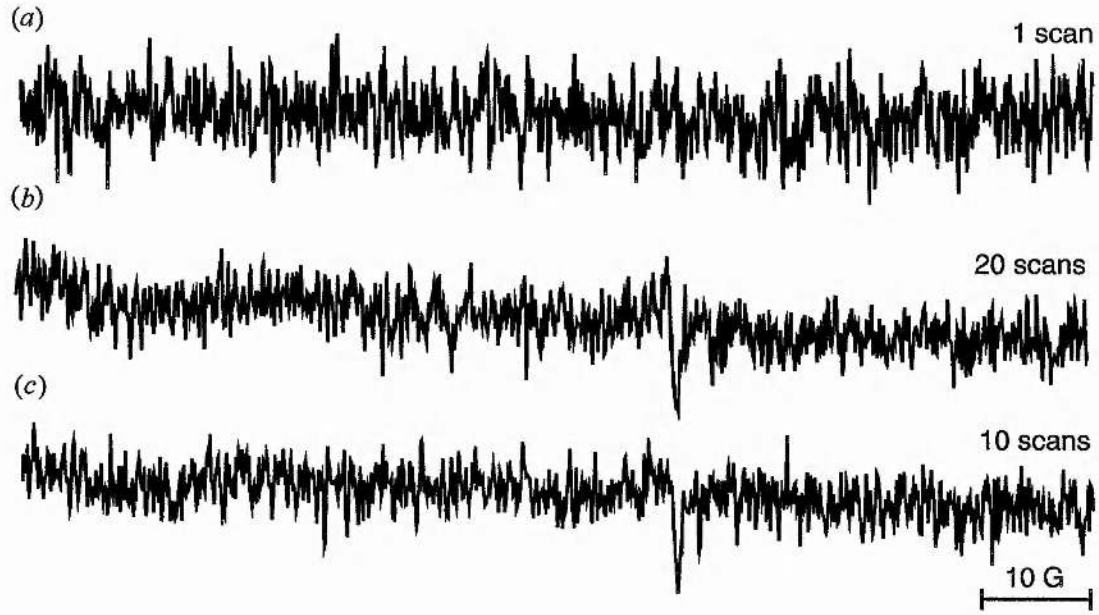

Fig. 4.8 EPR spectra obtained during the decomposition of furoxan derivatives in deaerated pH 7.4 phosphate buffer (50 mM) in the presence of DBNBS. (*a*) **2b** oxalate (1 mM) incubated at 37 °C for 10 min. (*b*) **2b** oxalate (1 mM) incubated at 37 °C for 10 min with *N*-acetyl-DL-penicillamine (10 mM). (*c*) **3b** oxalate (1 mM) incubated at 37 °C for 10 min.

4.3 Product analysis from furoxan decomposition

EI mass spectra of the major decomposition product from **3b** oxalate were dominated by peaks at 279 $[M–H]^+$, 167, and 149. Typical abundance ratios were approximately 15%, 35% and 85% respectively. The accurate masses were determined to be 279.159735, 167.034102 and 149.023738. Although a possible species from the decomposition process could be formulated with a molecular mass of 279, it is an unlikely product and there exhibits a discrepancy in the accurate mass of more than 0.1 mass units. It appears very likely that these peaks were due to the presence of dibutyl phthalate in the sample. An additional peak present at 157 mass units in one spectrum may well be due to the fragmentation of diisooctyl phthalate, although no peak at $[M–H]^+$ at 390 mass units was observed for this species. These are plasticisers widely used in industry to mould many plastic materials including PVA, PVB (polyvinylbutyral) and PVC. It can be extracted from rubber tubing, plastic tubing, plastic containers and plastic seals in glass bottles. It is seen as a contaminant in many extracted materials where solvents have been concentrated to small volume, leaving the involatile phthalates in the residue. This contamination made analysis of the decomposition products difficult. However, the available ^1H and ^{13}C NMR data seem to point to the formation of (2-phenylsulfonyl-1-(2-dimethylamino-ethylsulfanyl)-2-nitroso-ethenol from decomposition of **3b** oxalate, which would be consistent with the mechanisms proposed in schemes 4.3 and 4.4.

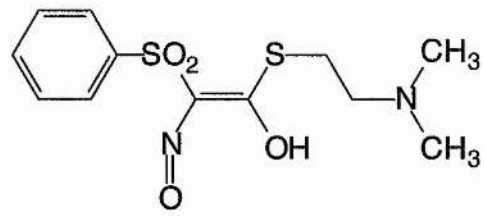

(2-phenylsulfonyl-1-(2-dimethylamino-ethylsulfanyl))-2-nitroso-ethenol

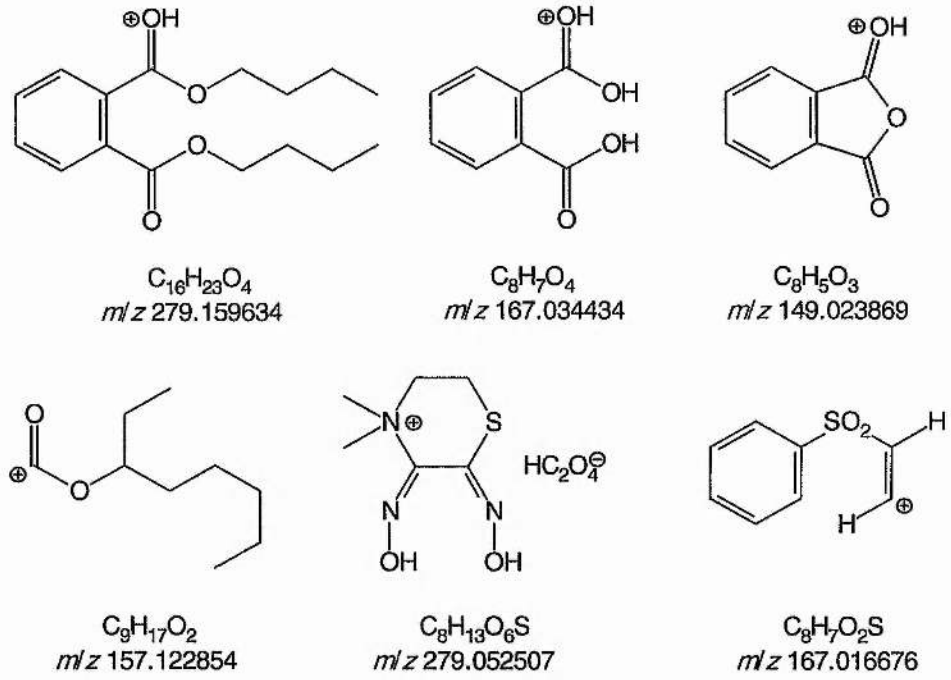

Fig. 4.9 Fragmentation pattern of dibutyl phthalate and other possible species accounting for similar *m/z* ratios arising from furoxan decomposition.

Fig. 4.9 shows these fragments and the possible species arising from the decomposition process with masses close to those observed.

4.4 Conclusions

The successful trapping of nitric oxide from the decomposition of these furoxan derivatives indicates that radical decomposition pathways such as those outlined in Schemes 4.2 and 4.4 are valid, although from the weakness of the EPR signals the most reasonable conclusion is that this is a minor decomposition mode, *i.e.* < 1%. The detection of such small quantities of NO does not necessarily imply that the *in vivo* activity will be limited by this factor, since it is well known that nitrite may be reduced to nitric oxide under physiological conditions. For instance, Yoshioka *et al.*[193] have used this same EPR trapping system with Fe^{2+}–MGD to characterise the nitrite reducing activity of human red blood cells, umbilical vein endothelial cells and aortic

smooth muscle cells independent of thiols or ferrous haem. It is unsurprising that approximately 90% of the nitrogen-containing decomposition product of these furoxan derivatives is nitrite since it may be formed either by the intermediacy of a nitrosothiol followed by reduction to a disulfide, or simply by attack of hydroxide ions from the solvent according to the speculative mechanism in Scheme 4.3. As Gasco and co-workers have demonstrated, this can easily be quantified using the Griess test.[8] If the enzymatic assay is considered to be reliable, then ammonia can account for the remaining 10% of the nitrogen-containing decomposition product under physiological conditions. This is a sufficiently significant result to merit consideration when assessing the toxicity of potential therapeutic treatments based on furoxan derivatives. One further point which emerges from these results is that since the furoxan ring system is attacked by hydroxide ion and softer, sulfur-centred nucleophiles it ought to be relatively stable under acidic conditions such as those encountered in gastric fluids. One potential advantage of this property is that orally-administered preparations containing furoxans as intended NO-donor compounds will be more likely to survive passage through the gastro-intestinal tract until they can be suitably absorbed into the bloodstream than, say, nitrosothiol-based drugs. The pH of the small intestine is approximately 8, at which the $t_{½}$ of furoxan derivatives is approximately 10 min. Indeed, this particular characteristic has been exploited by Sorba *et al.*[164] and Fruttero *et al.*[194] in the synthesis of hybrid drugs with mixed NO-donating and α_1 or H_2-receptor antagonist properties. Since H_2-receptors control a variety of responses including histamine, gastrin and acetylcholine, the latter would prove useful in treating gastric hypersecretion and ulcers.

In summary, it is apparent that although the Capdevielle reaction for one-pot conversion of aldehydes to nitriles is a very convenient and widely applicable

synthetic procedure, whenever any functional group transformations are attempted on furoxans, caution must be exercised since there is scope for a wide range of remarkable rearrangements, isomerizations and secondary reactions. These are thoroughly outlined in the review by Gasco and Boulton. Given the atypical coincidences which favoured the formation of this product, it would be unsound to suggest the reaction could be usefully incorporated into a synthetic methodology. The formamide formed because that particular furoxan derivative favoured such a rearrangement. The ability of the substrate to act as a bidentate ligand for $CuCl_2$ probably facilitated formation of the carbamoyl radical cation and the large excess of pyridine used undoubtedly lead to reaction with a minor aromatic impurity which would not normally have presented a problem. The 4-substituted 3-aminofurazan moiety forms the backbone of classical histamine H-2 receptor antagonists.[195,196] However, the method utilised here would not offer a convenient method of preparing derivatives other than 4-methyl or 4-phenyl due to the difficulty in preparation and handling of the intermediate furoxan carbaldehydes.

5 Experimental

Melting points were carried out on an Electrothermal 9100 apparatus and are uncorrected. CHN microanalyses were performed on a Carlo-Erba Model 1106 elemental analyser. Routine ^{1}H and ^{13}C NMR spectra were obtained with a Varian Gemini 200 spectrometer; chemical shifts are indirectly referenced to TMS *via* the solvent signal. Other work was performed with a Varian Unity*plus* machine operating at 11.74 T (500.3 MHz for ^{1}H, 125.8 MHz for ^{13}C and 50.7 MHz for ^{15}N). *J* values are given in Hz. NMR assignments for the AYV tripeptide and *N*-methyl-D-glucamine dithiocarbamate were made using a variety of 2D pulse sequences. $[\alpha]_D^{22}$ values were measured on an Optical Activity AA–1000 polarimeter using a 5 cm path length cell and are given in deg cm^2 g^{-1}. Infra-red spectra were obtained on a Perkin Elmer 1710 FTIR spectrometer, uv-visible spectra on a Philips PU8700 spectrophotometer and mass spectra either on a VG 70–25 SE, a Kratos MS–50 spectrometer or by the SERC service at Swansea using a VG AZB–E. An Applied Photophysics Model SX–17MV stopped flow spectrometer was used for determination of fast reaction rates. A Bruker ER–200D spectrometer was used in preliminary EPR investigations. However, reported spectra were recorded on a Bruker EMX–10/12. Photolysis was achieved in the spectrometer cavity using an unfiltered 500W super pressure Hg lamp. EPR spectral manipulation and simulation were carried out using the WIN-EPR and SimFonia® software (Bruker AG). The computer program Scientist® by MicroMath Scientific Software, USA was used for kinetic simulations. The software was run on an IBM-compatible personal computer equipped with an Intel 80586 Pentium® II processor of 233 MHz clock speed with MMX™ technology and 64 Mb RAM. Visualisation of crystal structures was accomplished using the WebLab ViewerPro software from Molecular Simulations Inc. Reference citation counts were obtained from the Bath Information and Data Service (BIDS).

5.1 Reaction of $H^{15}NO_3$ with *N*-acetyl-L-tyrosine

Spectra were acquired using a 5 mm–Inv probe for 8 scans with a 25 ° pulse and 14.672 s recycle (pulse repetition) time. Proton decoupling was off. [^{15}N] nitrobenzene contained in a sealed soda glass capillary placed in the NMR tube was referenced externally to liquid ammonia at 25 °C. *N*-Acetyl-L-tyrosine was purchased from Sigma and used without further purification. $H^{15}NO_3$ (0.25 cm^3, 40%, 98% atom N), sodium nitrite (0.25 cm^3, 0.004 M) and *N*-acetyl-L-tyrosine (0.0223 g) were placed in an NMR tube along with distilled water (0.5 cm^3) and D_2O (0.025 cm^3). Final concentrations were 0.100 M (*N*-acetyl-L-tyrosine), 2.25 M (nitric acid) and 0.001 M (sodium nitrite). The temperature of the NMR probe was regulated at 37 °C. The precipitate formed during the experiment analysed as [^{15}N]$_1$ 3-nitro-*N*-acetyl-L-tyrosine, mp 185–187 °C (Found: C, 49.17; H, 4.52; N, 10.42. $C_{11}H_{13}(^{15}N)NO_6$ requires C, 49.08; H, 4.49; N, 10.77%); δ_H(200 MHz; DMSO-d_6) 1.80 (3 H, s, COC*H*$_3$), 2.75–3.10 (2 H, m, *J* 5, CC*H*$_2$), 4.42 (1 H, m, *J* 5, *Hα*), 7.07 (1 H, d, *J* 8, Ar*H*2), 7.44 (1 H, dd, *J* 8 and 2, Ar*H*3), 7.78 (1 H, d, *J* 2, Ar*H*2′), 8.21 (1 H, d, *J* 8, N*H*); δ_C (50 MHz; DMSO-d_6) 22.6 (CO*C*H$_3$), 35.6 (Ar*C*H$_2$), 53.5 (α*C*), 119.3 (Ar*C*3′), 125.6 (Ar*C*2), 129.2 (Ar*C*2′), 136.5 (Ar*C*NO$_2$), 136.6 (Ar*C*1), 151.1 (Ar*C*OH), 169.5 (*C*OCH$_3$), 173.1 (*C*O$_2$H); δ_N(50.7 MHz; H_2O/D_2O; NH_3 (l)) 370.3; *m/z* (EI) 270 (M-H, 11%), 251 (81), 210 (100).

5.2 Reaction of alkaline [^{15}N] oxoperoxonitrate(1–) with L-tyrosine

Spectrometer conditions were identical to those described for the reaction of *N*-acetyl-L-tyrosine with $H^{15}NO_3$. $ONOO^-$ (1 cm^3 containing 5% D_2O, approx. 0.1 M) and L-tyrosine (0.0045 g, 0.025 M) were placed in an NMR tube. The temperature of the NMR probe was regulated at 25 °C. 100 mM pH 7.0 phosphate buffer was made up by dissolving 1 part Na_2HPO_4 to 9 parts NaH_2PO_4 in distilled water.

5.3 Reaction of [^{15}N] oxoperoxonitrate(1–) with frozen pH 7.4 phosphate buffer containing L-tyrosine, *O*-methyl-L-tyrosine, *N*-acetyl-DL-penicillamine or L-alanyl-L-tyrosyl-L-valine

A 10 mm broadband tunable probe was used but otherwise, spectrometer conditions were identical to those described for the reaction of *N*-acetyl-L-tyrosine with $H^{15}NO_3$. Starting lock level was between 20 and 25% and final lock level had fallen to around 5%. A solution of the appropriate substrate (0.05 M) was made up in a volumetric flask of 2 cm^3 capacity using 100 mM pH 7.4 phosphate buffer. This was transferred to a 10 mm NMR tube and a 5 mm NMR tube was inserted into the solution. The liquid was carefully frozen around the smaller tube by slowly lowering the 10 mm tube into an ethanol/dry ice bath. In this way, the liquid could expand upwards rather than outwards and hence the risk of cracking the fragile glass was avoided. When the solution had solidified, hot ethanol was added to the 5 mm tube to melt the substrate/buffer solution sufficiently to allow the 5 mm tube to be withdrawn leaving a coaxial channel in the frozen solution. The 10 mm tube was returned to the ethanol/dry ice bath for a short time to halt further melting and then placed in the freezer compartment of a refrigerator until required. A solution of [^{15}N] oxoperoxonitrate(1–) of nominal 0.1 M concentration and containing 10% D_2O was made in a 2 cm^3 volumetric flask in the manner previously described. This was left for at least 15 min to ensure complete reaction of the alkyl nitrite and the hydrogen peroxide. The liquid was then cooled in a refrigerator at 3–5 °C until required. To initiate the run, the peroxynitrite was added to the frozen solution along with the ^{15}N nitrobenzene reference contained in a sealed soda glass capillary tube.

5.4 Synthesis of [^{15}N] compounds

Technical grade $Na^{15}NO_2$ (98%+ atom N) and [^{15}N] nitrobenzene were obtained from Cambridge Isotope Laboratories and used without further purification. All chemical shifts are quoted downfield relative to liquid ammonia at 25 °C and were measured relative to [^{15}N] nitrobenzene (δ_N 370.3) as an external standard contained in a sealed soda glass capillary placed inside the NMR tube.

5.5 [^{15}N] 1-Ethoxy-2-nitrosooxy-ethane. Prepared according to the method of Noyes[197] for n-butyl nitrite. 2-Ethoxyethanol of spectrophotometric grade (99%) was purchased from Aldrich. $Na^{15}NO_2$ (1.0 g, 0.014 mol) was dissolved in distilled water (4 cm^3) and cooled to 0 °C. A mixture of concentrated sulfuric acid (0.37 cm^3), distilled water (0.27 cm^3), and 2-ethoxyethanol (1.33 cm^3) was cooled to 0 °C and by means of a dropping funnel introduced slowly beneath the surface of the nitrite solution, with stirring. The alcohol solution was added over a period of 1½–2 h so that practically no gas was evolved and the temperature remained at ± 1 °C. After this time, the reaction mixture separated into layers which were decanted from the precipitated sodium sulfate into a separating funnel and the organic liquid drawn off with a Pasteur pipette. 1.17 g (73%). density/g cm^{-3} 1.0077; ν_{max} (neat liquid)/cm^{-1} 2980 (CH_3 asymm.), 2935 (CH_2 asymm.), 2873 (CH_3CH_2O str.), 1624 (^{15}N=O str., *cf.* 1654 ^{14}N=O str.) and 1128 (C–O–C str.); λ_{max} (CH_3OH)/nm 266 (ε/M^{-1} cm^{-1} 82), 320 (29), 330 (43), 341 (57), 353 (59) and 366 (39); δ_H (200 MHz; $CDCl_3$) 1.19 (3 H, t, CH_3), 3.54 (2 H, q, CH_3CH_2O), 3.71 (2 H, m, OCH_2CH_2); δ_C (50 MHz; $CDCl_3$) 15.4 (CH_3), 67.2 (CH_3CH_2O), 67.7 (OCH_2), 68.9 (CH_2ONO); δ_N (50.7 MHz; neat liquid; NH_3 (l)) 576.4.

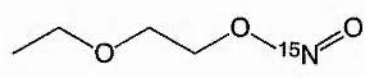

5.6 Standardisation of potassium manganate(VII), $KMnO_4$. A freshly prepared potassium permanganate solution of approximately 0.1 M was standardised against sodium oxalate using the following procedure. Analytical grade sodium oxalate (approx. 1.7 g, 12.7 mmol) was weighed out accurately and transferred to a 100 cm^3 titration flask. H_2SO_4 (5 M, 6 cm^3) was added to the flask together with distilled water (25 cm^3). The solution was warmed and sufficient potassium permanganate added to form a pale pink colour which turned colourless after standing for about 1 min. The solution was further heated to 50–60 °C and the titration continued until half a drop of permanganate afforded a permanent faint pink colour. Titrations were repeated until two results agreed to within 0.02 cm^3. The reaction is represented by eqn. (1).

$$2MnO_4^{\ominus} + 16H^{\oplus} + 5C_2O_4^{2\ominus} \longrightarrow 2Mn^{2\oplus} + 10CO_2 + 8H_2O \quad (1)$$

5.7 Standardisation of hydrogen peroxide, H_2O_2. '100–volume' (>35%) hydrogen peroxide (density 1.137 g cm^{-3}) was standardised in the manner described below against standard potassium permanganate. Hydrogen peroxide stock was diluted by 1 cm^3 in 100 cm^3 of distilled water in a volumetric flask. A 25 cm^3 aliquot of this solution was transferred to a 250 cm^3 titration flask and diluted with 200 cm^3 of distilled water. H_2SO_4 (3.6 M, 20 cm^3) was added. This solution was titrated with the permanganate until half a drop afforded a permanent faint pink colour. Titrations were repeated until two results agreed to within 0.02 cm^3. A typical batch of hydrogen peroxide was approximately 11.3 M. Mixtures containing hydrogen peroxide were kept refrigerated at 3–5 °C when not in use to discourage decomposition to water and oxygen The '100–volume' stock was assumed to have a useful shelf life of three months. The reaction is represented by eqn. (2).

$$2MnO_4^{\ominus} + 5H_2O_2 + 6H^{\oplus} \longrightarrow 2Mn^{2\oplus} + 5O_2 + 8H_2O \quad (2)$$

5.8 Preparation and standardisation of sodium chlorate(I), NaOCl. Sodium hypochlorite (1 M) was prepared by saturating a solution of NaOH (2 M) with chlorine gas generated by the action of concentrated HCl on $KMnO_4$. The solution thus prepared was stored in a refrigerator to minimise disproportionation of the product. Standardisation was carried out using an iodometric method. The sodium hypochlorite (approx. 1 M) was diluted by a factor of 10. Potassium iodide (2 g) free of trace iodate was added and glacial acetic acid (10 cm^3) was added. The liberated iodine was titrated with 0.1 N sodium thiosulfate according to eqns. (3) and (4).

$$I_2 + 2S_2O_3^{2\ominus} \longrightarrow 2I^{\ominus} + S_4O_6^{2\ominus} \quad (3)$$

$$OCl^{\ominus} + 2I^{\ominus} + 2H^{\oplus} \rightleftharpoons Cl^{\ominus} + I_2 + H_2O \quad (4)$$

5.9 [^{15}N] Oxoperoxonitrate(1–). Prepared according to the method of Leis *et al.*[21] Milli-Q® deionised water was used for preparation of aqueous solutions. [^{15}N] Oxoperoxonitrate was synthesised as required in 2 cm^3 aliquots by the reaction of a solution containing hydrogen peroxide (0.883 cm^3, 11.3 M) and sodium hydroxide (0.60 g) per 100 cm^3 of deionised water with an equimolar quantity of 1-ethoxy-2-nitrosooxy-ethane (0.0238 cm^3). λ_{max} (H_2O)/nm 302 (ε /M^{-1} cm^{-1} 1670 ± 50); δ_N (50.7 MHz; H_2O/D_2O; NH_3 (l)) 554.6.

5.10 [^{15}N]$_1$ 3-Nitro-L-tyrosine. Prepared according to the method of Dall'asta and Ferrario.[198] To a suspension of L-tyrosine (0.48 g, 5.33 mmol) in distilled water (4 cm^3), $H^{15}NO_3$ (0.5 cm^3, 40%, 9.01 M) was added with stirring at room temperature over a period of ½ h. After allowing the solution to cool in an ice bath to 5–8 °C,

$H^{15}NO_3$ (0.5 cm^3, 40%, 9.01 M) was added over 2 h. The temperature increased to 23 °C over that time and a yellow precipitate formed. Stirring was continued for 5 h at room temperature then the solution refrigerated overnight. The orange-yellow product (X-$H^{15}NO_3$) was filtered off and washed with an aqueous solution of $NaHCO_3$ yielding the title compound (0.44 g, 75%), mp 215–217 °C dec. δ_H (200 MHz; D_2O/DCl) 3.13 (2 H, m, *J* 7 and 2, ArCH_2), 4.23 (1 H, t, *J* 7, *α*H), 6.98 (1 H, d, *J* 9, Ar*H*2), 7.40 (1 H, dd, *J* 9 and 2, Ar*H*3), 7.85 (1 H, d, *J* 2, Ar*H*2′); δ_C (50 MHz, D_2O/DCl) 37.1 (ArCH_2), 56.4 (*αC*), 123.2 (Ar*C*3′), 128.7 (Ar*C*2), 129.2 (Ar*C*2′), 136.8 ($^1J_{NC}$ – 13.7, Ar$C^{15}NO_2$), 141.2 (Ar*C*1), 155.7 (Ar*C*OH), 173.6 (*C*O_2H); δ_N (50.7 MHz; H_2O/D_2O; NH_3 (l)) 375.3.

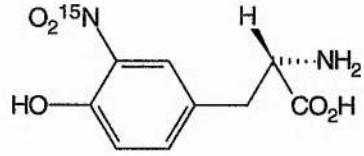

5.11 **[^{15}N]$_1$ *S*-Nitroso-*N*-acetyl-DL-penicillamine**. Prepared according to the method of Field *et al.*[199] A solution of [^{15}N] $NaNO_2$ (0.5 g, 7.25 mmol) in water (5 cm^3) was added during 20 min to a solution of *N*-acetyl-DL-penicillamine (0.69 g, 3.62 mmol) in MeOH–1 N HCl (10 cm^3, 1:1) with vigorous stirring at room temperature. Stirring was continued for a further 15 min, after which time the mixture was filtered, washed with water and air-dried to give the title compound as deep green crystals with red reflections (0.68 g, 85%), mp 152–154 °C dec. δ_H (200 MHz; DMSO-d_6) 1.88 (3 H, s, Ac-CH_3), 1.96 (6 H, d, *J* 5.2, *β*-CH_3), 5.18 (1 H, d, *J* 9.5, *αH*), 8.55 (1 H, d, *J* 9.5, N*H*); δ_C (50 MHz; DMSO-d_6) 22.5 (Ac-CH_3), 25.5 and 26.5 (*β*-CH_3), 58.6 (*C*-SNO), 59.4 (*αC*), 169.9 (Ac–*C*=O), 171.1 (–*C*O_2H).

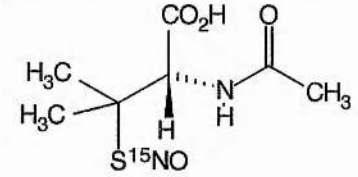

5.12 ***N*-Heptanoyl-DL-penicillamine**. Prepared according to the method of Greig.[200] DL-Penicillamine (6 g, 40.2 mmol) and sodium heptanoate (12.2 g, 80.8 mmol, 2 eq.) were stirred in a solution of 90% aqueous THF cooled in an ice-water bath. Heptanoic anhydride (10.5 cm^3, 40.2 mmol, 1 eq.) was added and the mixture stirred at room temperature overnight. The solvent was removed *in vacuo* and the oily residue dissolved in water. Concentrated HCl was added until precipitation occurred. The solid product was filtered off, washed with water and dried in a vacuum desiccator. The title compound was obtained as a white powder (9.3 g, 89%), mp 118–119 °C (hexane). (Found: C, 54.22; H, 8.90; N, 5.25. $C_{12}H_{23}NO_3S$ requires C, 55.14; H, 8.87; N, 5.36%); δ_H (200 MHz; DMSO-d_6) 0.9 (3 H, m, heptanoyl C*H*$_3$), 1.25–1.5 (10 H, m, heptanoyl CH_2), 2.2 (6 H, m, pen. C*H*$_3$), 2.95 (1 H, s, S*H*), 4.45 (1 H, d, *J* 9, C*H*), 8.1 (1 H, d, *J* 9, N*H*); δ_C (50 MHz; DMSO-d_6) 14.2, 22.3, 25.6 and 28.5 (heptanoyl), 29.8 and 30.2 (HSCH_3)$_2$, 31.2 and 35.2 (heptanoyl), 45.4 (HS*C*(CH)$_2$), 61.5 (HNCHR), 171.6 and 172.7 (heptanoyl and *C*O_2H); *m/z* (FAB) 262 (M^+, 50%), 187 ($M^+ - 75$, 100%; $(CH_3)_2CHSH^+$).

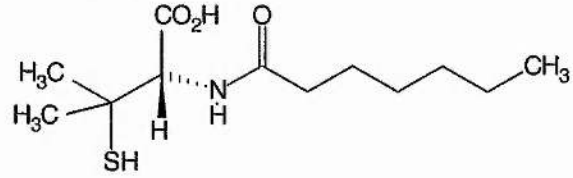

5.13 **[^{15}N]$_1$ *S*-Nitroso-*N*-heptanoyl-DL-penicillamine**. *N*-Heptanoyl-DL-penicillamine (0.28 g, 1.09 mmol) in MeOH–1 N HCl (20 cm^3, 1:1) was added to $Na^{15}NO_2$ (0.075 g, 1.09 mmol) in distilled water (10 cm^3) with concentrated sulfuric acid (0.5 cm^3) during 20 min with vigorous stirring. After a further 15 min, the title compound was isolated by filtration, washed well with water and air-dried to give green dichroic crystals with red reflections. (0.18 g, 57%), mp 77.5–78.0 °C. (Found:

C, 43.98; H, 6.92; N, 7.30. $C_{12}H_{22}N_2O_4S$ requires C, 49.46; H, 7.61; N, 9.99%.)[†] ; δ_H (200 MHz; DMSO-d_6) 0.86 (3 H, t, CH_3), 1.30–1.55 (6 H, m, CH_2), 1.97 (2 H, m, CH_2), 2.17 (2 H, m, CH_2), 5.20 (1 H, d, *J* 10, C*H*), 8.46 (1 H, d, *J* 10, NH); δ_C (50 MHz; DMSO-d_6) 14.2, 22.3, 25.6 and 26.6 (C(CH_3)$_2$), 25.4, 28.4, 31.2, 35.0 and 58.6 (*C*(CH_3)$_2$), 59.2 (*C*H), 171.1 and 172.9 (*C*(O)NH_2 and *C*O_2H); δ_N (50.7 MHz; DMSO-d_6; NH_3 (l)) 466; *m/z* (FAB) 521 (disulfide, 50%), 292 (M–H, 22%), 260 (M–H – 32, 52%, – ^{15}NO), 228 (M–H – 64, 100%).

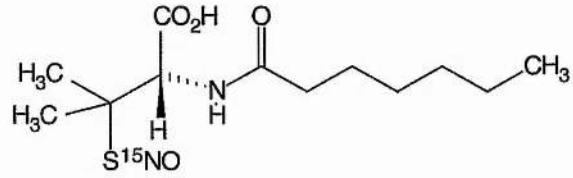

5.14 ***N*$^{\alpha}$-*tert*-Butoxycarbonyl-L-alanine**. Prepared according to the method of Tarbell *et al.*[201] A solution of L-alanine (4.45 g, 50 mmol) in a mixture of 1,4-dioxane (100 cm^3), water (50 cm^3) and 1 N NaOH (50 cm^3) was stirred and cooled in an ice-water bath. Di-*tert*-butyldicarbonate (12 g, 55 mmol) was added and stirring continued at room temperature for approximately 30 min. The solution was concentrated *in vacuo* to 10 to 15 cm^3, cooled in an ice-water bath, covered with a layer of ethyl acetate (30 cm^3) and acidified with a dilute solution of $KHSO_4$ to pH 2–3. The aqueous phase was extracted twice with ethyl acetate (15 cm^3). The combined organic extracts were washed twice with water (30 cm^3), dried over anhydrous $MgSO_4$ and reduced *in vacuo* giving the title compound (8.3 g, 88%), mp 76–78 °C. (lit. 80–82 °C). δ_H(200 MHz; $CDCl_3$) 1.41 (3 H, d, CH_3CH), 1.44 (6 H, s, (CH_3)$_3$C), 4.17 (1 H, q, *αH*), 6.94 (1 H, s, N*H*), 10.17 (1 H, bs, CO_2H); δ_C(50 MHz $CDCl_3$), 18.9 (CH_3), 28.8 (CH_3)$_3$C), 49.5 (*αC*), 80.8 (CH_3)$_3$*C*), 155.9 (*C*=ONH), 177.7 (*C*O_2H).

[†] Elemental analyses of acceptable accuracy (± 0.4%) could not be obtained for either *N*-acetyl-DL-penicillamine or the *S*-nitroso derivative due to loss of mass on weighing. In the latter instance this is due to thermal decomposition of the *S*-nitroso group.

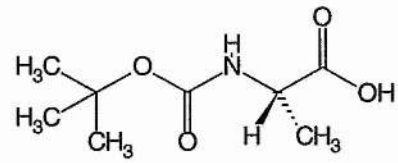

5.15 **L-Tyrosine benzyl ester hydrochloride**. Prepared according to the method of Erlanger and Hall.[202] L-Tyrosine (5.44 g, 30 mmol) was added to a mixture of benzyl alcohol (62.5 cm^3) and polyphosphoric acid (12.5 g). The mixture was stirred and heated at 90–95 °C for 4 h. The solution was then poured into 250 cm^3 of water containing 25 cm^3 of concentrated HCl. Diethyl ether was added and the water layer collected. The ether layer was then washed three times with 2% HCl. All aqueous fractions were collected, brought to a pH of about 10 with solid Na_2CO_3 and shaken with diethyl ether (three 100 cm^3 portions). The ether layer was dried over anhydrous magnesium sulfate and nearly saturated with HCl gas. The title product precipitated as a white solid (5.4 g, 66%), mp 193–194 °C (ethyl acetate); δ_H (200 MHz; DMSO-d_6) 2.94–3.19 (2 H, m, Y; CH_2), 5.13 (2 H, s, CH_2OPh), 6.70 (2 H, d, Yε), 6.96 (2 H, d, Yε), 7.25–7.35 (5 H, m, Bnz Ar*H*), 8.81 (2 H, bs, NH_2), 9.60 (1 H, bs, O*H*); δ_C (50 MHz; DMSO-d_6) 35.4 (Y; *C*H_2), 53.7 (Y; α*C*), 67.2 (Ph*C*H_2O), 115.7 (Y; Ar*C*3), 124.5, 128.6 and 130.6 (Ar*C*), 135.1 (Bnz; Ar*C*1), 157.0 (Y; Ar*C*4), 169.2 (Y; O-*C*=O).

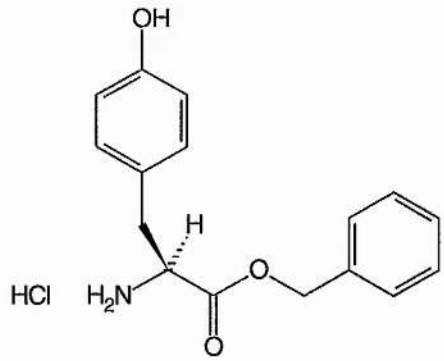

5.16 **L-Tyrosine benzyl ester *p*-toluenesulfonate**. L-tyrosine (9.06 g, 50 mmol) and *p*-toluenesulfonic acid monohydrate (9.51 g, 50 mmol) were added to a

mixture of freshly distilled benzyl alcohol (20 cm^3) and toluene (10 cm^3). The mixture was heated under reflux and the water formed trapped in a Dean-Stark receiver. When no more water appeared in the distillate, the mixture was allowed to cool to room temperature, diluted with diethyl ether (100 cm^3) and cooled further in an ice-water bath for approximately 2 h. Washing with diethyl ether (50 cm^3) and drying in air gave L-tyrosine benzyl ester as the crystalline *p*-toluenesulfonate salt. (20 g, 90%), mp 174–176 °C (MeOH–diethyl ether); δ_H (200 MHz; CD_3OD) 2.37 (3 H, s, *p*–Ts–C*H*$_3$), 3.09 (2 H, d, *J* 6.6, Y; C*H*$_2$), 4.27 (1 H, t, *J* 6.4, Y; *α*C*H*), 5.21 (2 H, d, *J* 2.9, PhCH_2O), 6.71 (2 H, d, *J* 8.1, Y*ε*), 6.96 (2 H, d, *J* 8.1, Y*ε*), 7.23 (2 H, d, *J* 8.5, *p*–Ts–Ar*H*), 7.29–7.39 (5 H, m, *J* 4.3, Bnz; Ar*H*), 7.72 (2 H, d, *J* 8.0, *p*–Ts–Ar*H*); δ_C (50 MHz; CD_3OD) 21.6 (*p*–Ts–*C*H$_3$), 37.0 (Y; *C*H$_2$), 55.6 (Y; *α*CH), 69.4 (Ph*C*H$_2$O), 117.2 (Y; Ar*C*3), 125.7 (*p*–Ts–CH$_3$ Ar*C*2), 127.6 (Y; Ar*C*1), 130.1 (Y; Ar*C*2), 130.2, 130.4, (Bnz; Ar*C*2/3) 131.8 (*p*–Ts–CH$_3$ Ar*C*3), 136.5 (Bnz; Ar*C*1), 142.1 (*p*–Ts–CH$_3$ Ar*C*1), 158.1 (Y; Ar*C*4), 170.4 (Y; O–*C*=O).

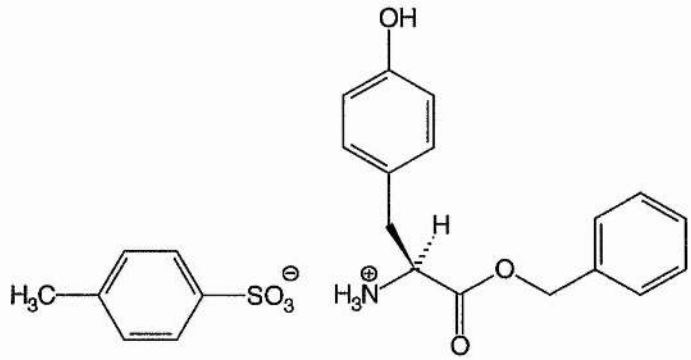

5.17 Preparation of N^{α}-*tert*-Butoxycarbonyl-L-alanyl-L-tyrosine benzyl ester. A solution of L-tyrosine benzyl ester *p*-toluene sulfonate (4.44 g, 10 mmol) in DMF (20 cm^3) was prepared by gentle warming. The solution was cooled to room temperature and treated with triethylamine (1.01 g, 1.40 cm^3, 10 mmol). A solution of N^{α}-*tert*-butoxycarbonyl-L-alanine (2.23 g, 10 mmol) in dry THF (50 cm^3) was cooled to – 15 °C in an ice-acetone bath and neutralised with *N*-methylmorpholine (1.01 g,

1.10 cm^3, 10 mmol). Isobutyl chloroformate (1.37 g, 1.32 cm^3, 10 mmol) was added, followed, about 2–3 min later by the of L-tyrosine benzyl ester *p*-toluene sulfonate described above. About 2 cm^3 of DMF was used for rinsing. The reaction mixture was allowed to warm up to room temperature. The hydrochlorides of *N*-methylmorpholine and triethylamine were removed by filtration and washed with THF. The combined filtrate and washings were concentrated *in vacuo* to about 25 cm^3 and diluted with water (50 cm^3). The solution was extracted with ethyl acetate, washed with HCl (50 cm^3, 1 M) , NaOH (50 cm^3, 1 M), reduced *in vacuo* yielding the title product as an oil (3.36 g, 81%), δ_H (200 MHz; $CDCl_3$) 1.32 (3 H, d, Aβ), 1.43 (9 H, s, $(CH_3)_3$), 3.03 (2 H, dd, Yβ), 4.12 (1 H, q, Aα), 5.30 (2 H, s, PhCH_2O), 6.67 (2 H, d, Yε), 6.82 (2 H, d, Yε), 7.31–7.38 (9 H, m, Bn; Ar*H*), 7.86 (1 H, s, A; NH); δ_C (50 MHz; $CDCl_3$) 18.8 (A; CH_3), 28.8 (Boc-CH_3), 37.4 (Y; CH_2), 50.6 (A; $CH(CH_3)$), 53.8 (Y; *C*H), 67.8 (PhCH_2O), 77.8 $(CH_3)_3C$), 116.0 (Y; ArC3), 127.5, 128.1, 128.3, 128.4, 129.1, 130.9 (Ar*C*), 156.1 (A; Boc *C*=O), 171.8 (A; *C*=O), 173.0 (Y; *C*=O).

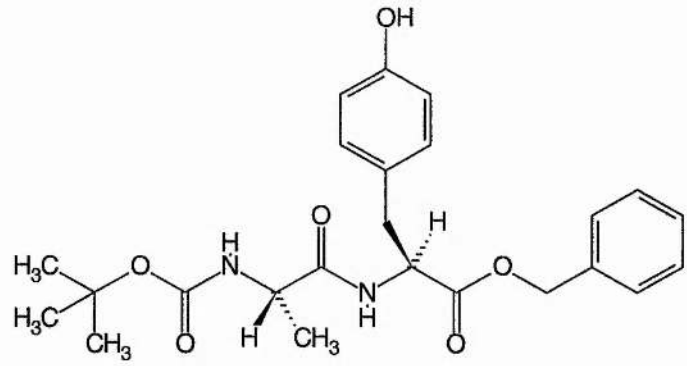

5.18 ***N*$^{\alpha}$*-tert*-Butoxycarbonyl-L-alanyl-L-tyrosine**. *N*$^{\alpha}$*-tert*-Butoxycarbonyl-L-alanyl-L-tyrosine benzyl ester (3.36 g, 10.4 mmol) was dissolved in ethanol (100 cm^3) contained in a hydrogenation flask and 10% palladium on charcoal (300 mg) was added. The flask was attached to a hydrogenation apparatus until hydrogen uptake was complete. The reaction mixture was filtered over a bed of Celite to remove the catalyst. The filtrate was reduced *in vacuo* to a yellow oil which was used in the next

stage without any additional purification (2.44 g, 93%), δ_H (200 MHz; DMSO-d_6) 1.18 (3 H, d, Aβ), 1.37 (9 H, s, (CH_3)$_3$), 2.05 (1 H, m, Vβ), 2.95 (1 H, dd, Yβ), 3.99 (1 H, q, Aα), 4.23 (1 H, dd,Vα), 4.35 (1 H, q, Aα), 6.65 (2 H, d, Yε), 6.99 (2 H, d, Yε), 7.82 (1 H, bs, A; NH); δ_C (50 MHz; DMSO-d_6) 18.4 (A; *C*H$_3$), 28.4 (Boc-*C*H$_3$), 36.2 (Y; *C*H$_2$), 49.9 (A; *C*H(CH$_3$)), 53.9 (Y; *C*H), 78.3 (CH$_3$)$_3$*C*), 115.2 (Y; ArC3), 127.5, 130.4 (Ar*C*), 155.2 (Boc *C*=O), 156.2 (Y; ArC4), 172.8 (A; *C*=O), 173.2 (Y; *C*=O).

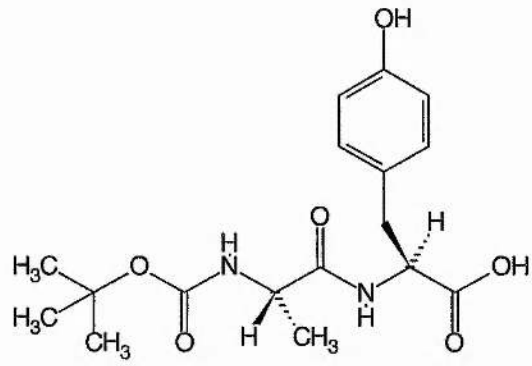

5.19 N^{α}-*tert*-Butoxycarbonyl-L-alanyl-L-tyrosyl-L-valine methyl ester. Mixed anhydride coupling was performed according to the procedure for N^{α}-*tert*-butoxycarbonyl-L-alanyl-L-tyrosine benzyl ester to give the title compound (2.65 g, 78%), δ_H (200 MHz; DMSO-d_6) 0.83 (6 H, m, Vγ), 1.28 (3 H, d, Aβ), 1.40 (9 H, s, (CH_3)$_3$), 2.05 (1 H, m, Vβ), 2.94 (1 H, dd, Yβ), 3.70 (1 H, q, Aα), 4.18 (1 H, dd,Vα), 4.42 (1 H, m, Yα), 6.70 (2 H, d, Yε), 6.98 (2 H, d, Yε); δ_C (50 MHz; DMSO-d_6) 18.8 (A; *C*H$_3$), 28.6 (Boc-*C*H$_3$), 37.8 (Y; *C*H$_2$), 50.8 (A; *C*H(CH$_3$)), 55.1 (Y; *C*H), 57.9 (V; *C*–H), 77.8 (CH$_3$)$_3$*C*), 116.0 (Y; Ar*C*3), 127.8, 130.9 (Ar*C*), 156.1 (A; Boc *C*=O), 171.5 (A; *C*=O), 172.2 (Y; *C*=O), 173.4 (V; *C*=O).

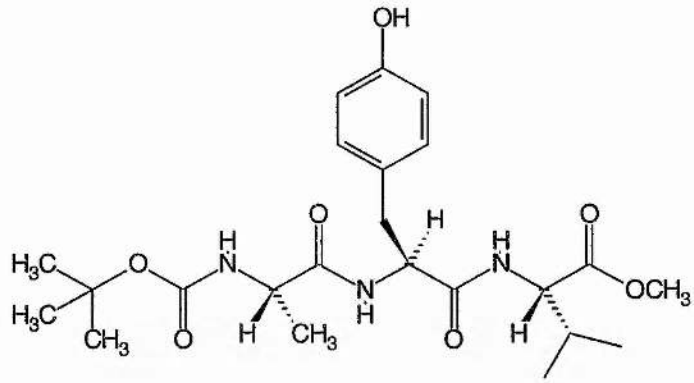

5.20 **L-Alanyl-L-tyrosyl-L-valine**. N^{α}-*tert*-Butoxycarbonyl-L-alanyl-L-tyrosyl-L-valine methyl ester (2.65 g, 5.9 mmol) was dissolved in acetonitrile (10 cm^3). TMSI (trimethylsilyl iodide, 3.21 cm^3, 21.1 mmol, 3.6 eq.) was added via a dry syringe under an atmosphere of nitrogen. The reaction mixture was stirred with heating to 60–70 °C for 9 h. and at room temperature overnight. After this time, methanol (6 cm^3) was added to quench the reaction mixture and the volatile components removed *in vacuo*. The residue was dissolved in a mixture of diethyl ether (10 cm^3) and 30% acetic acid (10 cm^3). The aqueous phase was separated and the extraction repeated three times with 10 cm^3 portions of diethyl ether. Evaporation of the aqueous phase to dryness *in vacuo* gave the deprotected tripeptide isolated as a water-soluble viscous oil which showed evidence of contamination with iodine. This was removed by adding a solution of sodium thiosulfate with swirling until the solution turned colourless and cloudy. The liquid was removed *in vacuo* and the tripeptide extracted from the mixture of sodium tetrathionate, sodium iodide and organic material by shaking with dry THF and filtering and reduction *in vacuo* once more. Purification by column chromatography (3:2 THF, DCM) yielded the title compound as a white powder (1.1 g, 55%), mp 238–239 °C (THF–ethyl acetate); $[\alpha]_D^{22}$ +22.0 (*c* 0.0028 in MeOH); δ_H(500.3 MHz; DMSO-d_6) 0.88; 0.91 (6 H, m, Vγ, Vγ), 1.32 (3 H, d, Aβ), 2.06 (1 H, m, Vβ), 2.70 (1 H, dd, Yβ), 2.92 (1 H, dd, Yβ), 3.78 (1 H, q, Aα), 4.20 (1 H, dd,Vα), 4.62 (1 H, m, Yα), 6.67 (2 H, d, Yε), 7.09 (2 H, d, Yε), 7.86 (2 H, bs, A; NH_2), 8.29

(1 H, d, V; NH), 8.46 (1 H, d, Y; NH), 9.16 (1 H, bs, Y; OH); δ_C(125.8 MHz; DMSO-d_6), 18.9 (Aβ), 19.8 (Vγ'), 20.5 (Vγ), 31.5 (Vβ), 38.5 (Yβ), 49.6 (Aα), 55.8 (Yα), 59.0 (Vα), 113.7 (Yδ), 116.5 (Yε), 129.0 (Yγ), 157.4 (Y ζ), 171.1 (A; C=O), 172.8 (Y; C=O), 173.2 (V; C=O); *m/z* (CI) 352.1872 (MH^+, 100%).

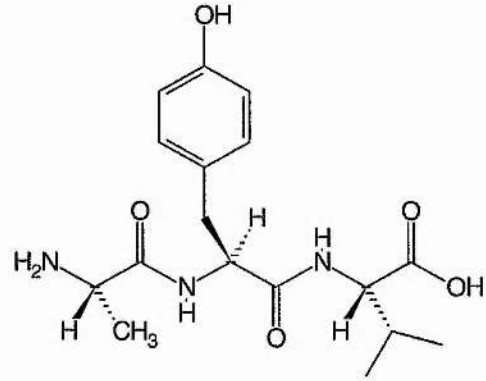

5.21 (2-Oxy-4-phenyl-furazan-3-yl)-methanol. Prepared according to the method of Gasco *et al.*[165] To a stirred solution of 3-phenyl-prop-2-en-1-ol (cinnamyl alcohol) (5.37 g, 40 mmol) in glacial acetic acid (8 cm^3), saturated aqueous sodium nitrite (8.28 g, 120 mmol) was added dropwise over ½ h so that the temperature was kept in the range 65–70 °C. Stirring was continued at room temperature for 1 h and then the reaction mixture was diluted with water (100 cm^3) and extracted several times with diethyl ether. The combined ether extracts were washed with brine, then $NaHCO_3$, dried over anhydrous $MgSO_4$ and distilled *in vacuo*. The oily red residue was purified by flash chromatography using a column of 5 cm diameter packed to a height of 30–35 cm with 220–440 mesh (particle size 0.035–0.070 mm) silica gel (eluent petroleum ether–ethyl acetate, 4:1) to yield the title compound as white crystals (3.23 g, 42%), mp 66–67 °C (toluene–petroleum ether). (Found: C, 56.96; H, 3.89; N, 14.46. $C_9H_8N_2O_3$ requires C, 56.25; H, 4.20; N, 14.58%); ν_{max}(thin film)/cm^{-1} 3394 (OH), 2928, 2869 and 2842 (CH_2OH), 1602 ($C=N^+-O^-$), 1467 ($=N^+-O^-$); δ_H (200 MHz; $CDCl_3$) 2.99 (1 H, bs, CH_2OH), 4.76 (2 H, s, CH_2OH), 7.55–7.86 (5 H, s,

C_6H_5); δ_C (50 MHz; $CDCl_3$) 53.9 (CH_2OH), 115.6 (*C*3), 126.6 (Ar*C*1), 128.3 (Ar*C*2), 129.9 (Ar*C*3), 131.8 (Ar*C*4), 156.8 (*C*4).

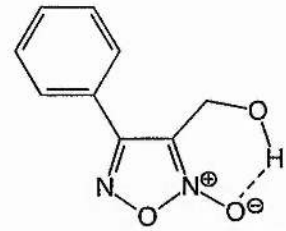

5.22 2-Oxy-4-phenyl-furazan-3-carbaldehyde. Prepared according to the method of Gasco *et al.*[165] To a stirred solution of (2-oxy-4-phenyl-furazan-3-yl)-methanol (0.96 g, 5 mmol) in chloroform (50 cm^3), activated manganese dioxide (6 g) was added. The mixture was vigorously stirred at room temperature for 4 h and then filtered. The filtrate was concentrated *in vacuo* to yield the title compound (0.81 g, 82%), mp 64–65 °C. (Found: C, 57.66; H, 3.03; N, 14.53. $C_9H_6N_2O_3$ requires C, 56.85; H, 3.18; N, 14.73%); ν_{max}(thin film)/cm^{-1} 2925 and 2856 (H–CO), 1707 (C=O), 1592 (C=N^+–O^-), 1479 (=N^+–O^-), 1311 (N–O); δ_H (200 MHz; $CDCl_3$) 7.50–7.63 (3 H, m, C_6H_5), 7.87–7.97 (2 H, m, C_6H_5), 9.98 (1 H, s, C*H*O); δ_C (50 MHz; $CDCl_3$) 114.1 (*C*3), 125.4 (Ar*C*1), 129.2 (Ar*C*2), 129.5 (Ar*C*3), 132.5 (Ar*C*4), 155.4 (*C*4) and 178.7 (H*C*=O).

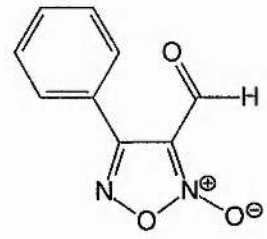

5.23 2-Oxy-4-phenyl-furazan-3-carbaldehyde oxime. Prepared according to the method of Gasco *et al.*[203] A mixture of 2-oxy-4-phenyl-furazan-3-carbaldehyde (0.5 g, 2.6 mmol), hydroxylamine hydrochloride (0.5 g, 7.2 mmol), ethanol (5 cm^3) and pyridine (0.5 cm^3) was heated under reflux for 1 h. The ethanol was removed by

distillation on a water bath. Water (5 cm^3) was added to the cooled residue with cooling in an ice bath and stirring until the oxime crystallised. The precipitated solid was filtered off, washed with water and dried to yield the title compound (0.29 g, 54%), mp 168–170 °C (EtOH). (Found: C, 52.47; H, 3.23; N, 20.22. $C_9H_7N_3O_3$ requires C, 52.69; H, 3.44; N, 20.48%); δ_H (200 MHz; $CDCl_3$) 7.54–7.57 (3 H, m, C_6H_5), 7.70–7.74 (2 H, m, C_6H_5), 8.07 (1 H, s, C*H*=N), 8.68 (1 H, bs, N–O*H*); δ_C (50 MHz; $CDCl_3$) 112.9 (*C*3), 128.0 (Ar*C*3), 130.0 (Ar*C*2), 130.3 (Ar*C*4), 132.4 (Ar*C*1), 136.7 (*C*4) and 157.5 (*C*H=N).

5.24 2-Oxy-4-phenyl-furazan-3-carbonitrile 1. Prepared according to the method of Medana *et al.*[166] To a stirred and ice-water cooled solution of 2-oxy-4-phenyl-furazan-3-carbaldehyde oxime (200 mg, 0.97 mmol) in anhydrous DMF (2 cm^3) was added thionyl chloride (0.3 cm^3). The reaction was monitored by TLC and when complete the mixture poured into ice. The precipitated product was filtered, washed with water, and dried yielding the title compound (165 mg, 90%), mp 73–74 °C (petroleum ether 3:2), (Found: C, 57.96; H, 2.44; N, 22.25. $C_9H_5N_3O_2$ requires C, 57.76; H, 2.69; N, 22.45%); ν_{max}(thin film)/cm^{-1} 2243w (C≡N), 1624 (C=N^+–O^-), 1458 (=N^+–O^-); δ_H (200 MHz; $CDCl_3$) 7.54–7.66 (3 H, m, C_6H_5), 7.90–7.96 (2 H, m, C_6H_5); δ_C (50 MHz; $CDCl_3$) 95.0 (*C*3), 107.0 (*C*≡N), 124.3 (Ar*C*1), 127.4 (Ar*C*2), 129.8 (Ar*C*3), 133.0 (Ar*C*4), 154.8 (*C*4).

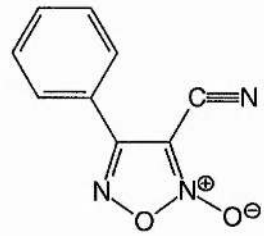

5.25 Formation of [^{15}N]$_3$ *N*-(4-phenyl-furazan-3-yl)-benzamide (attempted preparation of [^{15}N]$_3$ 2-oxy-4-phenyl-furazan-3-carbonitrile). The method of Capdevielle *et al.*[170] was followed. [^{15}N]$_2$ (2-Oxy-4-phenyl-furazan-3-yl)-methanol was prepared using Na^{15}NO$_2$ and then oxidised to [^{15}N]$_2$ 2-oxy-4-phenyl-furazan-3-carbaldehyde following procedures 5.21 and 5.22. In a dry flask, a mixture of [^{15}N]$_2$ 3-formyl-4-phenyl-1,2,5-oxadiazole 2-oxide (152 mg, 0.8 mmol), copper powder (76 mg, 1.2 mmol, 1.5 eq.) and ^{15}NH$_4$Cl (85 mg, 1.6 mmol, 2 eq.) in pyridine (15 cm^3) was stirred at 60 °C for 24 h in an oxygen atmosphere. The reaction liquor was then poured over a mixture of crushed ice and concentrated HCl (50 cm^3, 1:1) and extracted three times with diethyl ether. The combined ether extract was washed with brine, dried over anhydrous MgSO$_4$ and reduced *in vacuo* to give the crude product. 74 mg (69%). This was was purified by flash chromatography using a column of 1 cm diameter packed to a height of 15 cm with 220–440 mesh (particle size 0.035–0.070 mm) silica gel (eluent petroleum ether–ethyl acetate, 3:2); mp 148 °C; δ_H (200 MHz; $CDCl_3$) 7.47–7.90 (9 H, m, *J* 3.9 and 7.7, Ar*H*), 8.18 (~0.5 H, s, furazan N*H*), 8.64 (~0.5 H, s, O*H*); δ_C (50 MHz; $CDCl_3$) 125.67, 128.05, 128.14, 129.54, 129.85, 131.34 (*C*6), 132.50 (m, J_{NC} 10, N=*C*–OH), 133.69 (*C*10), 149.21 (m, J_{NC} 11, *C*1), 150.40 (d, *C*2), 165.73 (d, J_{NC} 12, *C*=O); δ_N (50.7 MHz; $CDCl_3$; NH_3 (l)) 100.3, 102.1, 394.5, 412.4. (Found: M$^+$, 268.0969. $C_{15}H_{11}{}^{15}N_3O_2$ requires M, 268.0762); *m/z* (EI+) M$^+$ (17%), M–163 (100%, $C_6H_5C{=}O^+$), M–191, (37%, $C_6H_5^+$).

Crystal data

$C_{14}H_{10}N^{15}N_3O_2$, M = 268.25. Monoclinic, a = 9.030(4), b = 5.011(5), c = 14.196(4) Å, α = 90°, β = 90.81(3)° γ = 90°, V = 642.2(7) Å^3 (by least squares refinement on diffractometer angles for 14 reflections, λ = 0.710 69 Å), space group $P2_1/n$ (alt. $P2_1c$, No. 7), Z = 2, D_x = 1.372 g cm^{-3}. Colourless plates, μ = 0.094.

Data collection and processing

AFC7S diffractometer, $\omega/2\theta$ mode with ω scan width = 0.85 + 0.35 tan θ, ω scan speed 1.3–6.8 deg min^{-1}, measurement temperature 293.2 K, graphite-monochromated Mo-Kα radiation; 1126 reflections measured ($1.5 \leqslant \theta \leqslant 25°$, $+h,k,l$), 726 unique.

Structure analysis and refinement

Direct methods. Full-matrix least-squares refinement with σ weighting scheme and Zachariasen type 2 Gaussian isotropic extinction method. Extinction coefficient 24.45293. Final R and R_w values are 0.0460 and 0.0442. Computing data collection and cell refinement: MSC/AFC Diffractometer Control. Data reduction and structure solution: teXsan.

5.26 Hydroxyimino-phenyl-acetaldehyde oxime. Prepared according to the method of Ponzio.[204] To a solution of 2-isonitrosoacetophenone (phenylglyoxaldoxime) (50 g, 0.34 mol) in ethanol (180 cm^3) was added a solution of hydroxylamine hydrochloride (24 g, 0.34 mol) and sodium acetate trihydrate (45 g, 0.34 mol) in water (75 cm^3). The mixture was heated at 70–80 °C until it began to separate, a process which was completed on cooling. The title compound was isolated as white crystals by precipitation on addition of water (36 g, 64%), mp 168–170 °C dec. (Found: C, 59.11; H, 5.12; N, 17.08. $C_8H_8N_2O_2$ requires C, 58.53; H, 4.91; N, 17.06%); δ_H(200 MHz; DMSO-d_6) 7.39–7.42 (3 H, m, C_6H_5), 7.56–7.59 (2 H, m, C_6H_5), 8.49 (1 H, s, C–*H*), 11.57 (1 H, s, O*H*), 12.00 (1 H, s, O*H*), δ_C(50 MHz; $CDCl_3$) 128.1 (Ar*C*3), 128.8 (Ar*C*2), 129.0 (Ar*C*4), 134.3 (Ar*C*1), 141.0 (C–*C*(=N–OH)), 151.2 (Ar–*C*(=N–OH)).

5.27 Chlorohydroxyimino-phenyl-acetaldehyde oxime. Prepared according to the method of Ponzio.[204] Hydroxyimino-phenyl-acetaldehyde oxime (10 g, 61 mmol) was dissolved in the minimum amount of hot glacial acetic acid. After cooling to room temperature, chlorine gas (generated by the action of concentrated hydrochloric acid on potassium permanganate) was passed through the solution by means of a Pasteur pipette bubbler. The exhaust gas was passed through scrubbing apparatus charged with aqueous sodium hydroxide. Empty Dreschel bottles were inserted in the gas line between the gas generating flask and reaction flask and reaction flask and scrubbing apparatus to discourage suck back. After a short time the pure chlorohydroxyimino-phenyl-acetaldehyde oxime separated out as white prisms which were washed with acetic acid and dried in a vacuum desiccator over self-indicating silica gel (10.5 g, 87%), mp 197.5 °C (Lit. 199–200 °C dec.) (Found: C, 48.03; H, 3.30; N, 13.65. $C_8H_7N_2O_2Cl$ requires C, 48.38; H, 3.55; N, 14.11%); δ_H(200 MHz; DMSO-d_6) 7.28–7.46 (5 H, m, C_6H_5), 12.13 (1 H, s, O*H*), 12.60 (1 H, s, O*H*); δ_C(50 MHz; $CDCl_3$) 128.1 (Ar*C*3), 128.8 (Ar*C*4), 129.0 (Ar*C*2), 131.8 (Ar*C*1), 135.9 (Ar–*C*(=N–OH)), 151.0 (C–*C*(=N–OH)–Cl).

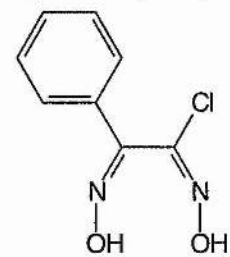

5.28 *N*-Hydroxy-2-hydroxyimino-2-phenyl-thioacetimidic acid phenyl ester. Prepared according to the method of Sorba *et al.*[205] To a stirred suspension of chlorohydroxyimino-phenyl-acetaldehyde oxime (10 g, 50 mmol) in a solution of thiophenol (5.50 g, 55 mmol) in dry ether (200 cm^3), triethylamine (7.6 cm^3, 55 mmol) in dry ether (20 cm^3) was added dropwise. The reaction mixture was stirred for 1 h at room temperature and then washed first with dilute hydrochloric acid and then with water. The organic layer was evaporated *in vacuo* to yield the title compound (9.3 g, 68%), mp 183.3–183.6 °C (ethyl acetate, lit. 190 °C). An additional crop of material was obtained by adding petroleum ether to the ethyl acetate, combined yield 11.2 g, 82%; (Found: C, 62.07; H, 4.42; N, 10.31. $C_{14}H_{12}N_2O_2S$ requires C, 61.75; H, 4.44; N, 10.29%); δ_H(200 MHz; DMSO-d_6) 7.11–7.28 (10 H, m, C_6H_5), 11.70 (1 H, s, O*H*), 12.13 (1 H, s, O*H*); δ_C(50 MHz; DMSO-d_6) 127.9, 128.7, 128.9, 129.0, 129.0, 129.2, 131.3, 134.8 (2 × C_6H_5), 148.8 (C=N–OH), 149.0 (CCH_2).

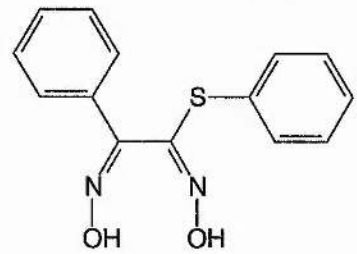

5.29 4-Phenyl-3-phenylsulfanyl-furazan 2-oxide and 3-phenyl-4-phenylsulfanyl-furazan 2-oxide. Prepared according to the method of Sorba *et al.*[206] To a stirred solution of *N*-hydroxy-2-hydroxyimino-2-phenyl-thioacetimidic acid phenyl ester (5.00 g, 18 mmol) in DCM (50 cm^3), was added a solution of dinitrogen tetroxide in DCM (10 cm^3, 1.03 M) dropwise over ½ h. The mixture was stirred for a further ½ h at room temperature then washed with water. Solvent removal gave a crude oily mixture of the title compounds. The mixture was resolved by column chromatography (petroleum ether–DCM, 2:1); 4-phenyl-3-phenylsulfanyl-furazan 2-

oxide eluted first (77%), mp 30–31 °C (petroleum ether); δ_H(200 MHz; $CDCl_3$) 7.31–7.56 (8 H, m, Ar*H*) and 7.93–7.98 (2 H, dd, *J* 2.3, Ar*H*); δ_C(50 MHz; $CDCl_3$) 110.2 (*C*3), 126.0 (Ar*C*1), 127.6 (Ar*SC*2), 128.6 (Ar*SC*4), 128.8 (Ar*C*2), 128.9 (Ar*SC*1), 129.5 (Ar*SC*3), 130.5 (Ar*C*3), 131.2 (Ar*C*4), 157.3 (*C*4) and 3-phenyl-4-phenylsulfanyl-furazan 2-oxide eluted second (13%), mp 67–68 °C (petroleum ether); δ_H(200 MHz; $CDCl_3$) 7.31–8.00 (10 H, m, Ar*H*); δ_C(50 MHz; $CDCl_3$) 114.3 (*C*3), 122.0 (Ar*C*1), 126.1 (Ar*SC*1), 127.5 (Ar*SC*2), 128.8 (Ar*C*2), 129.6 (Ar*SC*3), 129.8 (Ar*SC*4), 130.6 (Ar*C*4), 133.9 (Ar*C*3), 154.1 (*C*4)

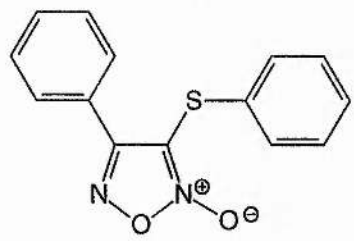

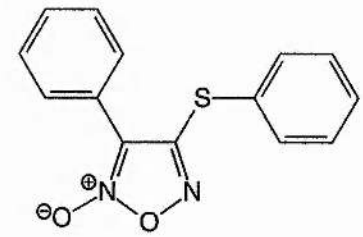

5.30 4-Phenyl-3-benzenesulfonyl-furazan 2-oxide and 3-phenyl-4-benzenesulfonyl-furazan 2-oxide. Prepared according to the method of Sorba *et al.*[205] To a stirred and water-cooled solution of the appropriate phenylthio derivative (6.53 g, 24 mmol) in acetic acid (65 cm^3) potassium permanganate (11.40 g, 74 mmol) was added in portions. The mixture was stirred at room temperature overnight and was then diluted with water. The excess of potassium permanganate and the manganese dioxide which formed were destroyed with sodium sulfite. The precipitate was filtered, partially dried, dissolved in DCM and filtered on a bed of silica gel. Solvent removal *in vacuo* yielded the title products 3-benzenesulfonyl-4-phenyl-1,2,5-oxadiazole 2-oxide (75%), mp 132–133 °C (MeOH); (Found: C, 56.18; H, 3.07; N, 9.27. $C_{14}H_{10}N_2O_4S$ requires C, 55.62; H, 3.33; N, 9.27%); δ_H (200 MHz, $CDCl_3$) 7.6–8.0 (10 H, m, Ar*H*); δ_C (50 MHz, $CDCl_3$) 117.6 (*C*3), 124.8 (Ar*C*1), 128.5 (Ar*C*2), 128.8 (Ar*C*3), 129.4 ($ArSO_2C2$), 129.5 ($ArSO_2C3$), 131.5 (Ar*C*4), 135.5 ($ArSO_2C4$),

137.0 ($ArSO_2C1$), 154.5 ($C4$) and 3-phenyl-4-benzenesulfonyl-1,2,5-oxadiazole 2-oxide (80%), mp 102–103 °C (MeOH); δ_H (200 MHz, $CDCl_3$) 7.6–8.0 (m, 10H, Ar*H*); δ_C (50 MHz, $CDCl_3$) 112.2 ($C3$), 120.3 ($ArC1$), 128.9 ($ArC2$), 129.0 ($ArC3$), 129.4 ($ArSO_2C2$), 129.5 ($ArSO_2C3$), 131.4 ($ArC4$), 135.5 ($ArSO_2C4$), 136.0 ($ArSO_2C1$), 158.7 ($C4$).

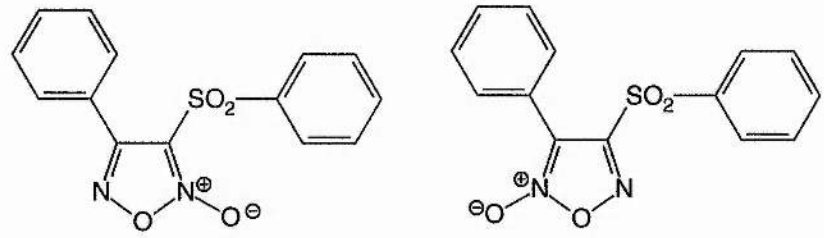

5.31 Dimethyl-[3-(2-oxy-4-phenyl-furazan-3-yloxy)-propyl]-ammonium oxalate 2b. Prepared according to the method of Sorba *et al.*[206] To a stirred solution of 4-phenyl-3-benzenesulfonyl-furazan 2-oxide (1 g, 3.3 mmol) in THF (20 cm^3) was added 3-(dimethylamino)propanol (1.16 cm^3, 9.9 mmol) and then NaOH solution (50% w/w, 0.79 g, 9.9 mmol) in portions while the temperature was maintained at 25 °C. The reaction mixture was stirred at room temperature for over ½ h and then evaporated *in vacuo*. The residue was treated with water and extracted with DCM. The combined organic layers were dried over magnesium sulfate and concentrated *in vacuo*, and the oily residue was filtered on a short silica gel column (CH_2Cl_2–MeOH, 95:5) to give the title product as an oily free base (0.45 g, 52%). The base was immediately transformed into the corresponding oxalate, mp 134–135 °C dec. (MeOH). (Found: C, 51.16; H, 5.45; N, 11.83. $C_{15}H_{19}N_3O_7$ requires C, 50.99; H, 5.42; N, 11.89); δ_H(200 MHz; DMSO-d_6) 2.15 (2 H, m, CCH_2), 2.71 (6 H, s, NCH_3), 3.12 (2 H, t, NCH_2), 4.52 (2 H, t, OCH_2), 7.6–7.9 (5 H, m, C_6H_5); δ_C(50 MHz; DMSO-d_6) 24.7 (CCH_2), 42.6 (NCH_3), 53.7 (NCH_2), 70.3 (OCH_2), 131.2 ($C3$), 151.2 ($C4$), 125.3 ($PhC1$), 128.7,129.5 ($PhC2/C3$), 131.7 ($PhC4$).

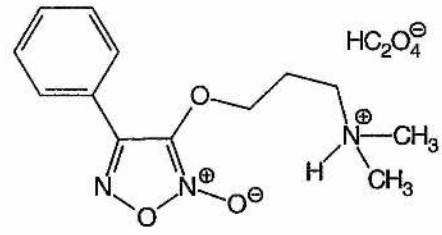

5.32 Phenyl nitromethyl sulfone. Prepared according to the method of Kelley *et al.*[177] To a stirred, ice cold mixture of potassium *tert*-butoxide (11.2 g, 0.10 mol) in DMF (75 cm^3) was added dropwise a solution of nitromethane (6.7 g, 0.11 mol) in 12 cm^3 of DMF. After ½ h, sodium benzenesulfinate (16.4 g, 0.10 mol) and iodine (12.7 g, 0.10 mol) were added to the white mixture. The resulting orange reaction mixture was then stirred at ambient temperature overnight, after which a concentrated solution of sodium sulfite in water was added until the dark colour had disappeared. The reaction was poured over 1 dm^3 of ice water and acidified with dilute hydrochloric acid. The recrystallised product was dried in a vacuum desiccator and exhibited dimorphism: fine needles, mp 126–127 °C (MeOH) and plates, mp 70–72 °C (EtOH). (Found: C, 41.88; H, 3.34; N, 6.83. $C_7H_7NO_4S$ requires C, 41.79; H, 3.51; N, 6.96%); δ_H(200 MHz; $CDCl_3$) 5.63 (2 H, s, CH_2), 7.61–7.99 (5 H, m, C_6H_5); δ_C(50 MHz; $CDCl_3$) 90.7 (CH_2), 129.8, 130.3, 136.2 (C_6H_5).

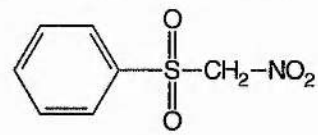

5.33 3,4-Bis-benzenesulfonyl-furazan 2-oxide. Prepared according to the method of Kelley *et al.*[177] A stirred mixture of phenyl nitromethyl sulfone (20.1 g, 0.10 mol), acetic acid (70 cm^3), and 90% nitric acid (35 cm^3) was heated at 60–65 °C for 1 h. The cooled reaction mixture was poured over ice water, filtered yielding the title product (32.9 g, 90%), mp 77–78 °C (EtOH). $C_{14}H_{10}N_2O_6S_2$ requires C, 45.89; H,

2.75; N, 7.65%); δ_H(200 MHz; $CDCl_3$) 7.4–8.3 (10 H, m, 2 × Ar*H*); δ_C(50 MHz; $CDCl_3$) 129.7, 130.1, 130.2, 130.3, 130.4, 130.7, 136.4, 136.7 (2 × Ar*H*).

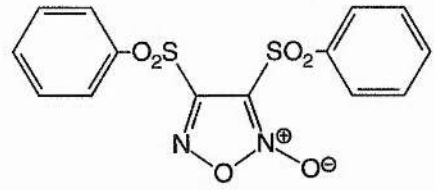

5.34 Dimethyl-[2-(2-oxy-3-benzenesulfonyl-furazan-4-ylsulfanyl)-ethyl]-ammonium oxalate 3a and dimethyl-[2-(2-oxy-4-benzenesulfonyl-furazan-3-ylsulfanyl)-ethyl]-ammonium oxalate 3b. Prepared according to the method of Sorba *et al.*[205] To a stirred solution of 3,4-bis-benzenesulfonyl-furazan 2-oxide (2 g, 5.46 mmol) in THF (25 cm^3) kept under nitrogen was added first 2-(dimethylamino)ethanethiol hydrochloride (1.54 g, 11 mmol) and then, in portions, NaOH solution (50% w/w, 1.75 g, 22 mmol). The temperature during the addition was kept at 25–30 °C. The reaction mixture was stirred at room temperature for 1 h. The solvent was removed *in vacuo*, and the water solution of the residue was extracted with DCM. The combined organic layers were dried over magnesium sulfate and evaporated *in vacuo* to afford a mixture of the two title isomers. The mixture was resolved by flash chromatography (EtOAc–MeOH, 95:5); first eluted was dimethyl-[2-(2-oxy-4-benzenesulfonyl-furazan-3-ylsulfanyl)-ethyl]-amine (0.82 g, 45%), second eluted dimethyl-[2-(2-oxy-3-benzenesulfonyl-furazan-4-ylsulfanyl)-ethyl]-amine (0.22 g, 12%). Both isomers were transformed into the corresponding oxalates by adding a stoichiometric quantity of oxalic acid in water and evaporating to dryness in a vacuum desiccator. Dimethyl-[2-(2-oxy-3-benzenesulfonyl-furazan-4-ylsulfanyl)-ethyl]-ammonium oxalate, mp 143–144 °C dec. (MeOH–H_2O); δ_H(200 MHz; DMSO-d_6) 2.72 (6 H, s, NCH_3), 3.32 (2 H, m, SCH_2), 3.55 (2 H, m, NCH_2), 7.6–8.1 (5 H, m, C_6H_5); δ_C(50 MHz; DMSO-d_6) 42.6 (NCH_3), 54.7 (NCH_2), 24.8 (SCH_2), 117.3 (*C*3),

136.4, 136.5 (Ph*C*1/Ph*C*4), 130.2, 128.5 (Ph*C*2/*C*3), 152.8 (*C*4). Dimethyl-[2-(2-oxy-4-benzenesulfonyl-furazan-3-ylsulfanyl)-ethyl]-ammonium oxalate, mp 144–145 °C dec. (MeOH–H_2O); (Found: C, 39.72; H, 4.01; N, 9.79. $C_{14}H_{17}N_3O_8S_2$ requires C, 40.09; H, 4.09; N, 10.02%); δ_H(200 MHz; DMSO-d_6) 2.59 (6 H, s, NCH_3), 2.95 (2 H, t, SCH_2), 3.23 (2 H, t, NCH_2), 7.8–8.1 (5 H, m, C_6H_5); δ_C(50 MHz; DMSO-d_6) 42.5 (NCH_3), 56.1 (NCH_2), 26.0 (SCH_2), 108.9 (*C*3), 136.0, 136.4 (Ph*C*1/Ph*C*4), 130.3, 129.3 (Ph*C*2/*C*3), 159.7 (*C*4).

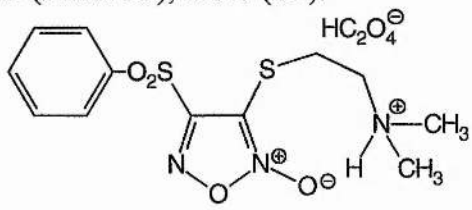

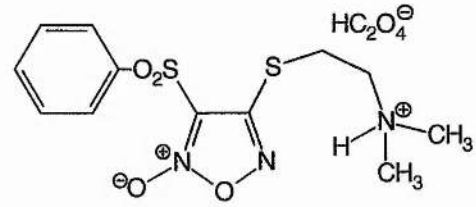

5.35 Sodium *N*-methyl-D-glucamine dithiocarbamate monohydrate. Prepared according to the method of Shinobu *et al.*[207] Sodium hydroxide (10 g, 0.25 mol) was dissolved in water (200 cm^3) in a 1 dm^3 beaker. Ice (25 g) was added to the solution, followed by *N*-methyl-D-glucamine (46.8 g, 0.25 mol), and the mixture was stirred with a magnetic stirrer until all the solid had completely dissolved. The resulting solution was cooled in an ice bath and a solution of carbon disulfide (25 cm^3, 0.42 mol) in absolute ethanol (75 cm^3) was added dropwise with continual stirring. The temperature of the reaction mixture was kept between 0 and 10 °C during the carbon disulfide addition to minimise the formation of coloured by-products. After all the carbon disulfide solution had been added, methanol (250 cm^3) was added and the beaker covered to prevent evaporation. The preparation was allowed to stand overnight to facilitate the formation of larger crystals. The solid was collected by filtration, washed with methanol and air dried. The filtrate and washings were refrigerated to obtain a second crop of crystals. The first crop dried to a white powder (59 g, 75%). The second crop was slightly yellow in colour (8 g, 10%). The literature

preparation reports only a CHN elemental analysis. mp 179–180 °C. (Found: C, 30.89; H, 5.98; N, 4.37. $NaC_8H_{16}NO_5S_2.H_2O$ requires C, 30.86; H, 5.82; N, 4.49%); δ_H(500.3 MHz, DMSO-d_6, 30 °C); 3.38 (1 H, m, *H*6'), 3.39 (3 H, s, NC*H*$_3$), 3.52 (3 H, m, *H*3, *H*4 and *H*5), 3.57 (1 H, m, *H*6), 3.80 (1 H, dd, *H*1'), 3.92 (1 H, m, *H*2), 4.28 (1 H, t, C6O*H*), 4.42 (1 H, d, C5O*H*), 4.46 (1 H, m, C4O*H*), 4.49 (1 H, d, *H*1), 4.72 (1 H, d, C3O*H*), 5.14 (1 H, d, C2O*H*); δ_C(125.8 MHz, DMSO-d_6, 30 °C) 42.72 (N*C*H$_3$), 57.44 (*C*1), 63.23 (*C*6), 68.72 (*C*3), 71.31 (*C*5), 72.27 (*C*2), 72.80 (*C*4) and 213.84 (*C*S$_2$).

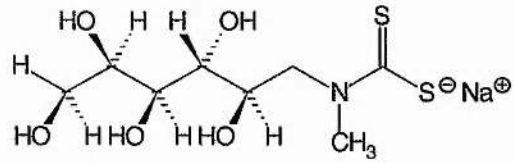

5.36 3,5-Dibromo-4-nitrosobenzenesulfonate (DBNBS). Prepared according to the method of Kaur *et al.*[188] A solution of 3,5-dibromo-4-aminobenzenesulfonic acid (3.31 g, 10 mmol) in a mixture of glacial acetic acid (30 cm^3), aqueous hydrogen peroxide (30%, 70 mmol), and anhydrous sodium acetate (0.82 g, 10 mmol) was warmed gently to dissolve the solids. The solution was allowed to stand at room temperature until crystallisation had occurred. The product was isolated as straw-coloured blades (1.14 g, 31%). mp >300 °C (EtOH); (Found: C, 18.83; H, 0.33; N, 3.31. $NaC_6H_2Br_2NO_4S$ requires C, 19.64; H, 0.55; N, 3.82%); δ_H(200 MHz, DMSO-d_6) 7.98 (2 H, s, Ar*H*); δ_C(50 MHz, DMSO-d_6) 107.4 (Ar*C*–Br), 113.3 (ArC-SO_3^-), 130.0 (Ar*C*H), 152.3 (Ar*C*–N=O).

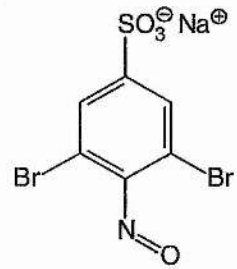

5.37 Bis(*N*-methyl-D-glucamine dithiocarbamate) iron(II). The ferrous complex of *N*-methyl-D-glucamine dithiocarbamate was prepared fresh as required by the addition of *N*-methyl-D-glucamine dithiocarbamate to a solution of ferrous ammonium sulfate (1:5) in 50 mM pH 7.4 phosphate buffer. HPLC-grade water was used throughout.

5.38 Procedure for ammonia assay. Solutions of **1** or **2b** oxalate and *N*-acetyl-DL-cysteine were made up using pH 7.4 phosphate buffer (100 mM) using HPLC-grade water and analytical grade methanol (99.99% purity) according to the conditions given in Table 5.1.

Table 5.1 Conditions for decomposition of **1** and **2b** oxalate in the presence of *N*-acetyl-L-cysteine at 37 °C.

Experiment	Furoxan	[Furoxan]/M	[Thiol]/M	Solvent
1	**1**	5×10^{-5}	2.5×10^{-3}	pH 7.4 buffer
2	**2b**	5×10^{-5}	2.5×10^{-3}	pH 7.4 buffer
3	**1**	0.01	0.01	pH 7.4 buffer–MeOH, (1:1)
4	**2b**	0.01	0.01	pH 7.4 buffer–MeOH, (1:1)

The solutions were sealed in volumetric flasks and incubated in a water bath at 37 °C for 24 h and then tested according to the following protocol using an ammonia assay kit from Sigma. The test solutions were made up in quartz cuvettes according to Table 5.2.

Table 5.2 Contents of cuvettes for ammonia assay.

Cuvette	Contents
1 (blank)	2.0 cm^3 ammonia assay solution.
	0.2 cm^3 water.
2 (control)	2.0 cm^3 ammonia assay solution.
	0.2 cm^3 ammonia control solution
3 (test 1)	2.0 cm^3 ammonia assay solution.
	0.2 cm^3 furoxan (*a*)
4 (test 2)	2.0 cm^3 ammonia assay solution.
	0.2 cm^3 furoxan (*b*)

The cuvettes were stoppered, gently inverted and allowed to equilibrate for approximately 3 min at a temperature between 25 and 35 °C. The initial absorbance was recorded against HPLC-grade water as the reference. L-Glutamate dehydrogenase solution (0.02 cm^3) was added to each cuvette followed by gentle inversion to facilitate efficient mixing and then the cuvettes returned to the spectrophotometer for approximately 5 min for the reaction to complete. After this time, the absorbance of each cuvette was recorded using the same reference.

5.39 Decomposition product of 3b oxalate (2-phenylsulfonyl-1-(2-dimethylamino-ethylsulfanyl)-2-nitroso-ethenol contaminated with dibutyl phthalate). The title compound (150 mg, 0.36 mmol) was dissolved in pH 7.0 phosphate buffer (100 cm^3) and incubated at 37 °C for 24 h. After this time, the solution was placed in an evaporating dish inside a vacuum desiccator over self-indicating silica gel until all the water had been removed. The residue was shaken with methanol to extract the organic products from the inorganic buffer salts. The

organic solvent was then removed *in vacuo* and the oily material purified by flash column chromatography using 220–440 mesh (particle size 0.035–0.070 mm) silica gel (eluent ethyl acetate–MeOH, 95:5). TLC showed the presence of two components (R_F = 0.92 and 0.44) in addition to baseline material. For the component with R_F = 0.92: EIMS *m/z* 157 (M^+, 8%), 149 (12%), 141 (25%). For the component with R_F = 0.44: ν_{max}(thin film)/cm^{-1} 3500 (–OH), 1725 (C=O), 1655w, 1415, 1370, 1157; *m/z* (EI) 279 (M^+, 31%), 167 (32%), 157 (75%). For the baseline components: δ_H (200 MHz; CD_3OD) 1.91 (6 H, s, NCH_3), 3.32 (2 H, t, NCH_2), 7.4–7.8 (5 H, m, C_6H_5); δ_C (50 MHz; CD_3OD) 24.4 (SCH_2), 45.5 $(NCH_3)_2$, 125.5, 127.2, 129.6, 131.6 (Ar), 105.3 (=*C*(OH)SR), 146.5 (*C*-NOH) 181.1 (*C*=O).

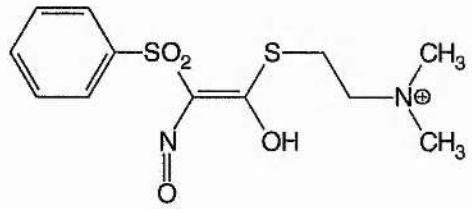

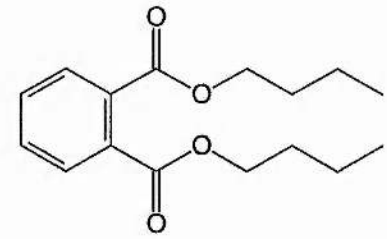

5.40 Conditions for EPR experiments. Aqueous phosphate buffer (50 mM, pH 7.4) and methanol (HPLC grade) were deaerated by alternately applying an oil pump to the flask until boiling off of the dissolved gases had effectively ceased and then vigorously bubbling a stream of oxygen-free nitrogen through the solution for 10–15 min. This procedure was repeated twice. For C-centred spin trapping, the solvents were saturated with DBNBS to a concentration of approximately 50 mg in 50 cm^3. For NO spin trapping, the furoxan was added to the 50 mM pH 7.4 Fe^{2+}–MGD to make the final solution 1 mM and this was subsequently incubated at 37 °C for approximately ½ h prior to the EPR spectra being run. In the case of **1** and **2b** oxalate, sufficient *N*-acetyl-DL-penicillamine was also added to achieve a final concentration of 10 mM. The samples were contained in capillary tubes made from

soda-glass long form Pasteur pipettes sealed at the tip. The test solution was added to ensure a depth of about 4–5 cm in the capillary and the open end was sealed with a rubber septum.

5.41 NO-trapping with Fe-MGD. The Fe^{2+} complex of MGD [Fe^{2+}–MGD] was used to scavenge NO formed during the reaction. Fresh stock solutions of Fe–MGD (1:5 w/w) were prepared by adding ferrous ammonium sulfate to solutions of MGD (1 mM) in 50 mM pH 7.4 phosphate buffer. HPLC-grade water was used throughout. ^{14}N and ^{15}N SNAP were synthesised as previously described in section 5.11.

6 References

1 D. M. Short, *Chem. Ind.*, 1997, 848.

2 E. Culotta and D. E. Koshland Jr., *Science*, 1992, **258**, 1862.

3 P. L. Feldman, O. W. Griffith and D. J. Stuehr, *Chem. Eng. News*, 1993, **71**, 26.

4 N. N. Greenwood and A. Earnshaw, *Chemistry of the Elements*, 1993 (Pergamon Press), p.512.

5 R. F. Furchgott and P. M. Vanhoutte, *FASEB J.*, 1989, **3**, 2007.

6 D. A. Wink, J. F. Darbyshire, R. W. Nims, J. E. Saavedra and P. C. Ford, *Chem. Res. Toxicol.*, 1993, **6**, 23.

7 V. G. Kharitonov, A. R. Sundquist and V. S. Sharma, *J. Biol. Chem.*, 1994, **269**, 5881.

8 (*a*) J. P. Griess, *Ber. Dtsch. Chem. Ges.*, 1897, **12**, 426; (*b*) B. E. Saltzman, *Anal. Chem.*, 1954, **26**, 1949.

9 R. F. Furchgott and J. V. Zawadzki, *Nature*, 1980, **288**, 373.

10 P. A. Craven and F. R. DeRubertis, *J. Biol. Chem.*, 1978, **253**, 8433.

11 E. M. Schuman and D. V. Madison, *Science*, 1991, **254**, 1503.

12 T. J. O'Dell, R. D. Hawkins, E. R. Kandel and O. Arancio, *Proc. Natl. Acad. Sci. USA*, 1991, **188**, 11285.

13 J. M. Hevel and M. A. Marletta. *Biochem.*, 1992, **31**, 7160.

14 H-G. Korth, R. Sustmann, C. Thater, A. R. Butler and K. U. Ingold, *J. Biol. Chem.*, 1994, **269**, 17776.

15 J. O. Edwards and R. C. Plumb, *Prog. Inorg. Chem.*, 1994, **41**, 599.

16 W. A. Pryor and G. L. Squadrito, *Am. J. Physiol. (Lung Cell. Mol. Physiol.)*, 1995, **12**, 699.

17 A. Baeyer and V. Villiger, *Ber.*, 1901, **34**, 755.

18 F. Raschig, *Z. Angew. Chem.*, 1904, **17**, 1419.

19 N. V. Blough and O. C. Zafiriou, *Inorg. Chem.*, 1985, **24**, 3504.

20 H. M. Papée and G. L. Petriconi, *Nature (London)*, 1964, **204**, 142.

21 J. R. Leis, M. E. Peña and A. Ríos, *J. Chem. Soc., Chem. Commun.*, 1993, 1298.

22 A. Saha, S. Goldstein, D. Cabelli and G. Czapski, *Free Radical Biol. Med.*, 1998, **24**, 653.

23 M. Anbar and H. Taube, *J. Am. Chem. Soc.*, 1954, **76**, 6243.

24 K. Gleu and E. Roell, *Z. Anorg. Allg. Chem.*, 1929, **179**, 233.

25 (*a*) W. A. Pryor, R. Cueto, X. Jin, W. H. Koppenol, M. Ngu-Schwemlein, G. L. Squadrito, P. L. Uppu and R. M. Uppu, *Free Radical Biol. Med.*, 1995, **18**, 75; (*b*) R. M. Uppu, G. L. Squadrito, R. Cueto and W. A. Pryor, *Methods in Enzymology*, 1996, **269**, 311.

26 M. N. Hughes and H. G. Nicklin, *J. Chem. Soc. (A),* 1968, 450.

27 E. Halfpenny and P. L. Robinson, *J. Chem. Soc.*, 1952, 928.

28 W. G. Keith and R. E. Powell, *J. Chem. Soc. (A)*, 1969, 90.

29 R. M. Uppu and W. A. Pryor, *Anal. Biochem.*, 1996, **236**, 242.

30 D. S. Bohle, B. Hansert, S. C. Paulson and B. D. Smith, *J. Am. Chem. Soc.*, 1994, **116**, 7423.

31 W. J. Lo, Y. P. Lee, J. H. M. Tsai and J. S. Beckman, *Chem. Phys. Lett.*, 1995, **242**, 147.

32 E. H. Appelman and D. J. Gosztola, *Inorg. Chem.*, 1995, **34**, 787.

33 J. S. Beckman, T. W. Beckman, J. Chen, P. A. Marshall and B. A. Freeman, *Proc. Natl. Acad. Sci. U.S.A.,* 1990, **87**, 1620.

34 R. M. J. Palmer, D. S. Ashton and S. Moncada, *Nature*, 1988, **333**, 664.

35 E. Cadenas, *Annu. Rev. Biochem.,* 1989, **58**, 79.

36 R. Radi, J. S. Beckman, K. M. Bush and B. A. Freeman, *J. Biol. Chem.,* 1991, **266**, 4244.

37 N. Hogg, V. M. Darley-Usmar, A. Graham and S. Moncada, *Biochem. Soc. Trans.*, 1991, **21**, 358.

38 V. M. Darley-Usmar, N. Hogg, V. J. O'Leary, M. T. Wilson and S. Moncada, *Free Rad. Res. Com.*, 1992, **17**, 9.

39 N. D. Seago, J. H. Thompson, X-J. Zhang, S. Eloby-Childress, H. Sadowska-Krowicka, J. L. Rossi, M. G. Currie, P. T. Manning, D. A. Clark and M. J. S. Miller, *Mediat. Inflamm.*, 1995, **4**, 19.

40 M. I. Bukrinsky, H. S. L. M. Nottet, H. Schmidtmayerova, L. Dubrovsky, C. R. Flanagan, M. E. Mullins, S. A. Lipton and H. E. Gendelman, *J. Exp. Med.*, 1995, **181**, 735.

41 D. Rachmilewitz, J. S. Stamler, F. Karmeli, M. E. Mullins, D. J. Singel, J. Loscalzo, R. J. Xavier and D. K. Podolsky, *Gastroenterology*, 1993, **105**, 1681.

42 J. S. Beckman, Y. Z. Ye, P. G. Anderson, J. Chen, M. A. Accavitti, M. M. Tarpey and C. R. White, *Biol. Chem. Hoppe-Seyler*, 1994, **375**, 81.

43 C. R. White, T. A. Brock, L. Y. Chang, J. Crapo, P. Briscoe, D. Ku, W. A. Bradley, S. H. Gianturco, J. Gore, B. A. Freeman and M. M. Tarpey, *Proc. Natl. Acad. Sci. U.S.A.*, 1994, **91**, 1044.

44 I. Fridovich, *J. Biol. Chem.*, 1989, **264**, 7761.

45 S. K. Kong, M. B. Yim, E. R. Stadtman and P. B. Chock, *Proc. Natl. Acad. Sci. USA.*, 1996, **93**, 3377.

46 T. H. Mondoro, B. C. Shafer and J. G. Vostal, *Free Radical Biol. Med.*, 1997, **22**, 1055.

47 M. R. Gunther, L. C. Hsi, J. F. Curtis, J. K. Gierse, L. J. Marnett, T. E. Eling and R. P. Mason, *J. Biol. Chem.*, 1997, **272**, 17086.

48 O. Bagasra, F. H. Michaels, Yong Mu Zheng, L. E. Bobroski, S. V. Spitsin, Zhen Fang Fu, R. Tawadros and H. Koprowski, *Proc. Natl. Acad. Sci. USA.*, 1995, **92**, 12041.

49 G. Prota, *J. Invest. Dermatol.*, 1980, **75**, 122.

50 P. C. Joshi, C. Carraro and M. A. Pathak, *Biochem. Biophys. Res. Commun.*, 1987, **142**, 265.

51 A. van der Vliet, C. A. O'Neill, B. Halliwell, C. E. Cross and K. Harparkash, *FEBS Letts.*, 1994, **339**, 89.

52 H. Musso, *Angew. Chemie*, 1963, **2**, 723.

53 H. I. Joschek and S. I. Miller, *J. Am. Chem. Soc.*, 1966, **88**, 3273.

54 S. O. Anderson, *Acta Physiol. Scand.*, 1966, **66** Suppl. 263, 1.

55 S. S. Lehrer and G. D. Fasman, *Biochem.*, 1967, **6**, 757.

56 G. Deliconstantinos, V. Villiotou and J. C. Stavrides, *Experimental Physiology*, 1996, **81**, 1021.

57 E. Gilad, S. Cuzzocrea, B. Zingarelli, A. L. Salzman and C. Szabo, *Life Sciences*, 1997, **60**, PL69.

58 W. A. Pryor, X. Jin and G. L. Squadrito, *J. Am. Chem. Soc.*, 1996, **118**, 3125.

59 H-H Tsai, T. P. Hamilton, J-H. M. Tsai, M. van der Woerd, J. G. Harrison, M. J. Jablonsky, J. S. Beckman and W. H. Koppenol, *J. Phys. Chem.*, 1996, **100**, 15087.

60 H-H Tsai, T. P. Hamilton, J-H. M. Tsai, J. G. Harrison and J. S. Beckman, *J. Phys. Chem.*, 1996, **100**, 6942.

61 W. H. Koppenol, J. J. Moreno, W. A. Pryor, H. Ischiropoulos and J. S. Beckman, *Chem. Res. Toxicol.*, 1992, **5**, 834.

62 W. A. Pryor, personal communication, October 27, 1997.

63 S. V. Lymar and J. K. Hurst, *J. Am. Chem. Soc.*, 1995, **117**, 8867.

64 R. M. Uppu, G. L. Squadrito and W. A. Pryor, *Arch. Biochem. Biophys.*, 1992, **327**, 335.

65 R. M. Uppu and W. A. Pryor, *Biochem. Biophys. Res. Commun.*, 1996, **229**, 1996.

66 W. A. Pryor, J.-N. Lemercier, H. Zhang and R. M. Uppu, *Free Radical Biol. Med.*, 1997, **23**, 331.

67 H. Zhang, G. L. Squadrito, R. M. Uppu, J.-N. Lemercier, R. Cueto and W. A. Pryor, *Arch. Biochem. Biophys.*, 1997, *339*, 183.

68 A. Gasco and A. J. Boulton, *Adv. Heterocycl. Chem.*, 1981, **29**, 251.

69 A. Kekulé, *Liebigs Ann. Chem.*, (*a*) 1857, **101**, 200; (*b*) 1858, **105**, 279.

70 H. Wieland, *Liebigs Ann. Chem.*, 1903, **329**, 225; (*b*) H. Wieland and L. Semper, *Liebigs Ann. Chem.*, 1907, **358**, 36.

71 A. Werner, *Lehrbuch der Stereochemie*, 1904, Fischer, Jena, p.260.

72 R. Koreff, *Ber. Dtsch. Chem. Ges.*, 1896, **19**, 176.

73 P. Tönnies, *Ber. Dtsch. Chem. Ges.*, 1880, **13**, 1845.

74 A. Angeli, *Ber. Dtsch. Chem. Ges.*, 1893, **26**, 593.

75 R. Calvino, A. Gasco, A. Serafino and D. Viterbo, *J. Chem. Soc., Perkin Trans. 2*, 1981, 1241.

76 G. A. Taylor, *J. Chem. Soc., Perkin Trans. 1*, 1985, 1181.

77 G. Barbaro, A. Battaglia and A. Dondoni, *J. Chem. Soc. B.*, 1970, 588.

78 R. A. Firestone, *Tetrahedron*, 1977, **33**, 3009.

79 A. Dondoni, A. Mangini and S. Ghersett, *Tetrahedron Lett.*, 1966, 4789.

80 T. Osawa, Y. Kito and M. Namiki, *Tetrahedron Lett.*, 1979, 4399.

81 H. Wieland, *Ber. Dtsch. Chem. Ges.*, 1909, **42**, 803.

82 G. Ruggeri, *Gazz. Chim. Ital.*, 1925, **55**, 72.

83 L. I. Peterson, *Tetrahedron Lett.*, 1966, 1727.

84 M. Z. Jovitchitch, *Ber. Dtsch. Chem. Ges.*, 1902, **35**, 151.

85 R. Behrend and H. Tryller, *Liebigs Ann. Chem.*, 1894, **283**, 209.

86 R. Behrend and J. Schmitz, *Liebigs Ann. Chem.*, 1893, **277**, 310.

87 L. W. Kissinger, W. E. McQuistion, M. Schwartz and L. Goodman, *Tetrahedron*, 1963, **19**, Suppl. 1, 131.

88 J. F. J. Engbersen and J. B. F. N. Engberts, *Synth. Commun.*, 1971, **1**, 121.

89 F. Yamakura, H. Taka, T. Fujimura and K. Murayama, *J. Biol. Chem.* 1998, **273**, 14085.

90 L. A. MacMillan-Crow, J. P. Crow and J. A. Thompson, *Biochem.*, 1998, **37**, 1613.

91 H. Ischiropoulos, L. Zhu, J. Chen, M. Tsai, J. C. Martin, C. D. Smith and J. S. Beckman, *Arch. Biochem. Biophys.*, 1992, **298**, 431.

92 J. A. Tainer, E. D. Getzoff, J. S. Richardson and D. C. Richardson, *Nature*, 1983, **306**, 284.

93 J. S. Beckman, personal communication, 9 October 1998.

94 (*a*) A. H. Clemens, J. H. Ridd and J. P. B. Sandall, *J. Chem. Soc., Perkin Trans. 2*, 1984, 1659; (*b*) A. H. Clemens, J. H. Ridd and J. P. B. Sandall, *J. Chem. Soc., Perkin Trans. 2*, 1984, 1667; (*c*) A. H. Clemens, P. Helsby, J. H. Ridd, F. Al-Omran and J. P. B. Sandall, *J. Chem. Soc., Perkin Trans. 2*, 1985, 1217; (*d*) A. H. Clemens, J. H. Ridd and J. P. B. Sandall, *J. Chem. Soc., Perkin Trans. 2*, 1985, 1227; (*e*) J.F. Johnston, J. H. Ridd and J. P. B. Sandall, *J. Chem. Soc., Perkin Trans. 2*, 1991, 623.

95 J. H. Ridd, *Chem. Soc. Rev.*, 1991, **20**, 149.

96 H. D. Roth, in *Encyclopedia of Nuclear Magnetic Resonance*, eds. D. M. Grant and R. K. Harris, John Wiley & Sons, New York, 1996, vol. 2, p. 1337.

97 H. R. Ward, in *Free Radicals*, ed. J. K. Kochi, John Wiley & Sons, New York, 1973, vol. 1, p. 239.

98 S. H. Pine, *J.Chem. Edu.*, 1972, **49**, 664.

99 R. Kaptein, *J. Chem. Soc., Chem. Commun.*, 1971, 732.

100 G. C. Levy and R. L. Lichter, *Nitrogen-15 Nuclear Magnetic Resonance Spectroscopy*, John Wiley and Sons, New York, 1979, p.2.

101 B. C. Challis and J. H. Ridd, *J. Chem. Soc.*, 1962, 5197.

102 A. V. Manuilov and V. A. Barkhash, *Usp. Khim.*, 1990, **59**, 304.

103 A. M. A. Abu-Namous, J. H. Ridd and J. P. B. Sandall, *Can. J. Chem.*, 1986, **64**, 1124.

104 S. L. Ioffe, A. L. Blyumenfel'd and A. S. Shashkov, *Izv. Akad. Nauk. SSSR, Ser. Khim.*, 1978, 246.

105 R. G. Coombes, J. G. Golding and P. Hadjigeorgiou, *J. Chem. Soc., Perkin Trans. 2*, 1979, 1451.

106 J. H. Ridd, S. Trevellick and J. P. B. Sandall, *J. Chem. Soc., Perkin Trans. 2*, 1992, 573.

107 Landolt-Börnstein, *Numerical Data and Functional Relationships in Science and Technology*, ed. K.-H. Hellwege, Springer-Verlag, Berlin, 1980, vol. 9, part d2, pp. 96.

108 E. Lippmaa, T. Pehk, T. Saluvere and M. Mägi, *Org. Magn. Reson.*, 1973, **5**, 441.

109 M. Ali and J. H. Ridd, *J. Chem. Soc., Perkin Trans 2*, 1986, 327.

110 Ref. 99, p.6.

111 N. A. Porter, G. R. Dubay and J. G. Green, *J. Am. Chem. Soc.*, 1979, **100**, 920.

112 J. R. Morton, K. F. Preston and S. J. Strach, *J. Phys. Chem.*, 1979, **83**, 533.

113 R. C. Sealy, L. Harman, P. R. West and R. P. Mason. *J. Am. Chem. Soc.*, 1985, **107**, 3401.

114 M. S. Blois, H. W. Brown and J. E. Maling, *Neuviéme Colloque Ampére, Geneva; Librairie Payot*, 1960, 243.

115 Landolt-Börnstein, *Numerical Data and Functional Relationships in Science and Technology*, ed. H. Fischer, Springer-Verlag, Berlin, 1987, New Series Group 2, vol. 17, part a, pp. 54-55.

116 (*a*) Younghee Ko, F.T Bonner, G. B. Crull and G. S. Harbison, *Inorg. Chem.* 1993, *32*, 3316; (*b*) F. T. Bonner, personal communication, 30 July 1998.

117 M. N. Hughes, H. G. Nicklin and W. A. C. Sackrule, *J. Chem. Soc. (A)*, 1971, 3722.

118 R. G. Coombes, A. W. Diggle and S. P. Kempsell, *Tetrahedron Lett.*, 1994, **35**, 6373.

119 A. R. Butler, T. J. Rutherford, D. M. Short and J. H. Ridd, *J. Chem. Soc., Chem. Commun.*, 1997, 669.

120 B. C. Challis and S. A. Kyrtopoulos, *J. Chem. Soc., Perkin Trans. 2*, 1978, 1296.

121 M. Grätzel, A. Henglein, J. Lilie and G. Beck, *Ber. Bunsengesellschaft Phys. Chem.*, 1969, **73**, 646.

122 A. Schaarschmidt, *Z. Angew. Chem.*, 1924, **37**, 933.

123 P. Golding, J. L. Powell and J. H. Ridd, *J. Chem. Soc., Perkin Trans. 2*, 1996, 813.

124 M. L. McKee, *J. Am. Chem. Soc.*, 1995, **117**, 1629.

125 J. L. Powell, J. H. Ridd and J. P. B. Sandall, *J. Chem. Soc., Chem. Commun.*, 1990, 402.

126 C. E. Richeson, P. Mulder, V. W. Bowry and K. U. Ingold, *J. Am. Chem. Soc.*, 1998, **120**, 7211.

127 S. Pfeiffer, A. C. F. Gorren, K. Schmidt, E. R. Werner, B. Hansert, D. S. Bohle and B. Mayer, *J. Biol. Chem.*, 1997, **272**, 3465.

128 (*a*) J. P. Eiserich, C. E. Cross, A. D. Jones, B. Halliwell and A. van der Vliet, *J. Biol. Chem.*, 1996, **271**, 19199; (*b*) J. P. Eiserich, M. Hristova, C. E. Cross, A. D. Jones, B. A. Freeman, B. Halliwell and A. van der Vliet, *Nature*, 1998, **391**, 393.

129 Work carried out in conjunction with Hazel Cox and first reported in H. L. Cox, Senior honours project, University of St. Andrews, 1996.

130 E. W. Wilson, Jr. and R. B. Martin, *Arch. Biochem. Biophys.*, 1971, **142**, 445.

131 D. M. E. Reuben and T. C. Bruice, *J. Am. Chem. Soc.*, 1976, **98**, 114.

132 R. K. Boggess, J. R. Absher, S. Morelen, L. T. Taylor and J. W. Hughes, *Inorg. Chem.*, 1983, **22**, 1273.

133 H. M. S. Patel and D. L. H. Williams, *J. Chem. Soc., Perkin Trans 2*, 1990, 37.

134 D. L. H. Williams, *Nitric Oxide: Biol. Chem.*, 1997, **1**, 522.

135 W. A. Pryor, D. F. Church, C. K. Govindan and G. Crank, *J. Org. Chem.*, 1982, **47**, 156.

136 E. A. E. Garber, S. Wehrli and T. C. Hollocher, *J. Biol. Chem.*, 1983, **258**, 3587.

137 B. W. Erickson and R. B. Merrifield, *J. Am. Chem. Soc.*, 1973, **95**, 3750.

138 B. Iselin, *Helv. Chim. Acta*, 1962, **45**, 1510.

139 Y. Trudelle and G. Spach, *Tetrahedron Lett.*, 1972, 3475.

140 R. S. Lott, V. S. Chauhan and C. H. Stammer, *J. Chem. Soc., Chem. Commun.*, 1979, 495.

141 G. A. Olah and S. C. Narang, *Tetrahedron*, 1982, 2235.

142 W. A. Pryor, *Free Radicals*, McGraw-Hill, New York, 1966; J. A. K. Hamony, *Methods Free-Radical Chem.*, 1974, **5**, 101; W. A. Pryor, J. H. Coco, W. H. Daly and K. N. Houk, *J. Am. Chem. Soc.*, 1974, **96**, 5591; W. A. Pryor in *Organic Free Radicals*, ed. W. A. Pryor, American Chemical Society, Washington D.C., 1978, p.33.

143 R. G. Lawler, personal communication, 23 July 1998.

144 R. A. Miller and B. E. Britigan, *J. Invest. Med.*, 1995, **43**, 39.

145 J. R. Lancaster, *Proc. Natl. Acad. Sci. USA*, 1994, **91**, 8137.

146 M. Fontecave and J-L Pierre, *Bull. Soc. Chim. Fr.*, 1994, **131**, 620.

147 M. Laurent, M. Lepoivre and J. P. Tenu, *Biochem. J.*, 1996, **314**, 109.

148 R. E. Huie, S. Padmaja, *Free Rad. Res. Commun.* 1993, **18**, 195.

149 A. R. Butler, I. L. Megson and P. G. Wright, *Biochim. Biophys. Acta. General Subjects*, 1998, **1425**, 168.

150 D. W. Johnson and D. W. Margerum, *Inorg. Chem.*, 1991, **30**, 4845.

151 J. M. Cachaza, J. Casado, A. Castro and M. A. López Quintela, *Can. J. Chem.*, 1976, **54**, 3401.

152 S. J. Kuhn and G. A. Olah, *J. Am. Chem. Soc.*, 1964, **83**, 4564.

153 C. D. Ritchie, D. J. Wright, D-S. Huang and A. A. Kamego, *J. Am. Chem. Soc.*, 1975, **97**, 1163.

154 C. D. Ritchie and P. O. I. Virtanen, *J. Am. Chem. Soc.*, 1972, **94**, 4966.

155 C. A. Bunton, E. A. Halevi and D. R. Llewellyn, *J. Chem. Soc.*, 1952, 4913.

156 K. Schofield, (1980) Aromatic Nitration, p.41 and 51, Cambridge University Press.

157 R. G. Coombes, J. G. Golding and P. Hadjigeorgiou, *J. Chem. Soc., Perkin Trans. 2*, 1979, 1451.

158 M. S. Ramezanian, S. Padmaja and W. H. Koppenol, *Chem. Res. Toxicol.*, 1996, **9**, 232.

159 Q. Jiang and J. K. Hurst, *J. Biol. Chem.*, 1997, **272**, 32767.

160 (*a*) J. Kenner, *Nature*, 1945, **156**, 369; (*b*) J. Weiss, *Trans. Faraday Soc.*, 1946, **42**, 116; (*c*) G. A. Benford, C. A. Bunton, E. S. Halberstadt, E. D. Hughes, C. K. Ingold and R. E. Reed, *Nature*, 1945, **156**, 688.

161 L. Eberson, M. P. Hartshorn, F. Radner and O. Persson, *J. Chem. Soc., Perkin Trans. 2*, 1998, 59.

162 A. Pross, *Adv. Phys. Org. Chem.*, 1985, **21**, 99; A. Pross, *Acc. Chem. Res.*, 1985, **18**, 212; S. S. Shaik, *Prog. Phys. Org. Chem.*, 1985, **15**, 197; S. S. Shaik, *J. Am. Chem. Soc.*, 1981, **103**, 3692.

163 M. Feelisch, K. Schonafinger and E. Noack, *Biochem. Pharmacol.* 1992, **44**, 1149.

164 G. Sorba, A. Gasco, G. Coruzzi, M. Adami, C. Pozzoli, G. Morini and G. Bertaccini, *Arzneimittel-Forschung/Drug Research*, 1997, **47**, 849.

165 A. M. Gasco, R. Fruttero, G. Sorba and A. Gasco, *Liebigs Ann. Chem.* 1991, 1211.

166 C. Medana, G. Ermondi, R. Fruttero, A. Di Stilo, C. Ferretti and A. Gasco, *J. Med. Chem.* 1994, **37**, 4412.

167 H. C. van der Plas, *Acc. Chem. Res.*, 1978, **11**, 462.

168 H. Wieland, *Liebigs Ann. Chem.*, 1903, **328**, 154.

169 Roberta Fruttero, personal communication, 11th June 1996.

170 P. Capdevielle, A. Lavigne and M. Maumy, *Synthesis*, 1989, 451.

171 R. C. Bertelson, K. D. Glanz and D. B. McQuain, *J. Heterocycl. Chem.*, 1969, **6**, 317.

172 H. Wieland and E. Gmelin, *Liebigs Ann. Chem.*, 1910, **375**, 297.

173 A. F. Holleman, *Recl. Trav. Chim. Pays-Bas*, 1892, **11**, 258.

174 A. J. Boulton, Personal communication, 10th November 1998.

175 F. Minisci, A. Citterio, E. Vismara and C. Giordano, *Tetrahedron*, 1985, **41**, 4157.

176 C. E. Stoner, A. L. Rheingold, T. B. Brill, *Inorg. Chem.*, 1991, **30**, 360.

177 J. L. Kelley, E. W. McLean and K. F. Williard, *J. Heterocycl. Chem.* 1977, **14**, 1415.

178 S. P. Singh, J. S. Wishnock, M. Keshive, W. M. Deen and S. R. Tannenbaum, *Proc. Natl. Acad. Sci. USA*, 1996, **93**, 14428.

179 P. K. Bhattacharyya and B. P. Dailey, *J. Chem. Phys.*, 1973, **59**, 5820.

180 R. Zamora, A. Grzesiok, H. Weber and M. Feelisch, *Biochem. J*, 1995, **312**, 333.

181 M. N. Hughes, *Q. Rev.*, 1968, **22**, 1.

182 H. C. van Anken and M. E. Schiphorst, *Clin. Chim. Acta*, 1974, **56**, 151.

183 W. E. Neeley and J. Phillipson, *Clin. Chem.*, 1968, **34**, 1868.

184 A. Mondzac, G. E. Ehrlich and J. E. Seegmiller. *J. Lab. Clin. Med.*, 1965, **66**, 526.

185 K. J. Reszka, C. F. Chignell and P. Bilski, *J. Am. Chem. Soc.*, 1994, **116**, 4119.

186 J. S. B. Park, Ph.D thesis, University of St. Andrews, July 1996.

187 Yong Xia and J. L. Zweier, *Proc. Natl. Acad. Sci. USA*, 1997, **94**, 12705.

188 H. Kaur, K. H. W. Leung and M. J. Perkins, *J. Chem. Soc., Chem. Commun.*, 1981, 142.

189 E. G. Janzen, Y. Y. Wang and R. V. Shetty, *J. Am. Chem. Soc.*, 1978, **100**, 2923.

190 E. G. Janzen and R. C. Zawalski, *J. Org. Chem.*, 1978, **43**, 1900.

191 M. J. Perkins, *Adv. Phys. Org. Chem.*, 1980, **17**, 1.

192 A. C. Whitwood, personal communication, 26 March 1998.

193 T. Yoshioka, N. Iwamoto, S. Manno, K. Irie, K. Ito, Y. Takakuwa and T. Muraki, *Jap. J. Pharmacol.*, 1997, **75** Suppl. 1, P–336.

194 R. Fruttero, D. Boschi, A. Di Stilo and A. Gasco, *J. Med. Chem.*, 1995, **38**, 4944.

195 A. De Filippi, G. Sorba, R. Calvino, A. Garrone, A. Gasco and M. Orsetti, *Arch. Pharm.*, 1988, **321**, 77.

196 G. Sorba, A. Gasco and M. Orsetti, *Eur. J. Med. Chem.*, 1989, **24**, 475.

197 W. A. Noyes, *Org. Synth.*, Coll. Vol. II, 1943, 108.

198 L. Dall'asta and P. Ferrario, *Helv. Chim. Acta*, 1962, **45**, 1065.

199 L. Field, R. V. Dilts, R. Ravichandran, P. G. Lenhert and G. E. Carnahan, *J. Chem. Soc., Chem. Commun.*, 1978, 249.

200 I. R. Greig, Ph.D. Thesis, University of St. Andrews, August 1997.

201 D. S. Tarbell, Y. Yamamoto and B. M. Pope, *Proc. Nat. Acad. Sci. USA*, 1972, **69**, 730.

202 B. F. Erlanger and R. M. Hall, *J. Am. Chem. Soc.*, 1954, **76**, 5781.

203 A. M. Gasco, C. Cena and A. Di Stilo, *Helv. Chim. Acta*, 1996, **79**, 1803.

204 G. Ponzio, *Gazz. Chim. Ital.*, 1930, **60**, 886.

205 G. Sorba, G. Ermondi, R. Fruttero, U. Galli and A. Gasco, *J. Heterocycl. Chem.*, 1996, **33**, 327.

206 G. Sorba, C. Medana, R. Fruttero, C. Cena, A. Di Stilo, U. Galli and A. Gasco, *J. Med. Chem.* 1997, **40**, 463.

207 L. A. Shinobu, S. G. Jones and M. M. Jones, *Acta. Pharmacol. Toxicol.*, 1984, **54**, 189.

Appendix 1: 2D NMR assignments for AYV tripeptide.

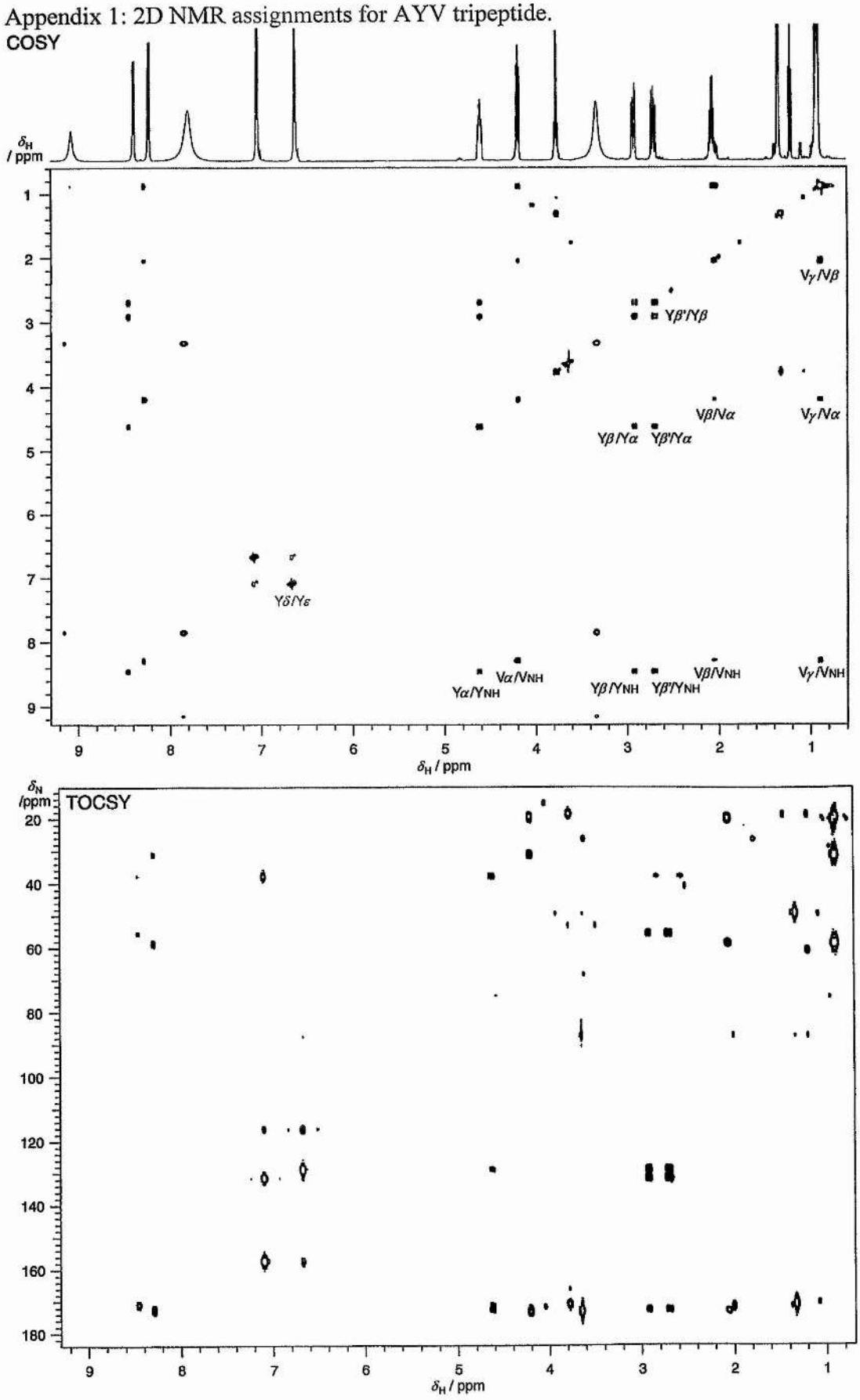

Appendix 2: 2D NMR assignments for *N*-methyl-D-glucamine dithiocarbamate

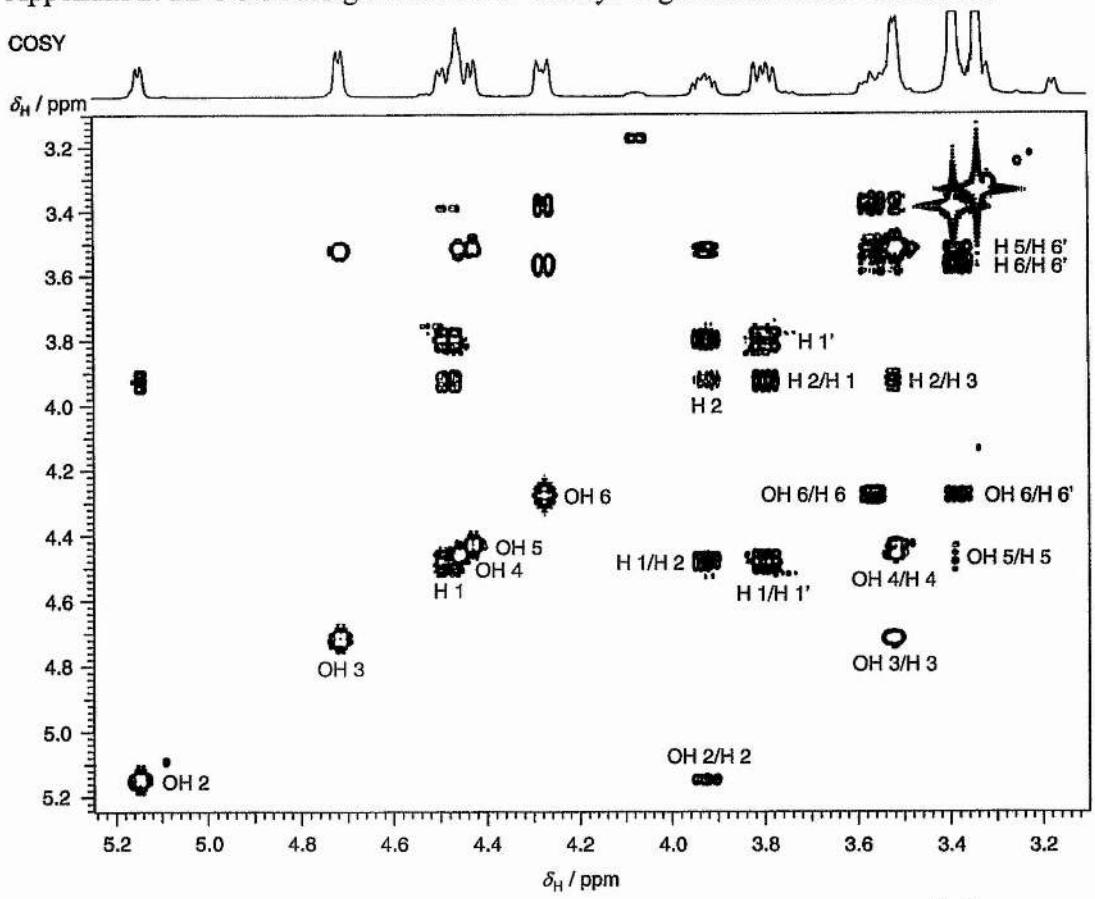

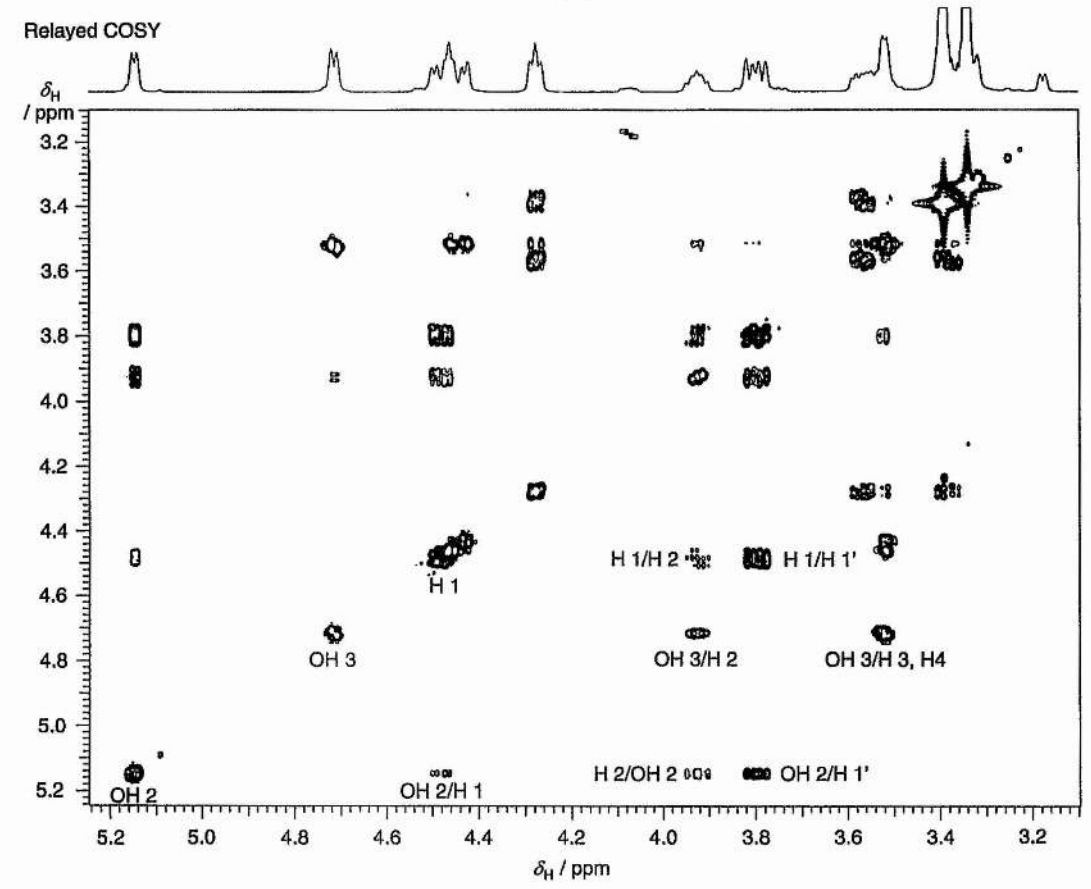

Appendix 2: 2D NMR assignments for *N*-methyl-D-glucamine dithiocarbamate

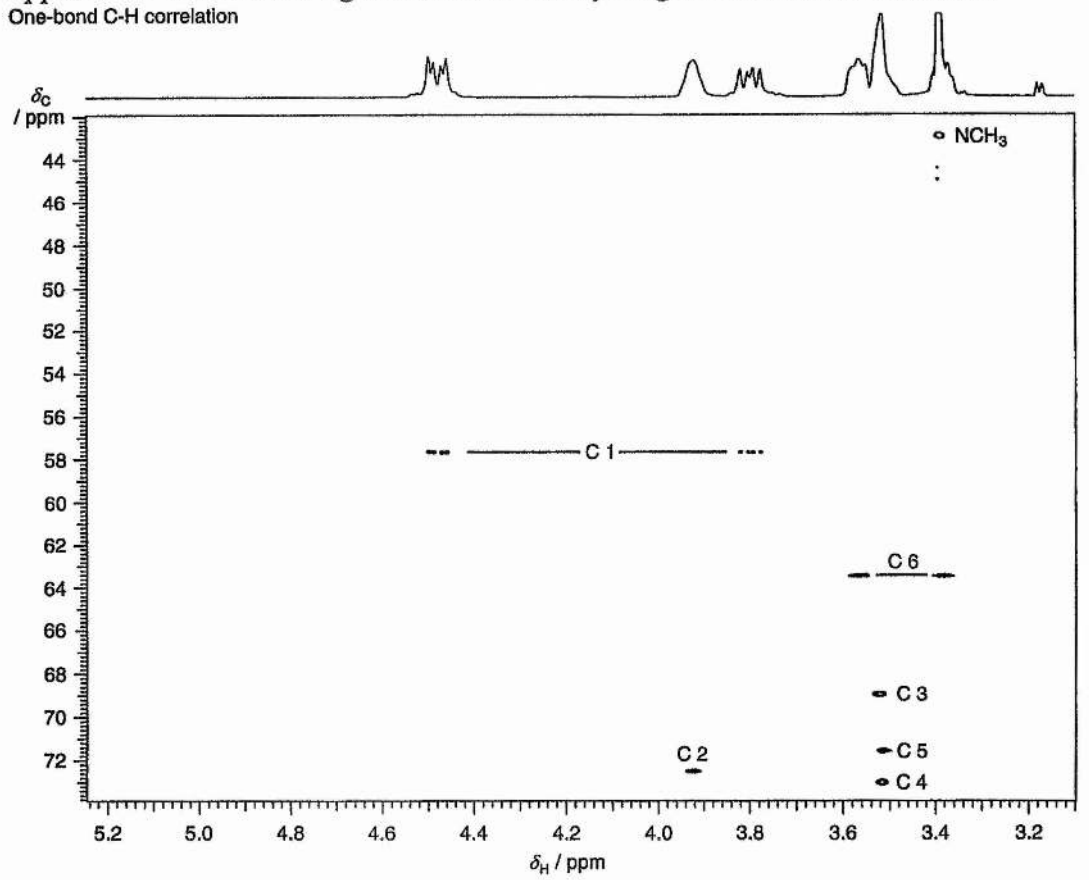

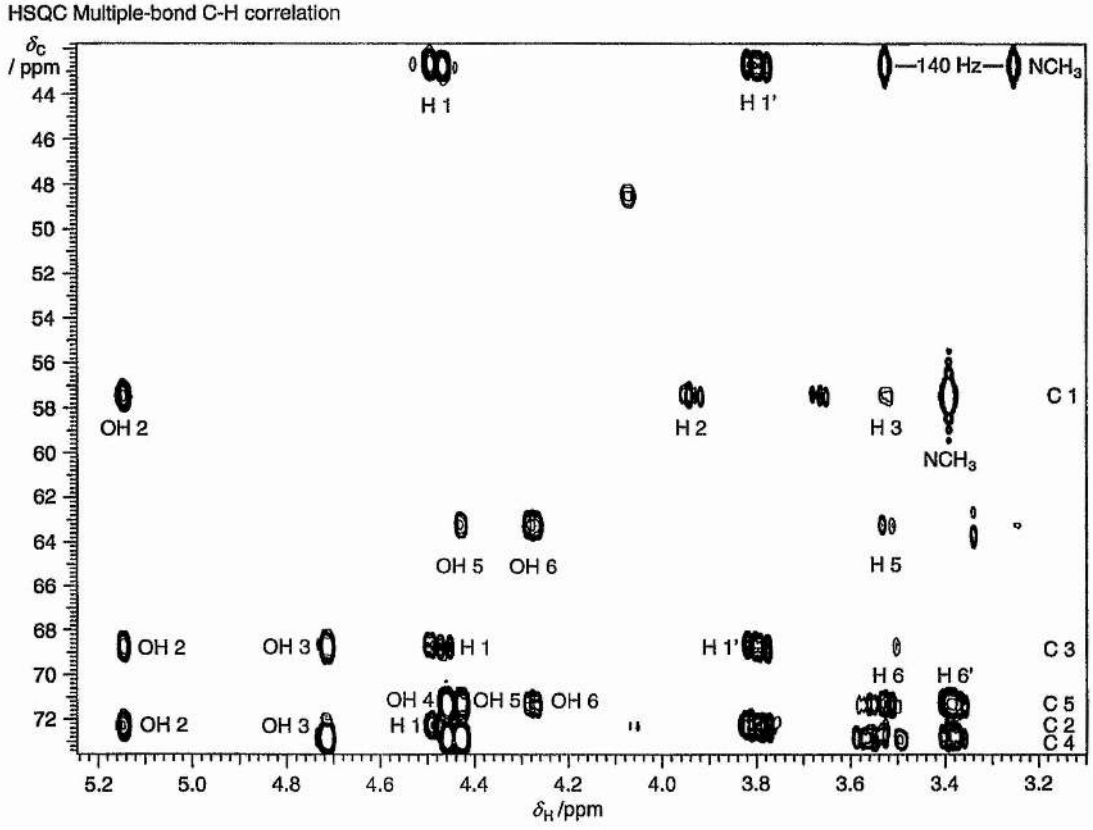

Appendix 3: Bond lengths, angles, refined coordinates, thermal parameters and their estimated standard deviations for crystal structure shown in Fig. 4.2

Atom 1	Atom 2	Bond length/pm	Atom 1	Atom 2	Atom 3	Bond Angle/°
O(1)	N(1)	1.397(9)	N(1)	O(1)	N(2)	111.6(5)
O(1)	N(2)	1.389(8)	O(1)	N(1)	C(2)	106.2(6)
O(2)	C(9)	1.210(7)	O(1)	N(2)	C(1)	103.9(6)
N(1)	C(2)	1.310(9)	C(1)	N(3)	C(9)	120.5(6)
N(2)	C(1)	1.308(9)	N(2)	C(1)	N(3)	118.3(7)
N(3)	C(1)	1.405(8)	N(2)	C(1)	C(2)	111.2(6)
N(3)	C(9)	1.384(8)	N(3)	C(1)	C(2)	130.4(6)
C(1)	C(2)	1.45(1)	N(1)	C(2)	C(1)	107.1(7)
C(2)	C(3)	1.45(1)	N(1)	C(2)	C(3)	119.5(7)
C(3)	C(4)	1.421(9)	C(1)	C(2)	C(3)	133.4(6)
C(3)	C(8)	1.40(1)	C(2)	C(3)	C(4)	122.6(7)
C(4)	C(5)	1.38(1)	C(2)	C(3)	C(8)	120.9(7)
C(5)	C(6)	1.38(1)	C(4)	C(3)	C(8)	116.5(7)
C(6)	C(7)	1.37(1)	C(3)	C(4)	C(5)	120.7(7)
C(7)	C(8)	1.37(1)	C(4)	C(5)	C(6)	121.6(8)
C(9)	C(10)	1.487(9)	C(5)	C(6)	C(7)	117.9(9)
C(10)	C(11)	1.394(10)	C(6)	C(7)	C(8)	122.1(8)
C(10)	C(15)	1.365(10)	C(3)	C(8)	C(7)	121.2(7)
C(11)	C(12)	1.39(1)	O(2)	C(9)	N(3)	121.5(6)
C(12)	C(13)	1.37(1)	O(2)	C(9)	C(10)	124.3(7)
C(13)	C(14)	1.39(1)	N(3)	C(9)	C(10)	114.1(6)
C(14)	C(15)	1.40(1)	C(9)	C(10)	C(11)	116.9(6)
			C(9)	C(10)	C(15)	123.2(7)
			C(11)	C(10)	C(15)	119.8(6)
			C(10)	C(11)	C(12)	119.4(7)
			C(11)	C(12)	C(13)	120.3(8)
			C(12)	C(13)	C(14)	121.2(8)
			C(13)	C(14)	C(15)	117.7(8)
			C(10)	C(15)	C(14)	121.6(7)

Appendix 3: Bond lengths, angles, refined coordinates, thermal parameters and their estimated standard deviations for crystal structure shown in Fig. 4.2

Atom No.	X Coordinate	Y Coordinate	Z Coordinate	U_{ij}
O(1)	-0.0313	-0.156(1)	0.3918	0.072(2)
O(2)	-0.2696(9)	0.2990(10)	0.6188(5)	0.048(2)
N(1)	0.057(1)	0.050(2)	0.4280(5)	0.063(2)
N(2)	-0.1355(10)	-0.240(1)	0.4565(6)	0.058(2)
N(3)	-0.1949(9)	-0.132(1)	0.6110(5)	0.040(2)
C(1)	-0.110(1)	-0.089(2)	0.5301(6)	0.043(2)
C(2)	0.012(1)	0.092(2)	0.5141(6)	0.043(2)
C(3)	0.0886(10)	0.285(2)	0.5729(6)	0.042(2)
C(4)	0.067(1)	0.303(2)	0.6716(6)	0.049(3)
C(5)	0.142(1)	0.489(2)	0.7249(6)	0.061(3)
C(6)	0.243(1)	0.661(2)	0.6851(8)	0.071(3)
C(7)	0.269(1)	0.637(2)	0.5903(8)	0.069(3)
C(8)	0.194(1)	0.458(2)	0.5348(7)	0.058(3)
C(9)	-0.273(1)	0.076(1)	0.6512(6)	0.037(2)
C(10)	-0.351(1)	0.002(1)	0.7390(6)	0.036(2)
C(11)	-0.470(1)	0.162(1)	0.7647(6)	0.049(3)
C(12)	-0.543(1)	0.110(2)	0.8481(7)	0.066(3)
C(13)	-0.495(1)	-0.093(2)	0.9059(7)	0.064(3)
C(14)	-0.376(1)	-0.254(2)	0.8817(7)	0.062(3)
C(15)	-0.306(1)	-0.202(2)	0.7966(6)	0.049(2)
H(1)	-0.0005	0.1847	0.7012	0.0588
H(2)	0.1248	0.4987	0.7906	0.0734
H(3)	0.2928	0.7922	0.7221	0.0858
H(4)	0.3414	0.7489	0.5625	0.0831
H(5)	0.2140	0.4504	0.4694	0.0694
H(6)	-0.2264	-0.3223	0.6253	0.0824
H(7)	-0.5012	0.3056	0.7254	0.0588
H(8)	-0.6257	0.2148	0.8651	0.0789
H(9)	-0.5445	-0.1233	0.9636	0.0768
H(10)	-0.3438	-0.3948	0.9217	0.0750
H(11)	-0.2253	-0.3103	0.7784	0.0592

Appendix 3: Bond lengths, angles, refined coordinates, thermal parameters and their estimated standard deviations for crystal structure shown in Fig. 4.2

atom	U_{11}	U_{22}	U_{33}	U_{12}	U_{13}	U_{23}
O(1)	0.091(5)	0.082(5)	0.043(3)	0.006(4)	0.017(3)	-0.010(3)
O(2)	0.059(4)	0.038(3)	0.047(3)	0.003(3)	0.014(3)	0.003(3)
N(1)	0.067(5)	0.074(5)	0.049(4)	-0.002(5)	0.020(4)	-0.002(4)
N(2)	0.068(5)	0.056(5)	0.049(4)	-0.002(4)	0.012(4)	-0.009(4)
N(3)	0.052(4)	0.026(3)	0.042(4)	-0.001(3)	0.013(3)	-0.003(3)
C(1)	0.050(5)	0.041(4)	0.039(5)	0.010(5)	0.005(4)	0.002(4)
C(2)	0.053(5)	0.045(5)	0.032(4)	0.013(4)	0.013(4)	0.000(4)
C(3)	0.039(5)	0.042(5)	0.044(4)	0.009(4)	0.009(4)	0.007(4)
C(4)	0.050(5)	0.055(5)	0.043(5)	0.000(5)	0.006(4)	0.004(4)
C(5)	0.051(5)	0.079(7)	0.053(5)	-0.005(5)	-0.002(4)	-0.010(5)
C(6)	0.062(6)	0.066(7)	0.086(8)	-0.014(6)	-0.011(5)	0.006(6)
C(7)	0.056(6)	0.071(7)	0.080(7)	-0.015(5)	0.000(5)	0.020(6)
C(8)	0.051(5)	0.065(6)	0.059(5)	0.000(5)	0.015(4)	0.020(5)
C(9)	0.044(5)	0.022(4)	0.044(4)	-0.007(4)	0.001(4)	0.000(4)
C(10)	0.046(5)	0.026(4)	0.035(4)	-0.007(4)	0.005(3)	-0.006(3)
C(11)	0.055(5)	0.040(5)	0.052(5)	0.007(4)	0.012(4)	-0.001(4)
C(12)	0.054(6)	0.082(8)	0.062(6)	0.003(5)	0.022(5)	-0.009(5)
C(13)	0.073(7)	0.068(6)	0.052(5)	-0.013(6)	0.025(4)	-0.005(5)
C(14)	0.085(7)	0.057(6)	0.046(5)	-0.008(5)	0.012(5)	0.004(4)
C(15)	0.052(5)	0.052(5)	0.045(5)	0.008(4)	0.006(4)	0.002(4)